METAKAOLIN-PORTLAND LIMESTONE CEMENTS: EVALUATING THE EFFECTS OF CHEMICAL ADMIXTURES ON EARLY AND LATE AGE BEHAVIOR

A Dissertation
Presented to
The Academic Faculty

by

Behnaz H. Zaribaf

In Partial Fulfillment
of the Requirements for the Degree
Doctor of Philosophy in the
School of Civil and Environmental Engineering

Georgia Institute of Technology
August 2017

METAKAOLIN-PORTLAND LIMESTONE CEMENTS: EVALUATING THE EFFECTS OF CHEMICAL ADMIXTURES ON EARLY AND LATE AGE BEHAVIOR

Approved by:

Dr. Kimberly Kurtis, Advisor
School of Civil and Environmental Engineering
Georgia Institute of Technology

Dr. T. Russel Gentry,
School of Architecture
Georgia Institute of Technology

Dr. Lawrence Kahn
School of Civil and Environmental Engineering *Georgia Institute of Technology*

Dr. Newell Washburn,
School of Chemistry and Biomedical Engineering
Carnegie Mellon University

Dr. Susan Burns
School of Civil and Environmental Engineering *Georgia Institute of Technology*

Dr. Sharad Mathur,
Product Applications Development and Quality Manager at *BASF*

Date Approved: 5/12/2017

ACKNOWLEDGEMENTS

I would like to acknowledge the contributions of a great many people to this work. First and foremost, I would like to express my greatest gratitude to my advisor, Dr. Kimberly Kurtis. I am grateful for all the insights you gave me in my Ph.D. journey, your advisement and mentorship did not only improve my research skills but also strengthen my leadership and mentorship skills.

I would also like to thank Dr. Lawrence Kahn for his guidance, I am grateful for your practical advice and encouragement in both my academic and my professional career. I would like to thank my committee members, Dr. Susan Burns, Dr. Newell Washburn, Dr. Sharad Mathur, and Dr. Russell Gentry for their thoughtful discussions, time, and support: this research was highly interdisciplinary, and I appreciate the variety of approaches and insights that each of you brought to the work. I would like to thank Dr. Uzal Burak for the insights he gave me when I first joined the group to find my research pathway in cement and admixtures compatibility.

This research was funded in part by Burgess Pigment Company and the Georgia Department of Transportation (GDOT) under project number 02-127. I would like to thank AJ Marisca and Charles Cleary from BASF for the great tour they gave us at BASF plant in Gordon and providing insightful information. Additional thanks belong to Andy Chafin at the Heidelberg Cement Technology Center for conducting chemical analyses on cement samples.

This research could not have been completed without the contributions of several collaborators. I would especially like to thank my groupmate Mehdi Rashidi for his great help on the modeling part of my research besides all the support he gave me during my

dissertation writing and defense. I would like to thank Elizabeth Nadelman that was my unofficial mentor in the group and gave me valuable advices on cement analytical and characterization techniques, and Ahmad Shalan who helped me with my concrete mixing and testing.

I would also like to thank my amazing group of undergraduate research assistants – Jamie Clark, Thibault Barbe, Mathieu Prevost, Claire Corbin, and Emily Cho – for their invaluable contributions to this research. I would also like to thank the past and present members of the Kurtis research group who have made my time in graduate school an enjoyable one: Dr. Passarin Jongvisuttisun, Dr. Nathan Mayercsik, Dr. Bradley Dolphyn, Dr. Álvaro Paul, Dr. Lisa Burris, Dr. Giovanni Loreto, Dr. Gun Kim, La Sasha Walker, Prasanth Alapati, Natalia Cardelino, Cole Spencer, and honorary group members Daniela Estrada and Dr. Guilherme Cordeiro. Thank you all for your friendship, conversations, encouragement, lunch times, game nights, and trivia shenanigans. Graduate school was a much richer and rewarding experience because of you.

Finally, I would like to thank my family for their unconditional support and love in my lifetime and special encouragement and support they gave in my Ph.D. life. I would like to specially thank my sister, Mary, for all her supports in my life as a mentor and my role model; I would not stand where I am without her.

TABLE OF CONTENTS

LIST OF TABLES

LIST OF FIGURES

LIST OF SYMBOLS AND ABBREVIATIONS

Abbreviations

AASHTO	American Association of State Highway and Transportation Officials
ASTM	American Society for Testing and Materials
BET	Brunauer-Emmett-Teller
CSA	Canadian Standards Association
DOT	Department of Transportation
DTG	Thermogravimetric derivative
EPA	United States Environmental Protection Agency
GDOT	Georgia Department of Transportation
GHG	Greenhouse gas
HRWRA	High-range water-reducer admixture
MK	Metakaolin
NIST	National Institute of Standards and Technology
OPC	Ordinary portland cement
PLC	Portland limestone cement
RCPT	Rapid chloride permeability test
SCM	Supplementary cementitious material
SD	Standard deviation
SEM	Scanning electron microscopy
SR	Surface resistivity
SRA	Shrinkage reducing admixture
SSA	Specific surface area
TGA	Thermogravimetric analysis
VP-SEM	Variable pressure scanning electron microscopy
WRA	Water-reducing admixture
XRD	X-ray diffraction

Cement Chemistry Abbreviations

AFm	Alumina-ferrite-monosulfate
AFt	Alumina-ferrite-trisulfate
C_2S	Dicalcium silicate ($2CaO \cdot SiO_2$)
C_3A	Tricalcium aluminate ($3CaO \cdot Al_2O_3$)
C_3S	Tricalcium silicate ($3CaO \cdot SiO_2$)
C_4AF	Tetracalcium aluminoferrite ($4CaO \cdot Al_2O_3 \cdot Fe_2O_3$)
$C\overline{C}$	Calcium carbonate ($CaCO_3$)
CH	Calcium hydroxide ($Ca(OH)_2$)
C-S-H	Calcium-silicate-hydrate
Hc	Hemicarboaluminate hydrate (hemicarbonate)
Mc	Monocarboaluminate hydrate (monocarbonate)
Ms	Monosulfoaluminate hydrate (monosulfate)

Symbols

D_{10}	10th percentile particle diameter
$D_{3,2}$	Surface area-weighted mean particle size

$D_{4,3}$	Volume-weighted mean particle size
D_{50}	50th percentile particle diameter
D_{90}	90th percentile particle diameter
D_a	Apparent diffusion coefficient
$H(t)$	Cumulative heat of hydration through time t
H_∞	Total heat of hydration upon complete hydration
H_{cem}	Total heat of hydration upon complete hydration of cement
H_{MK}	Total heat of hydration upon complete hydration of metakaolin
h_s	Height of capillary rise at the surface of a porous material
H_{slag}	Total heat of hydration upon complete hydration of slag
k	Permeability
p	Initial volume fraction of water (Powers' model)
p_c	Crystallization pressure
p_{cap}	Capillary pressure
p_i	Mass fraction of phase i in system of interest
p_w	Pore wall pressure
Q_t	Total charge passed by RCP test
r	Pore radius
R	Universal gas constant, 8.314 J/mol·K
RH	Relative humidity
S	Sorptivity
SG	Specific gravity
SG_b	Specific gravity of binder
T	Temperature
V	Voltage (Chapter 7 only)
V_{cs}	Volume fraction of chemical shrinkage
V_{cw}	Volume fraction of capillary water (capillary porosity)
V_f	Volume fraction of filler
V_{hp}	Volume fraction of hydration product
V_{uc}	Volume fraction of unhydrated cement
w/c	Water-to-cement mass ratio
w/b	Water-to-binder ratio, where the “binder” includes the cement, limestone, and any supplementary cementitious materials
α	Degree of hydration
α_u	Ultimate degree of hydration
β	Hydration shape parameter
θ	Contact angle (of a liquid-solid interface)
κ	Curvature (of a crystal)
ρ	Density
τ	Hydration time parameter

SUMMARY

One of the most effective and applicable ways to mitigate the greenhouse gas emissions contributed by cement production is to partially replace a portion of the cement clinker with alternative materials such as mineral filler (e.g., limestone) and pozzolanic materials (e.g., calcined clay or "metakaolin"), that require much less energy-intensive production processes compared to that of portland cement. However, the use of finer materials at higher rates has been limited by reductions in concrete workability, incomplete understanding of water reducing admixture (WRA) compatibility, and potential for increased shrinkage. To evaluate the combined use of metakaolin at higher replacement levels (> 10% by mass) with portland limestone cement (PLC) and their interaction with chemical admixtures, this investigation examines (1) early age hydration and microstructure development, (2) mechanical properties, and (3) durability including propensity for shrinkage-induced cracking in the context of understanding the interactions of water-reducing and shrinkage-reducing admixtures (WRAs, SRAs) with PLC-MK blended cements and concrete.

Among the four common WRA types, lignosulfonate (LS) was the least effective and polycarboxylate ether (PCE) the most effective admixture to improve the workability of PLC-MK blended cements. To improve predictions of heat of hydration in PLC-MK systems, a new model based on parameters obtained through isothermal calorimetry is proposed. Accelerated cement hydration in the presence of 30% MK lead to greater autogenous shrinkage in the first 3 days, but the 10% PLC-MK paste showed the greatest autogenous shrinkage at 28 days. The use of SRAs at 1% by mass of binder was effective

in mitigating autogenous shrinkage, decreasing shrinkage in PLC-MK by 50-60%, but also moderately delaying the cement hydration.

The use of MK in PLC concrete increased the compressive strength by more than 90% as early as one day and by 130% at 90 days of age. In comparing PCE with another WRA (i.e., polymelamine sulfonate, PMS), some retardation in strength development occurred and approximately 20% reductions in tensile strength and elastic modulus development were found; in contrast, improvements up to 43% in tensile strength and elastic modulus were found in the PCE PLC-MK compared to those of PLC concrete. This additional evidence points to the superiority of the PCE admixture in this system.

With respect to durability, the impermeability of PLC-MK concrete was significantly improved with increasing MK use. Although autogenous shrinkage was greater in the MK-containing pastes, MK-concrete exhibited *less* drying shrinkage, likely because less evaporable water is available during this period due to pozzolanic activity of MK, formation of new phases (e.g., secondary calcium silicate hydrates, carboaluminate), and the resulting densification of the paste. Overall, chemical admixtures were found to facilitate the use of MK at up to 30% by mass of PLC, with mixtures achieving similar or improved early and late age properties relative to PLC alone.

CHAPTER 1 INTRODUCTION

1.1.Motivation

Concrete is the most extensively used construction material in the world, and it can be used to produce durable and resilient structures of a variety of shapes. The high consumption of concrete is mainly due to the wide availability of its raw materials, its relatively low cost, and its versatility. More than 34 metric tons annually of portland cement concrete is produced annually with more than 4 million tons (Mt) of cement produced worldwide in 2015 [1], contributing 5-8% of all anthropogenic CO_2 emissions each year.

By virtue of the vast quantities produced each year, the cement industry is one of the major sources of carbon emissions (CO_2) through the combustion of fuels as well as calcinations of limestone in the manufacture of clinker. The cement consumption rate (Figure 1.1), shows that more than 50% of the cement worldwide is used in the rapidly developing countries, like India and China. With the ongoing industrial growth and urban development in those countries, the greenhouse gas (GHG) emissions from cement production are expected to continue at the current pace or higher. Therefore, environmental concerns regarding cement production have brought about pressures to reduce the associated emissions.

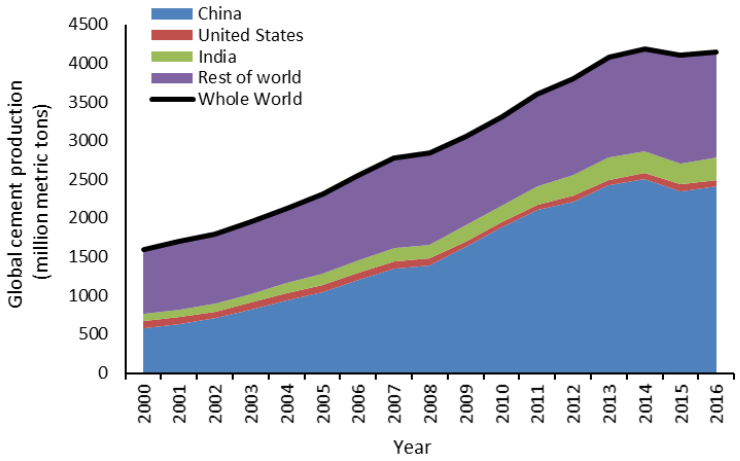

Figure 1.1.Contributions of China, India, and United States to global cement production from 2000-2016 [2].

The CO_2 emissions contributed by the portland cement production mainly derive directly from calcination and indirect sources of heating, electricity, and transportation. The majority of CO_2 emissions are contributed by the calcination process, which produces CO_2 and CaO by heating limestone (CaCO3) at the temperature typically lies between 600 and 850 °C [3] (Equation 1-1). The calcination process is a necessary step to produce CaO, which is a key component in portland cement clinker.

$$CaCO_3 + heat \rightarrow CaO + CO_2 \qquad 1\text{-}1$$

In 2009, the International Energy Agency (IEA) and Business Council for Sustainable Development (WBCSD) Roadmap proposed several CO_2 emissions and mitigation scenarios including increased energy efficiency, reliance on renewal energy, carbon capture and storage (CCS), and clinker substitution by SCMs to reduce the GHG emissions by cement industry [4]. One of the energy efficiency strategies was to use the

dry-kiln cement production process that consumes about 50% less energy than the wet kiln [5]. Another strategy is to use renewable sources of energy instead of fossil fuels for cements plants with the power plants on site. A recent technology to save the emitted CO_2 produced in cement production is carbon capture and storage (CCS). This technology works by capturing the CO_2 as emitted, compressing it to a liquid, and then transporting it in pipelines to be permanently stored deep underground [6] and was reported to potentially save about 46% of the emitted CO_2. Clinker substitution by SCMs is an important and well-established strategy with the advantage of reducing both the energy consumption and the direct CO_2 emission in the calcination process. This strategy is adopted in this study and will be discussed in more detail.

The clinker substitution strategy to reduce clinker-associated emissions is accomplished by blending SCMs with cement – either as a blended cement or during concrete batching – to reduce clinker fractions in concrete. SCMs can be naturally occurring, industrial waste, or products requiring relatively less energy to manufacture than that of cement. The use of SCMs in concrete improves the concrete sustainability not only by reducing the cement clinker fraction and embodied energy and GHGs but also by potentially improving durability through reducing permeability and increasing the mechanical properties of concrete through their pozzolanic reactivity. An estimated 800 Mt/yr. of SCMs are currently used in concrete, while the potential of using SCMs in concrete is much higher than that. Unacceptable performance issues observed with the use of SCMs limits their even broader utilization in concrete industry. Snellings [7] categorized the most common issues observed with the use of SCMs in concrete and suggested modifications to overcome those challenges (Table 1.1). The most common issue with using SCMs is lower workability due to the finer particles of SCMs.

Table 1.1. Challenging SCM properties for blended cements (From Ref. [7])

Physical incompatibility	**Effect on concrete properties**	**Suggested modification**
High fineness	High water demand, low workability	Superplasticizers, thermal treatment (sintering)
Insufficient fineness	Lowered performance	Grinding
High water absorption (porous components)	Excessive water demand	Selective removal, grinding
Intense color (red, black, brown…)	Undesirable color change	Selective removal of colored components, redox treatments
Chemical incompatibility		
Low reactivity	Low early strength	Activators, grinding, thermal activation
Expansive components (CaO, MgO, Al, …)	Volume instability, cracking, pop-outs	Maturation by hydration, carbonation, oxidation…
Corrosive components (Cl)	Corrosion of steel reinforcement	Cl removal (washing), use in concrete with no reinforcement
Durability impairing components (soluble alkalis, sulfate)	Long term expansion/cracking, efflorescence	Wet chemical pre-treatment
Environmental quality	Leaching of contaminants	Immobilization/removal by beneficiation pretreatments

The most commonly used SCMs in concrete are the industrial by-products fly ash (from coal-burning power plants) and slag (from blast furnace steel production). The use of fly ash in concrete typically ranges from 15 to 35% by mass of cement, but larger amounts of fly ash (up to 70%) have been used for roadways and dams. The use of fly ash reduces the water requirement and improves the concrete impermeability, strength, and freezing and thawing resistance through the pozzolanic activity of fly ash [8]. Despite the benefits of using fly ash, due to the varied quality of fly ash, only about one third of available fly ash can be used in concrete [9]. Also, as energy demand increases in cold weather, a time which is often not suitable for construction, some suitable fly ashes may

be disposed of because they cannot be utilized immediately. It should be also noted that the coal-burning power plant to produce electricity is by far the largest source of anthropogenic CO_2 and therefore the coal fired electricity production is being replaced by more sustainable renewable sources of energy. The coal power plant replacement and the recent availability of shale gas in North America has contributed to shortages of fly ash. With high demand of fly ash and its lower availability, the fly ash price is increasing. It was reported although fly ash is typically costs 50-60% of the cost of the cements, in areas where fly ash is not available and has been shipped long distances it was sold for higher prices than local portland cement [10].

The quality and availability of fly ash can vary around the world. In United States and Europe, the shift toward the use of more sustainable energy sources for electricity production has resulted in variation in the availability and characteristics of fly ash, such as mineralogy, particle size distribution, and morphology [11, 12]. In China, about 500 million tons per year (Mt/yr.) of fly ash is produced from coal-fired power plants. However, because the coal-fired plants are mainly located in the north and west of China while the economic development and population density are lower in those areas, around 3.5 billion tons of fly ash has been stored in China [13]. With the forecast of historical decrease in the construction growth in China, the utilization of this fly ash is not likely to happen in a close future [14].

Ground-granulated blast-furnace slag (GGBFS) can be substituted up to higher levels of 70% by mass of cement in concrete. However, the use of slag in concrete is limited by its availability. The blast furnace slag is only produced around 300-360 Mt/year with a decrease in production from 17% of global cement supply in 1980 to 8% in 2014 [15]. The

reduction in slag production is related to higher availability of recycled scrap steel and replacing the blast furnace iron production by more efficient steel making processes, i.e. electric arc furnaces (EAF). Currently, approximately 90% of the blast furnace slag is already used as an SCM in blended cements, and therefore there is not that much of potential left for further CO_2 reduction in cement industry.

With the limited supplies of slag and fly ash, and variety in quality and availability of fly ash, future reduction of embodied CO_2 emissions from the binder phases in concrete will need to depend on the extended used of other SCMs. Different types of SCMs and fillers can be considered for use in blended cement are shown, along with their compositions, in Table 1.2. The variation in composition, with respect to the main oxides associated with pozzolanic and latent hydraulic reactivity, of common SCMs are shown in Figure 1.2. It can be seen that unlike portland cement that contains lime and silicates, most SCMs are composed of aluminosilicates, although some, like slag and Class C fly ash, also contain lime.

Table 1.2. Overview of materials used or considered as SCMs (From Ref. [7])

Material	Components	Note
Blast furnace slag	$CaO\text{-}SiO_2\text{-}Al_2O_3$	Almost fully used
Fly ash- Class C (calcium rich)	$SiO_2\text{-}Al_2O_3$	LOI should be controlled
Fly ash- Class F (silica rich)	$CaO\text{-}SiO_2\text{-}Al_2O_3$	The LOI, CaO, MgO content should be controlled
Natural pozzolans	$SiO_2\text{-}Al_2O_3$	Large variety/variability, often high water demand
Silica fume	SiO_2	Used in high-performance concrete
Calcined clay	$SiO_2\text{-}Al_2O_3$	Metakaolin performs best, often high water demand
Limestone	$CaCO_3$	Cementitious contribution in combination with reactive aluminates
Biomass ash	$CaO.SiO_2$	Competition with use as soil amendment, high water demand
Waste glass	$CaO\text{-}SiO_2\text{-}Al_2O_3$	Glass recycling preferable, high alkali content

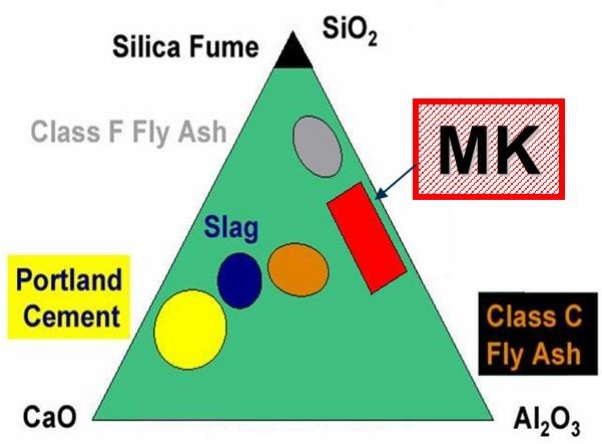

Figure 1.2. The difference in the chemical composition of fillers and SCMs

One important consideration in using SCMs is their availability. Figure 1.3 shows the quantity used of and overall availability of common SCMs and fillers. Sources of silica fume and water glass are very limited compared to that of portland cement. As it was mentioned before, slag availability is limited, and most of the available slag is already utilized, and there is not that much potential to increase the use of this SCM. The availability of fly ash is higher than that of slag, but not all that fly ash are usable in concrete because of its quality or timely accessibility. Natural pozzolans are reactive amorphous siliceous materials from natural sources that are available in limited regions around the world with about 75 Mt/yr. currently used as a pozzolan. The use of natural pozzolans in concrete can improve the concrete mechanical strength and impermeability of concrete but their uses are limited due to the localized sources and highly varied reactivity. Moreover, the non-spherical shapes and internal porosity of natural pozzolans can result in a higher water demand and workability difficulties [16]. The main type of bio-derived ash used as an SCM is rice husk ash (RHA), which when processed appropriately is a silica-rich pozzolan with a high surface area and high pozzolanic reactivity [17]. The use of bio-

derived ash is limited because of the seasonable and geographical variability, difficulty in processing, and competing use as a biofuel production source [9].

In contrast, sources of calcined clay, i.e. kaolin, and mineral fillers are abundant and thereby there is a great potential for their use in concrete. Kaolin sources are found worldwide, with United States, Uzbekistan, Germany and Brazil producing the highest kaolin [18]. In the United States, about 8.1 Mt kaolin is produced per year, with Georgia as the leading producer. The use of calcined clay can improve hardened concrete properties due to its high pozzolanic reactivity and small particle size. However, one of the challenges of working with calcined clay at higher substitution is workability challenges due to their high surface area. As a result, most practical applications of MK in concrete have relied on cement substitutions of 10% by mass or less [19, 20].

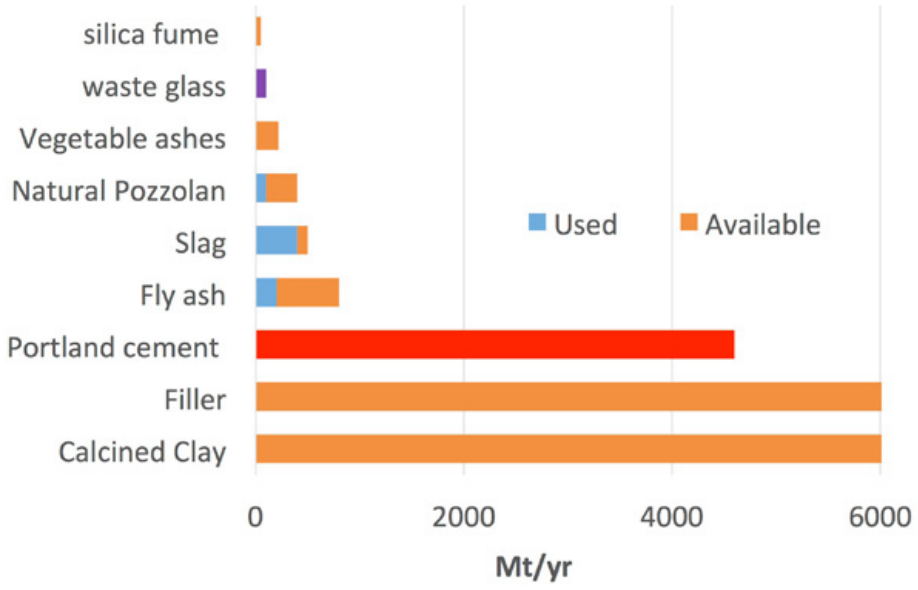

Figure 1.3. Use and estimated availability of possible SCMs and fillers compared to portland cement (From Ref. [9])

In addition to blending cement with SCMs, another option for reducing cement content in concrete is through clinker substitution with fillers. Fillers do not require heat or calcination processing, and thereby their use in concrete to replace cement clinker partially has significant environmental and economic benefits. One of the first applications of fillers in concrete was in Butte Dam in 1916 where cement was interground with granite and sandstone to produce blended cements with 50% filler content by mass. However, the use of fillers in cement as a common practice started in 1980s [21]. Today, the most commonly used filler in cement industry is the crushed limestone powders, which are used at substitution rates of up to 5% in ordinary portland cement and up to 15 and 35% in portland-limestone blended cements depending on prevailing standards. Some limitations associated with using fillers are their lower reactivity (which contributes to lower strength) and varied impurities. However, recent studies have shown that with optimizing the size

and quality of limestone fillers, limestone cement concrete showed similar performance to those of similarly composed portland cement concrete [22].

1.2.Research objectives

The primary objective of this study is to evaluate the potential utilization of metakaolin at higher fractions (≥10% by mass cement) and in combination with PLC conforming to ASTM C595 specifications. This research examines the influence of the rate of MK use on hydration, microstructure development, workability, early age property development, and hardened concrete properties (including mechanical properties, shrinkage, and permeability). Specifically, because the use of fine particles of metakaolin requires the addition of water-reducing admixtures (WRAs) to address workability, the interaction of water-reducing admixtures of varying chemistry on metakaolin-PLC blends are evaluated. Also because the use of MK can accelerate the cement hydration, increase the total heat of hydration, and consequently increase the rate and amount concrete shrinkage, the heat of hydration of PLC-MK blended cement are studied and models are developed to predict the heat of hydration for different MK substitutions rate. Finally, the application of shrinkage reducing admixtures toward mitigating the increases in shrinkage associated with faster hydration rates and finer pore structure is investigated.

The specific objectives of this research are:

1. To evaluate the influence of metakaolin substitutions of 10, 20, 30, and 40% by mass on the hydration and microstructural development of cement-based materials.

2. To understand the interactions of chemical admixtures, specifically water-reducing admixtures and shrinkage reducing admixtures, on the early age properties of metakaolin-limestone blended cements (PLC-MK).
3. To understand the effect of metakaolin and water-reducing admixtures on heat of hydration evolution when combined PLC and, further, to develop a model to predict the heat of hydration development.
4. To evaluate the mechanical properties and durability of hardened PLC-MK blends with 10, 20, and 30% metakaolin.

1.3.Organization of dissertation

Following with the objectives of this research effort, the structure of the dissertation is outlined below:

- Chapter 2 presents a review of the literature regarding the calcined clay and mineral fillers. The physical and chemical effects of metakaolin on the early age properties, hydration and microstructural development, and the hardened concrete properties of PLC-based materials is reviewed. The cement heat of hydration models developed in previous studies for different types cements and blended cements are presented. Finally, an overview of chemical admixtures including water-reducing admixtures (WRAs) and shrinkage reducing admixtures (SRAs) structure and applications are given in this chapter.
- Chapter 3 presents an investigation into the influence of MK on the early hydration and microstructural development of PLC-MK blends with 10, 20, and 30% MK. Besides, the effect of four commercial WRAs with different chemical structure on the early age properties of PLC-MK cement is evaluated.

- Chapter 4 shows the developed models for the cement heat of hydration and the effect of SCMs and admixtures in the previous models. The applicability and accuracy of previous models for PLC-MK blended paste was evaluated. A new model developed in this study using PLC-MK calorimetry data using linear regression analysis method is presented in this chapter.
- Chapter 5 evaluates the mechanical properties and durability of hardened PLC-MK blended cement concrete. The mechanical properties including compressive strength, tensile strength, elastic modulus, and Poisson's ratios of PLC-MK concrete with 10 and 30% MK and each PCE and PMS admixtures were measured and compared to those of PLC concrete. The concrete durability properties of PLC-MK concretes including the permeability measured by rapid chloride penetration test (RCPT) and surface resistivity, and dimensional stability measured by drying shrinkage of PLC-MK concrete was measured and compared to those of PLC concrete.
- Chapter 6 presents and compares the autogenous shrinkage of PLC and PLC-MK paste with 10, 20, and 30% after the final set time up to 28 days. The efficiency of shrinkage reducing admixtures in mitigating the shrinkage of PLC-MK at different dosages are shown. The effect of SRAs on the PLC-MK hydration, pore solution chemistry, and the surface tension of paste are evaluated.
- Chapter 7 summarizes the research performed as part of this dissertation and presents the primary conclusions regarding the influence of MK on the hydration, microstructural development, and hardened properties of PLC-based materials. Recommendations for practice and for future research are also presented.
- An appendix includes the results of the developed model for the PLC-MK heat of hydration, and the elastic modulus and Poisson's ratio at different loads.

CHAPTER 2 LITERATURE REVIEW

2.1. Calcined clay and its historical use in concrete

Kaolin rock is formed from the clay mineral kaolinite, which was formed in the Earth's crust by hydrothermal weathering of feldspar 65 to 100 million years ago [23]. Kaolin is usually associated with other minerals such as dickite, halloysite, nacrite and anauxite and some impurities such as hydrous oxide and colloidal materials [24]. While the main applications of kaolin are in paper, paint, and plastics, the calcined clays has been used in concrete constructions in the last decade. For example, calcined clay was used in a bridge construction (Bacalan bridge) in Bordeaux, France in 2009 [25] and in several dam constructions, such as Jupia dam in Brazil in 1962 [26], and more recently it was used in a New York city skyscraper, 432 Park Avenue building [27].

Historically, the identification of use of calcined clay in concrete derives from waste reutilization strategies in industrial production of clay-containing products. The ceramic industry, for example, generates 9 tons of clay waste for every ton of China clay produced [28]. This clay waste had been landfilled for the decades. However, the reutilization of this clay waste, after heat treating and grinding, in concrete is becoming a more common practice.

Another driving factor for increasing interest in calcined clay in concrete is lack of conventional SCMs in some regions. For example, the application of calcined clay in Brazil is quite important due to the lack of fly ash as the energy production there is mainly based on hydroelectricity. Brazil is a main producer of kaolin, producing 2Mt kaolin per year since 1970s. The Brazilian ceramic industry is the main consumer of kaolinite, while generating the significant amount of calcined clay waste. The Civil Engineering

Department of the Federal University of Rio de Janeiro has an ongoing program examining the use of ground calcined-clay brick as clinker replacement materials [29].

The application of clay wastes as partial substitutes of cement in concrete has led to savings in GHG emissions and embodied energy. However, the lower quality and purity of clay waste may have negative influences on concrete properties [30], and as a result, there has been a shift toward using more pure forms of kaolinite, which when calcined is called 'metakaolin.' Highly pure calcined clay is the focus of this research effort.

Metakaolin is produced through controlled heat processing of kaolinite, designed to give a uniform particle size and higher pozzolanic activity. With a more recently developed processing method, called 'flash-calcination', the dehydroxylation of powdered kaolinite clay happens within several tenths of a second, instead of traditional soak-calcinations, which require minutes at least. With flash-calcination, a high purity metakaolin is produced. MK is mainly composed of silica oxide at 50-55% and alumina oxide at 40-45%.

Studies have shown that MK produced from the flash-calcination process shows much better pozzolanic reactivity compared to that of standard metakaolin obtained by soak-calcination [31]. Metakaolin is classified as a Class N or natural pozzolan (ASTM C618 [32].) Most commercially available MK is produced by calcination at moderate temperature (650–800°C) of the hydrous aluminum silicate, kaolinite. Figure 1 shows kaolinite with a two-layered structure [33] and an approximate composition $Al_2Si_2O_5(OH)_4$ (39.8 % alumina, 46.3 % silica, 13.9 % water Heat treatment decomposes the kaolinite crystals, forming a highly reactive, amorphous pozzolan, metakaolin. After calcination, the product is ground to an average particle size of about one to two micrometers in average particle size. The micrographs of metakaolin is shown in Figure 2.1.

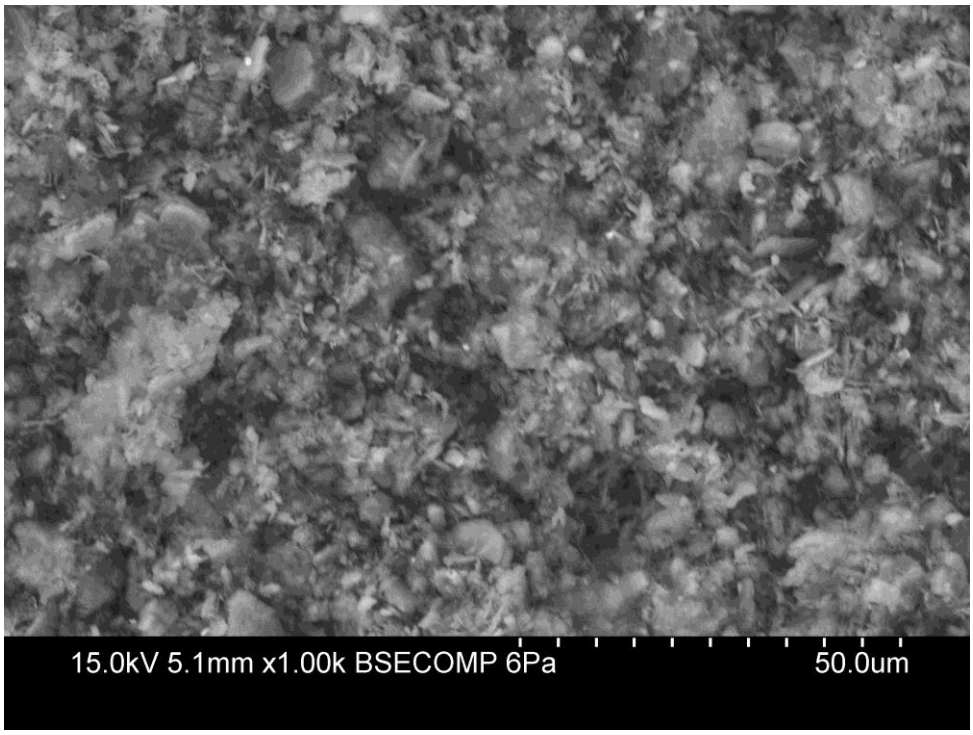

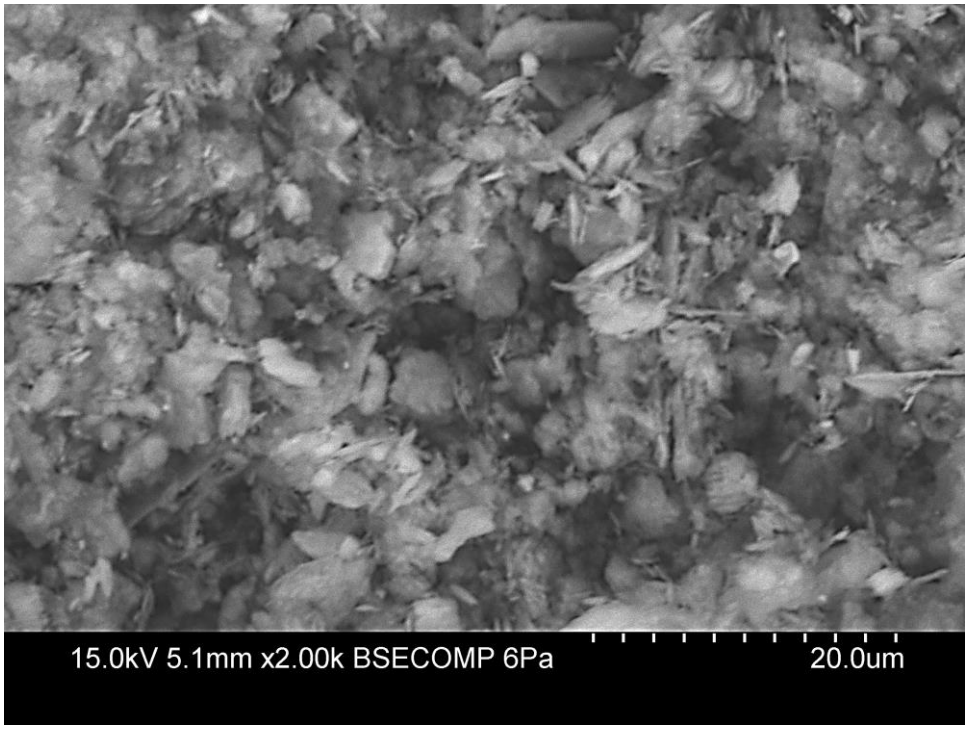

Figure 2.1. Scanning electron micrographs of metakaolin

The effect of calcination temperature on the physical and chemical properties of MK has been evaluated [35]. It was shown that calcination at 700 °C results in the highest concrete strength. The reactivity of the MK is reduced when the calcination temperature reaches 850°C, and little pozzolanic activity was observed for MK calcined at 1000°C [35]. Previous studies proposed different mechanisms for the dehydroxylation process of kaolinite but the general agreement is that metakaolin is formed between 300-700 °C by a gradual loss of the interlayer water (via dehydroxylation) (Equation 2-1), which occurs through diffusion, along with the change in the aluminum coordination [36].

$$Al_2Si_4O_{10}(OH)_8 \longrightarrow 2Al_2Si_2O_7 + 4H_2O \qquad 2\text{-}1$$

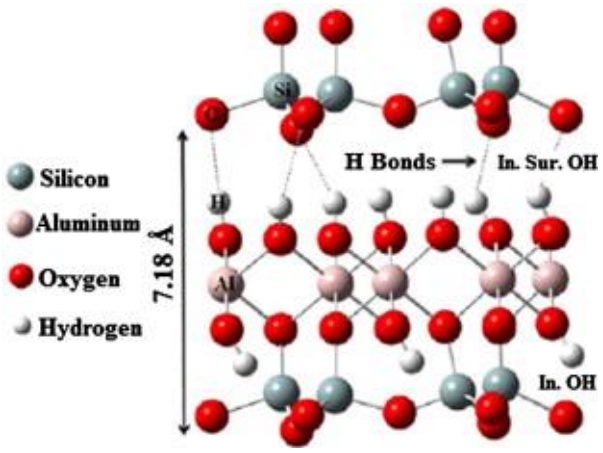

Figure 2.2.Schematic structure of kaolinite [36]

Georgia has one of the largest natural deposits of kaolinite in the USA and worldwide (Figure 2.3) located in south-middle Georgia. In fall 2015, our group had a visit to one of the metakaolin producers in mid-Georgia, BASF, that we observed the metakaolin production process (Figures 2.4-2.6).

Figure 2.3. Natural deposit of kaolinite in Gordon, GA.

Figure 2.4. Kaolin slurry during the metakaolin production process

Figure 2.5. Our research group in the visit to BASF

Figure 2.6. Metakaolin production processes at BASF, Gordon, GA

2.2.Mineral-based Fillers

In contrast to metakaolin, which is a highly reactive pozzolan, fillers are chemically inert particles that can also be blended with cements. The most common type of filler used in cement and concrete is limestone powder. Portland-limestone cements, or PLCs, originated in Europe in the 1960s. Spanish standards permitted the use of cements with up to 10% limestone in 1960, and French standards allowed up to 35% limestone by weight in blended cements in 1979 [37]. Following that, the European standards permitted the use of limestone cement in concrete, allowing up to 20 and 35% by mass limestone in cements referred to EN 197-1 CEM II/A-L (6-20 wt.%) and CEM II/B-L (21-35 wt.%) [38].

As previously noted, the use of PLC in North America was initiated with the growing concerns over the environmental impacts and energy consumption associated with cement manufacturing processes. However, the acceptance of PLC in North America standards was slower than in the European standards. It was not until the early 2000s that limestone cement was permitted in United States and Canada. In 2004, the American Society for Testing and Materials (ASTM) approved the use of limestone up to 5% by mass in blended cements specified in ASTM C150 [39]. In 2012, the inclusion of up to 15% limestone in blended cements denoted as Type IL was approved in ASTM C595 and AASHTO M240 [40, 41]. Similarly, the Canadian Standards Association (CSA) approved the use of limestone in cement up to 5% by mass in 2006 and up to 15% by mass in 2008 [42].

2.3.Metakaolin-blended cement

Metakaolin influences cement hydration and microstructure development through both chemical and physical effects. Chemically, the pozzolanic reaction is of primary importance. Physical influences include nucleation, dilution, and filler effects. In addition, there are synergetic chemical interactions between MK and PLC. These effects will be discussed in this section.

2.3.1. Physical effects of metakaolin on cement hydration

Previous studies identified three main effects of MK, the filler effect, which is immediate, the nucleation effect that accelerates the cement hydration occurs in the first 24 hours, and the pozzolanic reaction that happens in the first 2 to 14 days [20, 43]. In order to distinguish the metakaolin's physical effects from its pozzolanic activity, studies replaced cements with a powdered quartz with particle sizes similar to that of MK (i.e., 1-2 μm) and at the same substitution rate. It should be noted that the surface area of the reference quartz is important since heterogeneous nucleation effect becomes non-significant for specific areas lower than 50–100 m^2/kg [44].

One of the effects of finer SCMs, like metakaolin, and fillers on cement hydration is heterogeneous nucleation. The heterogeneous nucleation effect is directly related to surface area, as finely divided particles promote surface adsorption and provide precipitation sites that result in improving the degree of cement hydration. The mechanism of heterogeneous nucleation is believed to be derived by the hydrates adsorbing on the surface of mineral grains and then catalyzing the nucleation process by lowering the energy barrier for growth [45]. The factors affect the nucleation process are:

- The fineness of the mineral particles, with the higher surface area increasing the nucleation effect
- The rate of substitution, since increasing the amount of minerals increases the nucleation sites and the probable rate of nucleation.
- The affinity of the mineral particles for cement hydrates, which is related to the nature of the minerals [45].

Given its fine particle size and high surface area (10-30 m^2/g) compared to 0.3-0.5 m^2/g for cement; MK can provide nucleation sites for cement hydration. Previous studies show that when MK is used at 10-15% substitution by mass, it can act as a nucleating agent that accelerates the rate of cement hydration and enhances the degree of hydration and [46]. The early age short-term acceleration of cement hydration and autogenous shrinkage can be related to the heterogeneous nucleation of the hydration products on MK particle surfaces.

Another effect of minerals such as MK particles on the cement hydration is the dilution effect that results from the replacement of cement by SCMs. The dilution effect is related to an increase in the effective water-to-cement ratio, by decreasing the portion of the cement in the binder. The dilution effect consequently enhances the cement hydration at both early and later ages. It should be noted that the dilution effect of MK is more significant when MK is used at 15-20 wt.% cement, since that results in a higher water-to-binder ratio (w/b) and less cement is available for hydration [46]. The binder is defined as the total of cement and metakaolin mass.

The filler effect of minerals, even if chemically inert, derives from the physical changes in particle packing in the initial cement-based materials microstructure. This effect is more significant in interfacial transition zone (ITZ) where finer minerals can produce more efficient packing at the cement paste-aggregate interface. Improved packing overall will result in less bleeding and produce a denser, more homogenous microstructure and a narrower ITZ [47]. Therefore, cement replacement by finer SCMs can lower the strength in cement paste, due to the dilution effect, and increase the concrete strength, due to both the filler and effect on the improved transition zone [20].

2.3.2. Pozzolanic activity of metakaolin

Metakaolin's primary chemical reaction occurs through aluminosilicate reaction with calcium hydroxide (CH) (derived from cement hydration) to form calcium silicate hydrate (C-S-H) and crystalline hydrated phases including C_2ASH_8, C_3AH_6, and C_4AH_{13}, with the products formed depending on the Si/Al of the metakaolin and the temperature [20]. The phases, C_2ASH_8 and C_4AH_{13}, formed early during the MK pozzolanic reaction are metastable and with prolonged curing will convert to the stable phase hydrogarnet. The rate of pozzolanic reaction of MK showed to be higher than that of SF in corresponding mixes with the same replacement ratio [48]. The pozzolanic reaction of MK with CH improves concrete strength and impermeability. It contributes to enhanced durability by increasing its resistance to chloride intrusion, sulfate attack, and alkali-silica reaction (ASR) [49, 50].

There are different methods for measuring the pozzolanic reactivity and can mainly categorized as direct and indirect methods [51, 52]. One indirect method is the use of electric resistance measurements to indirectly measure the lime consumption through the

electrical conductivity of the pore solution as the reaction proceeds [51]. However, unrelated variations in ionic concentration, such as those deriving from the use of chemical admixtures, and changes in solid conductivity, such as those from SCMs, can interfere with this test. Another indirect test method is the strength activity index, as outlined in ASTM C311[52]. In this test, the 7-day and 28-day compressive strength of mortar, cubes with 20% mass replacement of cement by pozzolan are compared with those of control samples with no pozzolans. Bentz et al. (2012) compared the results of the strength activity index with the heat of hydration of those blended cements [53]. A good correlation was observed between the cumulative heat evolution of the mortar and the measured compressive strength at 7 days, suggesting the potential of evaluating the pozzolanic activity of blended cements via calorimetric measurement on much smaller specimens.

The direct test methods of pozzolanic activity measurement are based on the measurement of the amount of lime consumed. The analytical instruments that are commonly used include thermogravimetry (TG), differential thermal analysis (DTA), X-ray diffraction (XRD) and calorimetric analysis. The results of these techniques can be used to study the kinetics of the MK pozzolanic reaction with lime. It should be noted that when direct methods are used parameters such as the method for stopping the hydration and the hydration temperature could play important roles on the reaction kinetic and the stability of the hydrated phases.

2.3.3. Synergy between limestone and metakaolin

Limestone powders were initially added to the cement clinker as an inert filler to replace cement partially to reduce the environmental impacts and fill the pores in concrete [54]. However, recent research studies have showed that limestone particles can have both

physical and chemical effect on cement hydration and microstructure development [55]. Specifically, it has been observed that calcium carbonate can react with C_3A phase to produce carboaluminate hydrate [56].

Recent studies have shown synergies between metakaolin and limestone powders with the idea that the alumina in metakaolin will react with limestone producing carboaluminate phases. There are studies that reported similar synergy between limestone cement with blast furnace slag, fly ash, and natural pozzolans, where mechanical properties were improved by 28 and 90 days [57]. Other studies have shown similar synergy between limestone cement and calcium aluminosilicate glass powder [58, 59].

The stoichiometric formation of monocarboaluminate hydrate (an AFm phase) is by reaction of one mole of metakaolin with one mole of calcium carbonate in the presence of water and calcium hydroxide, as shown generally in Equation 2-2[60].

$$Al_2Si_2O_7 + CaCO_3 + 3Ca(OH)_2 + H_2O \rightarrow 3CaO.Al_2O_3.CaCO_3.4H_2O + 2SiO_2 \qquad 2\text{-}2$$

Antoni et al. [60] showed by thermogravimetric analysis (TGA) and X-ray diffraction analysis that the calcium carbonate reacts with alumina in metakaolin forming hemicarboaluminate and to a lesser extent monocarboaluminate, depending on the MK replacement level, as early as one day [60]. In addition, the formation of the supplementary AFm phases helps to stabilize the ettringite formed by early calcium aluminate hydration in the presence of gypsum.

2.3.4. Early age properties of metakaolin-OPC and PLC blends

The influences of MK on the pore refinement and microstructure of paste and concrete containing limestone powders have been studied. For example, previous research studied the coupled substitution of metakaolin and limestone in portland cement paste by isothermal calorimetry, setting time, mercury intrusion, pore size distribution analysis, autogenous and chemical shrinkage measurements [60]. It should be noted that the limestone powder used in this study was blended with the cement in the lab and was not interground as PLC.

The effect of metakaolin (MK) on the heat of hydration evolution of ordinary cement paste was evaluated in previous studies using isothermal calorimetry [61]. There was an agreement that the addition of finely divided materials such as metakaolin can accelerate cement hydration and increase the early heat evolution due to its amorphous and highly reactive nature [19]. Williams et al. [62] showed that a paste with 10% MK could accelerate the calcium silicate hydration peak up to 4 hours and attributed this to the nucleation effect of MK. If temperature effects are not appropriately considered, the increase in the overall heat of hydration and the rate of hydration can have negative effects on the durability of concrete due to the potential delayed ettringite formation and the concrete cracking [62-64].

The acceleration of cement hydration by MK can result in shortening both initial and final setting time of MK concrete. A 10% metakaolin substitution for cement by mass was shown to shorten the initial and final setting time of mortars by up to 4 hours [62]. Some studies have shown a delay in setting by up to 2 hours with 10 and 20% MK replacements [65, 66]. It should be noted that the high-range water-reducing admixtures that are commonly used in MK concrete can work as retarders and delay the setting time of MK

concrete, and their use could contribute to the variations in setting time report with MK usage [67].

Mercury intrusion tests showed that metakaolin blended cement pastes with up to 15% MK have a much lower porosity than that of OPC cement pastes. Additionally, the portion of larger pores (> 0.02mm) and the total pore volume in paste decreases with increase in the metakaolin content [68]. Another study showed a high reduction in capillary porosity of the MK paste with up to 25% MK until 7 days. However, no significant difference in capillary porosity was observed after 14 days [69].

The more refined microstructure of the MK-OPC blends can affect the shrinkage of MK blended cement paste and concrete, in ways that can be difficult to predict. Different trends in autogenous shrinkage for MK-OPC cement pastes have been reported [65]. Gleize et al. (2007) showed that the early age autogenous shrinkage of the cement paste was reduced with the MK substation, but the long-term autogenous shrinkage (after 24 h) was increased [70]. Moreover, they showed that MK replacement level at 5% increased the total autogenous shrinkage at w/b = 0.55 while the replacement levels of 10 and 15% the total autogenous shrinkage decreased. Kinuthia et al. [71] also found that in MK-blended cement pastes (w/b = 0.50) with 5% and 10% MK, the autogenous shrinkage increased, while it significantly decreased when MK replacement level increased to 15% and 20% MK. Wild et al. [72] studied both autogenous and chemical shrinkage of MK blended cement paste with 5 to 25% MK. It was shown that both autogenous and chemical shrinkage increased with MK replacements of 10 and 15%. Because shrinkage behavior observed for MK-blended cement pastes is variable and difficult to predict, this remains a topic worthy of further research.

2.4.Heat of hydration modeling of supplementary cementitious materials

Cement hydration is an exothermic process that is a function of cement composition, the amount of supplementary cementitious material present, water-to-binder ratio (w/b) present, and cement fineness among other variables including time and temperature. In practice, undesirable or unanticipated temperature development may contribute to cracking in concrete and compromise durability and serviceability. Therefore, the heat development of concrete mixes should be controlled and evaluated prior to placement.

In a modeling approach, the total heat of hydration of cements can be estimated based upon cement composition (Equation 2-3), with the assumption of fully hydrated cement [73]:

$$H_{cem} = 500\rho_{C3S} + 260\rho_{C2S} + 866\rho_{C3A} + 420\rho_{C4AF} + 624\rho_{SO3} + 1186\rho_{FreeCaO} + 850\rho_{MgO} \quad 2\text{-}3$$

where, H_{cem} is total heat of hydration of the cement (J/g), and ρ_i is weight ratio of *i*-th compound in terms of total cement content. The approximate heat range of each clinker phase taken from Taylor (1999) shown in Table 2.1 [74]. This model suggested the cement heat of hydration with only considering the cement chemistry, however, the cement physical properties such as particle size and fineness showed to influence the cement hydration heat. Zayed et al. [75] evaluated the effect of fineness on the cement hydration by comparing the heat of hydration of cements with different fineness but same chemical compositions. The findings of this study indicate that the cement heat of hydrations varied for cements with similar chemistry but different fineness that signify the effect of fineness on the cement hydration. This study reported that the heat of hydration calculated from the

heat index limit introduced by ASTM C150 as "$4.75C_3A+ C3S<100$" for a particular cement (i.e. Type II (MH) cement) does not reliably correspond to the measured heat of hydration of the cement determined by isothermal conduction calorimetry. Blaine fineness and particle size distribution of portland cements were found to affect the heat generated by cement on hydration [75]. This study suggested a limit on the Blaine fineness of cements beyond Types II and IV cements. The limit of 240 m^2/kg for Types II/IV cements fineness was first added to the ASTM C150 in 2007 [76] and later increased to 245 m^2/kg in 2009. Similarly, AASHTO M85 also has a limit of 430 m^2/kg on the finesse of Types II and IV.

Table 2.1. Enthalpy of complete hydration[74]

Phase	Enthalpy of complete hydration (J/g)
C_3S	−517 ± 13
C_2S	−262± 3
C_3A	−1144 to −1672 (depending on reaction to give monosulfate or ettringite)
C_4AF	−418± 3

Calorimetry can be used to measure the cement hydration rate and cumulative heat released. The most common calorimetry technique used in cement research is the isothermal (heat conduction) calorimetry that measures the heat production rate directly. Paste or mortar specimens are usually used for determination of heat of hydration typically for the first 48 hours or 7 days as specified in ASTM C186 [77]. The heat of hydration can be converted approximately into degree of hydration (α), which is a measure of the extent of cement hydration in mixture, as the ratio of the cement hydration heat released, i.e., measured by calorimetry, to the total heat of hydration (H_{cem}). The degree of hydration is a function of time and varies between zero at the initial time and one when the hydration is fully completed (Equation 2-4).

$$\alpha_{(t)} = \frac{H_{(t)}}{H_{cem}} \qquad 2\text{-}4$$

Where, α(t) = degree of hydration at time, t,

and H(t) = cumulative heat of hydration released at time, t, (J/m^3).

Several models have been developed to predict the heat development of cementitious materials, based on cement composition and fineness [73, 78-80]. The first guide on heat development in concrete was ACI 207.2R, Report on Thermal and Volume Change Effects on Cracking of Mass Concrete [80], first published in 2002. This report showed the concrete adiabatic temperature rise over time for different cement types, fineness, and concrete placing temperature based on calorimetry tests performed on different types of cements over 60 years ago. It was shown that Type III cement with the highest fineness has the highest adiabatic temperature rise, followed by Type I and II. The cement fineness affects the rate of heat generation more than the total heat generation. The effect of SCMs, such as fly ash, on the hydration was not quantified in this report, but it was recommended to conduct a calorimetry testing when such materials are used [80]. Basma et al. [81] developed an artificial neural network (ANN) model to predict the cement degree of hydration from 390 specimens. An ANN was trained based on the different data sets. But, it has the limitation such models are applicable for the data set it was trained for. Also, because no analytical expression results from ANN training, this approach cannot be implemented widely in practice.

Schindler and Folliard [82] developed a model based on multivariate regression analysis to predict the ultimate degree of hydration, considering the effect of fly ash and slag on hydration. Their model was developed using 13 new datasets and 20 published

datasets with the degree of hydration was determined by calorimetry [83]. This model considered the effect of slag and fly ash on blended cement hydration as shown in Equation 2.5.

$$H_u = H_{cem}\rho_{cem} + 461\rho_{slag} + 1800\rho_{FA-CAO}\rho_{FA} \quad 2\text{-}5$$

The degree of hydration can be modeled with a three-parameter exponential relationship, shown in Equation 2.6.

$$\alpha_t = \alpha_u . \exp(-[\frac{\tau}{t_e}]^{\beta}) \quad 2\text{-}6$$

where, α_t = the degree of hydration at equivalent age *t*,

τ = hydration time parameter (hours),

β = hydration shape parameter, and

α_u = ultimate degree of hydration.

Schindler and Folliard (2003) used nonlinear regression analysis to model τ, β, $\alpha_{(u)}$ shown in Equations 2-7 through 2-9.

$$\alpha_t = \frac{1.031.{}^{w}\!/\!_{cm}}{0.194 + {}^{w}\!/\!_{cm}} + 0.50\rho_{FA} + 0.30\rho_{slag} \quad 2\text{-}7$$

$$\beta = 181.4\rho_{C3A}{}^{0.146}\rho_{C3S}{}^{0.146}Blaine^{-0.535}\rho_{SO3}{}^{0.558}\exp(-0.647\rho_{Slag}) \quad 2\text{-}8$$

$$\tau = 66.78\rho_{C3A}{}^{-0.154}\rho_{C3S}{}^{-0.401}Blaine^{-0.804}\rho_{SO3}\exp(2.187\rho_{slag} + 9.50\rho_{FA}\rho_{FA-CaO}) \quad 2\text{-}9$$

Another study by Ge [84] developed equations for τ, β, $\alpha_{(u)}$,similar to equations 2-7 through 2-9. This study conducted semi-adiabatic calorimetry tests on 23 different

concrete mixes and developed a combined model for predicting the degree of hydration and temperature development of concrete under various construction and environmental conditions. Their model considers the effects of the cement chemical and physical properties, the amount and chemical compositions of fly ash and slag, and water/cement ratio on the ultimate degree of hydration development. While Ge's two models [82, 84] can be used for cements blended with fly ash and slag, the effect of other SCMs including metakaolin or silica fume was not considered. Moreover, those models did not consider the effect of chemical admixtures on the cement hydration.

Riding et al. (2012) developed an empirical model for calculating the heat of hydration of concrete mixtures accounts for the effects of cement composition, aggregate type, w/b, SCM type and dosage, chemical admixture type and dosage, and temperature on heat of hydration [73]. Semi-adiabatic calorimetry was used to quantify the heat of hydration parameters for 204 concrete mixtures, and multivariate regression analysis was used to develop a predictive model for the heat of hydration parameters. A separate set of 57 heat-of-hydration parameters was used to validate the developed empirical model. The calculated hydration parameters based on the cement composition obtained from Rietveld analysis is shown in Equations 2-10 to 2-12.

$$\alpha_u = \frac{1.031.\,w/cm}{0.194+w/cm} + \exp(-0.297-9.73\rho_{C4AF}\rho_{Cem}-325.\rho_{Na_2eq}.\rho_{Cem.}-8.90\rho_{FA}\rho_{FA\text{-}CaO}-331.\mathrm{WRRET}-93.8\mathrm{PCHRWR}) \quad 2\text{-}10$$

$$\beta=\exp(-0.418+2.66\rho_{C3A}\rho_{Cem}-0.864\rho_{Slag}+108\mathrm{WRRET}+32.0\mathrm{LRWR}+13.3\mathrm{MRWR}+42.5\mathrm{PCHRWR}+11.0\mathrm{NHRWR}) \quad 2\text{-}11$$

$$\tau=\exp(2.95-0.972\rho_{C_3S}\rho_{Cem}+152\rho_{Na_2.eq}\rho_{Cem}+1.75\rho_{Slag}+4.00\rho_{FA}\rho_{FA\text{-}CaO}-11.8ACCL+95.1WRRET) \quad 2\text{-}12$$

where ρ_i is the mass of i component to total cement content ratio as determined by Rietveld analysis; ρ_{Na2Oeq} is the wt.% alkalis as Na_2O equivalent; ρ_{cem} is the wt. % cement in mixture; low-range water-reducer/ retarder (WRRET), LRWR is the ASTM Type A water reducer dosage; MRWR is the mid-range water-reducer dosage; NHRWR is the ASTM Type F naphthalene or melamine-based high-range water-reducer dosage; and PCHRW is the ASTM Type F polycarboxylate-based high-range water-reducer dosage. All SCM dosages are by mass ratio of cementitious material. All admixture dosages are percent solids (by mass) per mass of cementitious material. While this more comprehensive model and considers the effects of chemical admixtures, in addition to SCMs, the effect of other SCMs such as metakaolin is still not considered. This reveals the need for a comprehensive model that considers the effects of a broader range of SCMs, including metakaolin, as well as chemical admixtures.

2.5.Chemical admixtures

Chemical admixtures are used in concrete to modify or improve different properties in concrete such as workability, setting time, and shrinkage rate. The eight types of admixtures are categorized in ASTM C494 [85] as follows: Type A—water reducing; Type B—retarding; Type C—accelerating; Type D—water reducing and retarding; Type E—water reducing and accelerating; Type F—water reducing, high range; Type G—water reducing, high range, and retarding; and Type—S Specific Performance. The admixtures examined in this study are Type A— water-reducing admixtures, Type F—high-range water-reducers,

and Type—S shrinkage reducing admixtures and will be described in the following sections. The effectiveness of an admixture depends on several factors including the composition, fineness and amount of cement and SCMs, water content, mixing time and method, and the temperature of the concrete, among other factors [86].

Cement-admixture incompatibility and incompatibility between admixtures can produce problematic behavior in fresh concrete, such as cement hydration inhibition, slump loss, air loss, and early stiffening (flash set) [87, 88]. Incompatibilities between supplementary cementitious materials and chemical admixtures have also reported recently [89].

Chemical admixture incompatibility does not only affect the fresh concrete properties, but can also impact the long-term hardened concrete performance. The cement-admixture incompatibility issues can be addressed by understanding the chemistry and mechanisms of action for each admixture in combination with a particular cement. The chemistry and mechanisms of action for two types of admixtures, water-reducing admixtures and shrinkage reducing admixtures, which were used in this study will be described in the following sections.

2.5.1. water-reducing admixtures (WRAs)

water-reducing admixtures (WRAs), ASTM C494 Types A and F [85], are admixtures that reduce the quantity of required mixing water by 5-15% while producing concrete of a given consistency [90]. High-range water-reducing admixtures (HRWRAs) are admixtures that reduce the required mixing water by a greater extent of at least 12% and up to 30% [90]. This reduction in the mixing water content, without compromising the concrete workability, can decrease permeability and improve mechanical properties in concrete by reducing the

porosity of concrete. The examples of concrete durability improvements can be decreasing the intrusion rate of water, carbon dioxide, dissolved solids such as deicing salts, thus providing concrete with increased resistance to freezing and thawing, alkali-silica reaction, salt scaling, delayed ettringite formation, and thermal stresses [91]. The effect of WRAs on reducing the water content and thus water-to-cement ratio has been shown to increase both the compressive strength and impermeability of concrete [92].

WRAs mainly work by adsorption at the cement grain surface and deflocculate and disperse the cement particles through charge repulsion and, with some WRA chemistries, steric hindrance between adsorbed polymeric molecules and neighboring polymers [93]. The WRAs are mainly composed of a backbone molecule with negative functional side and end groups (Figure 2.7). This surface adsorption can consequently retard cement hydration and setting time, however, it may not adversely affect the strength development rate [94].

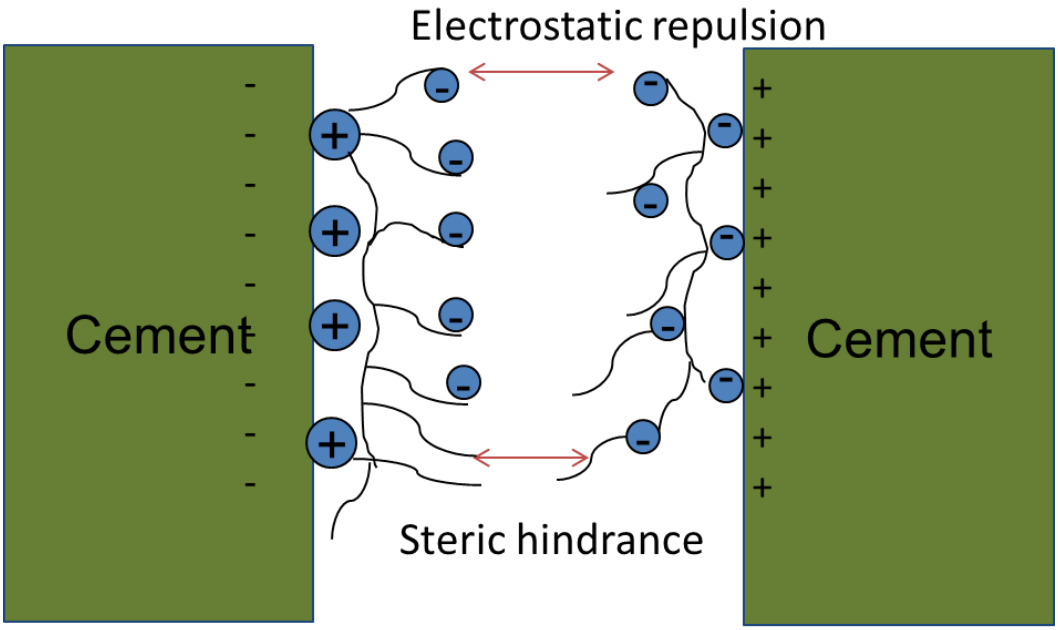

Figure 2.7. Interaction of admixtures with cement grains

WRAs are mainly salts of sulfonate or polycarboxylic acids. The admixtures used in this study are calcium lignosulfonate (LS), naphthalene formaldehyde condensate (PNS), polymelamine sulfonate (PMS) and polycarboxylate ether (PCE). Lignosulfonates are by-products of the acid sulfite wood-pulping process and may contain impurities such as pentose and hexose sugars. These impurities can cause retardation and are usually removed by fermentation, followed by a distillation process if the lignosulfonate is to be used only as a water-reducing admixtures (i.e., not as a retarder also). Calcium and sodium salts are most commonly used in lignosulfonate admixture production with calcium being less expensive and less effective as a WRA and sodium being more soluble and, hence, less likely to precipitate [94]. The sulfonated naphthalene formaldehyde condensate (PNS) and sulfonated melamine formaldehyde condensate (PMS) admixtures have similar chemistry and structure. The organic parts of these admixtures are negatively charged while the

overall balance is kept neutral by the addition of a cation in solution (usually sodium or calcium). Dispersion mechanism of these admixtures is considered principally to be the electrostatic repulsion, either caused by the anion adsorbed on the cement particle, resulting in the cement particle to be net negatively charged and thus keeping the particles apart by charge repulsion. PMS and PNS admixtures have similar potential water reduction capacity (10-25%) but vary in the intrinsic air content entrained in the concrete [74].

The compatibility of sulfonate-based admixtures, LS, PNS and PMS, with cement-based materials and their effect on portland cement hydration has been examined in previous studies [95-99]. The similar chemistry between the sulfonate ($-SO_3^-$) and sulfate group ($-SO_4^{2-}$) sulfonate-containing molecules can take part in some of the reactions involving the sulfate ions such as ettringite formation. The presence of sulfonate groups may play a crucial role in the initial hydration of the aluminate phases, particularly C_3A, and alter the hydration products [95, 96]. It was shown that the ettringite formed in the presence of sulfonated-admixtures has a regular polyhedral morphology, instead of its needle-shaped morphology, and the ettringite crystals tend to be substantially smaller [97]. Another study showed that in samples containing LS the initial ettringite formation seemed to be accelerated and the ettringite peak shifted to higher decomposition temperatures with increasing amount of LS present; this is interpreted as a sign of a more stable crystal structure [100]. Studies have shown that the adsorption of PNS on the hydrating cement grains slows down or inhibits the ettringite formation at the early ages. However, when all the admixture molecules are consumed, normal growth of ettringite resumes [98]. Aitcin et al. [99] showed that the cement with very low levels of alkali can exhibit poor compatibility with sulfonated admixtures. Gu et al. [101] studied the effects of PNS and

PMS on cement hydration and concluded that the adsorbed molecules disperse the water and calcium ions at the cement-solution interface. Moreover, they showed that the WRAs molecules could form Ca-containing complexes and inhibit the nucleation and precipitation of Ca-containing products. It should be noted that most of these studies used WRAs at dosages higher than commonly used in practice, to exacerbate the effect of admixtures. This difference in the dosages can result in inconsistency between laboratory experiments and field results [101].

Hydrocarboxylic acid admixtures, i.e. polycarboxylic ether (PCE) are known as the most effective HRWRAs, with the most soluble sodium salts in commercially used admixtures. PCE admixture works by both mechanisms of electrostatic repulsion and molecular hindrance, by limiting the diffusion of water and calcium ions at the cement-pore solution interface [102]. PCE molecules also form complexes with calcium ions that may inhibit nucleation or alter growth kinetics and morphology of the hydration products. Lothenbach et al. [103] have shown that the carboxylated admixtures strongly retard C_3S dissolution and also C-S-H formation at early ages, but after 6 days there was no significant difference between the amount of calcium silicate hydrates in the control sample and the one with PCE. The effect of PCE on ettringite formation was less distinct. It was shown that no significant complex was formed between PCE and dissolved ions such as Na, K, Ca, or Al in the pore solution of hydrating cements. It was concluded that the retardation effect of PCE is not due to the interactions with dissolved Ca^{2+} or other ions but rather based on steric and electrostatic dispersion mechanisms [103]. The interaction between different PCE-architectures and cements with different C_3A-contents has been examined in a previous study by calorimetric, rheological, adsorption, and zeta potential

measurements. This study showed that with decreasing side chain density, the PCE molecules adsorb more strangely and thus, lower the yield stress of a cement paste by primarily by steric stabilization. It is also shown that PCE molecules with long side chains delaying the setting of the cement paste to a lesser extent than PCE molecules with shorter side chains [104].

The use of higher than recommended concentrations of WRAs can cause excessive bleeding, retardation or flash setting, lower early strength, and high air content. These issues are common when finer SCMs at high fractions are used and there is a need to use higher dosages of water-reducing admixtures [105, 106]. Therefore, there is a need to study the interactions of WRAs with finer SCMs such as metakaolin to predict their compatibility and effectiveness with those SCMs.

2.5.2. Shrinkage reducing admixtures (SRAs)

SRAs were first discovered in 1980s can potentially reduce the shrinkage and cracking in concrete and consequently increase the durability of concrete exterior exposed structures such as bridge decks, floors slabs, and buildings [107]. Shrinkage reducing admixtures (SRAs) are surfactant monomers consist of a hydrophobic tail and a hydrophilic head dissolved in water. Propylene glycol and polyoxyalkylene alkyl ether are the common types of SRAs used in concrete industry.

SRAs may have different chemistries but their mechanism of action is generally the same. SRAs reduce the shrinkage by accumulating at the solution-air interface and reducing the interfacial tension of the pore solution in nano- to microscopic capillary pores [108-110]. It was observed that the pore solution surface tension decreases with increase

in the dosage of SRAs, up to a threshold "critical micelle concentration" (CMC) and then becomes almost constant with further increase in the dosage. This behavior is because of the self-aggregation tendency of SRAs to form micelles and that can limit the surface tension capacity of SRAs [111, 112]. At concentrations below the CMC, SRA surfactants at the interfaces of air and pore solution in partially filled capillary pores decrease the surface tension with increasing surfactant concentration. Above the CMC, excess surfactant molecules form micelles in the bulk water and cannot serve to further reduce the surface tension [113].

SRAs can also alter the microstructure in cement-based materials. They act to refine the pore structure of the concrete by increasing the ratio of the pores with diameters of 0.1 to 1.0 μm. The capillary stress in those pores are lower than those of in pores with the diameter of less than 0.1 μm [114, 115].

Previous studies showed that the SRA admixtures also retard the cement hydration and slag activation [114]. The retardation behavior of SRAs have contributed to reduced alkali content in the pore solution in their presence [116]. The reduction in the alkali concentration and pH of the pore solution results in an increase in the calcium concentration; the net effect can be a retardation of C_3S hydration [117] [118]. The lower alkali content in the pore solution can also retard the C_3A dissolution. The retardation effect of SRAs can result in up to 5% lower degree of hydration at 48 hours [119].

SRAs have been shown to decrease the drying shrinkage of concrete in the laboratory tests, by up to 25-50% [117]. Borsoi et al. [120] evaluated the effect of SRAs in the presence of superplasticizers in concrete and showed that combining both SP and SRA

can actually be more effective in reduction of drying shrinkage. The relative humidity (RH) also affects the effectiveness of SRAs on reducing shrinkage of concrete. A study showed that the SRAs can reduce the shrinkage of concrete by up to 85% and 50% at RH of 99% and 50%, respectively [114].

While SRAs generally decrease the chemical and autogenous shrinkage of cement pastes, some studies showed that the addition of an SRA could result in a period of expansion shortly after the final set. This expansion can provide a considerable benefit in shrinkage mitigation even at later ages. One study showed a 60% reduction in the total shrinkage arises from this expansion [121]. However, it should be noted that this expansion can induce a compressive stress in the system and should be controlled [122]. Sant et al. [121] concluded that the origin of this expansion is due to the effect of SRAs on increasing the portlandite oversaturation level in pore solution that can result in higher crystallization stresses and produce expansion.

Despite the benefits of SRAs in mitigating the shrinkage of concrete, several side effects such as delays in hydration, reducing the rate of strength development, and delays in setting time have been reported [116, 117, 123-125]. Balogh [124] showed the setting time of the concrete with SRA (1.5% by mass of cement) was delayed up to 30 min. compared to the control concrete and up to 50 min. when SRAs and high-range water-reducers (HRWR) were used together. (It should be noted that SRAs showed a negligible effect on the required dosage of HRWRs when used together). Another study showed a more significant delay - up to 2 hours - on the initial and setting time when SRAs are used at 1.5% by mass of cement [117]. SRAs have been shown to reduce the early age compressive strength of concrete by up to 25% at 1 day and 10% at 28 days [117, 123].

This strength decrease was mainly attributed to the retarding effects of SRA on cement hydration [123].

Previous studies focused on evaluating the interactions of SRAs with pore solutions of portland cement pastes and compared the mechanical properties of concrete with and without SRAs. However, the interaction and compatibility of SRAs with SCMs such as MK was not evaluated.

2.6.Metakaolin-blended cement concrete: Hardened properties

Two aspects of the effect of metakaolin on hardened concrete properties can be evaluated: mechanical properties and durability. The effect of MK on increasing the mechanical properties of concrete has been comprehensively addressed in previous studies [20, 126, 127]. Those show that higher mechanical properties of MK concrete are achieved at early ages. These increases can be attributed to the combination of the filler and nucleation effects of MK as well as due to the relatively rapid pozzolanic reaction of MK with CH produced from the cement hydration; the pozzolanic reaction extends for some time, leading to further increases in strength at later ages as well [128]. The increase in the mechanical properties of MK concrete can depend on MK quality, the thermal activation processing of kaolinite, cement composition and fineness, and mixing and curing temperature, among other factors.

The higher or similar compressive strength of MK concrete, compared to ordinary concrete, has been observed for different MK replacement levels at all ages. For example, Wild et al. [20] reported that the greatest compressive strength improvement was achieved by 20% by mass cement replacement level. Other studies, however, showed that

compressive strength increased with the increase in the metakaolin content, up to 10% MK content [65, 129, 130]. Generally, in practice – due to constraints on workability and cost – metakaolin contents in concrete are limited to 8 to 10% by mass of cement.

Razak and Wong [131] developed a mathematical model for estimating compressive strength of concrete with MK or silica fume based on the pozzolanic and dilution effects of those particular pozzolans (Equation 2.13). It was showed that the key parameters involved in the model are the pozzolanic and dilution factors, which can be correlated to the pozzolan content in the mixture.

$$S_p = \alpha S_p + \beta \qquad 2\text{-}13$$

Where α and β are factors related to the pozzolanic and dilution effects of the particular pozzolan respectively. This study presented a figure based on the ANOVA analysis to estimate α, β based on the pozzolan type (MK or SF), the replacement level, and the w/b. These relationships were based on mixtures designed with up to 15% mass replacement of OPC with metakaolin and silica fume, and mixtures with w/bfrom 0.27 to 0.33, to estimate the strength of concrete at 28 days or higher.

Justice and Kurtis [61] evaluated the effect of MK with two different fineness at 8% replacement by mass on the mechanical properties of concrete. It is showed that compressive and flexural strength of MK concrete were greater (by 15-50%) than the control concrete with OPC. The MK concrete with the finer MK showed the higher strength and the faster rate of strength gain. The influence of fineness on the increased mechanical propertied of concrete is more significant at later ages of 7 days or more. Qian and Li [132]

investigated the tensile strength, bending strength, and elastic modulus of concrete incorporating 5, 10, and 15% metakaolin as partial replacement of cement. It was shown that the tensile and compressive strength of concrete increased with increasing metakaolin content, especially at early ages, while only a small increase in the elastic modulus of MK concrete was observed compared to the control concrete with no MK. Moreover, the ratios of tensile-to-compressive strength decreased with increasing metakaolin content, which indicates increasing brittleness of the concrete with increasing metakaolin content [132]. An increase in the microhardness of metakaolin mortars with 10% MK has been reported, and this was attributed to the effect of MK on strengthening the aggregate/paste interfacial transition zone (ITZ), which also contributes to greater stiffness in cement-based composites [133].

The effect on MK in improving the durability of concrete has also been reported in previous studies [134]. The higher durability of MK concrete has been related to several factors, including a decrease in the total porosity of concrete, refinements in pore size and improvements in the ITZ microstructure, and transforming calcium hydroxide crystals by MK pozzolanic activity into C-S-H [135, 136]. Moser et al. [50] has evaluated the potential of binary blends of MK and ternary blends with MK and Class C fly ash on mitigating the alkali-silica reaction (ASR) with the highly reactive aggregates. The results of accelerated mortar bar test (AMBT) and concrete prism test (CPT) methods has shown that binary blends of metakaolin or Class C fly ash reduced expansion by 55–90% and 25–37% compared to the control. Ramlochan et al. [134] reported that substituting MK at 10 and 15% by mass of cement is effectives in controlling the expansion due to the alkali-silica reaction, which was attributed to the lower permeability of MK mortar bars and entrapment

of alkalis by MK's secondary C-S-H formation, which together act to inhibit or delay the alkali-silica reaction. Several studies have evaluated the chloride penetration resistance of concrete with w/b of 0.30 and 0.40 and MK replacement levels of 8 and 12%. The results show that higher metakaolin content and lower w/b decrease the diffusion rate, permeability, and conductivity [137, 138]. Thomas et al. [137] showed that MK concrete with 8 and 12% MK exhibit a reduction of 50 and 60% in diffusion coefficients compared to control specimens. Batis et al. [139] studied the corrosion resistance of reinforced MK mortars by total immersion in 3.5% NaCl solution up to 8 months. The corrosion rate of reinforcing steel was determined by measuring the mass loss of bars. It was observed that the use of MK at 10 or 20% improve the corrosion resistance of mortar specimens while the higher percentage of metakaolin decreases the corrosion resistance. Cabrera and Nwaubani [140] reported that MK paste have lower chloride diffusion coefficients than that of portland cement paste and even more so than fly ash concrete. Courard et al. [135] examined the effect of metakaolin additions by 5-20% on the durability of concrete. The results of the chloride diffusion and sulfate resistance studies show that concrete with 10 and 15% MK showed the lowest chloride diffusion coefficient and the highest sulfate resistance. Khatib and Wild [141] evaluated the effect of metakaolin on sulfate resistance of mortar, and showed that incorporating MK decreased the expansion of mortar with an increasing improvement associated with increases in MK content, in the range 5–20% by mass of cement. Studies have reported that substitution of MK at 10 and 15% increase the sulfate attack resistance of mortars compared to portland cement specimens [141, 142]

CHAPTER 3 EARLY AGE PROPERTIES OF METAKAOLIN-PLC BLENDS

3.1.Introduction

One of the primary objectives of this research is to evaluate the effect of metakaolin on the early hydration and microstructural development of PLC-MK blends. Previous studies have shown that metakaolin could have pronounced effects on portland cement hydration through a combination of physical and chemical processes. As reviewed in Chapter 2, the influences of inorganic or mineral additions to cement include the following primary physical effects:

1. The **dilution effect** of SCMs and fillers results in reducing the available cement for reaction, and thereby increasing the water-to-cement ratio (w/c) of the system and consequently increasing the degree of hydration of the clinker at early ages.
2. Another effect of finely divided SCMs and fillers with higher surface area is providing the **heterogeneous nucleation sites** for the formation of hydration products that results in a higher degree of early hydration and ultimately amore defined microstructure. Gleize et al. [70] showed that the addition of MK can accelerate cement hydration due to the nucleation on the finely divided MK particles.
3. It has also been understood that inert materials blended with cements may affect the hydration of the clinker phase through filler effect. The **filler effect** is dominant in the early age hydration of clinker hydration when the reactivity of SCMs has not started yet or is very small compared to the extent of cement hydration [143].

With cement hydration, the alkalinity of the pore solution increases and production of early hydration products including calcium hydroxide and ettringite occurs during the very early stages of reaction. The chemical reactivity of SCMs starts to increase after the first few days, and includes the following effects:

1. The **pozzolanic activity** of MK results in reaction with calcium hydroxide produced from cement hydration and water to form calcium silicate hydrates (C-S-H) and, due to the alumina content, also crystalline hydrated phases including C_2ASH_8, C_3AH_6, and C_4AH_{13}. The products formed depend on the Si/Al of the metakaolin.
2. Moreover, in limestone-containing cements such as PLCs, the reaction of MK with limestone results in **formation of AFm phases** such as mono- and hemicarboaluminate phases that can change the microstructure (including reducing porosity) and influence ettringite stability. The formation of AFm stabilize the ettringite by leaving more sulfate in the pore solution and delay or prevent ettringite conversion to monosulfate [60, 144].

In addition to influencing hydration (through various means described above), various studies have shown that MK generally decreases setting time at lower replacement levels and increases time to set at higher replacement levels. For example, the setting time of MK-blended cement was shown to be longer than that of the control sample with no MK [145] [139]. Likewise, Badogiannis et al. [146] showed that cements with 10% metakaolin exhibit similar setting times to that of PC, while for 20% metakaolin content there is a delay in the setting time. However, one study observed that MK accelerates the hydration

and shorten the initial and final setting times in mortars with relatively high replacement rate 30% MK [19]. Therefore, some inconsistency remains in the understanding of the influence of MK on setting time, and this may be related to the influence of admixtures used to improve workability, particularly at higher replacement rates.

The effect of WRAs on the setting time of neat cements was evaluated in previous studies [147-149]. It was shown that most WRAs retard cement hydration and delay the setting time of cement by 2.1 to 3.1 times compared to that of control sample. The retardation in setting in the presence of superplasticizers was attributed to adsorption of superplasticizers over the cement surface [150, 151]. The adsorbed polymer molecules can hinder the diffusion of water and calcium ions at the surface of the cement clinker grains and thereby retard the cement hydration by mainly retarding the dissolution of alite [151].

The workability of metakaolin mixes decreases with increase in metakaolin content, a potential limiting factor in the practical use of higher (>10% by mass of cement) metakaolin dosages. The use of WRAs can improve workability, but the type and dosage of admixtures can be critical because metakaolin-admixture compatibility has not been previously well-explored in the literature.

While WRAs can improve workability, they can also affect cement hydration and phase development, depending on their chemistry and dosages used. For example, PCE admixtures were shown to retard the C_3S dissolution rate, and this effect was increased with higher calcium hydroxide concentration [152]. Lignosulfonate admixtures accelerate ettringite formation, but are more effective at retarding the C_3S hydration [153]. It should be noted that the impurities in these admixtures could produce ancillary effects. To more comprehensively examine the influence of admixture composition not only on workability

but also early age hydration and behavior, this study examined four commonly used WRAs chemistries – polycarboxylate ether (PCE), calcium lignosulfonate (LS), naphthalene formaldehyde condensate (PNS) and polymelamine sulfonate (PMS) – and assessed their effectiveness in metakaolin-portland limestone cement (PLC-MK) blends.

Thermogravimetric analysis (TGA) and x-ray diffraction (XRD) are commonly used to characterize the early age products of hydration. To prepare the samples for TGA and XRD, it is important to stop the hydration instantaneously at a predetermined time by complete removal of free water. Several techniques can be applied to remove the free water, including low pressures D-Drying [154], freeze-drying [155], vacuum drying [156], and oven drying [157] at high temperatures, and solvent exchange [157]. Each technique has its own benefits and side effects. For instance, oven drying at 105 °C can was found to accelerate hydration, favor carbonation and cause dehydration of some cement hydrates [158]. The solvent exchange and freeze-drying are the most common ones used in analytical analysis such as thermal analysis, ATR-FTIR, and XRD that powdered samples are required. Solvent exchange is a common technique to stop the cement hydration but it results in a strong absorption of solvents that are not completely removed by normal drying. This method has been criticized by several authors due to their potential interactions with cement hydrates that can lead to carbonation and producing false results in analytical techniques. Knapn et al. [159] showed that that the interaction between absorbed solvents and the cement hydrates could cause the formation of carbonate-like phases upon heating, i.e. during thermal analysis. Therefore, the estimation of the $Ca(OH)_2$ content and the degree of hydration by thermal analysis for hydrated cement pastes treated with solvents cannot be considered to be reliable. On the other hand, they showed that freeze-drying is

an easy and reliable technique free water from early-age hydrated cements compared with the solvent exchange technique. An additional advantage of vacuum drying is that no interaction products can be formed and that the calculated $Ca(OH)_2$ content and the degree of hydration by thermal analysis can be a reliable approximation and the disadvantage is that this method can decompose phases such as ettringite. Since freeze-drying has been found to be a satisfactory process for stopping cement hydration, this study adopted this technique prior to chemical analysis by TGA and XRD [158]. At desired times; crushed paste samples (of ~5 mm and smaller in size) were immersed in liquid nitrogen for 15 minutes and then held for 12 hours at temperature of –49°C and pressure 0.22 mbar in a laboratory lyophilizer. Subsequently, the paste was ground using an agate mortar and pestle prior to TGA or XRD characterization. The XRD and TGA tests were carried out on the highest MK content (MK30) paste samples to evaluate the highest effect of MK and highest dosages of WRAs.

In this chapter, the effect of metakaolin at different replacement levels of 10, 20, and 30% by mass on the hydration kinetics, microstructural development, and autogenous shrinkage of limestone-metakaolin blended cement are evaluated. Additionally, the effect of each admixture on PLC hydration and phase development in the presence of MK are assessed.

3.2.Materials

The cement used in this study is an ASTM C595 [41] Type IL portland limestone cement (LS ≤ 15% by mass), provided by Argos, with clinker produced in Calera, AL and finished in Roberta, GA. High purity metakaolin (Burgess Pigment Company, Sandersville, GA) was used as a replacement for cement at rates of 10% 20%, 30% and

40% by mass. These blends will be denoted according to their MK content as MK10, MK20, MK30 and MK40, respectively.

As reported in Chapter 2, metakolin is a white fine powder (Figure 3.1.) categorized as Class N Natural Pozzolan [32] and produced from a heat-treating of kaolinite. Typically, MK is produced from a three-stage process that includes a grinding process, calcination of the raw material for several hours in a rotary kiln, and followed by grinding of the burned material [160]. The high purity metakaolin used in this study is produced from flash calcination, which is an industrial process based on a rapid calcination of kaolinite, for only a few tenths of a second, rather than a traditional calcination (minimum 10 minutes duration) [161].

For mortar samples used in the setting time test (in the Vicat test), natural sand (Vulcan Materials, Lithia Springs, Georgia) with a fineness modulus of 2.40, saturated surface dry (SSD) specific gravity of 2.63 and an absorption capacity of 0.40% was used.

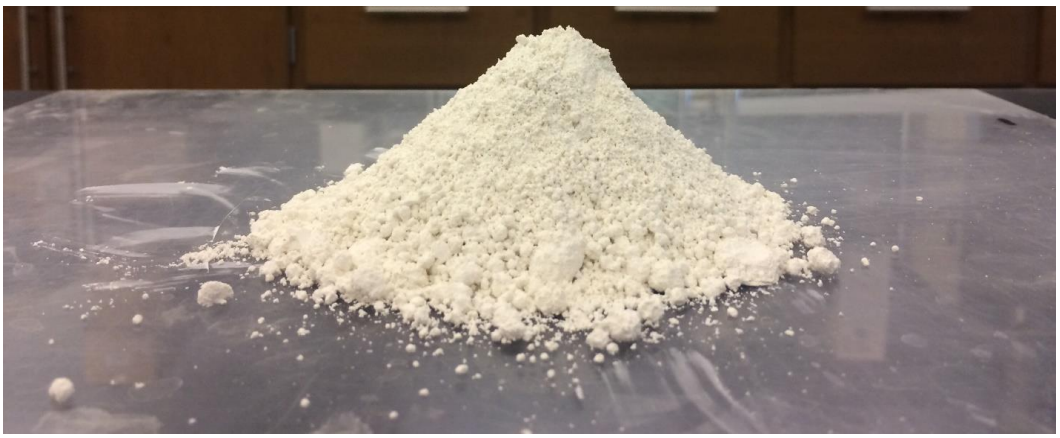

Figure 3.1. OPTIPOZZ Metakaolin provided by Burgess Pigment Company, GA, USA

The chemical compositions of cement was obtained by oxide analysis (ASTM C114 [162]) and quantitative x-ray diffraction (XRD) (ASTM C1365 [163]). The two common

methods for determining the unhydrated cement phases are the application of Bogue equations to oxide compositions and Rietveld analysis of the x-ray diffraction patterns. The oxide analysis is more commonly used to estimate the primary phase distributions in cement but the application of the Bogue equations to limestone cements requires *a priori* knowledge of the limestone composition and content [164]. The compositional data from chemical oxide analysis and the crystalline composition from quantitative X-ray analysis of the PLC and metakaolin are shown in Table 3.1. The results show that the PLC used in this study has 3% SO_3 content and 6.33% Loss on ignition (LOI) that meets the ASTM C595 chemical requirements of maximum %3 SO_3 content and 10% LOI. The Si/Al of the MK used in this study is 1.15 that, as it was mentioned, is important in determining the products produced from the MK pozzolanic reactivity.

The particle size distributions of the PLC and metakaolin were measured by laser diffraction (Malvern Mastersizer 3000E) on sonicated samples dispersed in ethanol. A small amount of sample (3-5g) was added and dispersed in ethanol until the laser obscuration reached approximately 7%. The dispersed sample was then sonicated for one min. and then at the rate of 840 rpm for about 10 mins to avoid sample agglomeration. The particle size distribution was determined as an average of five samples collected within 60-second intervals using Mie theory [165]. Refractive indices of 1.68 and 1.36 were selected for cement and ethanol, respectively, from the database included in the Mastersizer software. The results for the PLC and metakaolin (Figure 3.2) show that MK has a significantly finer particle size distribution than that of PLC with the mean particle sizes of 10.2 and 1.4 μm for PLC and MK, respectively. The particle size mean and distribution were provided by the producer (Burgess Pigment).

Table 3.1. Chemical composition of PLC and MK (left), and phase composition of PLC by quantitative x-ray diffraction (right)

	Portland limestone cement (PLC) (% by wt.)	**Metakaolin (% by wt.)**		**Portland limestone cement (PLC) (% by wt.)**
SiO_2	17.13	51.4	**C_3S**	50.83
Al_2O_3	4.16	44.8	**C_2S**	17.31
Fe_2O_3	2.86	0.424	**C_3A**	3.27
CaO	62.05	0.02	**C_4AF**	9.28
MgO	3.12	0.09		
Na_2O	0.07	0	**Lime**	0.1
K_2O	0.48	0	**Periclase**	2.23
Na_2O_e	0.38	0	**Quartz**	0.1
TiO_2	0.26	1.46	**Arcanite**	1.09
Mn_2O_3	0.05	0	**Gypsum**	0.75
BaO	0.09	0	**Bassanite**	1.6
SO_3	3.00	0	**Anhydrite**	0.12
$CaCO_3$	11.8	0		
Others	6.04	0	**Calcite**	11.80
LOI	6.33	1.05	**Portlandite**	1.18
Surface area (m^2/g)	-	15		
Blaine fineness (m^2/kg)	597	-		
Specific gravity (g/cm^3)	3.05	2.35		

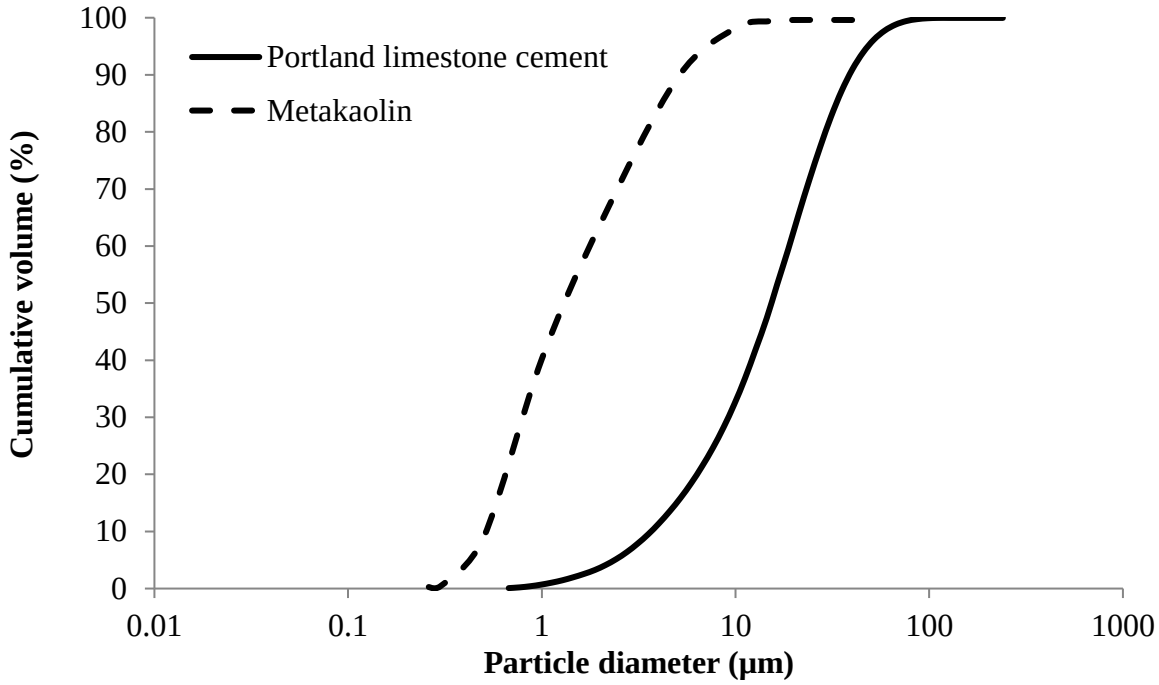

Figure 3.2. Particle size distribution of portland limestone cement and metakaolin

To understand the effect of WRAs on the early age reactions of metakaolin-portland limestone cement blends, four commercially available admixtures – polycarboxylate ether (PCE), calcium lignosulfonate (LS), naphthalene formaldehyde condensate (PNS) and polymelamine sulfonate (PMS) – were obtained from two different producers (GCP, BASF). PCE, PMS and, PNS are Type F high-range water-reducer (ASTM C494) and calcium lignosulfonate (LS) is a Type D water-reducer/retarder. WRA dosage rates are reported as the solid content per 100 grams of binder (i.e., cement + MK). The solid content of each WRA was measured by its residue after drying (ASTM C494) and are shown in Table 3.2 [90]. LS, PNS and PMS admixtures are considered to primarily disperse solid particles by electrostatic repulsion and by lowering the zeta potential, while the PCE admixture with its longer, grafted chains also involves steric repulsive forces based on the interaction between the adsorbed admixtures.

Table 3.2. Density and solid content of WRAs used in this study

water-reducing admixtures	**Density (g/cm^3)**	**Solid content (Mass %)**
Polycarboxylate ether (PCE)- liquid	1.08	30.6
Polycarboxylate ether (PCE)- powder	0.7	N/A
Calcium lignosulfonate (LS)- liquid	1.10	30.2
Naphthalene formaldehyde condensate (PNS) liquid	1.15	35.5
Polymelamine sulfonate (PMS)- solid	0.5-0.8	N/A

3.3.Experimental Methods

Paste samples were prepared at water-to-binder (w/b) of 0.40, with 0, 10, 20, 30% and 40% by mass MK replacement for. WRAs were each added first to the water and then the water and WRA was added to the cementitious materials. The mixing procedure consisted of manual stirring of the cement in deionized water for 30 s, followed by mechanical mixing of the paste mixture with a 5-speed hand mixer at low speed for 60 s and at medium speed for 60 s. In this study, mini slump tests were performed on paste samples at a common w/b of 0.40 to determine the dosage of each admixture required to produce equivalent slump of the control (cement only) paste. The dosages determined by mini slump were used in further tests with metakaolin paste.

The mini slump was performed using a polymethyl methacrylate (PMMA or “acrylic”) cone with a 19 mm top diameter, 38 mm bottom diameter, and a 57 mm height (Figure 3.3), based upon [166], where the dimensions are in the same proportions as the slump cone specified in ASTM C143 [167]. Paste samples were placed into the mold and the top surface was smoothed with a metal spatula. After 60s, the mold was raised vertically and the diameter of the subsided paste was measured in three directions, with the average of

these determining the pat area. The control PLC paste with no metakaolin exhibited a pat area of 27 mm^2 and was used as the basis for determining required WRA dosage for the other PLC-MK mixtures.

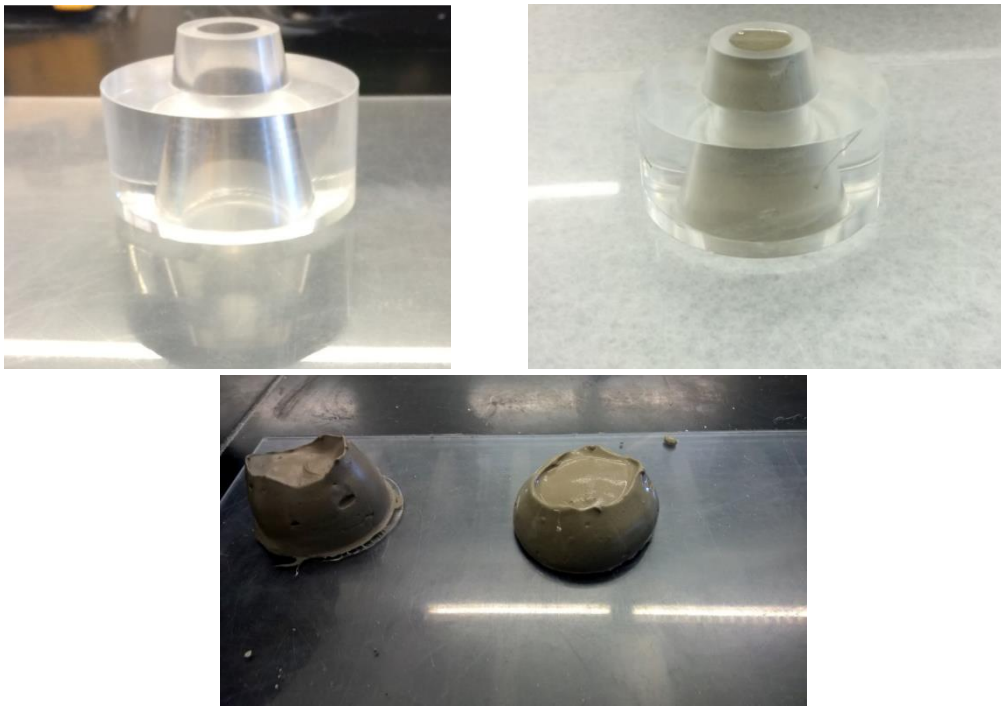

Figure 3.3. Mini slump test conducted to determine the required dosage of each WRA to produce equivalent slump of the control (cement only) paste

Hydration kinetics and cumulative heat of hydration were measured by isothermal calorimetry according to ASTM C1679 [168]. Pastes were mixed externally following ASTM C305 [169] prior to being placed in the calorimeter (Thermometric TAM AIR). Paste samples were prepared at water-to-binder (w/b) of 0.40, with 0, 10, 20, and 30% by mass MK replacement. Samples were prepared with no WRA and with dosages of each of four WRA type determined by mini slump to achieve equivalent flow. All pastes were prepared at w/b of 0.40 with water adjusted based on the water content of each WRA. The WRAs used in this study were LS that is a mid-range WRA and PMS, PCE, and PNS that

are HRWRAs. WRAs were each added first to the water and then the water and WRA was added to the cementitious materials.

Thermogravimetric analysis (TGA) and x-ray diffraction (XRD) were used to characterize the early age products of hydration. To prepare the samples for TGA and XRD, it is important to stop the hydration instantaneously at a predetermined time. Freeze drying has been found to be a satisfactory process for stopping cement hydration prior to chemical analysis by TGA [158]. At desired times, crushed paste samples (of ~5 mm and smaller in size) were immersed in liquid nitrogen for 15 minutes and then held for 12 hours at temperature of –49°C and pressure 0.22 mbar in a laboratory lyophilizer. Subsequently, the paste was ground using an agate mortar and pestle prior to TGA or XRD characterization.

Thermogravimetric analysis was performed on approximately 15 mg of paste using a HITACHI TG/DTA 7300 heated under N_2 environment with a 10°C/min ramp from 25°C to 800°C. Calcium hydroxide ($Ca(OH)_2$) generally decomposes between 400 and 500°C to CaO and H_2O [170], and therefore this change in mass (M_{CH}) between those temperatures can be used to calculate the amount of calcium hydroxide (CH) present in the sample [170]. The molecular weights of $Ca(OH)_2$, and H_2O are taken to be 74.09 g/mol, 18.01 g/mol, respectively. As the solid content changes over the decomposition period, the CH content is normalized by the anhydrous sample mass at 600 °C (m_{600}).

$$CH = \frac{m_{400} - m_{450}}{m_{600}} \times \frac{MW_{Ca(OH)_2}}{MW_{H_2O}} \qquad 3\text{-}1$$

The phases present in the cement phase were examined by the thermogravimetric derivative (DTG) curves. Some phases, such as monosulfate and monocarboaluminate occurring between ~130-150°C and ~140-160°C respectively, overlap with ettringite and C-S-H and could not be identified from the DTG curve. The decomposition temperatures for other phases are presented in Table 3.3.

Table 3.3. The temperature that each component decomposes for thermogravimetric analysis

Decomposition Temperature Range (°C)	**Phase**	**Chemical Formula**	**Reference**
90-120	Calcium silicate hydrates (CSH)		[171]
	Ettringite (E)	$CaAl_2(SO_4)_3(OH)_{12}.26H_2O$	[172]
140-160	Gypsum (G)	$Ca(SO_4)$	[170]
60-200, 600-650	Monocarboaluminate(MC)		[170]
190-250	Stratlingite (Str.)	C_2ASH_8	[173] [174]
	Tetra calcium aluminate hydrates (Tr.)	C_4AH_{13}	[173] [174]
310-350	Hydrogarnet (Hy)	C_3AH_6	[175]
400-450	Portlandite (CH)	$Ca(OH)_2$	[170]
650-700	Calcium carbonate (CC)	$CaCO_3$	[170]

X-ray diffraction (XRD) measurements were carried out on paste samples using a PANalytical EMPYREAN diffractometer with a CuKα (λ= 1.54 Å) source with a fixed divergence slit size of 1.58 millimeters and anti-scatter size of 6.35 millimeters. The tests were performed over a Bragg angle (2θ) range of 5–40° with a step size of 0.01 2θ and a

time per step of 50 seconds. HighScore Plus software was used to analyze the pattern and assign the peaks to phases.

The effect of MK substitutions on the initial and final setting times of mortar specimens were assessed by the Vicat test [176]. The Vicat test is a standard test for measuring the initial and final setting times of cement paste and mortar. Initial set is defined as the time at which the needle will not penetrate past a certain distance, i.e. 25 mm (ASTM C191) [177], from the top of the sample. Final set is defined as the time when there is no mark upon the surface from the needle, i.e., no penetration of the needle at all. The sand-to-cement ratio of 2.75 and w/b=0.485 were chosen for mortars following ASTM C109 for mortars composition [178]. The normal consistency test was not followed in this study, as the purpose of this study was to evaluate the effect of certain MK contents and WRAs dosages. The mixing of mortars followed the procedure in ASTM C305 [179]. The mortar was then shaped into a ball with gloved hands and toss six times between two hands while maintaining the hands about 150 mm (6 inches) apart following ASTM C191[180]. The ball was then rest on the palm of the hand and placed into the larger end of the ring and completely filling the ring with paste. The ring was flipped over, the excess mortar was removed, and it was set on its larger end onto the glass plate. Three mortar sets were made for each mix and the results were presented by taking an average of three readings. The samples were kept in the moisture environment for the whole test duration. The needle penetration was measured every 30 mins. In the case that the 25 mm penetration did not fall into one of the readings, the following equation (Equation 3-2, ASTM C191[180]) was used to calculate the initial setting time.

$$\frac{(H-E)}{(C-D)}\times(C-25)+E \qquad 3\text{-}2$$

Where:

E = time in minutes of last penetration greater than 25 mm,

H = time in minutes of first penetration less than 25 mm,

C = penetration reading at time E, and

D = penetration reading at time H.

3.4 Results

In this section, the results of WRAs dosage, calorimetry test, XRD and TGA patterns, and Vicat setting time results are presented to show the effect of MK and WRAs on the early age behavior of PLC cement paste.

3.4.1 Required WRA Dosages

The required dosage of each WRAs for MK replacements of 10, 20, 30, and 40% MK by mass of cement was examined. The WRAs were not capable of increasing the workability of MK40 paste to be close to the PLC paste and therefore for the rest of this study the MK content is limited to 30% MK by mass.

Figure 3.4 shows that the flowability of PLC-MK cement paste decreases by about 11% for each 10% increase in the metakaolin level measured by the mini slump test. The results reveal the need for the use of an efficient WRA to improve the flowability of PLC-MK specimens particularly with higher MK content.

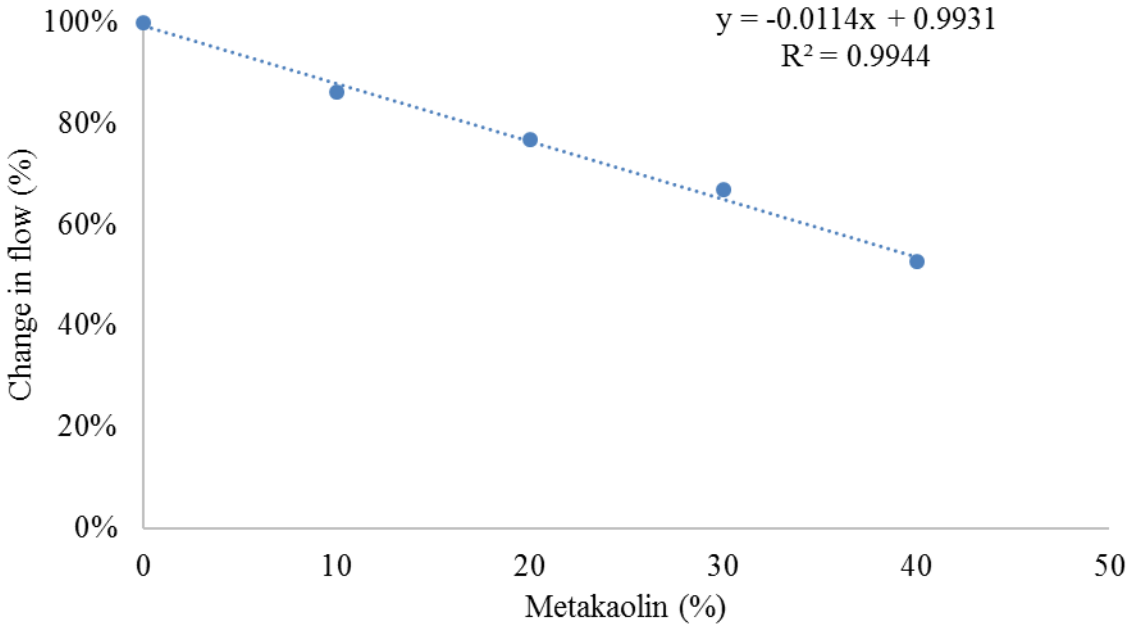

Figure 3.4. The change in the flow of metakaolin-containing cement paste with increase in the metakaolin replacement level (expressed as % by mass of cement) measured by the mini slump test.

The required dosages of each WRA to achieve equivalent mini-slump to the ordinary cement paste are presented in grams of solid/100g of binder in Figure 3.5; presenting the data in this manner allows for comparison between liquid and solid admixtures (e.g., the liquid PCE noted as PCE-L and the powder form as PCE-P). The dashed lines in Figure 3.5 show the maximum WRA dosage recommended by each of the admixture producers and can be viewed as a practical upper bound on dosage rate.

These results indicate that several types of WRAs, specifically LS and PNS, require significantly higher dosages than the maximum recommended to achieve flow values similar to those for the control sample. The use of WRAs at such high dosage rates may produce undesirable behavior, including set retardation or even cement hydration inhibition [181]. Moreover, higher variations were observed for LS dosages.

Both the PMS and PCE admixtures produced workability similar to the control samples within the recommended manufacturer dosage even at 30% MK replacement. Moreover, the relationship between the required PCE admixture dosage and the metakaolin replacement level was found to be linear. This is advantageous for predicting the required dosage of PLC-MK blends at different metakaolin replacement levels, and facilitates practical upscaling. Overall, a more predictable behavior was found for PCE (both powder and liquid) compared to the behavior of other WRAs evaluated. Furthermore, the required dosage was lower for PCE at each MK substitution rate examined than those for other WRAs.

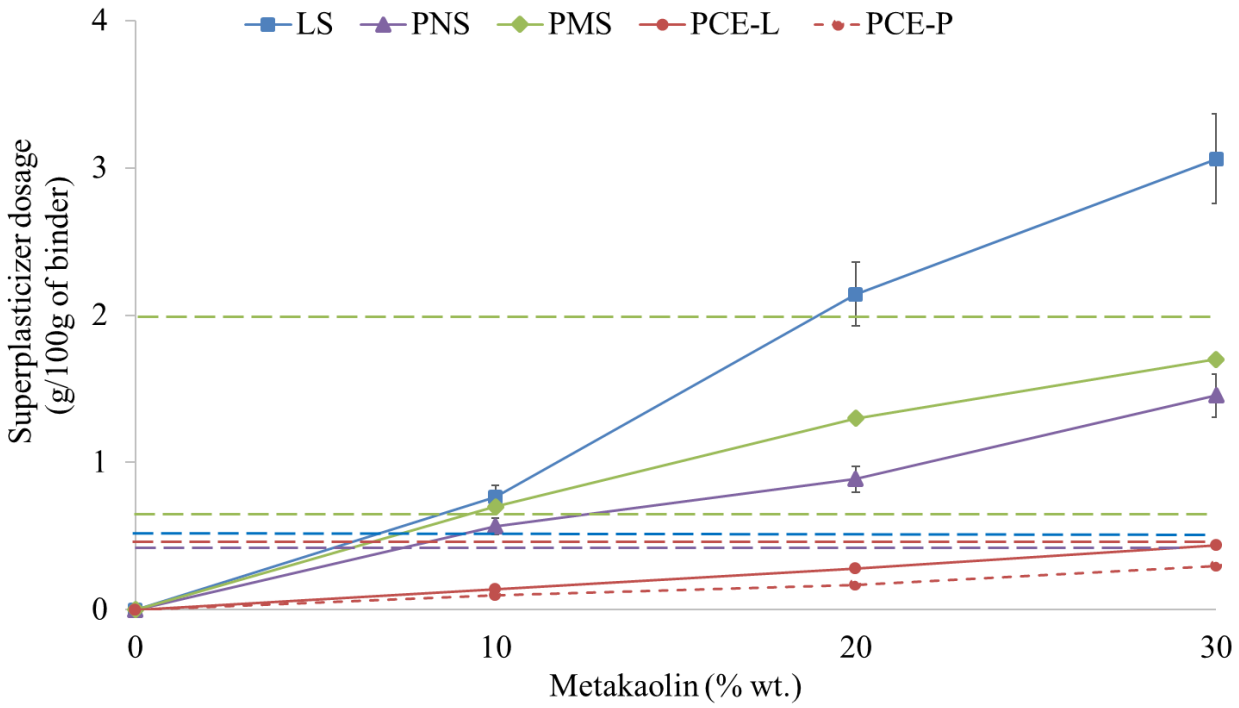

Figure 3.5. Required WRA dosage for each metakaolin substitution level to obtain equivalent flow to control pastes with no metakaolin, measured via mini slump. The dashed lines show the maximum recommended dosage for each admixture.

3.4.2 Flow loss

The prior data show that WRAs can improve the workability of MK pastes; however, the potential of these admixtures in retaining flow over time is also important. Flow loss is a common issue with the use of admixtures, and this can be a problem when concrete transported in the field. Understanding and anticipating flow loss is important for large scale production of such mixes.

Fresh concrete is assumed to retain its workability for between the 45 to 60 mins after initial mixing for concrete delivery and consistency performance. The quick slump loss can result in the operation problems like choking of pipe line because of dry, bleeding, or segregated concrete[182]. Here, the flow loss of PLC and PLC with 10 and 30% MK paste

with PMS and PCE was measured via mini slump test on the paste samples after each 10 mins of resting for the first 60 mins after initial mixing. (Figure 3.6). The paste was mechanically mixed for 10 sec before measuring the flow by mini slump cone each time. The highest flow loss (58% at 60 mins) was observed with the PMS admixture and that increased up to 80% with the increase in the MK content of 10 to 30% and increase in the admixture dosage. The MK paste with PCE showed similar flow loss (25% at 60 mins) to the PLC paste. It should be noted that the flow loss was consistently slightly lower for the MK30 paste with the higher PCE content. Therefore, in practice, PCE is recommended, based upon its flow retention properties in PLC-MK systems.

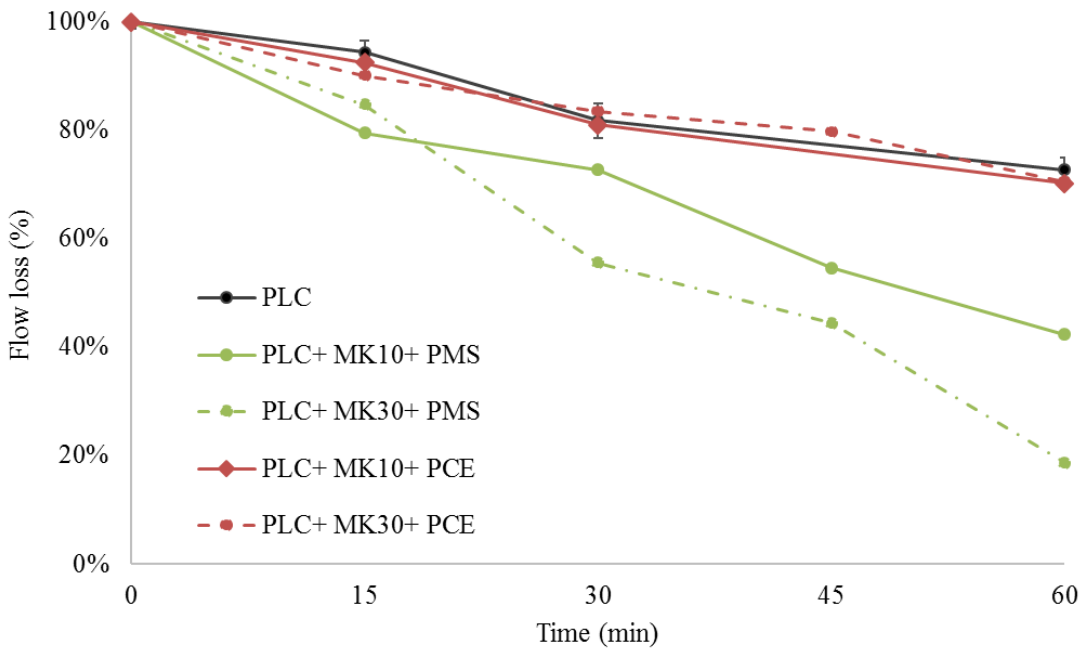

Figure 3.6. The flow loss of PLC and PLC with MK10 and MK30 paste with PMS and PCE admixture.

3.4.3 Hydration kinetics

It was shown in Chapter 2 that metakaolin addition can affect the cement hydration depending on metakaolin replacement levels [64]. The change in the cement hydration was attributed to the nucleation and filler effects of metakaolin depending on the replacement levels. The use of metakaolin particularly at the higher levels requires the use of WRAs at relatively higher dosages. The WRAs can affect the cement hydration kinetics depending on their chemistry and dosages, as was described in Chapter 2.In this section, the role of metakaolin at 10, 20, and 30% replacements on limestone cement hydration will be presented. Moreover, the effect of each WRA, at the dosage determined by the mini slump test, on the rate of cement hydration will be evaluated.

Following ASTM C1679 [183], three calorimetric peaks are typically observed during the hydration of a portland cement, the first peak (often only the descending portion is captured) is attributed to the dissolution of the clinker phases in the first hour of hydration, the second peak corresponds to the hydration of the C_3S phase, and the third peak corresponds to the hydration of the C_3A phase. A fourth broad shoulder may also appear after 24-36 hours, corresponding to the formation of AFm phases such as monosulfate and monocarbonate, but this peak is not always apparent. The trough between the second and the third peaks is related to sulfate depletion.

The inclusion of MK by 10% of mass of cement in PLC accelerates the hydration heat by about half an hour while increasing the rate and total heat of hydration compared to PLC by about 1.3 times (Figure 3.7). The addition of WRAs, except LS, delays the rate of heat evolution up to 3 hours with PCE showing the highest delay but the total heat of hydration after 48 hours are similar to that of control sample with no WRA (Figure 3.7). The total heat of hydration measurements show that the MK10 paste with no admixture showed the highest cumulative heat of hydration for the first 24 hours that shows the retardation effect of WRAs used in this study. The use of LS accelerates the heat of hydration rate up to 4 hours and increases the peak of hydration rate to be about 3 times higher than the control sample. The total heat of hydration of LS mix is only about 40% of control sample.

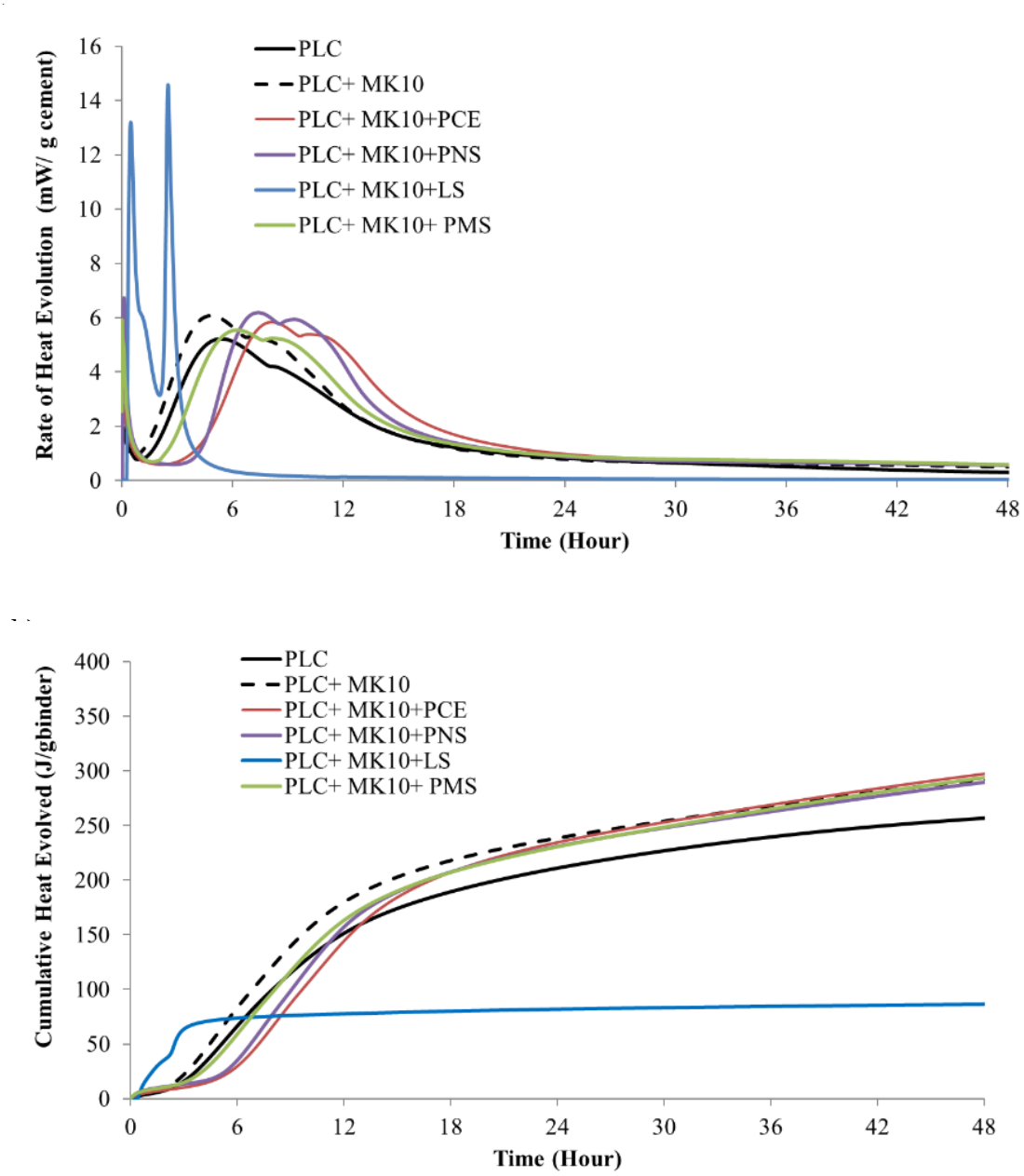

Figure 3.7. Isothermal calorimetry (25°C) results for portland limestone cement with 10% MK and each four types of WRAs a) rate of hydration b) cumulative heat of hydration

The combination of PLC with metakaolin at 20% (MK20) increases the rate of heat of hydration and the total heat over 48 hours compared to that of PLC mix paste. The use of metakaolin accelerated the heat of hydration by about 1.5 hours. The use of HRWRAs at the dosages determined by the mini slump test to improve the workability of metakaolin paste samples has led to delay the cement hydration up to 2 hours. The MK20 paste with

no admixture showed the highest cumulative heat of hydration for the first 12 hours of hydration while at 48 hours it became lower than that of MK20 with HRWRAs that is due to the delay caused by HRWRAs. The cumulative heat of hydration of MK20 paste with no admixture was higher than that of PLC mix at all ages in the first 48 hours. The use of LS highly accelerates the cement hydration by about 3-4 hours. While the addition of LS increases the heat of hydration rate peaks, it decreases the total heat at 48 hours by about one fifth compared to that of PLC with MK20.

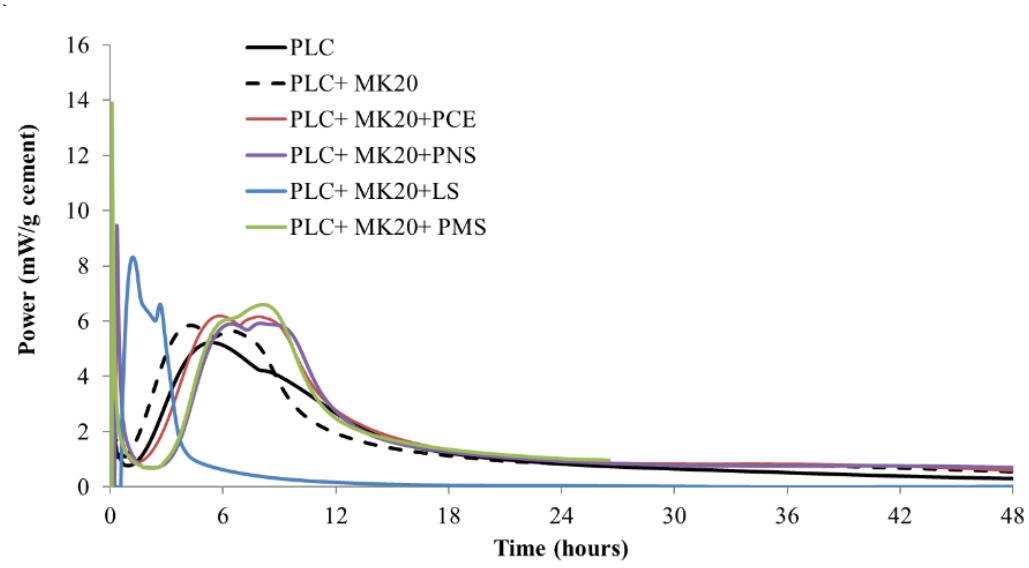

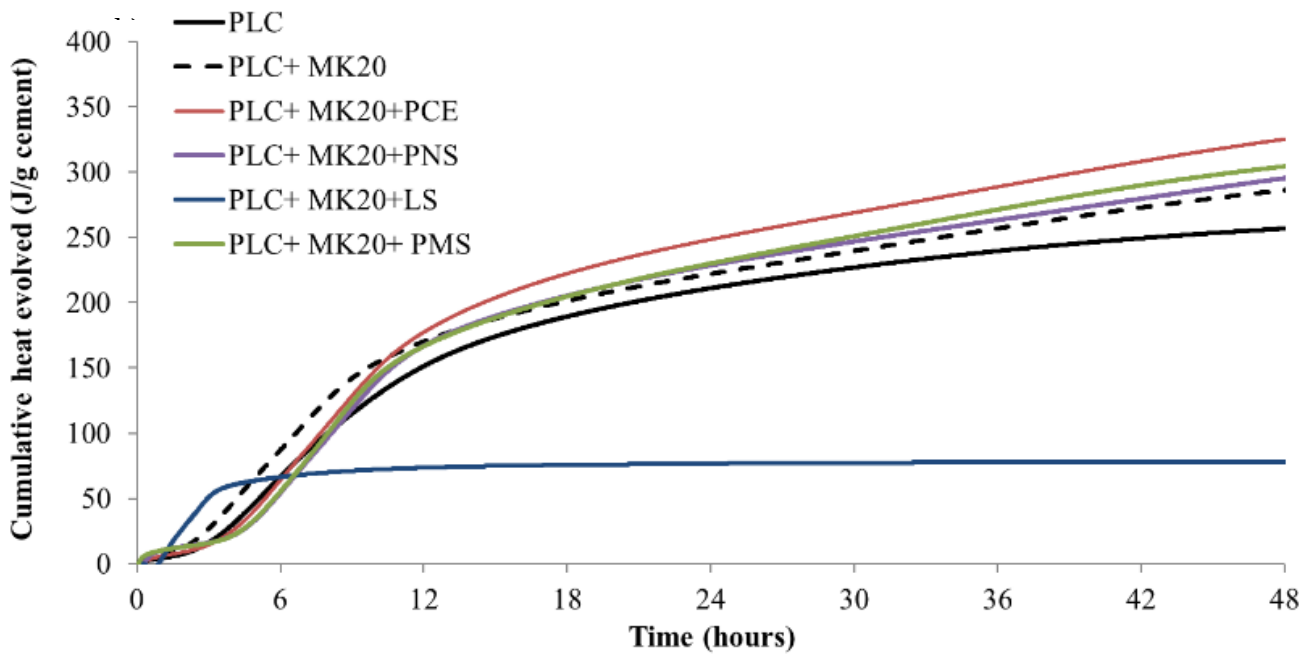

Figure 3.8. Isothermal calorimetry (25°C) results for portland limestone cement with 20% MK and each four types of WRAs at w/b 0.4 a) rate of hydration b) cumulative heat of hydration

The influence of WRAs on cement hydration can be particularly observed with respect to the silica and aluminate phases hydration reactions, as noted in prior studies [181]. The increase in the MK content to 30% further signify the effect of MK on the cement hydration. The more pronounced and sharper aluminate peak was observed in the MK30 paste. All high range WRAs (PCE, PMS, and PNS) when used in PLC paste with 30% MK increased the rate of heat evolution of silicate phases, when compared to PLC with 30% MK and no admixture (Figure 3.9). However, with both PCE and PNS, the silicate and aluminate phase hydration was both delayed by up to 4 hours. In this system, the LS water reducer exhibited a single peak, occurring 5 hours early than the initial peak in PLC paste with 30% MK.

a)

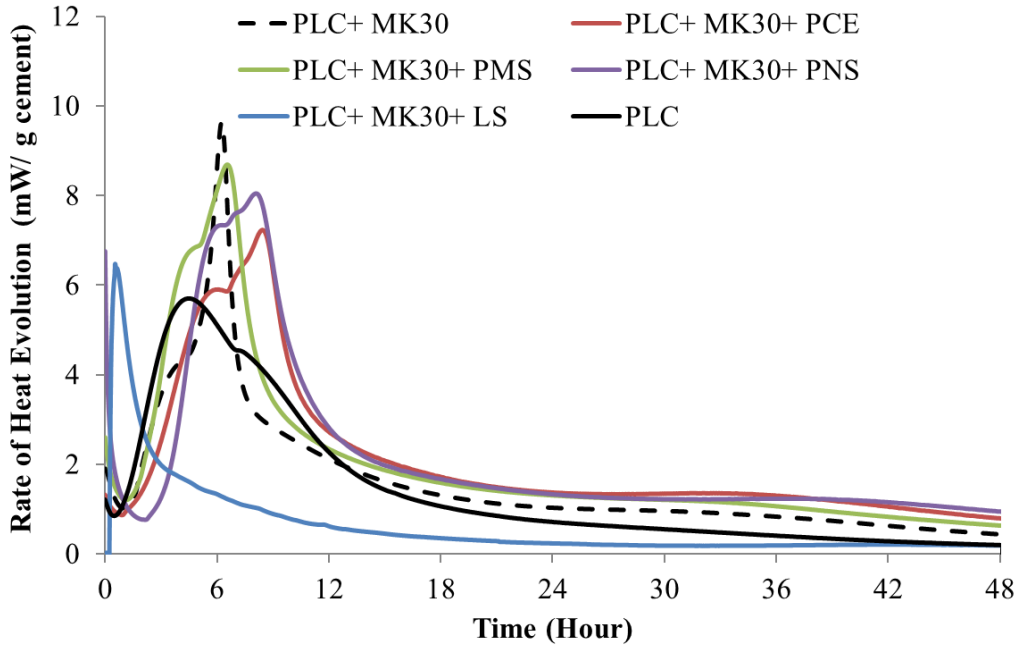
PLC+ MK30
PLC+ MK30+ PCE
PLC+ MK30+ PMS
PLC+ MK30+ PNS
PLC+ MK30+ LS
PLC
Rate of Heat Evolution (mW/ g cement)
Time (Hour)
0
2
4
6
8
10
12
0
6
12
18
24
30
36
42
48

b)

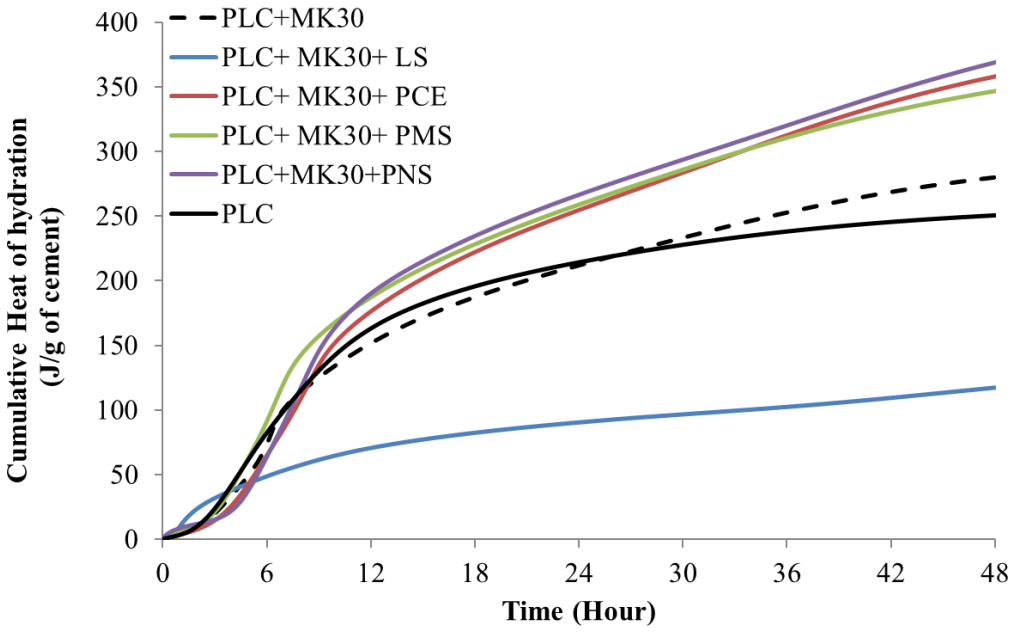
PLC+MK30
PLC+ MK30+ LS
PLC+ MK30+ PCE
PLC+ MK30+ PMS
PLC+MK30+PNS
PLC
Cumulative Heat of hydration (J/g of cement)
Time (Hour)
0
50
100
150
200
250
300
350
400
0
6
12
18
24
30
36
42
48

Figure 3.9. Isothermal calorimetry (25°C) results for portland limestone cement with 30% MK and each four types of WRAs a) rate of hydration b) cumulative heat of hydration

General trends were observed in all MK mixes of 10, 20, and 30% with and without WRAs. The use of MK at all levels increase the cement heat of hydration that can be due to nucleation and dilution effects of MK. The use of WRAs, with the exception of the LS mixture, led to increased cumulative heat at 48 hours. This effect can be interpreted as a result of improved dispersion in the pastes containing WRAs [184].

The lower cumulative heat of hydration of MK30 pastes with LS suggests that the hydration of C_3S, and consequently production of CH, was inhibited or highly delayed despite the very early initial exothermic peak. While cement pastes with lignosulfonate showed a very early hydration peak, the cumulative heat of hydration is considerably lower compared to the other pastes; this further suggests an anomalous interaction between the LS and the MK paste at this relatively high admixture dosage rates. The accelerated hydration peak in the lignosulfonate paste is likely a result of accelerated gypsum dissolution and catalyzed ettringite formation in the presence of LS [100, 185]; this will be explored in more detail subsequently.

To determine the effect of metakaolin on the cement hydration, Type IL cement with 3 metakaolin substitution rates, 10, 20, and 30% by mass, with appropriate dosages of PCE determined by mini slump test, were tested by isothermal calorimetry. Figure 3.10 shows the effect of MK substitution rates, 0-30% by mass of cement, on the kinetics of cement hydration. From these data, PLC paste samples with MK (10-30%) hydrated with a higher rate of heat evolution and generated greater total heat than those from cement pastes without MK during the first 48 hours. The higher heat of hydration in MK mixes in the

first 48 hours might be due to the nucleation and dilution effect of MK, as it was discussed in Chapter 2. The rate and cumulative heat of hydration increase with increase in MK replacement levels from 10 to 20, and 30% by mass.

Paste samples with 30% MK have the highest peak, particularly the C_3A peak, and cumulative heat of hydration. It seems that the nucleation effect might be more significant for the aluminate phase hydration products as it was shown in previous studies as well [186]. Le Saout and Scrivener [186] showed that the additions of the fine materials, corundum and rutile, have a slight impact on the silicate reaction but a much more significant impact on the aluminate reaction. The aluminate peak is sharpened, becoming narrower and higher. The MK30 paste with PCE showed a slight delay (~ 2-3 hours) in the peak of hydration compared to the PLC paste that can be due to the retardation effect of PCE used at a higher dosage with MK30. This delay was also evidenced in the total heat of hydration that the MK30 with PCE showed a lower cumulative heat of hydration for the first 10 hours while it showed the highest cumulative heat of hydration by 48 hours (Figure 3.10b). A fourth broad shoulder may also appear after 24-36 hours that can be attributed to the formation of AFm phases such as monosulfate and monocarbonate [187]. This peak is more significant in the MK30 mix probably due to the higher MK and aluminate content.

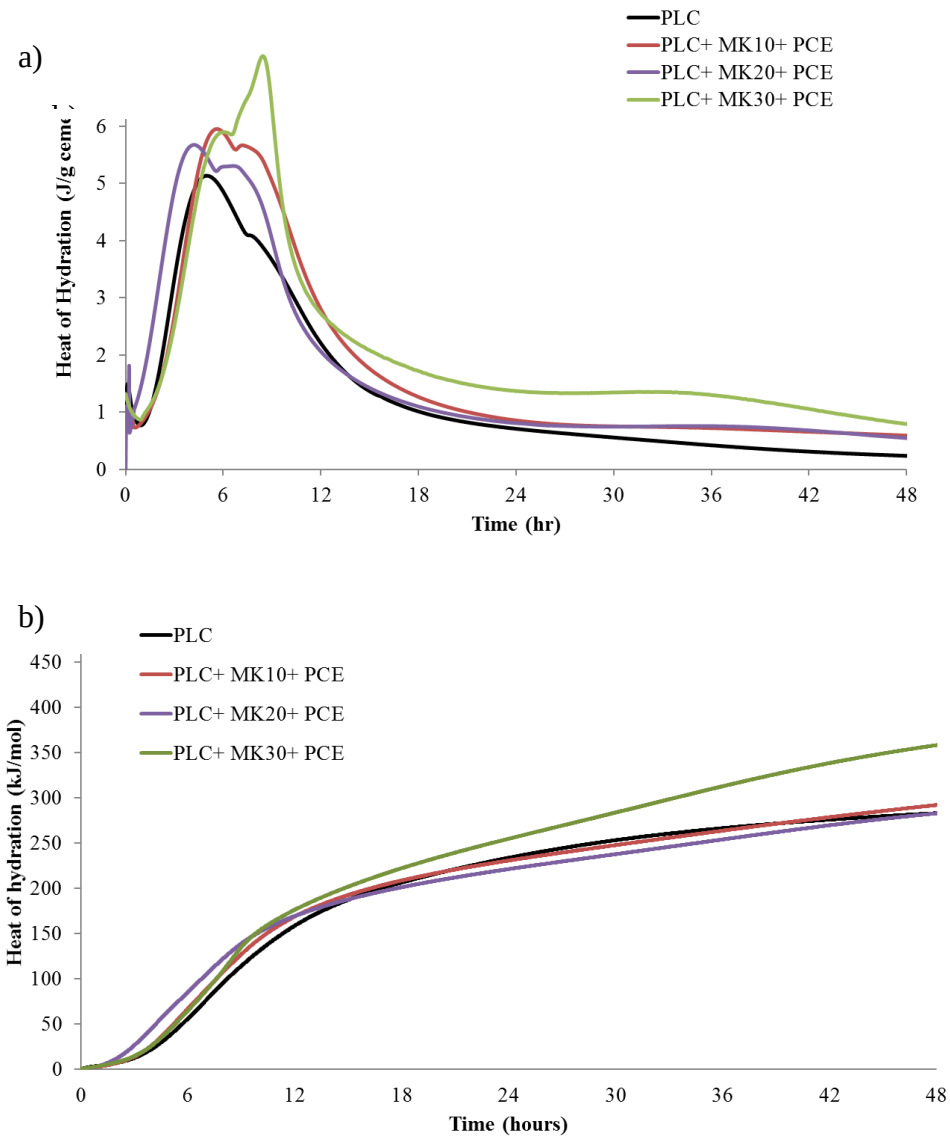

Figure 3.10. Isothermal calorimetry (25°C) results for portland limestone cement with 10-30% MK and PCE a) rate of hydration b) cumulative heat of hydration

3.4.4 XRD

The XRD patterns obtained at 2, 6, 12, and 48 hours (Figure 3.11) show the effect of metakaolin on the portland limestone cement (PLC) phase development and also the effect of WRAs on the type and rate of hydration products formed in the portland limestone

cement-metakaolin pastes. At 2 hours (Figure 3.11a), the calcium hydroxide (CH) peak is only observed PLC mix that can be because of the higher cement content of this mix that reacts with water and hydrates to produce higher CH. The unreacted gypsum peak at 11.8° is identified in PLC and PLC with MK mixes, except the LS mix; the C_3A peak at 33.9° is also the lowest in the LS mix, and an ettringite peak (at 25°) is apparent in LS mix at 2 hours. The higher ettringite peak and lower peak of gypsum and C_3A at 2 hours in LS paste provides evidence for accelerated formation of ettringite in the LS mix. The appearance of ettringite peak at 23° instead of 8.9°, which is usually the main peak for ettringite, may be result from intercalation in the ettringite structure, in the presence of the sulfonates derived from LS [188]. A similar peak is also evident for some of the other admixtures, most notably PMS at 12 hours.

By 6 hours (Figure 3.11b), the early hydration product calcium hydroxide (CH) is found in PLC mix and PLC with MK30 and PCE, PNS and no-WRA pastes, but not in the LS or PMS. The absence of a CH peak at 6-hour PMS and 12-hour LS paste samples further evidences the strong retardation effect of those WRAs. The CH peak does appear in the PMS mix at 12 hours, but this peak is not seen in LS mixes until 48 hours, and even at that time, is only a very small peak relative to observations in other mixtures. A relatively strong peak for C_3S at 29.0° in the LS mix at 48 hours is another evidence for a strong retardation of calcium silicate phase hydration and delay in CH formation in LS mixes. A stratlingite (C_2ASH_8) peak was only observed in the LS mix, apparent at 2 and 6 hours but not afterwards. It appears that LS delays the stratlingite conversion to hydrogarnet, a minor phase in this system measured by thermal analysis [188].

The peaks for monocarboaluminate (MC) and hemicarboaluminate (HC) appear in 48-hour XRD patterns for all mixes. These peaks may be a result of the reaction of metakaolin with the limestone powder in the mix in presence of excess calcium hydroxide and water [188]. The presence of MC and HC in the LS mix and absence of the CH peak suggests the reaction of MK with CH, leading to the depletion of CH.

a)

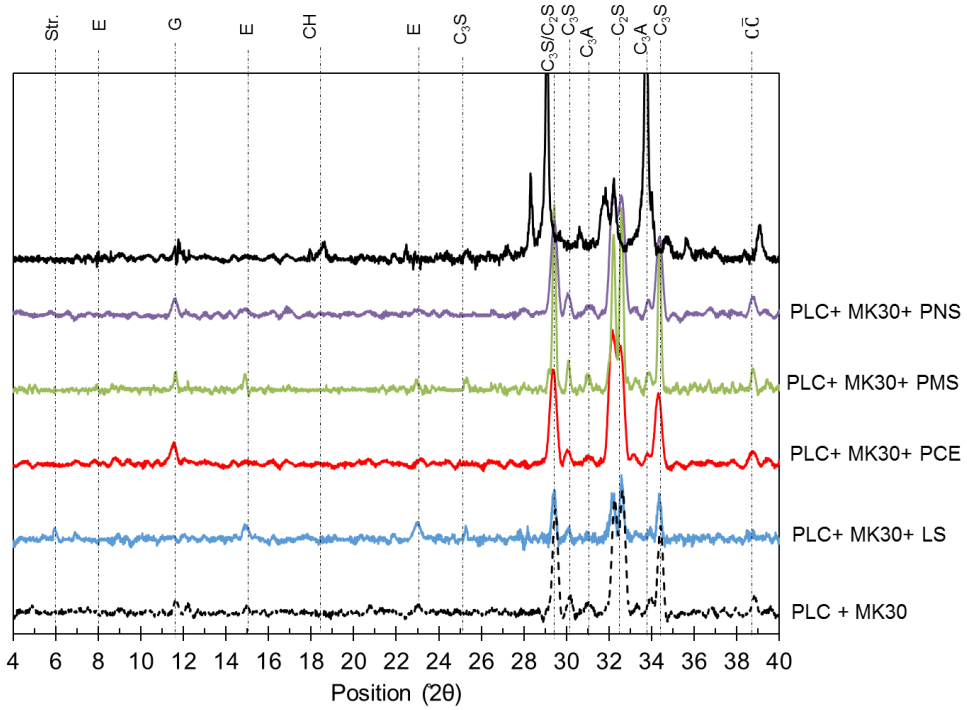

b)

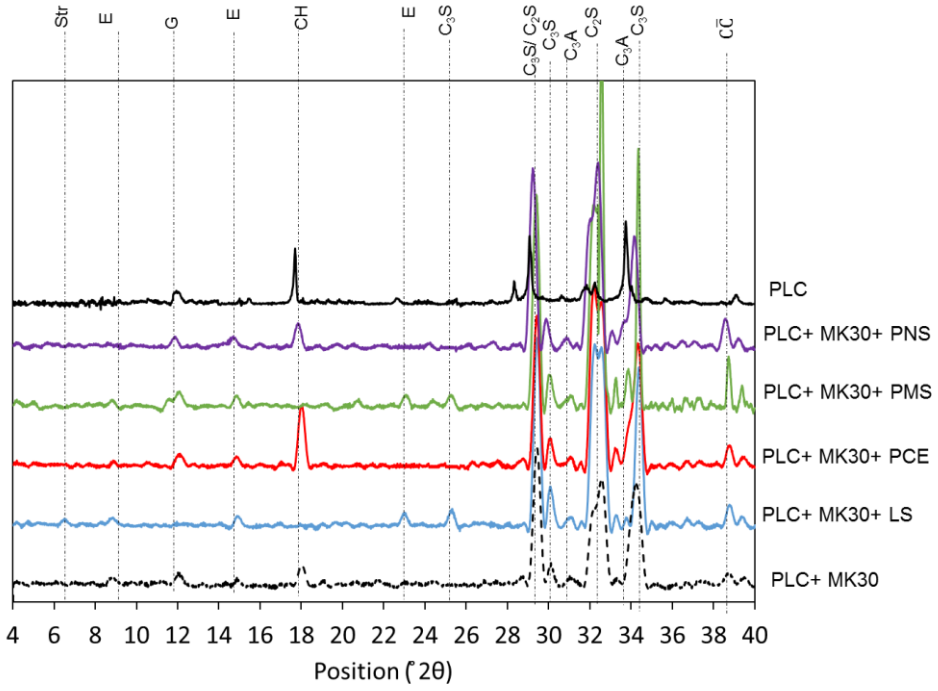
Str
E
G
E
CH
E
C3S
C3S/ C2S
C3S
C3A
C2S
C3A
C3S
CC
PLC
PLC+ MK30+ PNS
PLC+ MK30+ PMS
PLC+ MK30+ PCE
PLC+ MK30+ LS
PLC+ MK30
4 6 8 10 12 14 16 18 20 22 24 26 28 30 32 34 36 38 40
Position (°2θ)

c)

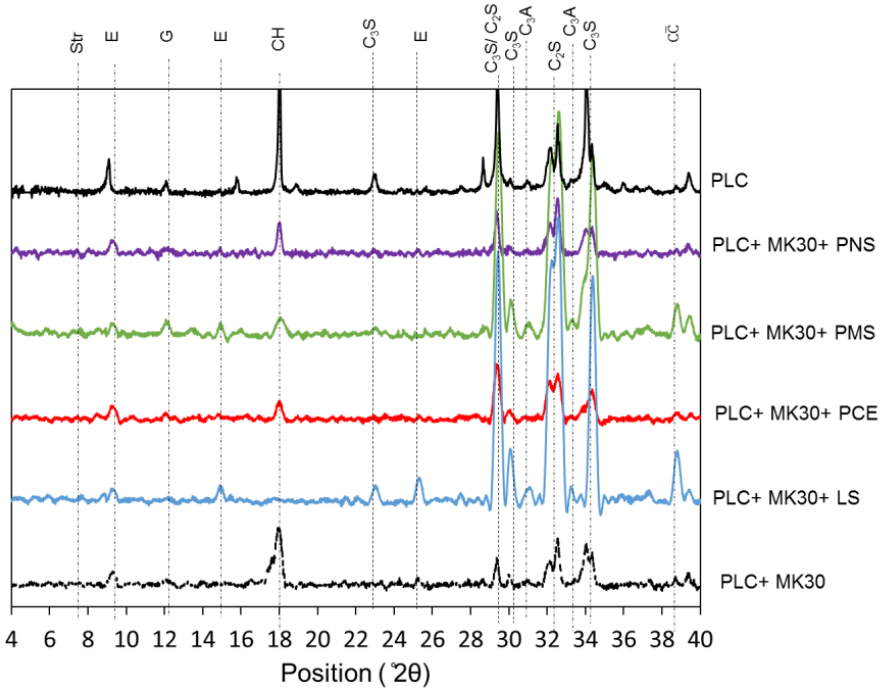
Str
E
G
E
CH
C3S
E
C3S/ C2S
C3S
C3A
C2S
C3A
C3S
CC
PLC
PLC+ MK30+ PNS
PLC+ MK30+ PMS
PLC+ MK30+ PCE
PLC+ MK30+ LS
PLC+ MK30
4 6 8 10 12 14 16 18 20 22 24 26 28 30 32 34 36 38 40
Position (°2θ)

d)

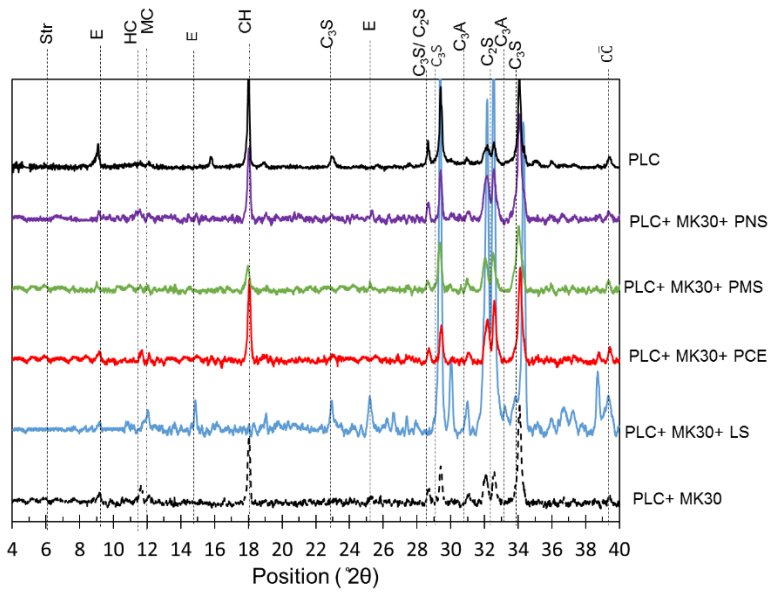

Figure 3.11. XRD patterns for portland limestone cement with 30% metakaolin and each type of WRA at a) 2 hours b) 6 hours c) 12 hours and d) 48 hours

3.4.5 Thermogravimetric analysis

Thermogravimetric analysis (TGA) is a widely used technique in cement research to measure the bound water and phase composition changes, following the reaction of portland cement and evaluating the reactivity of supplementary cementitious materials (SCMs). This study uses TGA to determine the calcium hydroxide (CH), calcium carbonate, and aluminate phases to determine the effect of MK and WRAs on the phase development in cement paste over time.

By as early as 2 hours (Figure 3.12a), compositional differences are apparent among the pastes prepared with PLC paste and MK30 paste with the different WRAs. The calcium hydroxide peak is the highest in the PLC mix with no MK that can be due to the higher cement content compared to MK30 mixes. Among the MK30 mixes, calcium hydroxide

(CH) is found in pastes prepared with PCE and PNS and in the one with no WRA, but it is not detected in LS and PMS paste. Gypsum (G) is observed in all mixes at 2 hours, with the exception of the lignosulfonate (LS) mix, with PLC showing the greatest trough for this phase. The higher trough of gypsum in PLC shows the slower ettringite formation in this mix compared to mixes with metakaolin. The absence of gypsum in LS mix is associated with greater early formation of calcium sulfoaluminate products, including ettringite, in the presence of LS [100]. The LS mix is also the only one where peaks for stratlingite (C_2ASH_8) and tetracalcium aluminum hydrate (C_4AH_{13}) are observed in the TGA data in 2 hours and persist up to at least 6 hours of age. (Recall that the XRD data confirms that the presence of stratlingite peak in the LS mix at 2 hours (Figure 3.13). Their presence is believed to result from the retardation effect of LS on the transformation of hexagonal C_2AH_8 and C_4AH_{13} to the cubic hydrogarnet phase C_3ASH_6 [100, 189]. In contrast, hydrogarnet is observed in 2-hour specimens containing PCE or PMS, where it can be formed through a direct reaction of metakaolin with lime or from the conversion of metastable phases (e.g., C_2AH_8, C_4AH_{13}). While this conversion reaction could increase porosity, a previous study showed that hydrogarnet produced in metakaolin-portland limestone cement blends does not have a significant effect on its microporosity because of its relatively small fraction in the paste [190]. The monocarboaluminate (MC) in LS mix at 2 hours can be due to the carbonation of ettringite, formed early in this mix, due to the limited availability of CH in this system at this early age.

By 6 hours, variations in composition (as related to reaction rate and as affected by the various WRAs) remain, but by 12 hours, the primary difference among the pastes is the relative amount of the phases present. For example, by 6 hours of age (Figure 3.12b),

unreacted gypsum persists in PMS and PNS mixes, presumably due to the delay in the hydration of C_3A; it is notable that ettringite formation in presence of those WRAs does not appear until 12 hours. The gypsum peak in PLC mix is being consumed and transforming from a peak to a broader shoulder. By 12 hours (Figure 3.12c), the hydration products, calcium hydroxide (CH), ettringite, C-S-H, and monocarboaluminate (MC) are observed in all mixes. By 12 hours, a small amount of CH is first observed in the LS paste, whereas that phase was observed by 2 hours for PCE, PNS, and the control mixes and by 6 hours for the PMS mix. By 48 hours, the CH trough in the PCE paste increased, while PLC still shows the deepest trough among all mixes (Figure 3.12d), and paste with PCE and PMS show the deepest trough for ettringite and C-S-H. The absence of monosulfate in mixes at 48 hours can be due to the higher lime content and formation of monocarboaluminate instead of monosulfoaluminate [144].

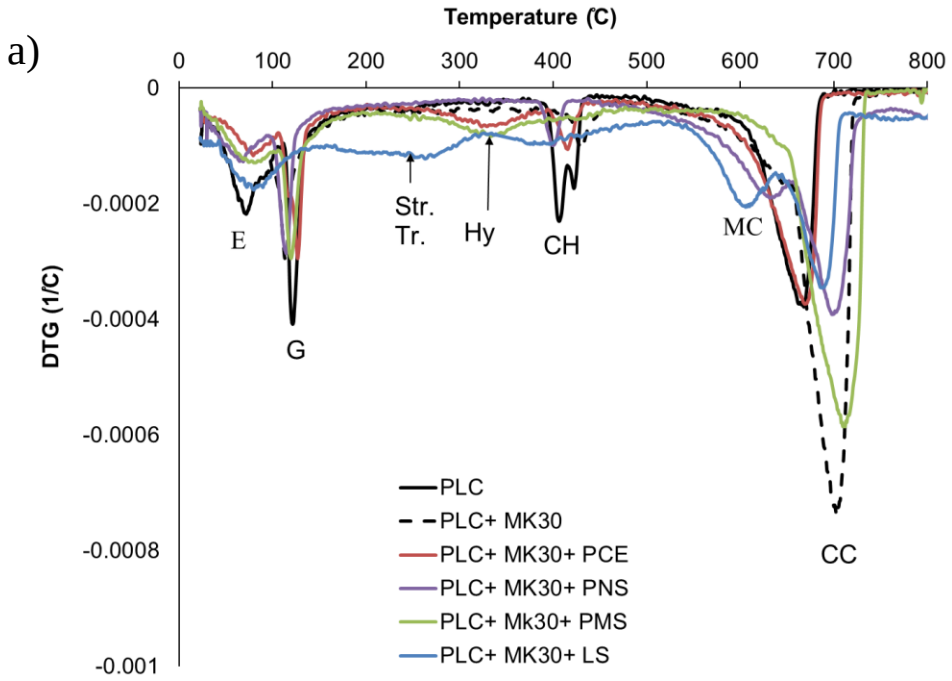

b)

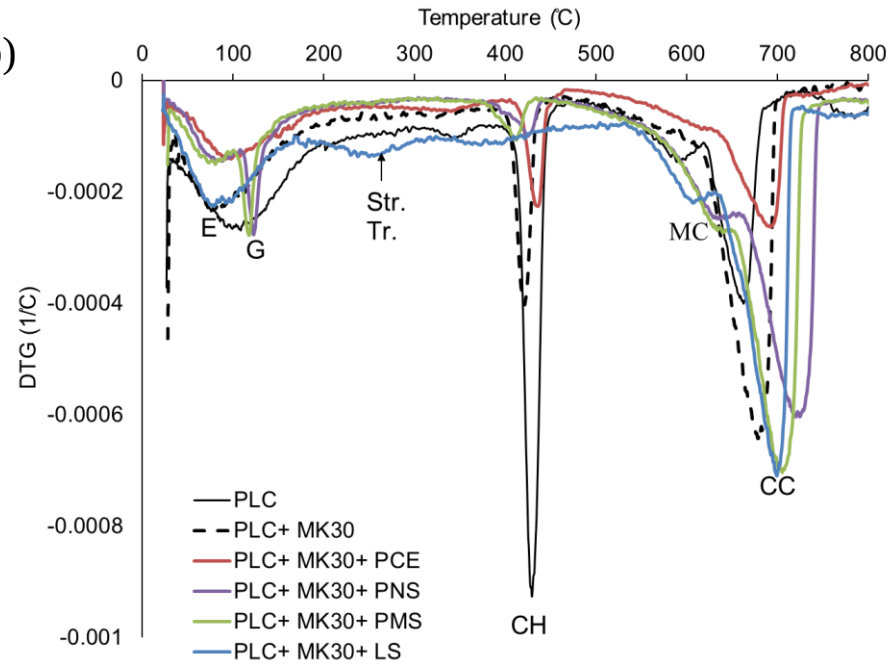
Temperature (℃)
0
100
200
300
400
500
600
700
800
0
-0.0002
-0.0004
-0.0006
-0.0008
-0.001
DTG (1/C)
E
G
Str.
Tr.
CH
MC
CC
PLC
PLC+ MK30
PLC+ MK30+ PCE
PLC+ MK30+ PNS
PLC+ MK30+ PMS
PLC+ MK30+ LS

c)

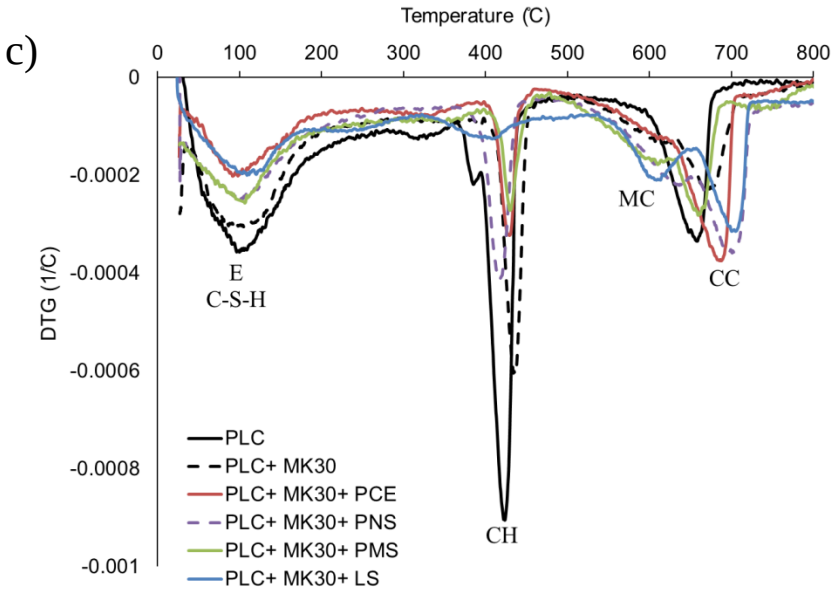
Temperature (℃)
0
100
200
300
400
500
600
700
800
0
-0.0002
-0.0004
-0.0006
-0.0008
-0.001
DTG (1/C)
E
C-S-H
CH
MC
CC
PLC
PLC+ MK30
PLC+ MK30+ PCE
PLC+ MK30+ PNS
PLC+ MK30+ PMS
PLC+ MK30+ LS

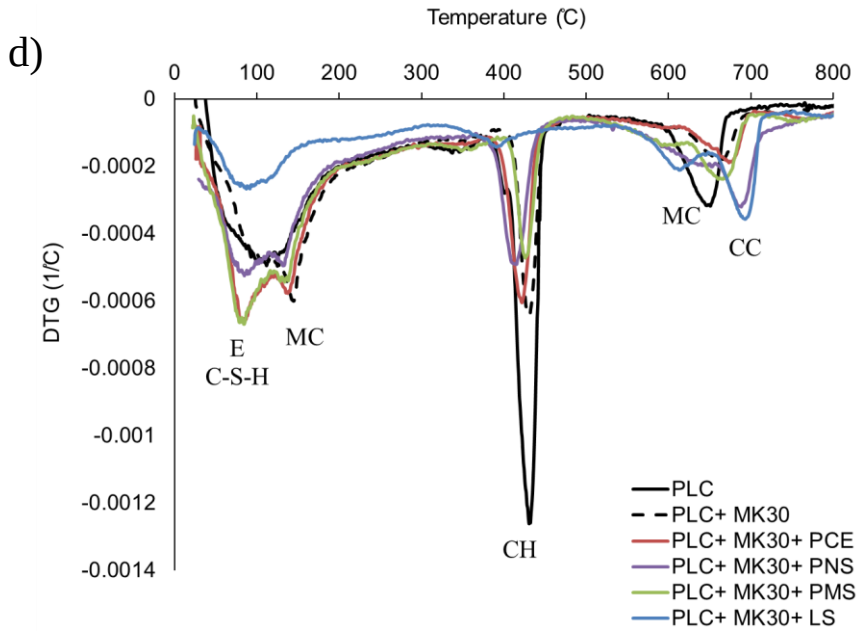

Figure 3.12. Time derivative of the mass loss as a function of temperature for MK30 samples with each WRA at a) 2 hours b) 6 hours c) 12 hours and d) 48 hours. G: gypsum, E: ettringite, Hy: Hydrogarnet, Str.: Stratlingite, Tr.: Tetra calcium aluminate hydrates, MC: m

Calcium hydroxide contents for each paste are calculated from the TGA data at 2, 6, 12, 24, and 48 hours (Equation 3.1). From these trends in Figure 3.12, it can be seen PLC mix has the highest CH content at all ages compared to the MK30 mixes due to the higher cement content. Moreover, all WRAs retard the early formation of calcium hydroxide, at least up to 12 hours. However, by 48 hours, the CH content of all mixes are similar, with the exception of the LS mix where the portlandite content remains a much lower. The observation of 43-65% lower CH content in MK mixes with WRAs up to 12 hours, compared to the case of MK without WRAs, further demonstrates the retardation of cement hydration with WRA addition, since the pozzolanic reaction of MK at these early ages is small to negligible [20].

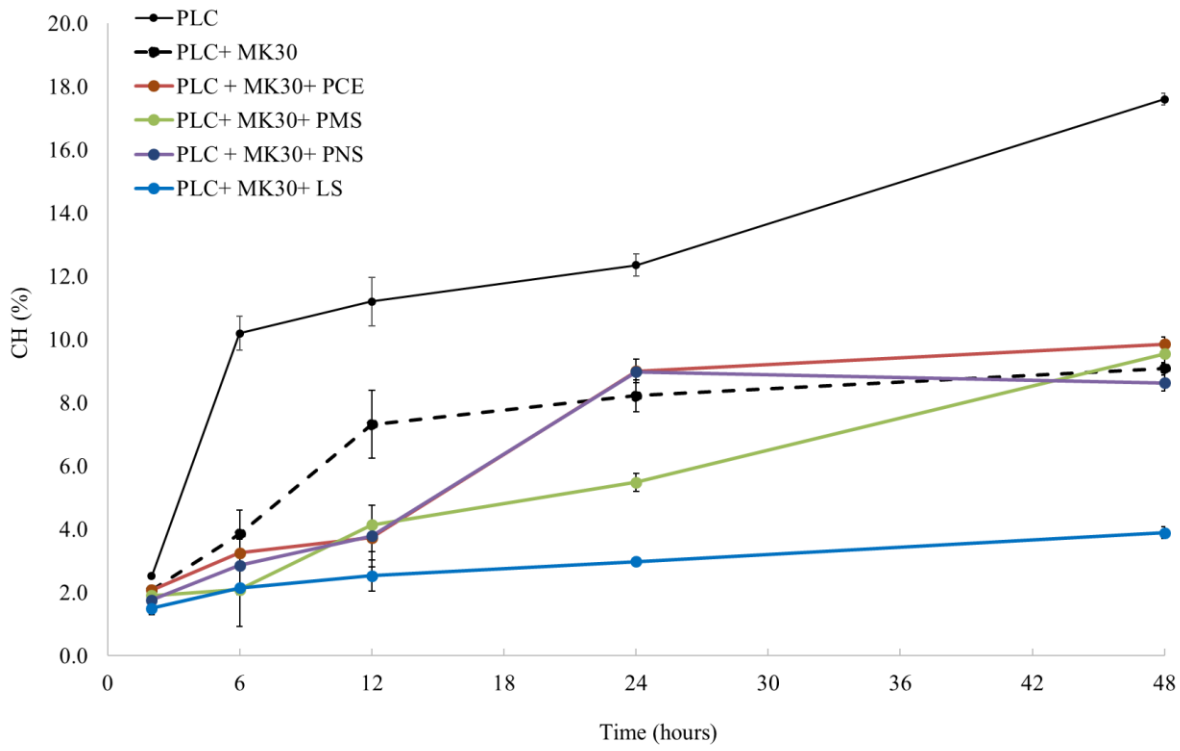

Figure 3.13. Calcium hydroxide content normalized by the paste weight at 600°C as a function of time for MK30 samples with each WRA

3.4.6 Time to set

This study used the Vicat apparatus to evaluate the effect of MK replacement and addition of each WRA on the setting time of mortar samples. Two MK substitution rates of 10% (MK10) and 30% (MK 30) by mass were chosen for measuring the setting time of MK mortar specimens. Mortar specimens were prepared with Types IL cement as a control specimen and Type IL cement with MK10 and MK30 with PCE, PNS, LS, and PMS, at the same dosage rates determined by the mini slump test. It should be noted that the MK30 with LS sets too quickly to measure the setting time

The initial and final setting times of mortars with PLC and PLC with MK10 and MK20 at w/b= 0.485 are shown in Figure 3.14. It was observed that the use of MK without WRAs shortens the initial and particularly the final setting times, which is consistent with prior findings [61]. The MK10 mortars showed a similar initial setting but a 40-min shorter final setting time compared to that of PLC mortars. The mortar samples with MK20 showed that both initial and final setting time of mortars were both shorten by about 40 mins. The mortar specimens with MK30 and no WRA were not workable enough for the Vicat test. The shorter set time of MK mortars can be due to the higher surface area of MK particles that provides more nucleation sites for the cement hydration that accelerates the hydration process. The shorter setting time of MK mortars, particularly the final setting time, can cause issues with finishing the concrete in the field.

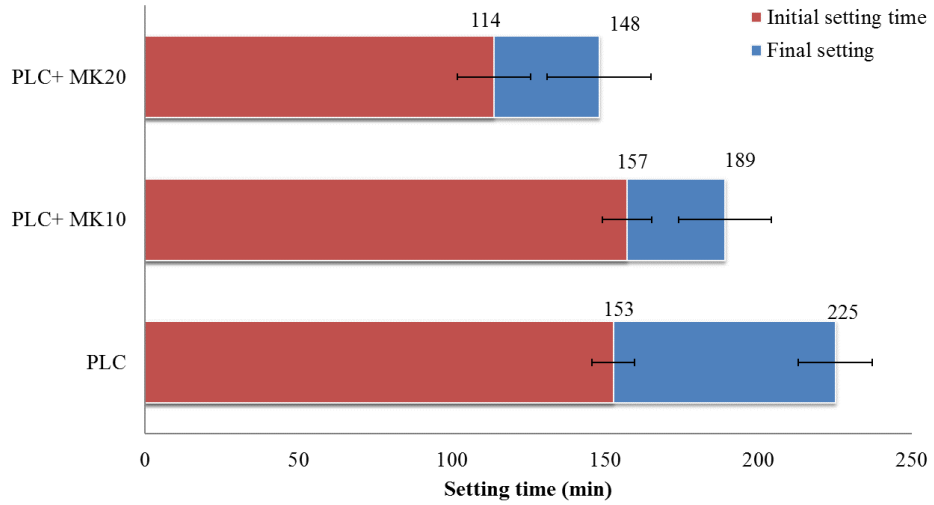

Figure 3.14. Setting time data for and Type IL cement mortars and Type IL blended with MK substitution of 10 and 20% by mass

Adding the appropriate dosage of WRAs, determined in the mini slump test, can result in setting times closer to those for the reference mortar specimens (i.e., no MK). The effect of each WRA on the setting time of MK mortars on MK 10 was measured (Figure 3.15a). The MK10 mix with no WRA shows the initial setting time similar (~ 4mins shorter) and the final setting of 40 mins shorter compared to that of PLC mortar. The MK10 mix with PMS shows the highest effect on increasing the setting time of mortars. The LS mix showed a shorter setting time compared to PLC mortars that can be due to the accelerated reaction of C_3A happens in LS mix as it was observed in calorimetry results (Figure 3.9). Similar results were observed for MK20 specimens, however, the effect of WRAs on MK20 on increasing the initial setting of specimens were more significant (Figure 3.15b). The MK20 with no WRA shows the further decrease in both initial and final setting time by about 30 mins compared to that of PLC mortar. The initial setting time of MK20 mortars with WRAs was similar to that of PLC while the final setting time of mix with PMS showed the longer final set time (20 mins) and the LS mix showed the shortest final set (~ 85 mins) compared to PLC mortar.

Figure 3.15c shows the effect of WRAs on the setting time of MK30 specimens. It should be noted that MK30 mortar was not workable enough to measure the setting time.

The WRAs, except PMS, were not able to increase the setting time of MK30 mortars enough to be close to that of control specimens.

a)

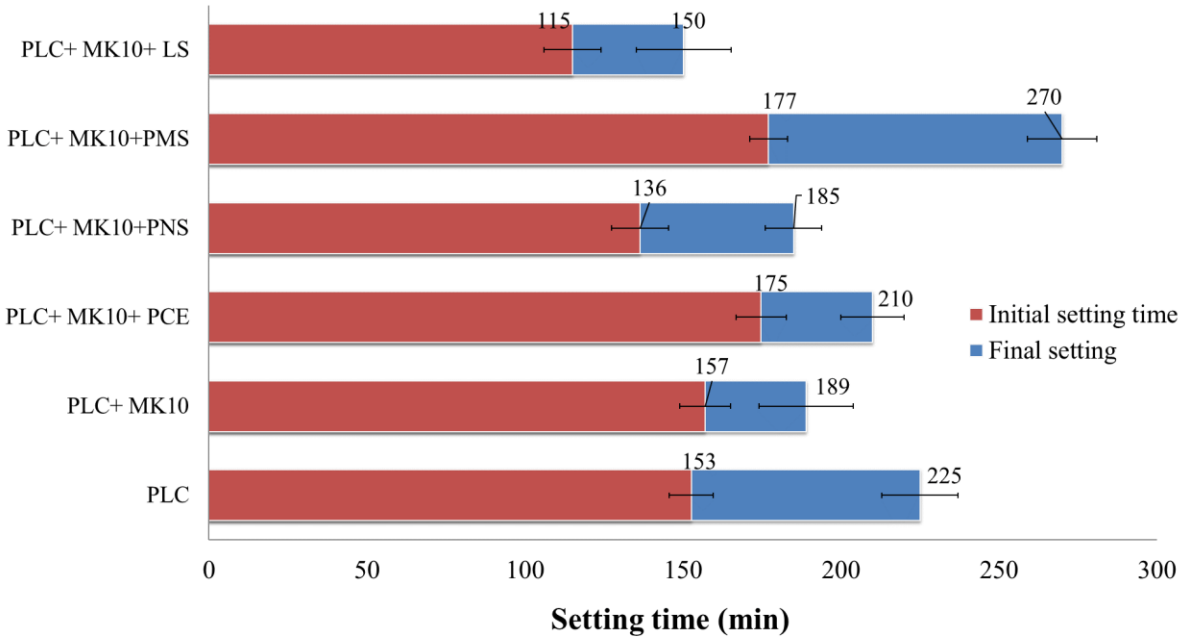

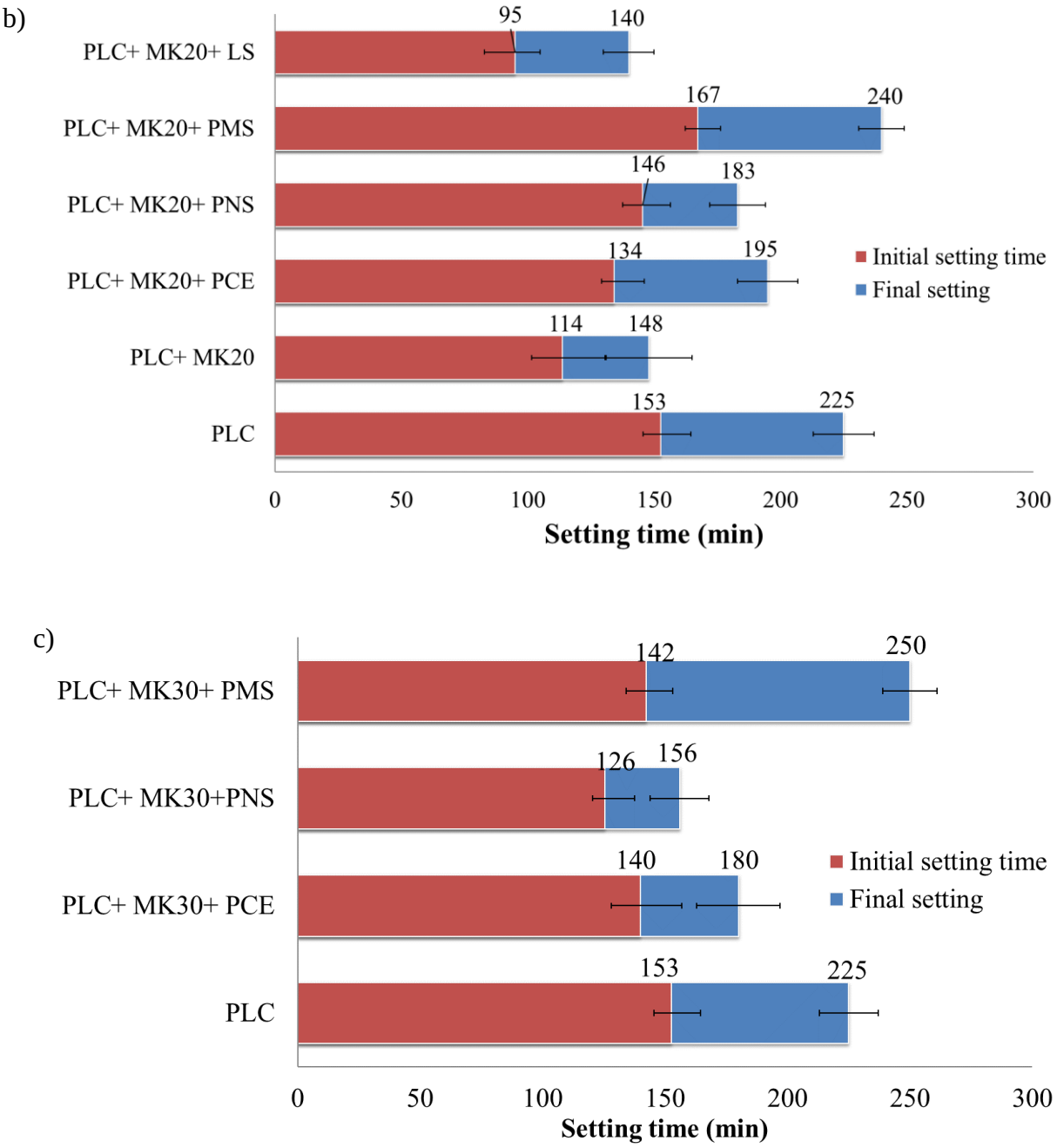

Figure 3.15. Setting time data for Types IL mortar specimens and Type IL cement with 10, 20, and 30% MK prepared with each type of WRAs

ASTM C494 [85] has physical requirements for mixes with WRAs to be accepted for use in concrete. One of the requirements of WRAs mixes is that the setting time of WRA mixes should not be more than 1 hour earlier nor than 1:30 hour later than those of the control specimen. In this study, specimens with MK10 and MK20 and LS showed the

setting time of 75 and 85 mins shorter than that of PLC mortar respectively and do not pass the ASTM C494 requirement. The MK30 specimen with PNS mix showed the final setting time of 69 mins shorter that the PLC mortar and does not pass the ASTM C494 requirement either. The conclusion here is that LS cannot be used for MK10 or 20 specimens and PNS cannot be used with MK30 specimens. PMS and PCE can be used for PLC mixes with 10, 20, and 30% MK.

The relation between the setting time data and time to maximum rate of heat evolution from calorimetry data is shown Figure 3.16. A correlation was observed for MK10 and MK20 specimens that with increase in the time to the peak of hydration, the setting time is increased as well. This correlation was not observed in MK30 specimens.

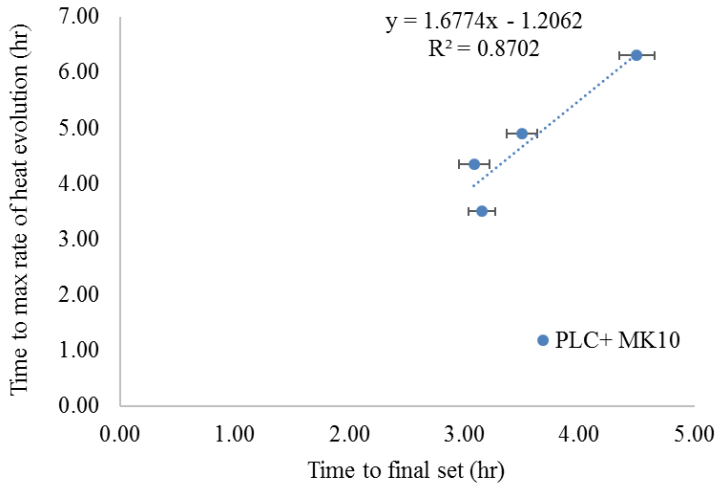

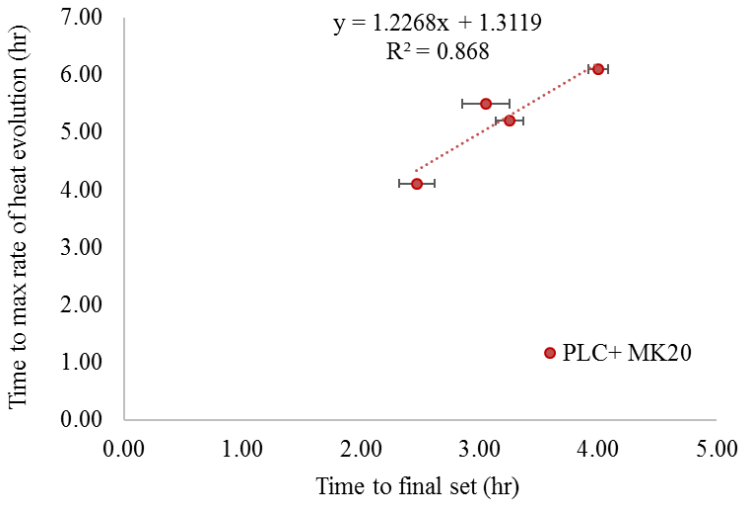

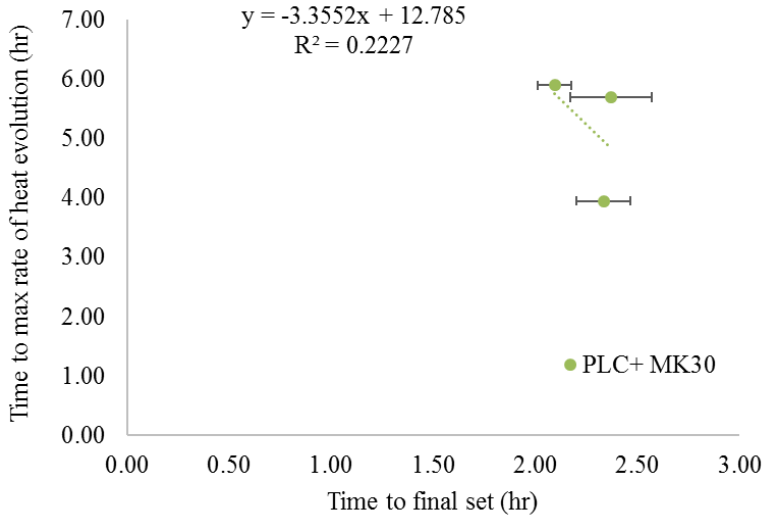

Figure 3.16. The correlation of time to final set and the rime to maximum rate of heat evolution from calorimetry data for MK10, MK20, and MK30

3.4.7 Life cycle assessment

Life Cycle Assessment (LCA) was used to evaluate the sustainability and compare among PLC-MK blends among different binders in concrete. The LCA study estimated the

energy and GHG emissions that can be saved by replacing portland cement with PLC and when PLC is combined with metakaolin at 10 and 30% by mass. The databases used for the LCA study were Simapro database, EIO-LCA, and previously published data [191-193]. The analysis considers the paste fraction only and assumes 1:1 replacement by mass.

It was observed that (Figure 3.17) the substitution of PLC (with up to 15% limestone) for ordinary portland cement can save up to 15% in the embodied energy and GHG emissions, as might be anticipated given the clinker fraction reductions. Moreover, blending PLC with MK further reduces the embodied energy and GHG emissions by up to 16-20% when MK10 and MK30 by mass are used with PLC.

Moreover, it was observed that contribution of metakaolin to GHG emissions and embodied energy is much lower than that of cement or PLC, with up to 18% to the embodied energy and 9% to GHG emissions. Because of the greater fineness of MK and some PLCs compared to portland cement, their use may require higher dosages of superplasticizer to achieve adequate workability. Therefore, the contribution of WRA was considered. The admixture used in this study was polycarboxylate ether (PCE). It was found to contribute up to 3% to the embodied energy and up to 11% to the GHG emissions in MK30 mixes.

a)

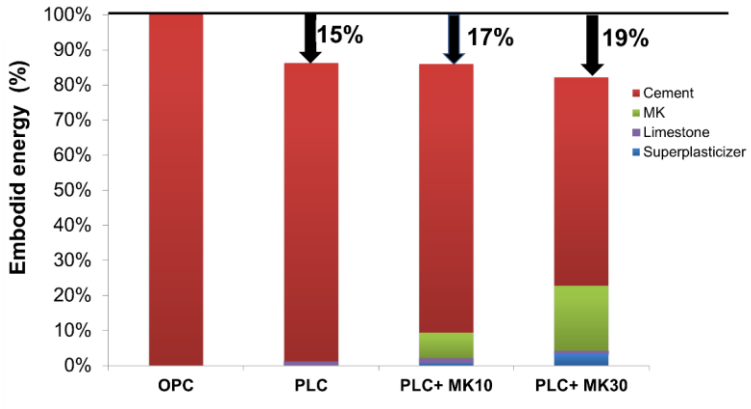

b)

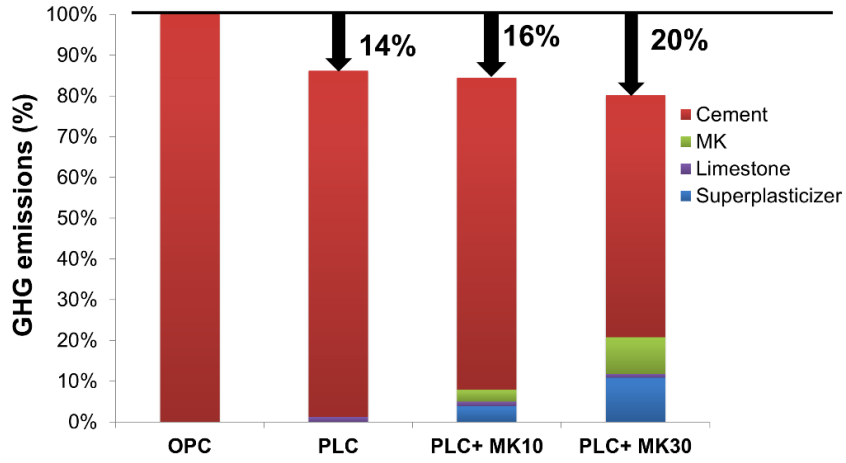

Figure 3.17. The life cycle assessment of cementious materials and admixtures a) embodied energy b) greenhouse gas (GHG) emissions

3.5 Conclusions and discussions

This chapter investigated the early-age hydration, phase development, and setting time of the metakolin-limestone blended cements with 10, 20, and 30% metakaolin. Moreover, the use of finer metakaolin particles requires the use of WRAs, and therefore the effect of WRAs chemistry on hydration and phase development of metakaolin-blended cements were evaluated. Finally, LCA considered the changes in binder composition and the use of WRAs on the embodied energy and GHG emissions in the concrete paste fraction.

The isothermal calorimetry results show that metakaolin inclusion accelerates the cement hydration and increase the rate and total heat of hydration of the cement. The accelerated hydration can be due to the nucleation effect of MK being dominant in the first 48 hours of cement hydration. Based on the calorimetry results, different WRAs have significantly varying effect on cement hydration and microstructural development of portland limestone cement-metakaolin pastes. The WRAs generally delay the cement hydration with the exception of the LS mix that the hydration was highly accelerated. The delay in the hydration can be attributed to the decrease in the C_3S dissolution rate in the presence of WRAs [152].

One key observation in this study is the high early peak of heat evolution in the isothermal calorimetry performed for MK30 with LS mix. This peak occurs 5 hours earlier than in the MK30 paste and can be interpreted, considering also the XRD and TGA data, to result from accelerated C_3A hydration and catalyzed formation of ettringite at early ages. Significant adsorption of LS on C_3A has been observed in previous studies, such that C_3A was described as "a sink" for that admixture [194]. The increase in the solubility of gypsum in the presence of LS reported in previous studies was also observed in the XRD and TGA data in this study, with the gypsum peak present in all samples at 2 hours *except* the LS sample [100]. The accelerated peak in the LS solution can be due to the increased solubility of gypsum in pore solution that accelerates the ettringite formation. It can also be presumably a result of a catalyzing ability of lignosulfonate in templating the ettringite formation. It has been reported that some small anionic groups, such as organic sulfonates derived from LS and PMS, can substitute in the ettringite structure (forming a lamellar structure), which contributes to the shift in peaks associate with ettringite (as noted in the

presentation of the XRD data). These sulfonate groups can also be incorporated into hydrated calcium aluminates, accelerating ettringite formation [20]. This can explain the ettringite peaks at 25° in LS and PMS mixes at 6 hours. In addition to the changes in C_3A hydration kinetics, data suggests that LS played a role in inhibiting the conversion of stratlingite (C_2ASH_8) and tetracalcium aluminate hydrate (C_4AH_{13}), to the stable phase, hydrogarnet (C_3ASH_6). This could occur by LS adsorption onto the metastable hexagonal products and prevents their conversion to the hexagonal stable phases [195]. This effect was observed in the TGA data and XRD patterns (Figures 3-12 and 3-13) where stratlingite peaks were observed in LS mixes at 2 and 6 hours, but were not observed in any other mix at any age. The TGA data shows that the hexagonal stable phase, hydrogarnet, was observed in PMS and PCE mixes at 2 hours; however, hydrogarnet was not detected in the XRD pattern probably due to the lower fraction of this phase in the mix.

The delays on calcium silicate phase hydration were observed in both the PMS and LS mixes, but the extent of the retardation was greater with LS. The XRD patterns show that while the C_3S peak at 23° does not appear in the control mix (with no admixture) after 2 hours, this peak persisted in the PMS mix up to 6 hours and up to 48 hours in LS mix. Additionally, the lower CH concentration in LS and PMS mixes up to 24 hours (Figure 3-14) further confirms the delayed silicate phase hydration. The adsorption of WRAs molecules on cement grain surfaces during the dissolution of Ca^{2+} ions can then lead to the formation of a surface complex around those ions in the pore solution. This complexation retards the nucleation and precipitation of hydration products [101] and occurs as soon as WRAs come into contact with Ca^{2+} ions.

The PNS admixture produced delays in C_3A hydration by 3 hours, which has been documented by other researchers as well [196]. This effect was also observed in the TGA data, with ettringite peaks not observed even after 6 hours (Figure 3-12). Based on calorimetry, thermogravimetric and XRD measurements, the PNS admixture did not appear to have an effect on hydration of the calcium silicate phases, although in a previous study found retardation of calcium silicate hydration with PNS [195]. The XRD data shows no C_3S peak at 23° in the PNS mix even at even at 2 hours, and the intensity of the C_3S peak at around 29° (which is a main peak for C_3S) decreases as the hydration reaction proceeds.

Of the four admixture chemistries examined, the PCE that appears to be the most effective admixture in increasing the workability of metakaolin-portland limestone cement blends paste and dispersing the cementitious materials without significantly altering the hydration kinetics. The calorimetry data shows delayed hydration of both silicate and aluminate phases by about 2-3 hours in the first 6 hours of hydration. However, after 6 hours, reaction of C_3S is apparent through XRD, which a decrease in C_3S in the PCE mixes. While the amount of calcium hydroxide (CH) formed in PCE mix was lower than that of control mix by up to 12 hours (Figure 3-11), the CH content of PCE mix is similar to and higher than that of control mix by 24 and 48 hours, respectively. The lower ettringite peak for the PCE mix at 6 and 12 hours (Figure 3-11b and c) suggests the effect PCE on delaying the hydration of the aluminate phase in PCE mixes. The XRD data at 48 hours (Figure 3-11d) shows that the peak for ettringite at 8.9° is similar to that of control mix.

The Vicat test was used to evaluate the effect of MK on the initial and final setting time of MK mortars. Moreover, the effect of each WRA on mortar setting time was evaluated. The use of MK without WRAs shortens the initial and particularly the final setting times.

The use of WRAs showed to increase the setting time of PLC-MK blends mortars to be close to that of control sample. The setting time of MK 10 and MK20 mortars with PMS showed the longest setting time and mixes with LS showed the shortest. For MK30 mortars, the mortar specimen with the PMS was the only mix with setting time close to that of control mortar. The delay in the setting time of mortars with PMS can be due to the delay effect of PMS on the C_3S hydration as it was shown in XRD and TGA data. The shorter setting time of LS can be related to the accelerated cement phase reaction in presence of LS as it was observed in calorimetry and TGA data. The use of LS for MK10 and MK20 and PNS for MK30 mortars did not meet the ASTM C494 and cannot be used in combination [85].

The LCA results show that the replacement of cements by MK can save the GHG emissions and embodied energy up to 20% when MK30 is used. The contribution of MK and PCE admixture to GHG emissions and embodied energy is much lower than that of portland cement.

This study suggests the use of PCE admixture as a WRA PLC-MK cements particularly when MK is used at higher rates (>10% by mass). The required dosage of WRA should be determined and its effect on cement hydration and phase development should be evaluated.

CHAPTER 4 HYDRATION OF METAKAOLIN-PLC BLENDS: EXPERIMENTS AND MODELING

4.1.Introduction

The pattern of heat development during hydration is a key parameter in determining the concrete microstructure development, setting behavior, mechanical property evolution, long-term durability, and potential for cracking. For example, in mass concrete undesirable temperature development may lead to cracking in concrete and compromise the concrete durability and serviceability [197]. In cold-weather or hot-weather concrete construction, knowledge of the rate of hydration can be useful for predicting setting and hardening rates, vital information in construction scheduling.

Many factors affect the cement heat development in concrete. These include water-to-binder ratio (w/b), cement composition and fineness, supplementary cementitious material (SCMs) composition, fineness, and dosage, and types and dosages of chemical admixtures. In concrete, other factors include the fraction of cement, the types of aggregate used, curing practices, and environmental conditions, among other variables.

In the evaluation of the ultimate heat development in different concrete mixtures, a primary step is the monitoring and measurement of the early age heat of hydration. Isothermal calorimetry is commonly used to measure and record the heat release rate for cement paste or mortars at a constant temperature. In comparison, adiabatic calorimetry measures the heat development of a concrete mixture when carefully isolated to prevent heat exchange with its environment; as a result, this is more difficult to achieve reproducibly in laboratory conditions. With the difficulties in isolation and variation in the

adiabatic measurement results, the use of isothermal calorimetry on paste and mortars samples has become more common.

As introduced in Chapter 2, the heat of hydration of cement largely depends on its chemical and physical properties. It is known that the hydration of C_3A and C_3S are rapid and highly exothermic and contribute the most to the cement heat of hydration. Moreover, the fineness of cement can affect the rate and extent of cement heat of hydration, with the finer cement showing higher early heat evolution and under appropriate curing conditions greater overall heat of hydration. The finer cement has a higher surface area-to-volume ratio giving a higher contact of cement with water that result in a higher heat of hydration.

Supplementary cementitious materials (SCMs) generally release heat at a lower rate than that of portland cement and are less exothermic in their reaction than the cement that they partially replace. The heat production of SCMs is a function of their type and replacement levels.

The use of chemical admixtures, particularly accelerators and retarders, can affect the cement hydration rate and heat development. water-reducing admixtures may work as retarders, Types D and F, or accelerators, Type E [85], can increase the cement heat of hydration rate. High-range water-reducers (HRWAs) usually work as retarders and can slow cement hydration and heat development rates.

The water-to-binder ratio (w/b) affects the rate and extent of cement hydration. With higher w/b, more water is available for the cement to react with, and thereby, higher of heat of hydration is evolved ultimately [198].

In addition, to monitoring the rate and extent of early hydration, isothermal calorimetry data can be further used to estimate or predict the degree of hydration of cements and cementitious materials. The degree of hydration, $\alpha_{(t)}$, is the fractional amount of cement that has reacted at a particular time (t) and varies between 0 at the initial time and 1 when the hydration is fully completed. Chapter 2 thoroughly reviews historical and modern approaches to hydration modeling, based upon isothermal calorimetry, and the reader is referred to Equations 2.6-2-11 presented there as a basis for the approach taken in this chapter.

In this research effort, the degree of hydration results are used to evaluate the influence of metakaolin substitution on the degree of hydration of the cement, $\alpha_{(t)}$. The physical effects of metakolin including dilution, nucleation, and filler effects are expected to increase degree of cement hydration as they increase the effective water-to-cement ratio and provide more sites for nucleation during early hydration. However, until now, MK has not been accounted for in existing hydration models.

4.2.Modeling Approach and Motivation

To estimate and compare the degree of hydration of cement and metakaolin blended cements used in this study, the Schindler equations (Equations 4-2 and 4-3) were used to estimate the total heat of hydration of two portland cements, two PLC sources, one Type V, and one Type II/V plain and each of these blended with MK at 10, 20, and 30% by mass. The cumulative heat of hydration of cementitious materials after 7 days was measured using isothermal calorimetry performed at 25 °C. Then, the degree of hydration was calculated by dividing the measured heat of hydration, by the total heat of hydration for cement that is fully hydrated (Table 4.1).

The use of the Schindler equations, which are commonly used for portland cement alone or blended with fly ash and/or slag, resulted in underestimations of heat of hydration for MK-blended systems, compared to their measured heat of hydration. This results in predicted degrees of hydration of greater than one, which are clearly not realistic.

One of the reasons for this discrepancy is coming from the fundamentally flawed assumption in previous studies that pozzolanic materials do not contribute to the heat of hydration. In contrast to most other SCMs, MK is known to increase the heat evolved in early cement hydration as it was shown in Chapter 3 (Figures 3.7 to 3-9). Another reason for underestimation of cumulative heat in previous models is that these models only considered the chemical compositions of cements that can contribute to the cement hydration while physical properties of cements such as fineness and particle size distribution showed to affect the cement heat of hydration. Zayed et al. [75] evaluated the effect of fineness on the cement hydration by comparing the heat of hydration of cements with different fineness but same chemical compositions. The findings of this study indicate that the heat of hydration calculated from the heat index limit introduced by ASTM C150 as "$4.75C_3A+ C3S<100$" for a particular cement (i.e. Type II (MH) cement) does not reliably correspond to the measured heat of hydration of the cement determined by isothermal conduction calorimetry. Blaine fineness and particle size distribution of portland cements were found to affect the heat generated by cement on hydration [75]. This study suggested a limit on the Blaine fineness of cements beyond Types II and IV cements. The limit of 240 m^2/kg for Types II/IV cements fineness was first added to the ASTM C150 in 2007 [76] and later increased to 245 m^2/kg in 2009. Similarly, AASHTO M85 also has a limit of 430 m^2/kg on the finesse of Types II and IV.

This difference demonstrates the need for a new model for estimating the heat evolution of the metakaolin-blended cement that considers the effect of MK on the early hydration.

Table 4.1. Predicted total heat of hydration (H∞), measured total heat of hydration H(t) and degree of hydration at 7 days for each mix using Riding et al. 2013 (Equations 2-2 to 2-4)

Cement Type	Cement Mixture Nomenclature	H∞, J/g	$H_{(t)}$, J/g	Degree of hydration at 7 days	$H_{(t)}/\rho_{MK}$, J/g
ASTM C150 Type I and blends	A	452.3	309.0	0.64	
	A+ MK10	407.3	353.0	0.78	290
	A+ MK20	362.1	384.1	0.96	300
	A+ MK30	315.2	430.1	1.16	270
ASTM C595 Type IL and blends	AL	414.8	301.1	0.69	
	AL+ MK10	378.9	297.3	0.83	280
	AL+MK20	336.9	305.0	1.02	295
	AL+ MK30	294.8	349.7	1.22	252
ASTM C150 Type I and blends	C	564.4	334.2	0.78	
	C+ MK10	507.7	410.3	0.97	420
	C+MK20	451.34	373.6	1.21	410
	C+ MK30	394.9	326.9	1.50	403
ASTM C595 Type IL and blends	DL	445.3	333.3	0.68	
	DL+ MK10	400.7	379.5	0.85	390
	DL+MK20	356.2	404.8	1.10	444
	DL+ MK30	311.7	443.1	1.37	423
1.1.1.1 ASTM C150 Type V and blends	E	464	337.1	0.72	
	E+ MK10	417.6	402.9	0.90	420
	E+MK20	371.2	445.7	1.24	410
	E+ MK30	324.8	456.6	1.38	397
1.1.1.2 ASTM C150 Type II/V and blends	F	453.5	318	0.72	
	F+ MK10	402.5	402	0.88	350
	F+MK20	363.1	426.4	1.10	400
	F+MK30	326.7	439.3	1.33	384

Next , the Schindler equations (Equations 2-6 to 2-8) and Riding et al. 2013 equations (Equations 2-9 to 2-11) were used to estimate the model fit parameters α, β, and τ used to predict the degree of hydration of metakaolin-blended cement after the first 7 days. The results (Figure 4.1) show that the data from this model was not a good fit to the experimental data, even for cements without metakaolin (Figure 4.1). This could be due to increased fineness and increased tricalcium silicate contents and reactivity achieved through increasing innovation in cement manufacture over the past decade, and the early dissolution and reaction of aluminate phase of MK [199, 200].

However, a more thorough parametric analysis is needed to fully isolate the factors contributing to the discrepancy between predicted and actual heat evolution in the neat pastes. It is also notable that the difference between the experimental data and Schindler model was even higher in mixes with metakaolin (Figure 4.1). In general, this model estimated the degree of hydration to be 10-40% lower than results from the experimental data for the cement pastes used in this study. This lower estimation, as it stated, is due at least in part to the assumption in previous equations that MK does not contribute to the cement hydration heat evolution. The mode recently developed model by Riding et al. [201] showed to overestimate the heat of hydration for neat cements and MK-blended cements. The reason can be that this model considers the effect of all admixtures, such as water-reducer admixtures or retarder admixtures, but in this study only one type of admixtures, HRWRA, was used. Another reason for this discrepancy is that this study did not consider the effect of MK neither the cement fineness in the suggested equations (Equations 2-2 to 2-4). The degrees of hydration of all mixtures from experimental data, and with using Schnidler model and Riding model are shown in Table 4.7.

The significant difference between the predicted degrees of hydration from the Schindler model and the experimental data reveals a need for improved models to predict the heat evolution in MK-PC and PLC-MK blends.

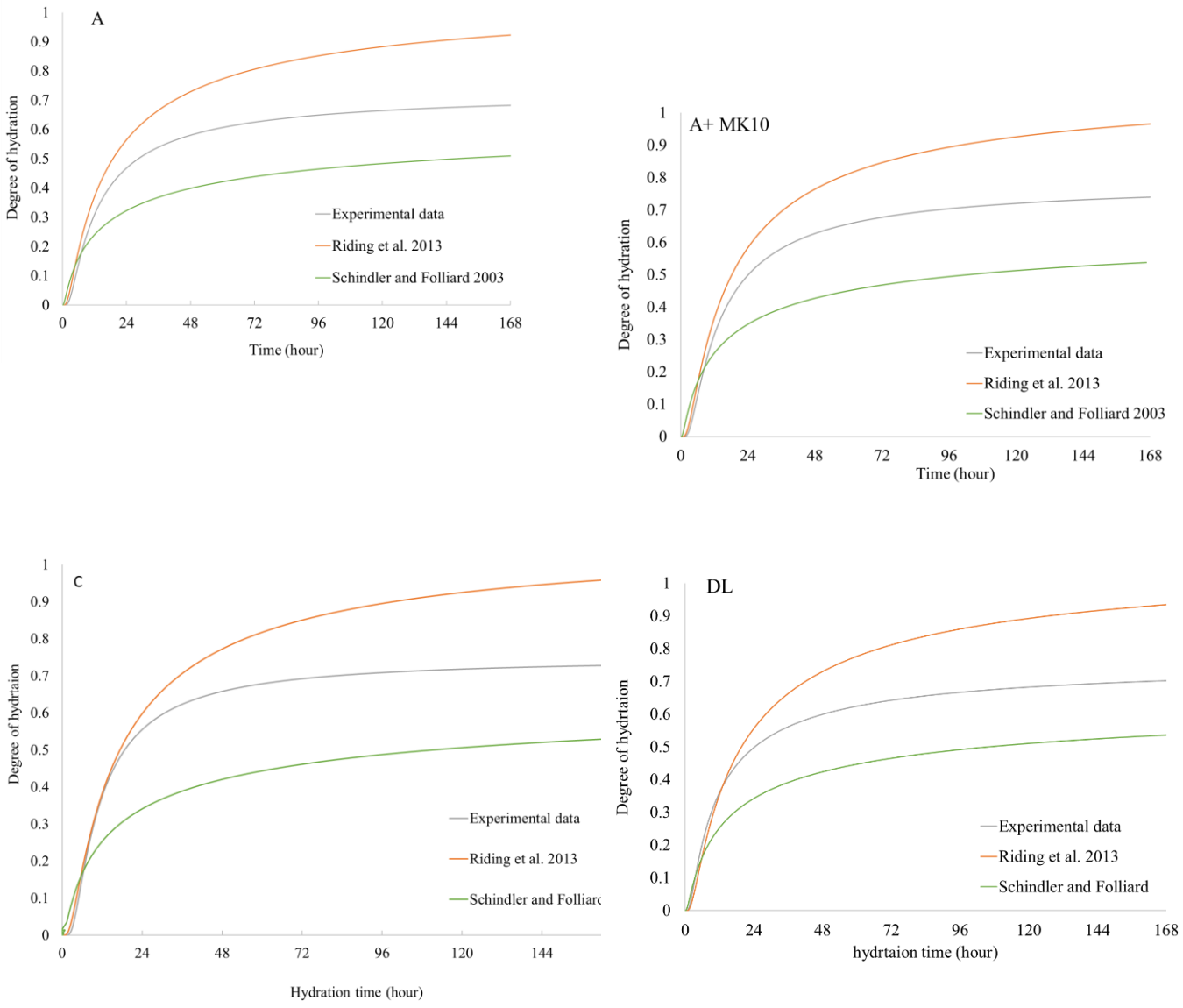

Figure 4.1. The degrees of hydration from experiments and predicted from Schindler et al. *[82]* model for cement pastes at w/b of 0.4 for Cement A, A+MK10, C, and DL

4.3.Materials and methods

This research monitors the heat of hydration developed during the first 7 days for 24 mixes of cement and cements blended with metakaolin. This study examines several cement compositions, including cements conforming to ASTM C150 Type I/II, III, V, and II/V and those conforming to ASTM C595 Type IL, and each of these blended with MK at 10, 20, and 30% by mass. The w/b used in this study was held constant at 0.40.The cement compositions, types, sources, and Blaine fineness are shown in Table 4.2. Composition was determined by oxide analysis and Bogue calculation for Types I/II, II/V, and V, and the adjusted equation (Equation 4.1) was used for Type IL cements.

$$X_f = X_b \times \frac{(100 - L - P)}{100} \qquad 4\text{-}1$$

High purity metakaolin (Burgess Pigment Company, Sandersville, GA) was used as a replacement for cement at rates of 10% 20%, and 30% by mass, denoted according to their MK content as MK10, MK20, and MK30, respectively. According to the results of the previous chapter (Ch. 3), PCE was the most effective admixture for MK mixes particularly at higher MK content, therefore, PCE admixture (Viscocrete 2100, SIKA) was used mixtures with MK for the heat of hydration modeling in this chapter. The required dosage of admixture was determined using mini slump test, as described in Chapter 3.

Table 4.2. The ASTM C150 or C595 cement Type, sources, Blaine fineness, and Bogue compositions.

Cement	Cement Type	Source	ρ_{C3S}	ρ_{C2S}	ρ_{C3A}	ρ_{C4AF}	ρ_{SO3}	ρ_{MgO}	ρ_{FreeCa}	ρ_{alkali}	Fineness (m2/kg)
A	I/II	Calera, AL &Roberta, GA	0.60	0.09	0.067	0.092	0.031	0.036	0.090	0.005	448
AL	IL		0.60	0.09	0.061	0.093	0.033	0.031	0.010	0.004	597
C	I/II	Holly Hill, SC	0.56	0.15	0.020	0.110	0.029	0.002	0.020	0.004	465
DL	IL	Theodore, AL	0.54	0.15	0.050	0.100	0.032	0.010	0.010	0.004	574
E	II/V	Victorville, CA	0.58	0.15	0.040	0.110	0.032	0.043	0.020	0.005	354
F	V	Leeds, AL	0.55	0.19	0.030	0.130	0.024	0.031	0.010	0.004	376

The heat of cement hydration was measured directly by the isothermal calorimetry for the first 7 days to calculate the total heat evolved at that time and to determine the degree of hydration.as used in previous studies as well [75, 202], The heats of hydration was measured by isothermal calorimetry according to ASTM C1679 [168]. The pastes were mixed externally following ASTM C305 [169]. Water-reducers, at the dosages determined by the mini slump, were each added first to the water and then the water and water-reducing admixtures was added to the cementitious materials. Pastes were mixed by hand mixer for 60s at a low speed, followed by mixing at medium speed for 60s. Two samples, each weighing 7.0 ± 0.5 g, were poured in to the plastic vials and then placed into the isothermal calorimeter. The calorimetry was performed at 25℃.

The ultimate degree of hydration was calculated for each mix, based upon its composition as determined by oxide analysis, using Equation 2-2. The degree of hydration was calculated by dividing the experimental ultimate heat of hydration by the calculated value. The hydration parameters of τ, β, $\alpha(u)$ were estimated by the best-fit model. The regression analysis was used to determine the independent parameters including cement composition, Blaine fineness, metakaolin content, and high-range-water-reducer admixtures (HRWRAs) dosage that may affect each of the hydration parameters. P-value analysis was used to quantify the significance of the correlation between the each hydration parameters and independent parameters with the lower p-value shows a higher correlation between a parameter and a hydration parameter. Finally, the linear multi-variant regression analysis was used to develop a model to predict the cement and MK-blended cements degrees of hydration based on the significantly related parameters.

4.4.Results

The ultimate heats of hydration of the neat portland and portland-limestone cements used in this study measured by calorimetry are shown in Table 4.1. Cement A has the highest heat of hydration, due to its higher tricalcium silicate phase content. The Type V Cement (Cement F) showed the lowest heat of hydration, as it was expected, due to the lower C_3S content.

Comparing the heat of hydration of neat cements and MK-blended cements (Table 4.1), the higher heat of hydration MK contains cement is correlated to the MK content. The MK heat per MK content is shown to be in the range of 290 to 444 J/ g with average of 363 J/g of MK. Previous studies show that MK contributes to the heat of hydration even after 7days with the total contributed heat of hydration to be 1.1 to 1.2 times higher at 28 days and 90

days compared to 7 days. Therefore, the MK heat is multiplied by the factor 1.15 to account for the further heat evolution of MK after 7 days, which is the maximum time of heat evolution measurement in this study.

The Riding et al. [201] equation was modified to account for the MK contribution to the heat of hydration. The proposed equation (Equation 4-2) was used to calculate ultimate heat of hydration the blended cement paste mixtures examined in this study:

$$H_u = H_{cement}.\rho_{cement} + 461.\rho_{slag} + 1800.\rho_{FA-CAO}.\rho_{FA} + 483\rho_{MK} \quad 4\text{-}2$$

4.4.1. Ultimate degree of hydration (α_u)

The degree of hydration, α, is a measure of the extent of the cement reactions with water. In practice, cement cannot be fully hydrated. Mills [203] reported that in most mixes, cement hydration stops before the cement is fully consumed. According to the Schnidler Equation (2-6), cements with the same w/b should have the same ultimate degree of hydration that does not hold true in field or laboratory experiments. It should be also noted that the ultimate degree of hydration, α_u, cannot exceed the theoretical value given by the following equation, which 0.4 is approximately the theoretical water–cement ratio necessary for full hydration, which is the sum of the chemically bound water ratio, about 0.25, and the gel water ratio, about 0.15.

$$\alpha_u \leq \frac{w/b}{0.4} \quad 4\text{-}3$$

This study used regression analysis to determine the independent variables affecting the ultimate degree of hydration of cements and MK-blended cements with considering a constant w/b ratio. The p-values of the parameters that are significant in determining the ultimate degree of hydration are shown in Table 4.3. The stepwise regression analysis only shows the parameters that are strongly related to the degree of hydration. It was observed that C_3S content, Blaine fineness, and MK content are significantly related to the ultimate degree of hydration. It should be noted that, while addition of HRWRAs can delay the cement hydration for the first 6-10 hours, their use was not found to affect the ultimate degree of hydration significantly.

Table 4.3. The p-values of the parameters related to ultimate degree of hydration showing that MK contents is highly related to the ultimate degree of hydration

Parameter	**P-value**
C_3S	1.18×10^{-5}
C_2S	
C_3A	
C_4AF	
SO_3	
Alkali	
Blaine	0.099
MK	3.63×10^{-8}
HRWRA	

Multi-variant linear regression analysis was used to develop an equation to predict the ultimate degree of hydration based on the significantly related parameters. Equation 4-4 shows the developed equation for the ultimate degree of hydration with an R2 of 0.90 for the 24 mixes used in this study. This equation shows that higher silica phase content of cements decrease the ultimate degree of hydration of the cements. The increase in the silicate phase increase the cement *potential* heat of hydration significantly (Equation 2.2),

while it may not have been achieved in the first 7 days, and that might be the reason for the lower degree of hydration with increase in the silicate phase content.

Blaine finenesses also increase the ultimate degree of hydration, as it increases the available surface area for the cement and water interaction and nucleation sites for early hydration products. The metakaolin addition increases the ultimate degree of hydration because metakaolin substitution for cement decreases the effective w/b (via a dilation effect) but also provides more nucleation sites for cement hydration.

$$\alpha_u = \frac{1.031 \times w/c}{0.194 + w/c} + \exp(-8.27\rho_{C3S} + 0.00255 \times Blaine + 1.69\rho_{MK}) \qquad 4\text{-}4$$

The developed equation (Equation 4-4) was used to estimate the ultimate degrees of hydration of cements and MK-blended cements used in this study (Table 4.4). Of those, Cement AL showed the highest ultimate degree of hydration owing to its higher fineness and C_3S content.

Table 4.4. The ultimate degrees of hydration for different types of cements and MK-blended cements

Cement mixture Nomenclature	α_u	Cement Type
A	0.71	Type I/II
A+ MK10	0.73	
A+ MK20	0.77	
A+ MK30	0.85	
AL	0.75	Type IL
AL+ MK10	0.75	
AL+MK20	0.81	
AL+ MK30	0.92	
C	0.72	Type I/II
C+ MK10	0.75	
C+MK20	0.81	
C+ MK30	0.91	
DL	0.73	Type IL
DL+ MK10	0.77	
DL+MK20	0.84	
DL+ MK30	0.98	
E	0.72	Type V
E+ MK10	0.74	
E+MK20	0.83	
E+ MK30	0.87	
F	0.72	Type II/V
F+ MK10	0.74	
F+MK20	0.79	
F+MK30	0.85	

4.4.2. Hydration slope parameter (β)

The hydration slope is one of the parameters in determining the degree of hydration of the cements that shows the rate of cement hydration in reaching the ultimate degree of hydration. The hydration slope, also referred to as the rate of hydration, is typically between 0.5 and 1.

Linear regression analysis was used to identify the parameters significantly affecting the hydration slope. Again, P-value analysis was used to show the significance of correlation of independent parameters to the hydration slope. Results (Table 4.5) show that the hydration slope influence by the amount of cement alkali content and calcium aluminate phases in the cement, cement alkali content, Blaine fineness, and the HRWRA dosage.

Table 4.5. The p-values of the parameters related to slope of hydration

Parameter	**P-values**
C_3S	
C_2S	
C_3A	
C_4AF	
SO_3	
Alkali	0.0068
Blaine	0.015
MK	
HRWRA	2.99×10^{-6}

The relationship of the hydration slope to the independent parameters (Equation 4-4) shows that the slope increases with increase in the cement alkali content, HRWRA dosage, and cement Blaine fineness. In cement manufacture, control of the Blaine fineness can change the slope of cement hydration. The addition of HRWRA was also shown to increase the rate of hydration (slope of hydration) due to the better dispersion provided. The R-square value of the equation below is 0.92.

$$\beta = \exp(-0.2855 + 102\rho_{alkali} + 33.862\rho_{HRWRA} + 0.00055Blaine) \qquad 4\text{-}5$$

4.4.3. Hydration time parameter (τ)

The hydration time is a parameter in quantifying the degree of hydration of cement over time that shows the time takes each cement to reach its ultimate degree of hydration.

The hydration time parameters shows the total time required for the cement to reach the ultimate degree of hydration. The parameters affecting the hydration time were determined using *P-value* regression analysis. The *P*-value analysis (Table 4.6) shows that the cement Blaine fineness and MK content along with the C_3A content are significantly related to the hydration time parameter.

Table 4.6. The p-values of the parameters related to the hydration time parameter (τ)

Parameter	***P*-value**
C_3S	0.14
C_2S	
C_3A	
C_4AF	
SO_3	
Alkali	
Blaine	9.074×10^{-5}
MK	
HRWRA	0.019

The relationship between the independent parameters and the hydration time (Equation 4-15) shows that an increase in the calcium silicate phase content and higher Blaine fineness decreases the hydration time, while increases in the HRWRA content increases it. Relative to MK-blends, neat cement pastes with higher C_3S phase can take a shorter time to hydrate while the use of HRWRAs retard the cement hydration and can delay the cement hydration and thereby increase the hydration time. The finer cements shows the higher rate of heat evolution and thereby a faster hydration and shorter time. The R^2 value of this equation, which is relevant to the cements with a high fineness (up to 597 m^2/kg), was 0.94.

$$\tau = \exp(3.45 - 1.12\rho_{C3S} - 0.0001\times Blaine + 33.182\rho_{HRWRA}) \quad 4\text{-}6$$

4.4.4. Degree of hydration

The three-parameter equation for the degree of hydration (Equation 4-16) is used to estimate the degree of hydration over time for each cement paste mixture. The independent parameters of α, β, and τ were estimated in the previous sections and t_e is the time in hours after the initial hydration started:

$$\alpha_t = \alpha_u . \exp(-[\frac{\tau}{t_e}]^{\beta}) \qquad 4\text{-}7$$

The predicted and experimental degrees of hydration for different cement types are shown in the following sections. The results of the degree of hydration at different ages of 24, 48, 72, and 168 hours, from experimental data as well as using previous models and the stepwise model used in this study are shown in Table 4.7 for Cement A and Cement A blended with MK. The results for other cements are shown in Appendix A.

Table 4.7. The degrees of hydration of Cement A and Cement A blended with MK from experimental data, previous models, and the stepwise model used in this study at different ages

	Degrees of hydration			
A	**24hr**	**48hr**	**72hr**	**168hr**
Experimental data	0.45	0.55	0.60	0.65
Stepwise model	0.48	0.60	0.65	0.71
Schindler and Folliard 2003	0.38	0.47	0.51	0.58
Riding et al. 2013	0.33	0.47	0.54	0.64
A+ 10%MK				
Experimental data	0.48	0.61	0.66	0.72
Stepwise model	0.48	0.62	0.67	0.74
Schindler and Folliard 2003	0.35	0.43	0.48	0.55
Riding et al. 2013	0.34	0.49	0.56	0.66
A+ 20%MK				
Experimental data	0.51	0.68	0.74	0.82
Stepwise model	0.48	0.64	0.70	0.78
Schindler and Folliard 2003	0.32	0.40	0.44	0.52
Riding et al. 2013	0.35	0.52	0.59	0.69
A+ 30%MK				
Experimental data	0.44	0.65	0.73	0.83
Stepwise model	0.46	0.65	0.72	0.81
Schindler and Folliard 2003	0.30	0.37	0.41	0.48
Riding et al. 2013	0.37	0.54	0.62	0.72

4.4.4.1.Type I/II cement

The predicted and experimental degrees of hydration of Type I/II cements (A and C) and blended with MK content of 10, 20, and 30% are shown in Figure 4.2. Good correlation between the experimental data and the predictions showing that this model is well applicable of predicting the degree of hydration of modern Type I/II cements.

The results also show that the ultimate degrees of hydration of these cements increase with the increase in the MK use at rates of from 10 to 20 and 30%, in both cements. Comparing the degrees of hydration of plain cement and MK blended cements shows that the increase in the MK content further increases the degree of hydration. The increase in the cement degrees of hydration in MK mixes can be due to the nucleation effect of MK that increases the cement hydration and also due to some exothermic reactions occurring that can be due early age reaction of aluminate phase in MK [64, 204] .

The increase in the degree of hydration with the increase in the MK content is more significant for Cement A, particularly for the MK30 case. The higher increase in the degree of hydration of Cement A with MK addition can be due to the lower degree of hydration of plain Cement A (0.64) compared to that of plain Cement C (0.69) at 7 days. The higher degree of hydration of Cement C can be, related at least in part to its higher surface area. It was also observed that the degree of hydration for both MK20 and MK30 combined with both cements were lower than that of the control mix (with no MK) for the first 24 hours, while after 48 hours the MK30 mix showed the highest degree of hydration. This delay in reaching the ultimate degree of hydration for metakaolin-blended cements can be due to the combined effect of dilution and the retardation effect of HRWRAs on the cement hydration. Particularly for cases with higher MK content that lower cement content and higher admixture dosages may have contributed to some retardation.

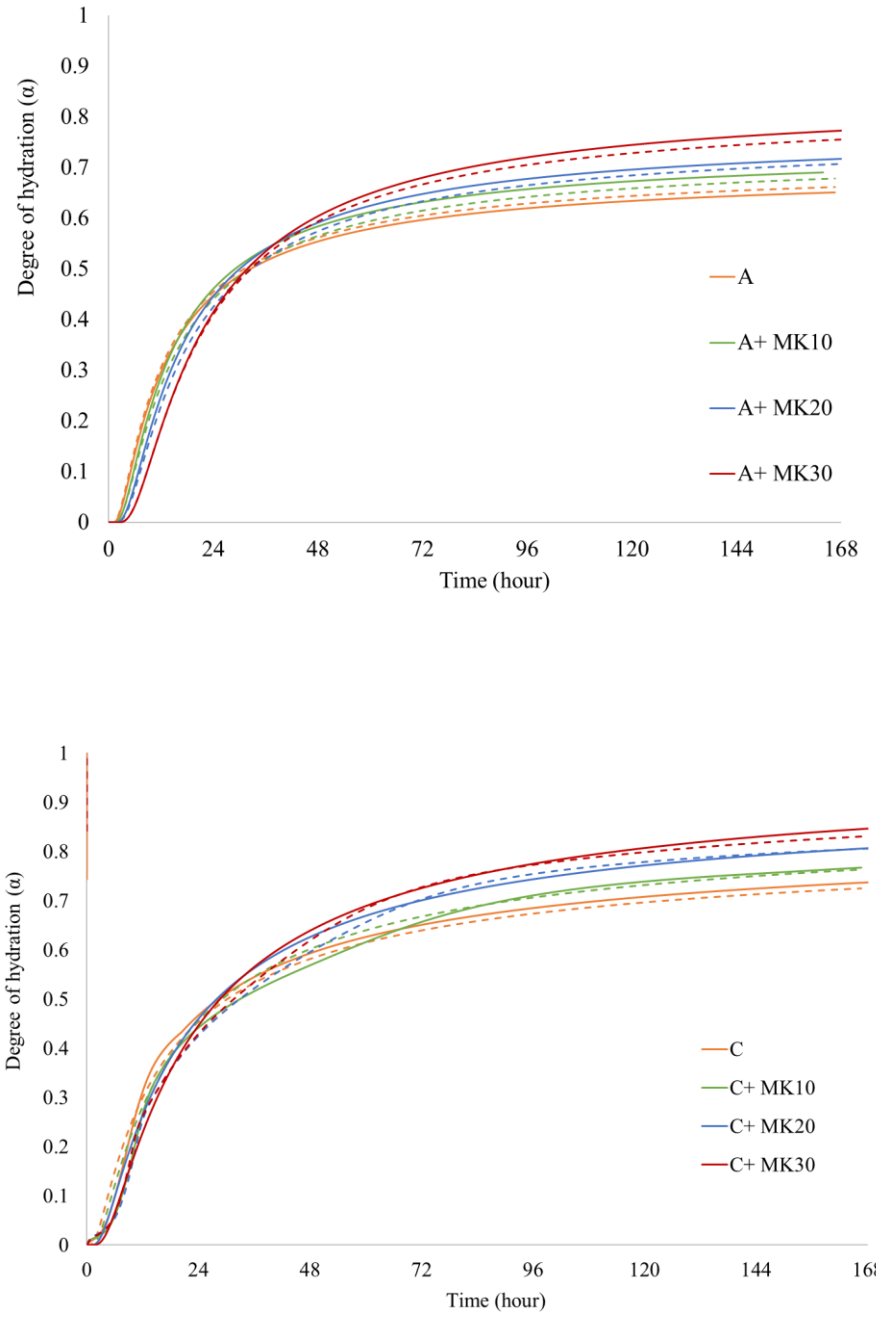

Figure 4.2. Degree of hydration of Type I/II cements (A and C) and MK blended cements, the solid lines showing the experimental data and the broken lines show the data from the model

4.4.4.2.Type IL cement

The predicted and experimental degrees of hydration of Type IL cements AL and DL, plain and blended with MK are shown in Figure 4.3. The similar results for the predicted and experimentally determined degrees of hydration further verifies the accuracy of this model in predicting the Type IL cement degree of hydration, among these compositions and at this w/b.

Comparing the degrees of hydration of plain cement and MK blended cements shows that the increase in the MK content further increases the degree of hydration. The increase in the cement degrees of hydration in MK mixes can be due to the physical and chemical effects of MK, as it was mentioned before [64, 204]. Moreover, it was observed that mixes with higher metakaolin content (i.e., MK20 and MK30) showed the lowest degrees of hydration in the first 24 hours. However, after 7 days, the MK30 mix showed the highest the ultimate degree of hydration. The lower early degrees of hydration of MK30 mixes can be related to the combined effect of dilution and the use HRWRAs that can act as retarders.

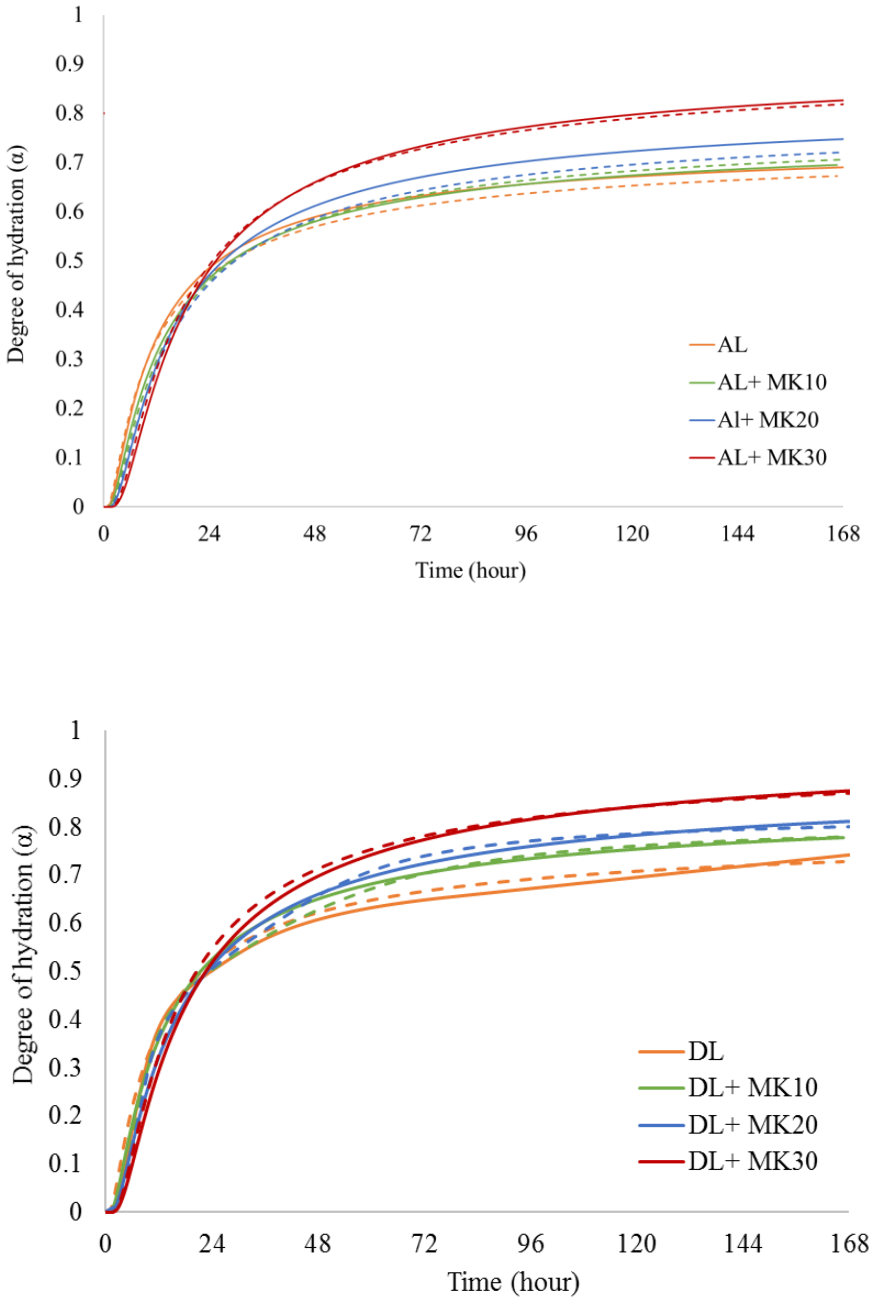

Figure 4.3. The predicted and measured degree of hydration of cement AL and DL limestone cement and blended with MK, the solid lines showing the experimental data and the broken lines show the predicted data

4.4.4.3.Types V and II/V cements

Cements E and F were tested to compare the predicted degrees of hydration with the experimental data for Type V and II/V cements, respectively. The results (Figure 4.4) show that the regression analysis model was capable of predicting the early age degrees of hydration of Cements E and F and Cements E and F when blended with MK. The predicted degrees of hydration of MK30 paste for cement F is lower (10-17%) than that of experimental data between 48 and 120 hours. The heat of hydration in this period is related to the C_4AF hydration, which might be delayed or inhibited by the HRWAs adsorption and was not accounted for in the model. The predicted ultimate degrees of hydration and experimental data for MK30 paste are similar after 7 days. Overall, the fits are reasonably good, for cements of these compositions at this w/b.

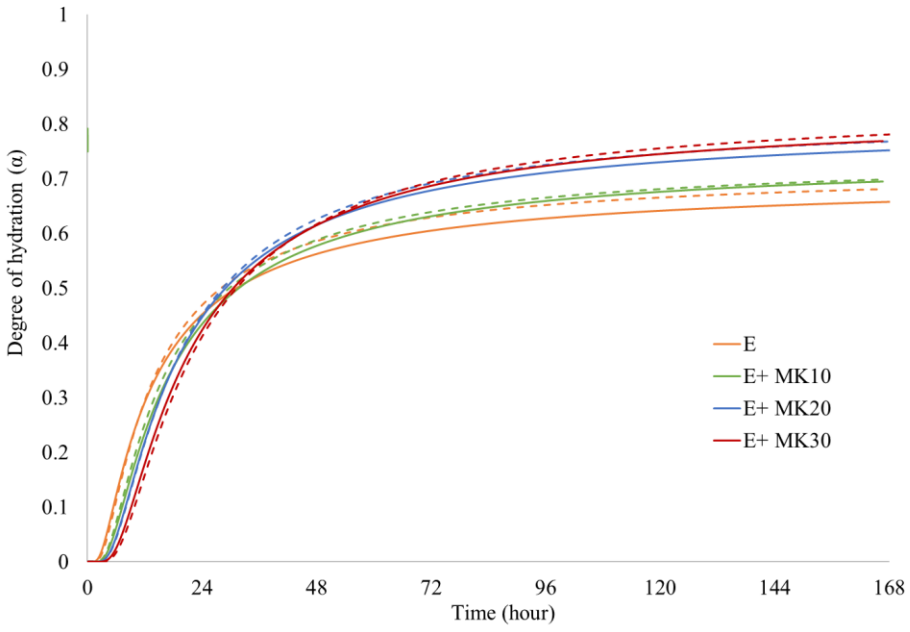

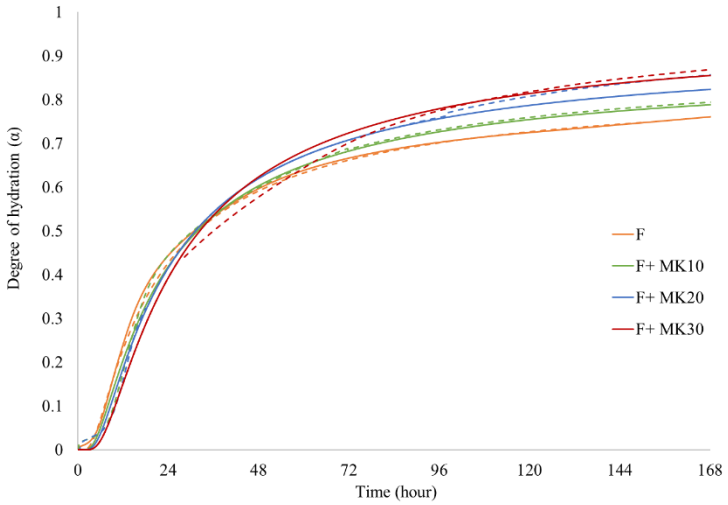

Figure 4.4. The predicted and measured degree of hydration of cement E and F and blended with MK, the solid lines showing the experimental data and the broken lines show the predicted data

4.5.Discussion

In this section, the effects of different parameters on the cement hydration model are discussed. Additionally, the validity of the developed model is evaluated using confidence interval analysis.

4.5.1. Effect of cement properties

The results of this study show that cement physical and chemical properties can affect the heat of hydration parameters, as has been observed in previous studies [80, 201]. The greater silicate phase contents in cements is shown to decrease the cement ultimate degrees of hydration. The hydration slope parameter showed to increase with an increase in the cement alkali contents. The underlying reason may be that the higher alkali content

in cement increases the cement phases dissolution rate and thus accelerates the cement hydration. The cement hydration time is affected by the cement composition, as the hydration time decreases with an increase in the calcium silicate phase content. The reason can be that with the increase in the calcium silicate phase, more heat is produced and thus reaches the ultimate degree of hydration faster.

In addition to the cement composition, the cement fineness was shown to affect the cement hydration [75]. The cement heat of hydration showed to increase with increase in the cement fineness. All hydration parameters showed to be affected by the cement Blaine fineness. The ultimate degrees of hydration showed to increase with increase in the cement fineness while the hydration slope and the hydration time showed to decrease with an increase in the cement Blaine fineness. This can be due to the increased contact between water and cement surface with increase in the cement fineness.

4.5.2. Effect of MK

The use of MK was shown to increase the cement heat of hydration, as has been shown in Chapter 3 and in previous studies [61, 64, 106] .The contribution of MK to the total heat of hydration was shown in the previous section (Equation 4-2). The increase in the MK content showed to increase the degree of hydration. This increase can be due to the effect of MK on increasing the cement hydration heat through nucleation as well as the reaction of MK itself that contributes to the heat of hydration, as it was observed in the calorimetry data in Chapter 3.

4.5.3. Effect of WRAs

The early age hydration calorimetry data showed that water-reducing admixtures (WRAs) delay the hydration and increase the setting time. The WRA used in this study was PCE, which is a HRWRA that can also work as a retarder. The heat of hydration modeling shows that the use of PCE can delay the cement hydration and increase the hydration slope that can be due to the better dispersion provided by this admixture. The early age heat of hydration was affected by PCE but the ultimate cement degree of hydration at 7days was not affected.

4.5.4. Model validity

To evaluate the developed model for the types of cements used in this study, the predicted and measured degrees of hydration of all cements are shown versus each other (Figure 4.5). It can be seen that with the 95% confidence interval all of the data set are within the confidence limit of the model. This validation test shows that the model presented in this study can successfully predict the cement degrees of hydration with varying cement chemistry, fineness, metakaolin content, and admixtures for the materials tested in this study. It should be noted that the constant w/b of 0.4 was used in this study.

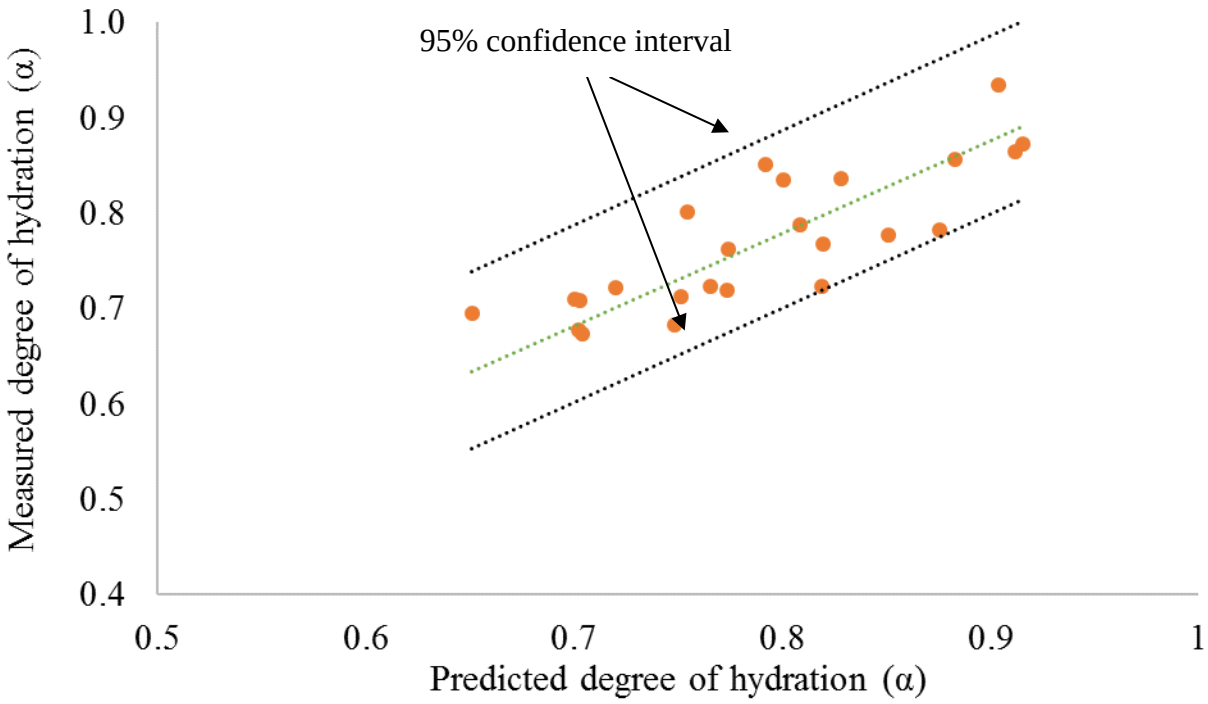

Figure 4.5. The predicted versus measured degrees of hydration for all of the cements mixtures, with and without MK using Equations 4-5 to 4-7.

4.6.Conclusions

An empirical model was developed, based upon and extending existing models, to predict the degree of hydration of modern cements and metakaolin-blended cements. The model is based on isothermal calorimetry data on cement pastes and was developed using linear regression analysis (stepwise model). Different cement types, Types I/II, IL, V, and I/II-V with no metakaolin and with 10, 20, and 30% metakaolin by mass, were used. In total, the experimental data from 24 different cement pastes were used in this study.

The degree of hydration was calculated based on cumulative heat evolved over the total cement heat of hydration, with the assumption that cement is 100% hydrated (H_u). The total heat of cement hydration is estimated based on the cement composition and the effect of MK.

A three-parameter equation based on the hydration parameters (α_u, ultimate degree of hydration, β, slope of hydration, and τ, hydration time parameter) was used to predict the degree of hydration. The hydration parameters were estimated for each cement mix based on isothermal calorimetry data analyzed using the least square regression analysis method. The linear regression analysis, using the *P*-value analysis, was then used to identify the independent factors, i.e., cement phase composition, cement fineness, MK content, that can significantly influence each hydration parameter. Multivariate non-linear regression analysis, stepwise analysis, was used to develop a model for each hydration parameter using the most significant parameters. This developed model showed that the ultimate degree of hydration is dependent of cement calcium silicate composition, cement Blaine fineness, and the MK content. The slope of hydration was shown to be dependent of the cement alkali contents and Blaine fineness of cement and HRWRA dosage, and the

hydration time be related to the cement calcium silicate, cement Blaine fineness, and HRWRA dosage. Therefore, the proposed form of a heat of hydration model accounting for the use of metakaolin at up to 30% by mass of cement with the w/b of 0.4 is as follows:

$$\alpha_u = \frac{1.031 \times w/c}{0.194 + w/c} + \exp(-8.27\rho_{C3S} + 0.00255 \times Blaine + 1.69\rho_{MK})$$

$$\beta = \exp(-0.15 - 0.94\rho_{C3S} - 1.48\rho_{C3A} + 149.31\rho_{alkali} + 0.71\rho_{MK})$$

$$\tau = \exp(3.45 - 1.12\rho_{C3S} - 0.0001 \times Blaine + 33.182\rho_{HRWRA})$$

Further research is needed to consider different w/b ratios, the use of other admixtures beside HRWRAs, other Types of cements, and the use of MK from other sources.

CHAPTER 5 EVALUATING THE HARDENED PROPERTIES OF METAKAOLIN-PORTLAND LIMESTONE CEMENT CONCRETE

5.1.Introduction

The primary goal of this investigation is to evaluate the effects of metakaolin (MK) use in concrete at higher substitution rates (>10%) and in particular when combined with portland limestone cement (PLC). The effect of MK at different replacement levels on the early age hydration and phase development was presented in the previous chapter. This chapter focuses on the hardened properties of metakaolin-portland limestone cement (PLC-MK) concrete.

Specifically, in this chapter, the effect of metakaolin use at rates of 10% or more on PLC concrete mechanical properties and durability are presented. The results of the previous chapter on early age properties showed that PCE and PMS are the most effective admixtures in improving the MK concrete workability, with the required dosages falling within in the manufacturer recommended dosage and showing the least adverse effects. As a result, in this work, these two admixtures are used for metakaolin concrete production. Two MK replacement levels - 10% by mass of cement for the lower end and 30% by mass of cement for the higher end - were chosen and compared to ordinary PLC concrete. Mechanical properties, including compressive strength development, splitting tensile strength, elastic modulus, and Poisson's ratio, are measured for PLC and PLC-MK concretes with either of PCE or PMS admixture. The durability of the PLC and PLC-MK concretes will be assessed based on concrete permeability measured indirectly by rapid

chloride permeability test (RCPT, ASTM C1202) and surface resistivity. The drying shrinkage of concrete is also assessed.

5.2.Materials

The cements used in this is ASTM C595 Type IL portland limestone cement (LS ≤ 15%) [41] provided by Argos where the clinker was produced in Calera, AL and finished in Roberta, GA. High purity metakaolin (Burgess Pigment Company, Sandersville, GA) was used as a replacement for cement at rates of 10% and 30% by mass of cement. These were denoted according to their MK content as MK10 and MK30 respectively. The chemical and physical properties of cements and metakaolin used in this study are presented in Table 3.1.

The concrete was cast with natural sand (Vulcan Materials, Lithia Springs, Georgia) with a fineness modulus of 2.40, saturated surface dry (SSD) specific gravity of 2.63 and an absorption capacity of 0.40% and combined with a #67 stone granitic gneiss (Lithonia, GA) with SSD specific gravity of 2.61 and absorption capacity of 0.58%. Concrete mix designs were developed based on the specifications in GDOT Section 500 for AA concrete [205] (Table 5.2). The same class of concrete was used for PLC concrete and PLC-MK concrete, while keeping water, fine and coarse aggregates and total binder contents constant. All the concretes were cast at w/b= 0.445. While the mid-range water-reducing admixture was used for PLC concrete and either PMS or PCE high-range water-reducing admixture (HRWRA) was used for the PLC-MK concretes. The dosage of each admixture, PCE and PMS, for MK10 and MK30 concrete were determined based on the concrete slump test, with an aim to be between 4 to 8 inches according to ACI 301 [28].

Table 5.1 Concrete mix designs with Type IL cements and Type IL cement with 10 and 30% MK by mass.

Materials	Type IL (lb./ yd^3)	Type IL+ MK10+ PCE (lb./ yd^3)	Type IL+ MK10 + PMS (lb./ yd^3)	Type IL+ MK30 + PCE (lb./ yd^3)	Type IL+ MK30 + PMS (lb./ yd^3)
Cement	635	572	572	445	445
Metakaolin	-	64	64	191	191
Water	282.6	280.4	279.8	277.1	271.6
WRA (fl. oz./ 100 lbs)	-	8	12	12	40
Coarse Aggregate (#67 granitic)	1889	1889	1889	1889	1889
Fine Aggregate (natural sand)	1260	1260	1260	1260	1260
w/b	0.445	0.445	0.445	0.445	0.445

5.3.Experimental methods

5.3.1. Fresh concrete properties

The slump of the PLC concrete and PLC with 10 and 30% MK were measured on fresh concrete following ASTM C143 [167]. The slump of concrete are specified in ACI 301 concrete to be at the maximum of 4 in. at the point of delivery while the maximum slump can be increased to 8 in. when high-range water reducing admixture is used [28].

The unit weight of PLC and PLC-MK concretes were calculated to estimate the air content of concrete following ASTM C138 [206]. To measure the unit weight, the mass of a standard cylindrical steel "measure" container (M_m) was measured, and then filled by concrete, compacted in a standard way, and struck off, the mass of measure and concrete

(M_c) were obtained. The unit weight (density) of the concrete was calculated by dividing the net mass by the volume of the measure, V_m, as follows (Equation 5-1):

$$D = (M_c - M_m) / V_m \qquad 5\text{-}1$$

The theoretical density of the concrete was determined by dividing the cumulative mass of ingredients by their cumulative absolute volume (Equation 5-2). The absolute volume of each ingredient in cubic feet is equal to the quotient of the mass of that ingredient divided by the product of its relative density times 62.4 lb./ft^3. The relative density and mass of aggregates are based on the saturated, surface-dry conditions and for cements the value of 3.15 g/cm^3 was permitted to be used according to ASTM C138 [206]. The air content can be estimated by calculating the difference between the calculated and theoretical unit weight called the gravimetric method as shown in Equation 5-3.

$$T = M / V \qquad 5\text{-}2$$

$$A = \frac{(T - D)}{T} \times 100 \qquad 5\text{-}3$$

The air content of concrete was also measured using the pressure method following ASTM C231 [207]. For this method, a standard container was filled with concrete on a flat and level surface with concrete added in three levels and each layer rodded 25 times uniformly. After each level was added, the bowl side was tapped 10 to 15 times with the mallet to release any air trapped and close the void left by the tamping rod. After filling,

the top surface was struck off. The main air valve between the air chamber and the container was opened and its sides tapped with the mallet. The pressure gauge was slightly tapped by hand to stabilize it, and the air content as a percentage was read. The air was then release through the main air valve.

5.3.2. Mechanical properties

After the fresh concrete properties were measured and recorded, concrete specimens were cast for later age property measurement. Cylinders, 4 by 8 in., were cast for compressive strength measurements at 1, 7, 28, and 90 days and 28-day splitting tensile testing. In addition, 6 by 12 in. cylinders were case for elastic modules tests and 4-in. square cross section prisms 11.25 in. long were cast for drying shrinkage tests. All specimens were demolded after 24 hours and were kept in limewater at 23°C until testing. The compressive strength of concrete cylinders were measured by applying a load at rate of 35 psi/s by a hydraulic machine as described by ASTM C39 [208]. The concrete strength is calculated by dividing the maximum bearing load at failure by measured cross-sectional area. Each cylinder diameter was measured and recorded to the nearest 0.01 in. before testing. The compressive strength tests were carried out on four cylinders at each age, and the results with the standard deviations are reported.

For the splitting tensile strength measurement, the diameter and length of each cylinder was measured and recorded to the nearest 0.01 in. The concrete cylinder was then located on the center of the wood strips along the center of the lower bearing plate with the lines marked on the ends of the specimens vertical and centered over the wood strip. The second wood strip was placed on the top of the cylinder parallel to the lower strip and the top bearing plate was placed on top of the wood strip with its center on the center of the

cylinder. The load was applied at the range of 100-200 psi/min and the maximum applied load at the time of failure was recorded. The type of failure and the appearance of the concrete was noted. The splitting tensile strength was calculated using the following equation from ASTM C496 [209]:

$$T = \frac{2P}{\pi.l.d} \qquad 5\text{-}4$$

where:

T = splitting tensile strength, MPa (psi),
P = maximum applied load indicated by the testing machine,
N (lbf), l = length (in.), and
d = diameter, (in.)

The elastic modules (E) was measured on four 6 by 12 in. cylinders following ASTM C469 [210] at 28 days of age. The concrete specimen was placed in the compressometer/extensometer, and rested on the lower bearing plate of the testing equipment. The specimen was carefully aligned to be in the center of the guard and then the screws at each end were tightened. The specimens was then loaded at a constant loading rate of 35 psi/s up to 40% of the average ultimate load determined by the compression test. Because the specimen sizes are different for compressive strength tests and the elastic modulus test, the conversion has been done to estimate the correct ultimate load for elastic modulus specimens. The first loading was not recorded but the performance of the gauges were evaluated to make sure there is no attachment or alignment defects. For the second and subsequent third loadings, each set of the applied load and longitudinal strain at that point was recorded for every 10,000 lbs load applied. ASTM C469 [210] requires to record,

without interruption of loading, the applied load and longitudinal strain at the point (1) when the longitudinal strain is 50 microstrain and (2) when the applied load is equal to 40 % of the ultimate load of the companion specimens. The relevant stress calculated based on the recorded load and the relevant strain were used to draw the strain-stress diagram and calculate the elastic modulus (E). The elastic modulus was calculated by:

$$E = \frac{S_2 - S_1}{\varepsilon_2 - 0.000050} \qquad 5\text{-}5$$

Where:

E = chord modulus of elasticity (psi),
S_2 = stress corresponding to 40 % of ultimate load (psi),
S_1 = stress corresponding to a longitudinal strain, ε_1, of 50 microstrain (psi), and
ε_2 = longitudinal strain produced by stress S_2.

The transverse strain was also measured at the same points to calculate the Poisson's ratio. The transverse strain is the measured change in specimen diameter divided by the original diameter. Poisson's Ratio defined as the ratio of the lateral strain to the longitudinal strain and can be expressed as [210]:

$$\mu = (\varepsilon_{t2} - \varepsilon_{t1}) / (\varepsilon_2 - 0.000050) \qquad 5\text{-}6$$

Where:

μ = Poisson's ratio
ε_{t2} = transverse strain at mid height of the specimen produced by stress S_2, and
ε_{tl} = transverse strain at mid height of the specimen produced by stress S_1.

5.3.3. Durability of concrete

The durability of concrete was assessed through indirect measure of its permeability through the rapid chloride permeability test (RCPT) and surface resistivity (SR). ASTM 1202 [211] and American Association of State Highway and Transportation Officials (AASHTO T277[212]) have similar standards on RCPT measurement [213], this study followed ASTM 1202 [211] for RCPT. This test method consists of monitoring the amount of electrical current passed through saturated 2-inch (50-mm) thick disks cut from 6-inch (150-mm) nominal diameter cylinders during a 6-h period. This test was carried on cut cylinders after 56 days of hydration in limewater at 23°C. The disks were vacuum-saturated for 18 ± 2 hr, and the rapid chloride permeability test was performed the following day in accordance with ASTM C1202/AASHTO T277 (Figure 5.1). A potential difference of 60V dc is maintained across the ends of the specimen, one of which is immersed in a sodium chloride solution, the other in a sodium hydroxide solution. The total charge passed, in coulombs, after 6 hours was measured on two concrete disks for each mixture, and the average was reported.

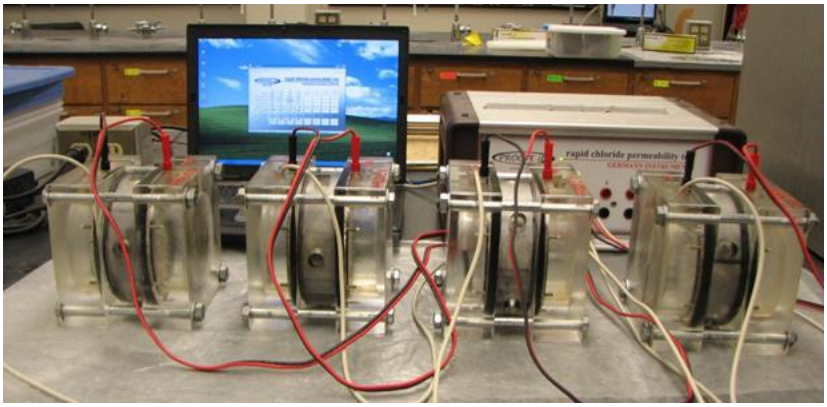

Figure 5.1. RCP test conducted in accordance with ASTM C1202/AASHTO T277.

The surface resistivity measurement was made on three 4 by 8 inch specimens using a four-probed Wenner array, in accordance with AASTHO T 358-15[214]. Measurements were made at quarter-points around the circumference of the cylinders, with eight measurements being made for each cylinder (two measurements per line). The samples were cured in a saturated calcium hydroxide (limewater) solution maintained at 23°C. After 1, 7, 14, and 56 days of hydration, the surface resistivity was measured again on the same specimens to obtain SR-development curves for each mix. SR values for limewater-cured specimens were multiplied by a factor of 1.1, as specified by the AASHTO standard [214], to account for an assumed 10% decrease in pore solution resistivity caused by the limewater.

5.3.4. Drying shrinkage

Drying shrinkage of concrete measured through changes in the length three companion 3 in. by 3 in. by 10 in. (76 by 76 by 254 mm) prisms, following ASTM C157 [215]. The measurements started after the prims were cured in a bath of saturated limewater at 23°C for 28 days. After that, the prisms were placed in a controlled environment with the temperature of 23°C and 50% relative humidity (RH). The measurements were carried out on prisms after

0, 4, 7, 28, 56, and 90 days of drying. The length change was calculated and reported based on the following equation (ASTM C157 [215]):

$$\Delta L_x = \frac{CRD - initialCRD}{G} \times 100 \quad \text{5-7}$$

Where:

ΔL_x = length change of specimen at any age, %,

CRD = difference between the comparator reading of the specimen and the reference bar at any age, and

G = the gage length (10 in. (250 mm))

These calculations were carried out for PLC and PLC with MK10 and MK30, each with PCE and PMS admixtures. The results were reported as the average of three specimens with standard deviation.

5.4.Results

This section presents the fresh and hardened properties of concrete with PLC, and PLC with MK10 and MK30 with either PCE or PMS admixture. First, the mechanical properties of concretes including compressive strength, splitting tensile strength, and elastic modulus of cylindrical concrete specimens are presented, and then the durability of concrete including permeability and drying shrinkage test results.

5.4.1. Fresh concrete properties

As part of regular quality assessment, the fresh properties of concrete were measured on concrete just after mixing and are shown in Table 5.2. The slumps of MK concrete with the same mix but different HRWRAs (PMS or PCE) are close to each other.

The slump of all concretes are in the range of 4-8 in. that is recommended by ACI 301 for concrete with HRWRs [28].

The fresh air contents were measured by the pressure and gravimetric methods, and similar results were achieved, which are generally in the range expected for non-air entrained concrete [216]. The air content of metakaolin concretes are in general lower than those of PLC concrete. In addition, with higher MK content, that is, increasing from 10 to 30% by mass, the air content decreased. The lower air content of MK concrete can be related to improved particle packing in the paste fraction and improvements in compactability with high range water reducing agents, as compared to midrange water-reducing admixtures used for the PLC [217]. The slightly higher air concrete in the MK concrete produced with PCE compared to that of concrete with PMS can be in part due to the air-entraining properties of PCE [218]. The lower unit weight of MK concrete in general compared to that of PLC concrete can be due to the lower density (2.35 g/cm^3) of MK compared to that of PLC (3.05 g/cm^3).

Table 5.2. Fresh concrete properties with Types IL cements and Type IL cement with 10% and 30% MK

Cementitious material	Admixture	Slump (in.)	Calculated unit weight (T) (lb./ ft^3)	Measured unit weight (D) (lb./ ft^3)	Air content (%)	
					Pressure method	**Gravimetric method**
Type IL	Midrange WRA	7.25	150.5	146.1	3.3%	3.3%
Type IL+ MK10	PCE (HRWRA)	4	150.2	148.3	2.6%	3.2%
	PMS (HRWRA)	4.5	150.1	146.4	2.5%	2.5%
Type IL+ MK30	PCE (HRWRA)	6	148.3	146.0	1.8%	1.5%
	PMS (HRWRA)	6	148.5	148.6	1.1%	0.6%

5.4.2. Hardened concrete properties

In this section, the hardened concrete properties are categorized to mechanical properties and durability. The first part of this section shows the effect of MK on the concrete strength and the second sections shows the effect of MK on the durability of concrete, including propensity for drying shrinkage-induced cracking.

5.4.2.1.Mechanical properties

The mechanical properties of PLC concrete and PLC with 10 and 30% metakaolin by mass are presented and compared in this section. Moreover, the difference in the mechanical properties of concrete with the same MK content but different admixture, PMS or PCE, are evaluated in this section. The mechanical properties includes the compressive strength measured at 1, 7, 28, 56, and 90 days, as well as tensile strength and elastic modulus measured at 28 days.

5.4.2.1.1. Compressive strength

Compressive strength results (Figure 5.2) show that in general PLC-MK concretes have equivalent or higher compressive strength than PLC concrete at all ages. This enhanced performance is due to the densify effect of MK by the filler effect, the acceleration of cement hydration, and the pozzolanic reaction of metakaolin with CH, as was reported in previous studies [141, 219].

Despite having a lower cement content, the MK concrete with PMS showed similar compressive strength to that of PLC concrete at 1 day, and its later age compressive strength was higher than that of PLC concrete at all ages examined. The 7-day compressive strength of MK10 and MK30 concrete with PMS was 7% and 34% higher compared to that of PLC concrete. The extent of the greater compressive strength of MK concrete with PMS further increased with the age of the concrete, particularly for the MK10 case. The 56-day compressive strength of MK10 and MK30 concrete with PMS were 19% and 37% higher than that of PLC concrete. At 90 days, both MK10 and MK30 concretes showed higher compressive strength (18 and 32%) than that of PLC concrete. The slower rate strength development of the PLC-MK concrete may be due to the retardation effects with PMS. The retardation effect of PMS was also observed on the cement paste hydration and phase development (Ch. 3). The other reason for lower compressive strength of PMS can be the lower efficiency of this admixture in dispersing the MK and cements.

The MK concrete with PCE exhibited significantly higher compressive strength compared to PLC concrete as early as one day of age. The 1-day compressive strength of MK10 and 30 with PCE are higher than that of PLC concrete by 50 and 93% respectively. The later age compressive strength of MK10 and MK30 concrete with PCE further

increased relative to the PLC concrete, with 7-day compressive strength concrete of up to 70 and 150% higher than that of PLC concrete. Finally, the 90-day compressive strengths of MK concrete with PCE showed 130% higher compressive strength compared to that of PLC concrete. It should be noted that MK concretes with significantly improved compressive strength contain 25 to 45% less cement than the OPC concrete.

The higher compressive strength of MK concrete with PCE can be due to the better dispersion provided by this admixture and a less significant retardation effect, compared to PMS, as described in Chapter 3. That the MK30 concrete with PCE showed higher compressive strength than the MK10 concrete shows the MK pozzolanic reactivity and filler effect overcome any dilution effect (even at 30% by mass replacement, when considering the compressive strength development of concrete. The failure of PLC-MK concrete through the aggregates show the strong adhesion of paste/aggregates in these concretes (Figures 5.3).

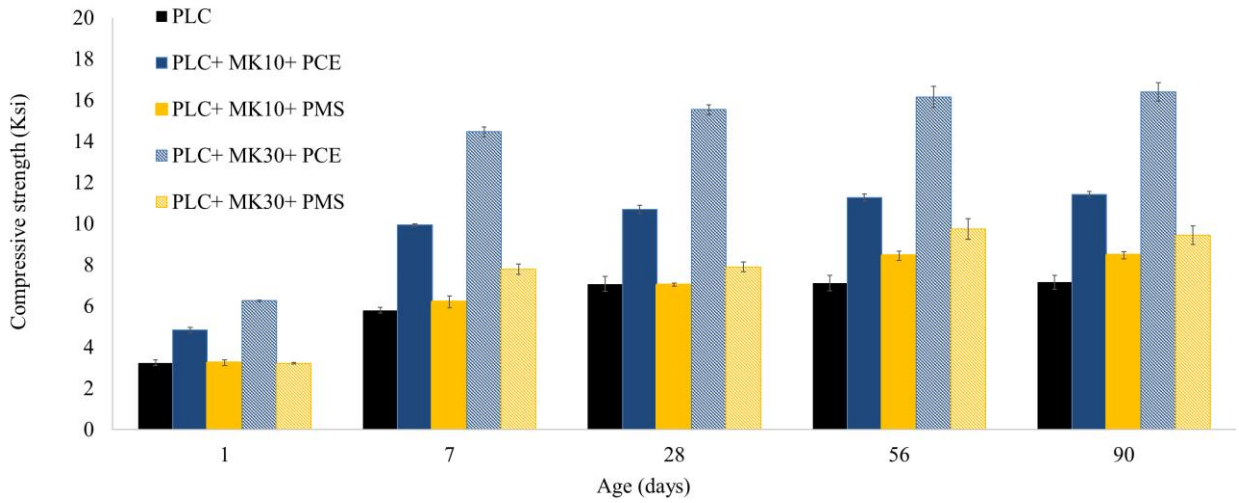

Figure 5.2. Compressive strength of portland limestone cement (PLC) concrete and PLC with MK10 and MK30 with PCE or PMS admixture measured on 4 by 8 in. cylinders.

The normalized compressive strength of MK concrete by the PLC concrete compressive strength (Figure 5.3) show that the MK concrete with PCE showed higher early strength while PMC concrete has a delay in strength gaining that can be due to the retardation effect of PMS. The failure analysis (Figure 5.4) of MK concretes showed that the concrete breaks mainly breaks the aggregates that shows the high strength of paste and a higher bond of paste/aggregates.

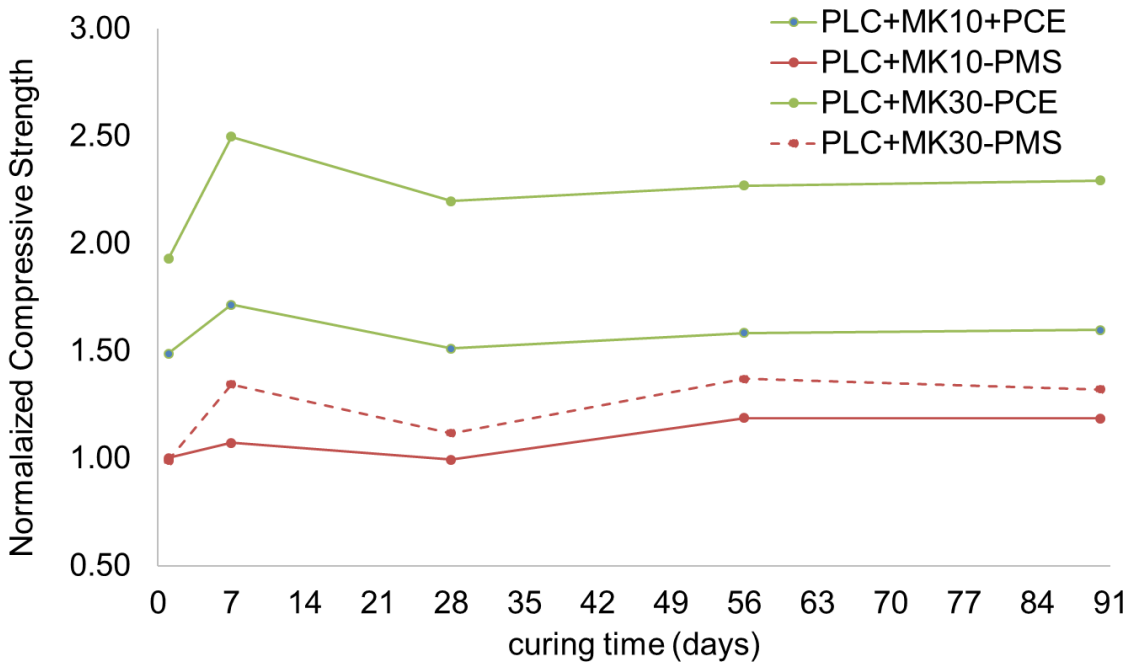

Figure 5.3. The normalized compressive strength gain of PLC-MK concrete by PLC concrete strength over 80 days

Figure 5.4. PLC-MK30 with PCE concrete cylinders failure mode after compressive test

5.4.2.1.2. Splitting tensile strength

The splitting tensile strength of PLC and PLC-MK concretes were measured at 28 days on 4 by 8 in. cylinders following ASTM C496 [209]. The results show that the tensile strength of MK concrete depends on the MK content and the HRWRA type. The tensile strengths of MK concrete with PCE were higher that PLC concrete, while those of the MK concrete with PMS were lower than that of PLC concrete. Specifically, the average tensile strengths of MK10 and MK30 with PCE are higher than that of PLC concrete by 15% and 42%, respectively. The higher tensile strength of MK concrete with PCE may result from enhanced dispersion of the cement and improved particle packing, with strengthens both the bulk paste and the ITZ in PLC-MK concrete.

In contrast, it should be noted that while the MK10 and MK30 concrete with PMS showed similar early compressive strength and higher 28-day compressive strength than

that of PLC concrete, its tensile strength is lower than that of PLC concrete. The tensile strength of MK concrete with PMS at 28 days is 22 and 13% lower than that of PLC concrete. The lower tensile strength of MK concrete with PMS can be due to the weaker interfacial transition zone (ITZ) perhaps because of poorer dispersion of MK and cement particles with PMS. The ITZ is generally the "weakest link" in the concrete matrix and can limit the splitting tensile strength and elastic modulus of concrete, as both of these measures are highly influenced by microscale defects in the ITZ. The fracture surfaces of the PLC-MK concrete with PMS shows that concrete failure mode occurs primarily through crack propagation along the paste/aggregates interface and through the paste, This is indicative of a lower bond between the aggregate and paste in the PMS case than in the PLC or PLC-MK with PCE concrete..

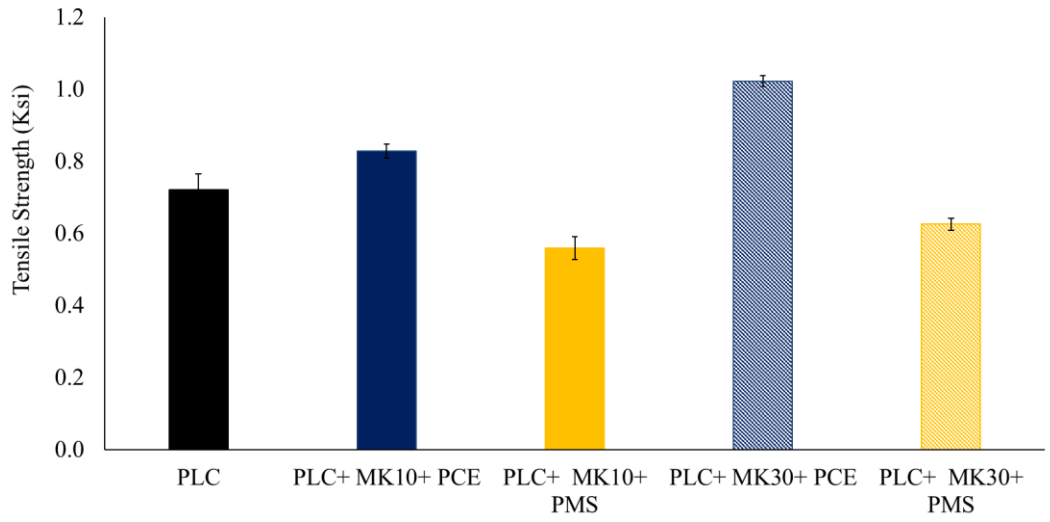

Figure 5.5. The splitting tensile strength of PLC concrete and PLC with MK and PCE or PMS high-range water-reducer-admixture

The tensile strength of concrete can be described as a function of its compressive strength. The increase in the compressive strength typically correlates with a higher tensile strength

but degree at which both increase is not the same. Therefore, the relationship between the compressive and tensile strength is not linear. Commonly, and for normal strength concrete, the tensile strength is about 7-12% of its compressive strength [220]. This estimation is a close approximation for the results of this study (Table 5.4).

Several equations have been developed in previous research to predict the tensile strength of concrete based on compressive strength [221, 222]. Those equations were used to estimate the tensile strength, and to compare them with the experimental data for PLC-MK concretes to evaluate the accuracy of these equations in predicting the tensile strength of PLC-MK concretes. The least square regression analysis method was used to evaluate the each equation in predicting the tensile strength of each concrete. A lower value in this method shows better correlation between experimental and predicted values.

The American Concrete Institute in its documents ACI-318 [221] and ACI-363 [222] has developed empirical equations for the relationship between compressive and tensile strengths of concretes. These equations were used to estimate and compare the experimental and predicted tensile strength of PLC-MK concrete. The comparison of previous models and the experimental data of this study (Figure 5.5) revealed that all those equations overestimate the tensile strength of MK concrete. The results (Table 5.4) show that the ACI-predicted tensile strengths are up to 3-4 times higher than the experimental results of this study for all MK concretes. Therefore, the ACI equations are non-conservative for PLC-MK concretes of the type examined in this study. Dewar [223] studied the studied the relationship between the indirect tensile strength (cylinder splitting strength) and the compressive strength of concretes having compressive strengths of up to 12,105 psi (83.79 MPa) at 28 days. He concluded that at low strengths, the indirect tensile

strength may be as high as 10 percent of the compressive strength but at higher strengths it may reduce to 5 percent.

Alternate relationships have also been proposed. Carino et al. [224] showed that the commonly used square root of the compressive strength is not the most applicable relation of tensile strength prediction. They, rather, used a simple power function to predict the tensile strength of wide range of concrete strengths. Their equation showed the best approximation to predict the tensile strength of MK concrete among the used equations in this study. Raphael [225] used the 12,000 individual test results of tensile strength form direct, splitting tension, and flexural tests to develop an equation between the tensile and compressive strength of concretes. The developed equation was the second best fit for the tensile strength of MK concretes in this study. It should be noted that this equation is mainly based on the results of concrete with the normal compressive strength (f_c<5800 psi), which can may the reason this equation does not apply to the PLC-MK concretes with the higher compressive strengths.

Noting the influence of SCMs on ITZ quality and overall microstructure, others have proposed equations with specific relevant to concrete containing SCMs. For example, Gardner et al. [226] developed an equation for tensile strength of concrete with Type I and III cement blended with fly ash. The developed equation showed the approximation of the tensile strength results of MK concrete in this study compared to the ACI equations. Arıoglu et al. [227] developed an equation to calculate the tensile strength based on the compressive strength of concrete with silica fume, but as shown in Table 5.3, their relationship does not appear to be applicable for MK concretes in this study. Overall, the difference between the results of the developed models and the experimental data for the

MK concretes here reveals a need to develop an equation for predicting the tensile strength of PLC-MK concrete.

Table 5.3. The experimental and predicted tensile strength based on the compressive strength results

	Equation	PLC	PLC+ MK10+ PCE	PLC+ MK10+ PMS	PLC+ MK30+ PCE	PLC+ MK30+ PMS	Sum of squares of differences
Experimental tensile strength		0.72	0.83	0.56	1.02	0.63	
Compressive strength (fc)		7.08	10.69	7.03	15.54	7.90	
Empirical equation [228]	$f_{tsp} = 0.1f_c$	0.71	1.07	0.70	1.55	0.79	0.39
ACI 363R [222]	$f_{tsp} = 0.59\ f_c^{\ 0.5}$	1.57	1.93	1.56	2.33	1.66	5.70
ACI 318 [221]	$f_{tsp} = 0.56\ f_c^{\ 0.5}$	1.49	1.83	1.49	2.21	1.57	4.75
Carino and Lew [224]	$f_{tsp} = 0.272fc^{0.71}$	1.09	1.46	1.09	1.91	1.18	1.91
Raphael [225]	$f_{tsp} = 0.313fc^{0.667}$	1.15	1.52	1.15	1.95	1.24	2.26
Ahmad and Shah [229]	$f_{tsp} = 0.46fc^{0.55}$	1.35	1.69	1.34	2.08	1.43	3.53
Aroiglu [227]	$f_{tsp} = 0.321fc^{0.661}$	1.33	1.72	1.32	2.18	1.42	3.72
Gardner [226]	$ftsp = 0.33fc^{2/3}$	1.20	1.58	1.20	2.02	1.29	2.63
This study	$f_{tsp} = 0.18fc^{0.64}$	0.65	0.83	0.64	1.04	0.69	0.02

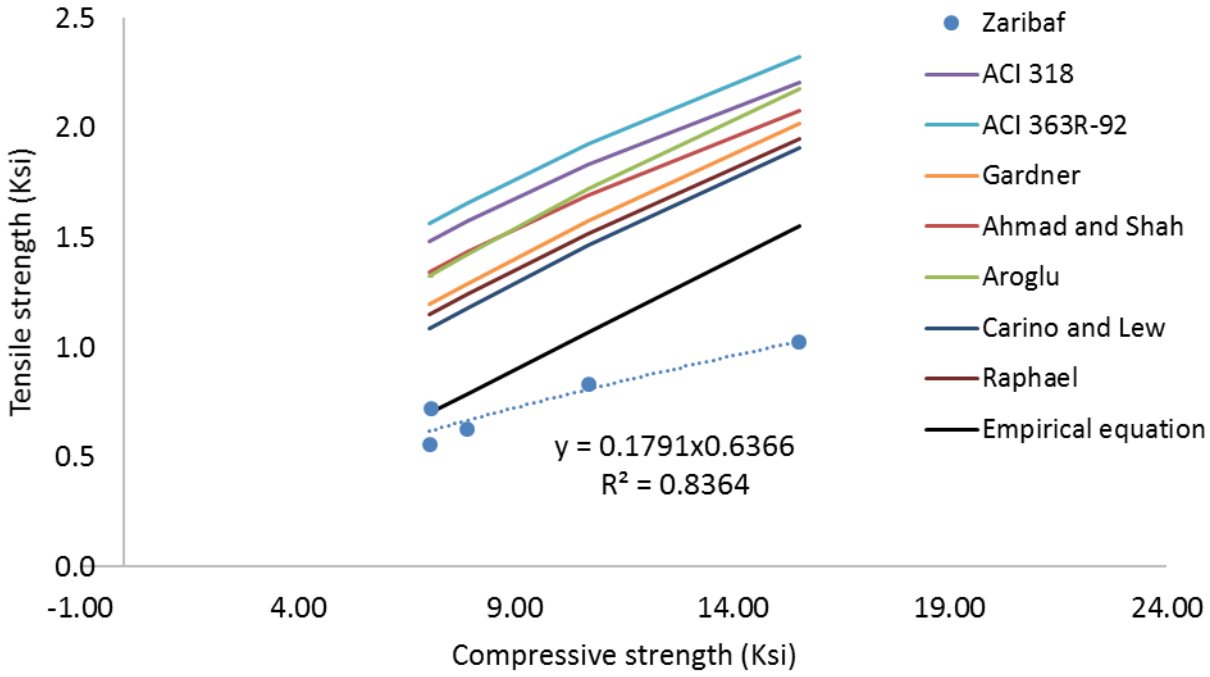

Figure 5.6. The comparison of predicted tensile strength based on previous models and the experimental data in this study on PLC-MK concrete with 10 and 30% MK. The predicted model developed in this study is also shown

This study used the tensile strength results of MK10 and MK30 concrete with PMS and PCE to develop the following equation (5-8) for predicting the tensile strength (f_{tsp}) of MK concrete based on their compressive strength (f_c). The developed model shows the sum of square differences of 0.02 between the experimental and predicted tensile strength data. The experimental and predicated tensile strengths (Figure 5.7) showed the significantly high correlation (R^2= 0.97) between the experimental and predicted data, as expected. The experimental data sets of this study were not large, but this primary equation can be used as a basis to predict the tensile strength of high strength PLC-MK concrete based on their 28-day compressive strength:

$$f_{tsp} = 0.18 \times f_c^{0.64} \qquad 5\text{-}8$$

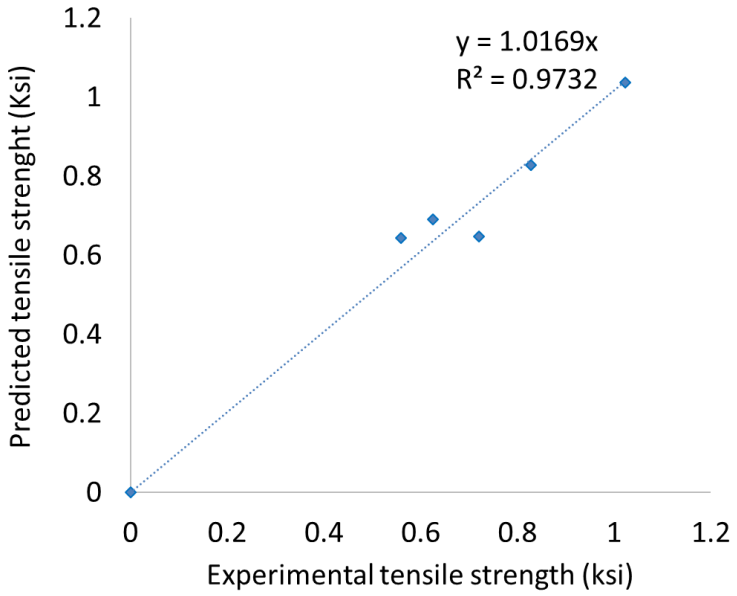

Figure 5.7. The experimental and predicted tensile strength of PLC-MK concretes using Equation 5.8.

The model developed in this study was used on compressive and tensile strength of MK concrete with 10-15% MK from previous studies [132, 230-232]. The results (Figure 5.8). show that the predicted results are in the 95% confident intervals of the experimental data.

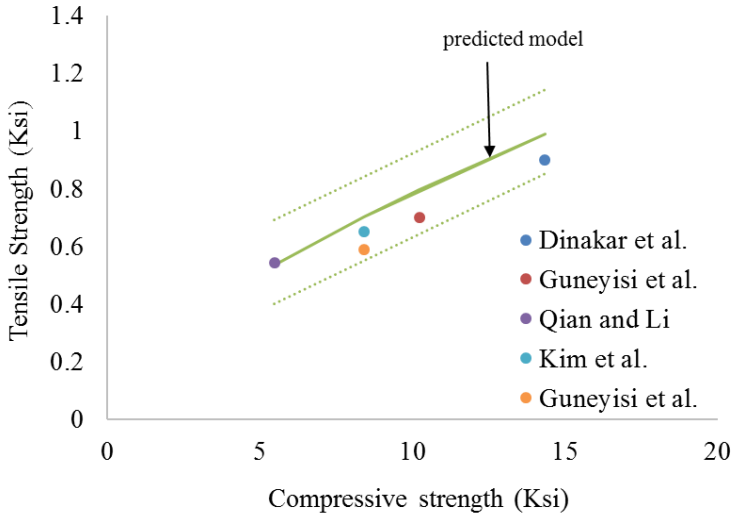

Figure 5.8. The experimental data from previous studies and predicted data using the model developed in this study shows that the experimental data are in the 95% confidence interval (dashed lines) of the predicted data

5.4.2.1.3. Elastic modulus

The elastic modulus and Poisson's ratio of PLC and PLC-MK concrete were measured on at 28 days to evaluate and compare the effect of MK. The results of elastic modulus (Figure 5.9) show that the elastic modulus is dependent of MK content and the admixture chemistry. The elastic modulus of all MK concretes are higher than the PLC concrete. The elastic modulus of MK concretes with PCE are significantly higher (up to 80% higher) compared to that of PLC concrete, and this increases with increasing MK content. The elastic modulus of MK10 and MK30 concrete with PMS are higher than the PLC concrete up to 77% and 35% higher, respectively. The lower elastic modulus of MK30 concrete with PMS can be due to the lower capability of this admixture in dispersing the MK and cement particle.

The elastic modulus of concrete is related to porosity of paste and aggregate and the ITZ of concrete [233]. The addition of MK densifies the paste matrix and reduces the

porosity of paste and thus increases the elastic modulus. Moreover, the higher elastic modulus with higher MK content can be because of the better packing due to the filler effect of fine MK particles, especially in the ITZ.

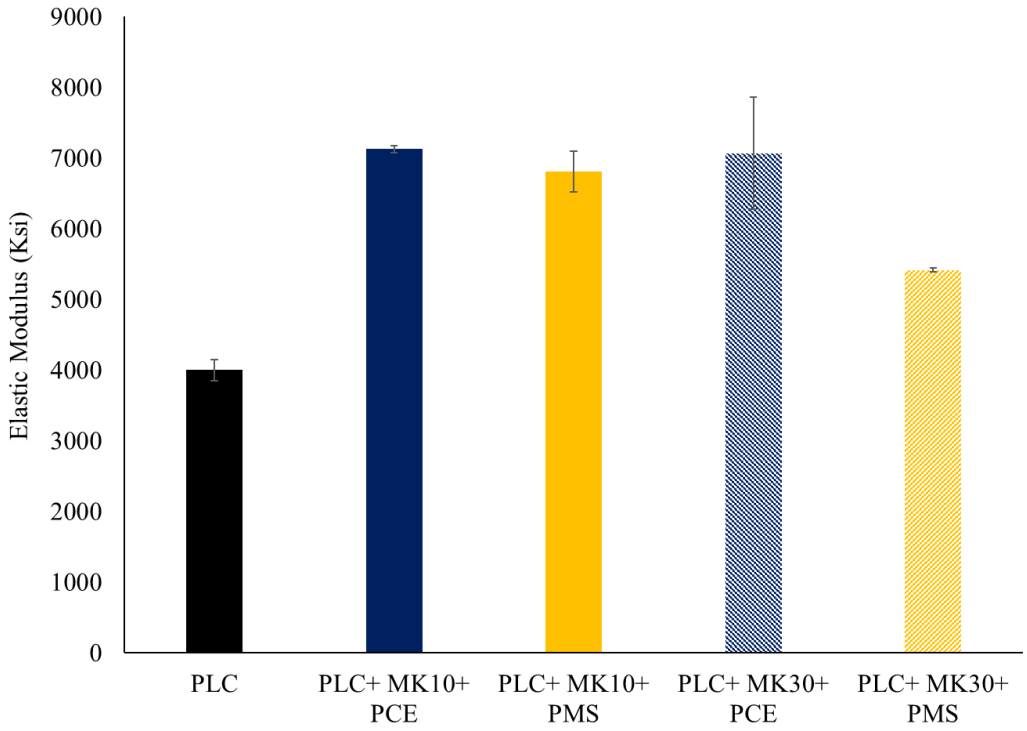

Figure 5.9. Elastic modulus of PLC and PLC with MK10 and MK30 concrete and PMS or PCE admixture

Strain-stress curves are helpful in visualizing the variations in behavior of concrete cylinders with MK10 and MK30 with PMS or PCE under axial loading (Figure 5.10). Comparing the PLC-MK10 concretes, the PLC-MK10 with PCE concrete showed a more consistent behavior as compared to those of concretes with PMS. It is proposed that the MK10 concrete cylinders with PMS showed different and early nonlinear behavior because of inherent microcracking which leads to crack propagation and ultimately fast fracture under increasing stress. Depending on the depth and direction of the preexisting defects,

the concrete may behave differently, accounting for some variability in the stress-strain response. The PLC-MK30 concretes with PMS and PCE both showed more predictable behavior than the MK10 concretes with the concrete with PCE showing a linear behavior with the higher ratio of stress to strain values that results in a higher elastic modulus value compared to PLC-MK30 concrete with PMS.

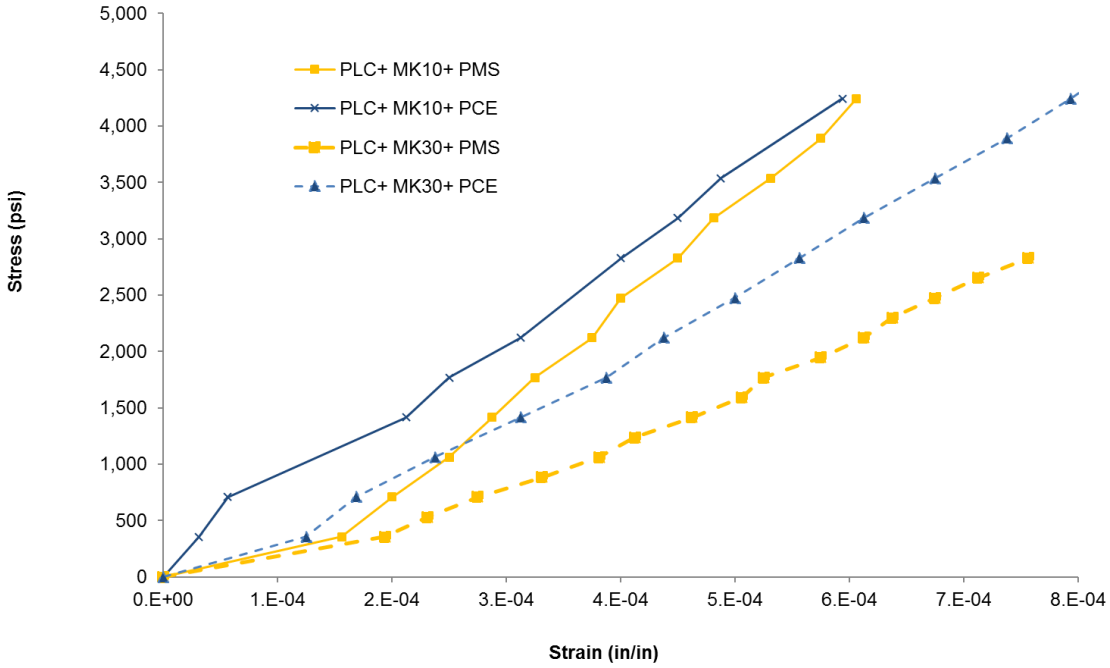

Figure 5.10. Stress/strain diagram for PLC with MK10 and MK30 concretes with PCE and PMS

Several equations have been developed to predict the elastic modulus (E) based on the compressive strength at 28 days [221, 222]. The Residual Sum of Squares (RSS) was used to evaluate the accuracy of these models in predicting the elastic modulus of concretes examined in this study (Table 5.5).

ACI 318 [221] suggested an equation to predict the elastic modulus based on the concrete unit weight and the compressive strength, as shown in Equation 5.9, where w is the concrete unit weight (lb/ft^3) and f_c is the 28-day compressive strength (psi):

$$E = 33 \times w^{1.5} \times f_c^{\,0.5} \qquad 5\text{-}9$$

The results of elastic modulus calculated based on this equation and the experimental data are shown in Figure 5.11 and Table 5.4. The predicted values of E were a better approximation for the higher strength concrete, MK10 and MK30 with PCE, while E is overestimated for other concretes.

ACI 363 [222] developed an equation to predict the elastic modulus of high-strength concrete (HSC), specifically with 28-day strength of 9,000 psi or higher. The MK concretes used in this study with PCE can be considered as HSC. The results of predicted elastic modulus using this equation (Figure 5.5 and Table 5.5) show that this model is capable of predicting the elastic modulus better than that of ACI 318 equation.

$$E = (40,000 \times f_c^{\,0.5} + 10^6) \times (w/145)^{1.5} \qquad 5\text{-}10$$

The American Association of State Highway and Transportation Officials for Bridge Design Specifications (AASHTO-LRFD) [234] developed the following equation to predict the modulus of elasticity of concrete:

$$E = (33,000 \times K_1 \times f_c^{0.5} + 10^6) \times (w/145)^{1.5} \qquad 5\text{-}11$$

Where:

K_1= correction factor for source of aggregates (equal to one unless determined by physical test, and as approved)

W= unit weight of concrete (Pcf)

f_c= specified compressive strength of concrete (ksi)

This equation was used to predict the elastic modulus of concrete used in this study. The results (Table 5.4 and Figure 5.10) show that this model showed comparable results for elastic modulus of high-strength concrete, including MK concrete with PCE, but was not successful in predicting the elastic modulus for other concretes. This model overestimated elastic modulus for normal-strength concrete, which is nonconservative.

Table 5.4. The experimental and predicted elastic modulus for PLC and PLC with MK10 and MK30

Specimen	28-day Compressive strength (psi)	Experimental E (psi)	ACI-318 Value (ksi)	ACI-363 Value (ksi)	AASHTO LRFD Value (ksi)
PLC	7077	4.0×10^6	4795	4593	5100
PLC+ MK10+ PCE	10700	6.8×10^6	5893	5403	6268
PLC+ MK10+ PMS	7034	3.8×10^6	4780	4582	5084
PLC+ MK30+ PCE	15500	7.1×10^6	7106	6299	7558
PLC+ MK30+ PMS	7900	4.9×10^6	5066	4793	5388
Residual Sum of Squares (RSS)			2.6E+06	1.0E+06	3.2E+06

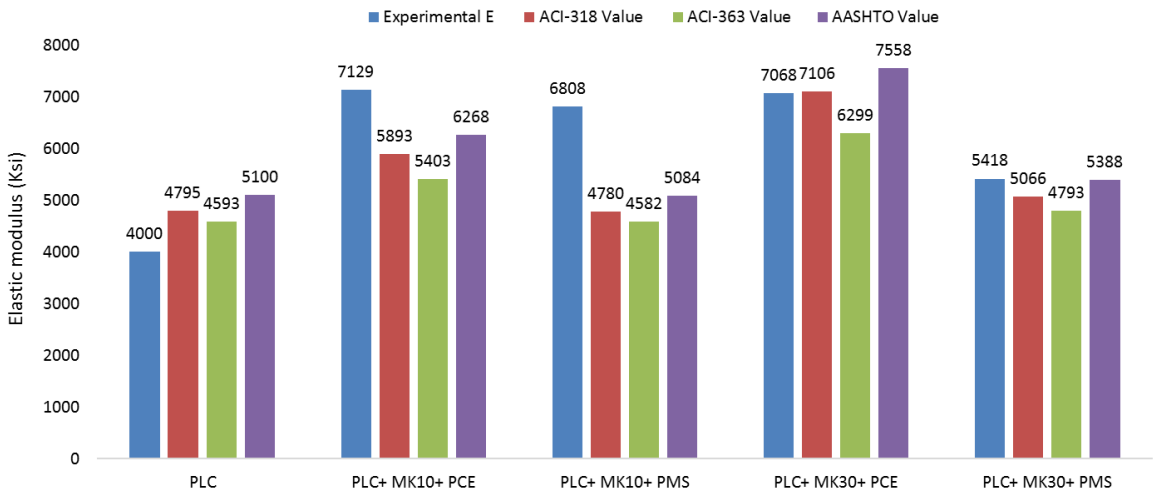

Figure 5.11. Measured and predicted elastic modulus of PLC and PLC with MK concretes

5.4.2.2.Poisson's ratio

This study followed ASTM C469 [210] to calculate the Poisson's ratio by determining the absolute value obtained by dividing the measured lateral strain by the measured longitudinal strain at stress applied up to 40% of the ultimate strength of the concrete with the load applied at 10,000 lb. intervals. It was observed (Appendix A) that the Poisson's ratio increased with the increase in the applied load. It can be explained that in brittle materials under high stress, microcracking starts to develop generally parallel to the direction of the stress and, because of this microcracking, the transverse strain increases at higher stress. Close to the ultimate strength, Poisson's ratio increases rapidly until failure occurs.

The Poisson's ratio of MK concrete with PCE is higher than that of concretes with PMS, similar to the trend was observed for the elastic modulus data. The Poisson's ratio is typically between 0.15 and 0.2 with in the elastic range for concrete and is stress-independent for normal strength concrete [233] while it is around 0.10-0.14 for high

performance concrete (HPC) [235, 236]. The Poisson's ratio showed to be adversely related to the compressive strength of concrete but there appears to be no consistent relationship between Poisson's ratio and concrete characteristics such as w/c ratio, curing age, and aggregates gradation [233] .

The Poisson's ratio of PLC concrete in this study was 0.24. The results of this study (Figure 5.12) show that MK concrete with PMS exhibits Poisson's ratios in the typical concrete range, but lower than that of PLC concrete. The MK concrete with PCE at both 10 and 30% MK showed to have Poisson's ratio higher than the typical range for concrete and closer to that of PLC concrete. The relatively higher Poisson's ratio of MK concrete with PCE compared to that with PMS can be due to the better dispersion provided by this admixture. Overall, these results suggest that historical values for Poisson's ratio - determined when cements were ground more coarsely, workability limited the extent to which water-to-cement ratios could be decreased, and finely divided fillers and SCMs were uncommon – required re-examination in the context of modern concrete materials and design practices. However, further studies are needed to validate these observations in a

broader context.

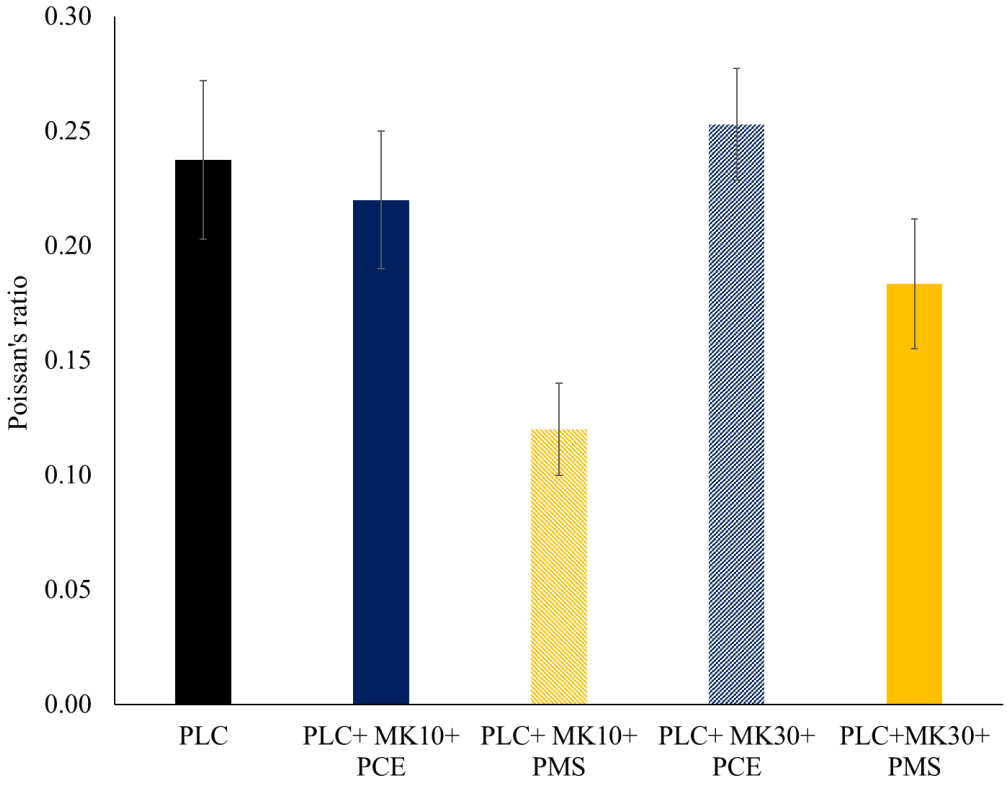

Figure 5.12. The Poisson's ratio of MK10 and MK30 concretes with PMS or PCE admixture

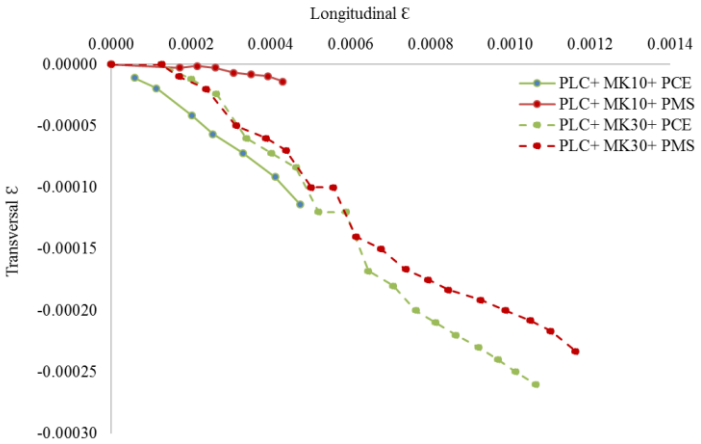

Figure 5.13. The longitudinal and transversal strain for PLC-MK pastes showing the Poisson's ratio rate

5.5.Durability assessment of PLC-MK concretes

In this section the durability of PLC-MK concretes are measured and compared to those of PLC concrete to evaluate the effect of MK on durability of concretes. The durability of concretes are evaluated based on the permeability measured by the rapid chloride penetration test and surface resistivity. The concrete potential for cracking is another aspect of durability that was assessed by free drying shrinkage.

5.5.1. Permeability

The permeability is important in determining the durability of concrete. The higher permeability of concrete results in water and chemical intrusion that leads to concrete deterioration. The permeability of concrete is related not only to the concrete porosity but also the pore interconnectivity. This study used the rapid chloride penetration test (RCPT)

and surface resistivity (SR) to evaluate the effect of MK and WRAs on PLC concrete permeability.

5.5.1.1.Rapid chloride penetration test (RCPT)

The rapid chloride penetration test was conducted following ASTM 1202/AASHTO T277 on PLC and PLC-MK concrete and PMS or PCE admixture. The concrete chloride ion penetrability was categorized based on the charge passed according to ASTM 1202 (Table 5.5). The lower charged passed indicates the lower permeability of the concrete.

Table 5.5. Permeability classifications for concrete tested according to the ASTM C1202/AASHTO T277 rapid chloride permeability test.

Classification	Charge Passed (Coulombs)
High	> 4000
Moderate	2000-4000
Low	1000-2000
Very Low	100-1000
Negligible	< 100

The results of the chloride permeability (Figure 5.14) show that the addition of MK decreases the permeability of concrete significantly. For concretes with w/b of 0.40, the classification was moderate for PLC concrete, and with MK it was low to very low. This decrease can be due to the effect of MK on densifying the concrete through filler effect and pozzolanic reaction of MK that decrease the permeability by filling the pores and densifying the concrete, particularly in the ITZ.

Moreover, the WRA chemistry was found to affect the concrete permeability. For MK10 concrete, both concretes with PCE and PMS exhibited a very low permeability. However, for the MK30 concrete, concrete cast with PCE showed very low permeability,

while the MK30 concrete with PMS showed low permeability. The lower permeability with PCE admixture particularly with higher MK content (MK30) can be because of the better dispersion provided by this admixture.

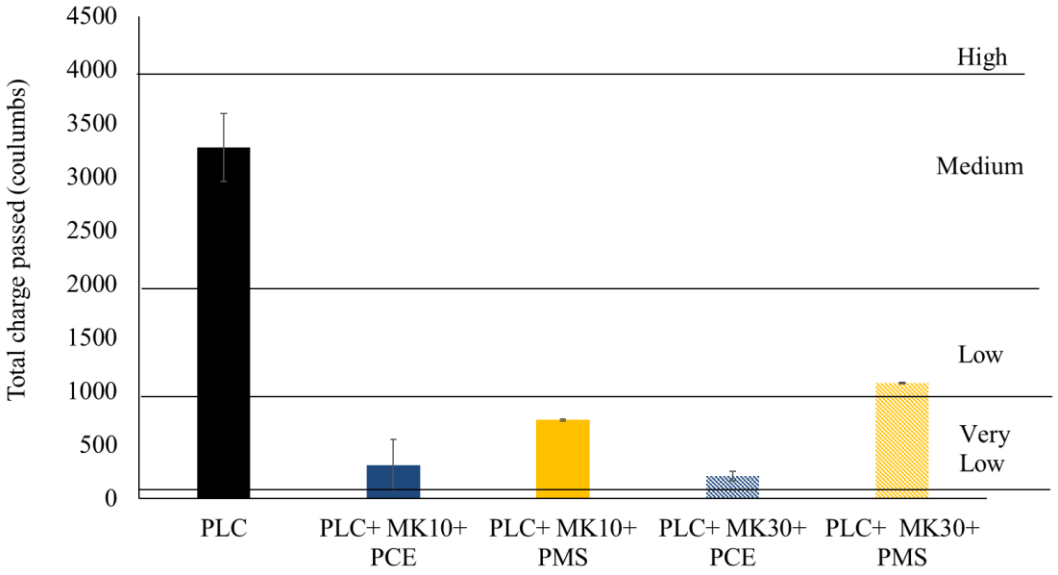

Figure 5.14. Total charge passed by RCPT for PLC and PLC with MK concretes, after 56 days of hydration. *Surface resistivity*

The evolution of surface resistivity (SR) over the first 56 days of hydration is shown in Figure 5.15 for the PLC concrete and PLC-MK concretes. To aid in the interpretation of the results, horizontal dashed lines are shown in all figures to indicate the permeability classifications defined by the standard (Table 5.7). The surface resistivity of PLC concrete is adopted from another study by Nadelman [237]. Note that the measurements were carried out every day for the first 10 days and then every three days after that.

In general, all mixes show increasing resistivity with time, as expected since the primary hydration of the cement and the secondary hydration of the SCMs reduce and

refine the porosity. The SR of concrete is inversely related to the permeability of concrete; that is, the higher surface resistivity of concrete corresponds generally with lower permeability. While the surface resistivity of PLC mixtures tends to reach a plateau after about 14 days of hydration, the MK concretes show further SR development up to and even beyond 28 days of hydration. This suggests continued microstructural development due to secondary pozzolanic of the MK.

All MK concretes exhibited higher surface resistivity than that of PLC plain concrete, while the change in the surface resistivity with increase in the MK content depends on the water reducer chemistry. With PCE admixture, the surface resistivity of MK30 concrete is higher than that of the MK10 concrete. However in PMS concrete, MK10 showed a higher resistivity than that of MK30. The higher SR of MK10 concrete than that of PLC concrete can be due to the filler effect and pozzolanic activity of MK that densifies the concrete microstructure. The increase in the SR of concrete from MK10 to MK30 with PCE can be due to the higher pozzolanic activity with higher MK content, which is facilitated at the higher MK fraction by the effective dispersion provided by PCE admixture. With other WRAs, the lower SR of concrete with increases in the MK content from MK10 to MK30 can be due to the higher MK and lower cement contents that PMS was not effective enough to disperse the higher fraction of MK particles, and hence the potential improvements to microstructure refinement were not fully realized.

Table 5.6. Permeability classifications for concrete tested according to the AASHTO T 358 [214] surface resistivity test.

Classification	SR limits (kOhm-cm)
High	< 12
Moderate	12 – 21
Low	21 – 37
Very Low	37 – 254
Negligible	> 254

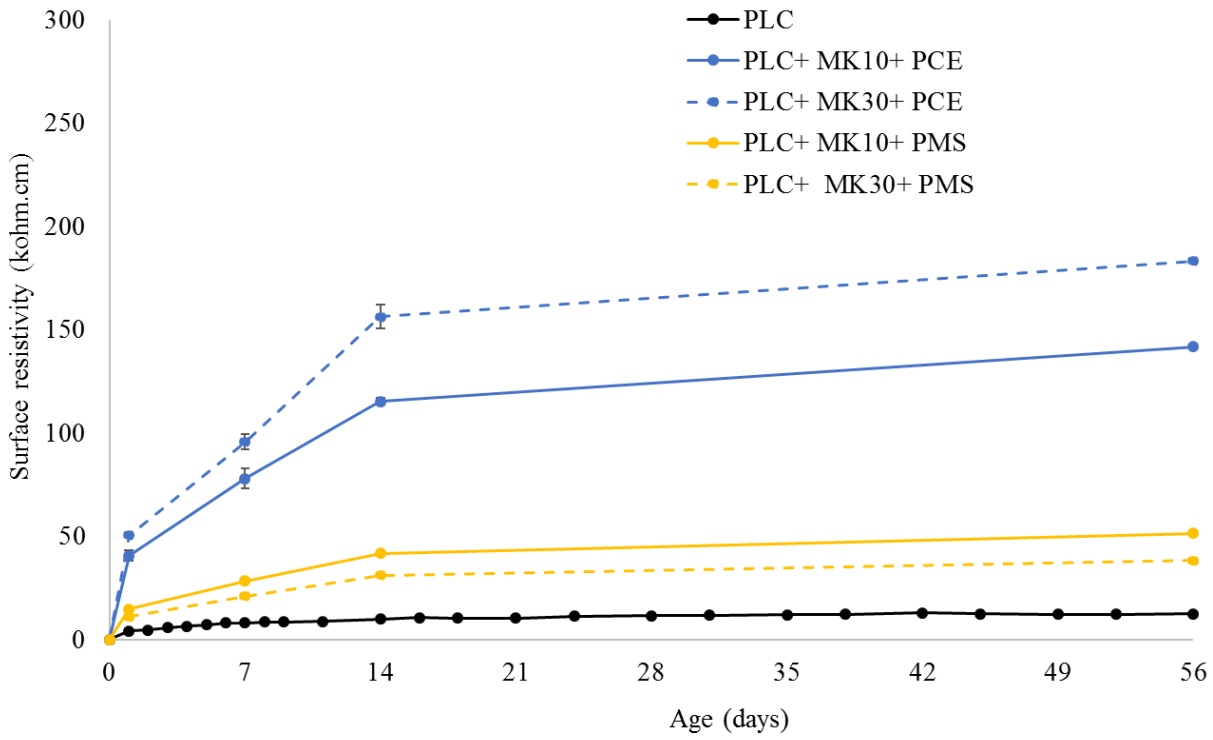

Figure 5.15. Surface resistivity measurements over the first 56 days of hydration for PLC and PLC-MK concretes. (AASHTO T 358)

Comparing the 56-day SR and RCPT results (Figure 5.16) shows that the two tests have a nearly perfect inverse relationship (with the R^2 of 0.99) to one another. Given the inverse relationship of conductivity (on which RCPT depends) and resistivity (measured

directly by the SR test) [237], a relationship is anticipated, but the strength of the correlation – given the complexities of the binder and use of WRAs – was not fully anticipated It should be noted that the results of RCPT and SR test methods in this study showed consistent results to one another because both tests are based on the microstructures of the concrete and also the factors, such as pore solution chemistry, that can affect both SR tests and RCPT results. Therefore, the results of both tests can be interpreted as combined effect of concrete microstructures and pore solution effects, as it was mentioned in previous studies as well [238]. Overall, The results of both tests showed that MK concrete permeability is the categorized as low to very low, suggesting very good durability.

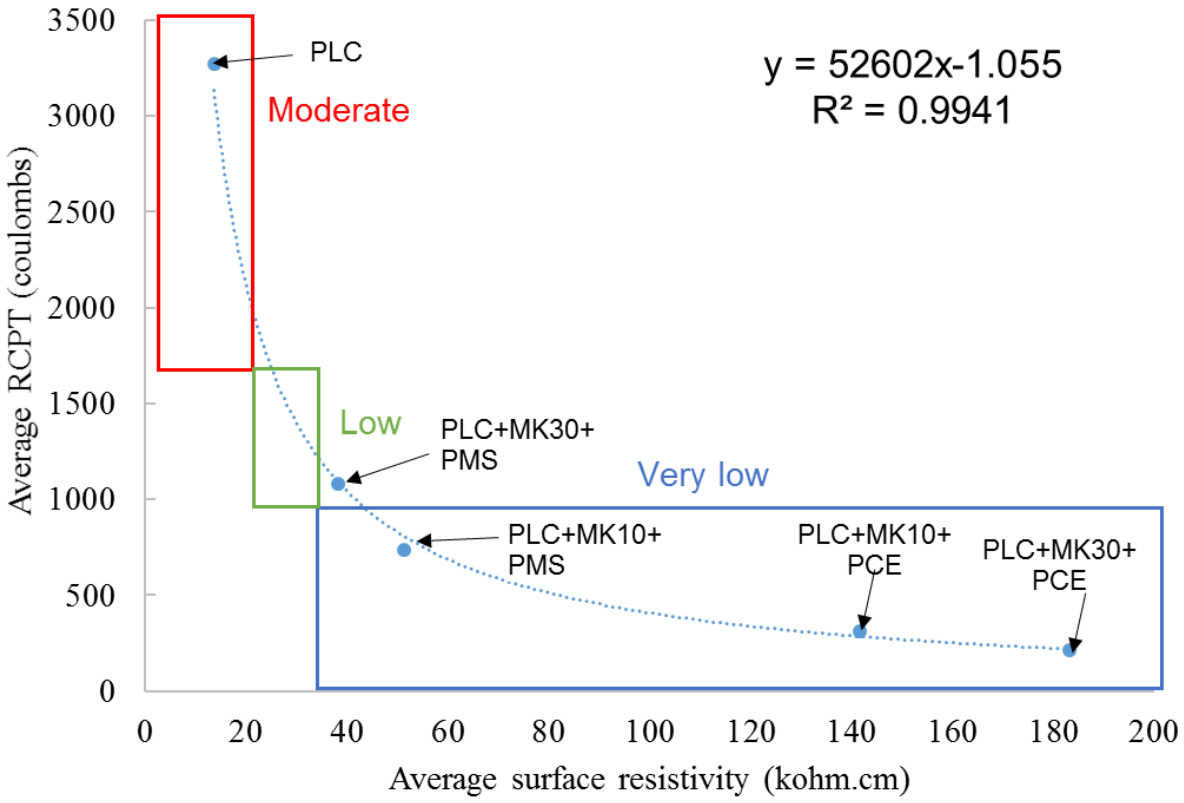

Figure 5.16. Correlation between SR and RCPT results for PLC and PLC with MK concretes.

5.5.2. Dimensional stability

The dimensional stability of concrete is important in determining the crack resistance due to shrinkage. Drying shrinkage in concrete is one the main components of deformation in hardened concrete, and this form of shrinkage is mainly due to the water loss in hardened concrete. In this section, the effect of MK on the drying shrinkage of concrete and the influence of WRAs chemistry is evaluated. The maximum drying shrinkage is usually limited to 600-750 microstrain.

5.5.2.1.Drying shrinkage

The drying shrinkage of PLC and PLC-MK with MK concrete was measured over 90 days of drying, as shown in Figure 5.17. The MK concretes, in general, showed relatively lower drying shrinkage, with the least shrinkage recorded for MK30 concretes with PCE. In the first days, the difference between amount of the drying shrinkage of PLC and PLC-MK concretes was small. But after about 2 weeks the different behaviors became much clear, and the shrinkage of concrete generally decreased with increasing replacement levels of MK. The lower shrinkage of MK concrete particularly after 2 weeks can be because due to pozzolanic activity that there is less evaporable water available in the mixes due to the combination of hydration and pozzolanic reactions [232] and also because the densification of the matrix can slow or decrease moisture migration out of the concrete. When the shrinkage strain at 60 days of drying was considered, the PLC-MK concrete had remarkably lower shrinkage strain in comparison to PLC case.

The shrinkage trend of MK concretes with the same MK content and different admixtures are similar to each other. This shows that the effect of MK content is more important in determining the shrinkage behavior than that of admixture. The admixture type is important in affecting the total shrinkage amount. MK10 concrete with PCE showed the similar or slightly higher shrinkage than that of control specimens (PLC concrete). With increase in the MK content (MK30 with PCE), the concrete shrinkage is similar to that of PLC concrete for the first 7 days while it further decreased to be as low as 47% of the PLC concrete at 90 days, suggesting a dominant dilution effect, potentially also combined with decreased potential for moisture migration. MK10 concrete with PMS showed less shrinkage compared to that of PLC concrete. A potential reason includes poor dispersion

of MK leading to a greater dilution effect. The MK30 with PMS showed the higher shrinkage for the first 24 hours and plateaus afterward.

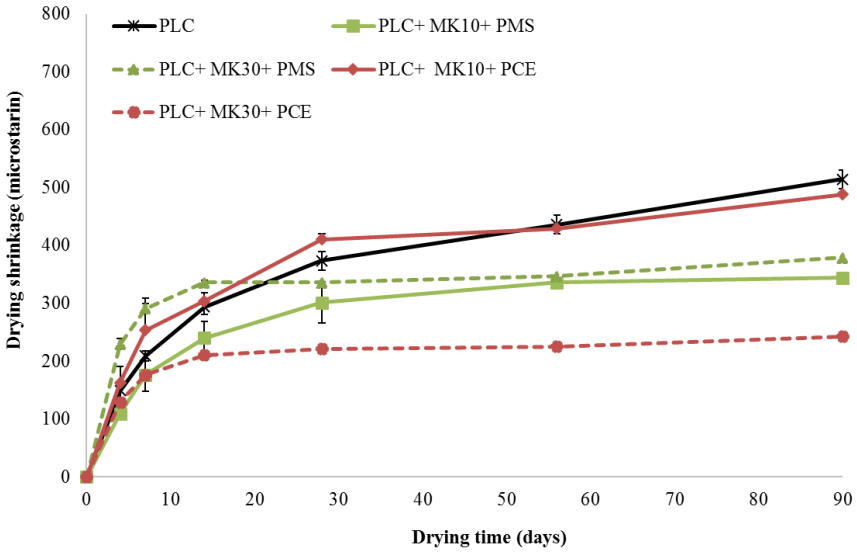

Figure 5.17. Drying shrinkage of PLC and PLC-MK concrete prisms over 90 days of drying. The concrete prisms were cured in limewater at 25°C for 28 days before drying in air at 50% RH.

Drying shrinkage of unreinforced concrete occurs in the paste fraction and develops stress in concrete, due to internal restraint provided by the aggregate. When this stress is higher than the tensile capacity of concrete (neglecting stress relaxation effects), concrete cracks.

The following equation (Equation 5-12) assumes linear-elastic behavior and uses Young's modulus of elasticity (measured in this study) and the shrinkage strain at 28 days to estimate the stress developed from the drying shrinkage strain. The calculated stress was then compared with the tensile strength of concrete at 28 days measured in this study (Table 5.7).

$$\sigma = E \times \varepsilon \qquad 5\text{-}12$$

Table 5.7. Comparison of developed stress due to the drying shrinkage with the measured tensile stress

	PLC	PLC+ MK10+ PCE	PLC+ MK10+ PMS	PLC+ MK30+ PMS	PLC+ MK30+ PCE
Elastic modulus (ksi)	4000	6842	6808	5418	7068
Tensile strength at 28 days (ksi)	0.72	0.83	0.56	1.02	0.63
Drying shrinkage strain at 28 days (με)	0.0004	0.0004	0.0003	0.0003	0.0002
Developed stress (ksi)	1.49	2.74	2.04	1.62	1.41

It can be seen that for all concretes, even for PLC concrete with no MK, the developed stress due to the drying shrinkage exceeds the tensile strength of concrete. In fact, the predicted tensile stress is almost double the tensile strength. While this is a simplistic analysis, one which neglects the ameliorating effects of stress relaxation but also does not consider the additive effects of chemical and autogenous shrinkage, the high magnitude of the anticipated stress due to drying shrinkage alone relative to the tensile strength suggests cracking in concrete of these mix proportions is a concern. The next chapter evaluates the use of shrinkage reducing admixture (SRAs) in concrete to mitigate cracking potential.

5.5.Conclusions and discussion

The use of MK in PLC concrete was found to affect the fresh and hardened concrete properties. Two HRWRAs, PCE and PMS, based on their higher effectiveness in addressing workability were compared in this study. In terms of fresh concrete properties, the PLC-MK concrete in general exhibited slightly lower air content, potentially due to

improved workability and improved packing. The MK concrete with PCE had a higher air content than that of PMS concrete, likely due to the foaming properties of PCE.

In terms of hardened concrete properties, MK addition in general increased the mechanical properties of concrete. The MK concrete with PMS showed similar compressive strength to PLC concrete at 1 day and was higher than that of PLC concrete at later ages. The MK concrete with PCE had a higher compressive strength than PLC concrete as early as one day. The higher mechanical properties of MK concrete at early age are believed to be related to the combination of the filler and nucleation effect of MK while the extension of these improvements at later ages can be due to the pozzolanic reaction of MK with CH produced by cement hydration. Similar to the compressive strength, the 28-day tensile strength of PLC-MK concrete with PCE was higher than that of PLC concrete. The tensile strength of PLC-MK concrete with PMS was lower than that of PLC concrete; observations of a failure mode dominated by cracking around the aggregate and through the paste, it can be interpreted that this is because of the weaker ITZ and lower bond of cement paste with the aggregates in this mixture. The ACI equation was not capable of predicting the tensile strength of MK concrete in this study and therefore, this study developed a new equation to predict the tensile strength of MK concrete based on the results of this study. The elastic modulus and Poisson's ratios of MK concretes followed the similar trend that MK10 and MK30 concretes with PCE showed higher elastic modulus and Poisson's ratios than those of PLC concrete, while the MK10 concrete with PMS exhibited a lower modulus and MK30 with PMS a higher elastic modulus. The higher elastic modulus with higher MK content can be because of the better packing due to the filler effect of fine MK particles. The higher elastic modulus with PCE can be due to the

better dispersion of MK particles and greater reaction of the MK. The predicted elastic modulus by ACI 363 showed the closest approximation to the experimental data.

The effect of MK on the durability and dimensional stability of concrete was evaluated through permeability and drying shrinkage. The results of the rapid chloride penetration test (RCPT) show that the addition of MK decreases the permeability of concrete significantly from moderate for PLC concrete to low and very low PLC with MK. The surface resistivity (SR) of MK concrete fell in the very low category defined by AASHTO T 358-15 [214]. This lower permeability of MK concrete can be due to the effect of MK on densifying the concrete through filler and pozzolanic effects, contributing to pore filling and densification of the concrete matrix. The WRA chemistry influenced the MK concrete permeability, and the MK concrete with PCE had lower permeability than that of MK concrete with PMS. Good correlation was observed between the RCPT and SR results.

The effect of MK on drying shrinkage of concretes showed that the MK addition decreased the concrete shrinkage, but that the concrete still had likely high cracking potential. The lower shrinkage of MK concrete may be because of the pozzolanic activity of MK that as a result, there is less evaporable water available in the mixes as hydration and pozzolanic reactions used up most of the free water and also because of decreased moisture migration due to matrix densification. The MK10 concrete with PCE exhibited similar shrinkage to that of PLC concrete, while with increase in the MK content to 30% the shrinkage decreased to be as low as 47% of the PLC concrete at 90 days. The MK10 and MK30 concrete with PMS showed a lower drying shrinkage at 60 and 90 days. The stress developed in concrete due to the shrinkage was calculated by linear-elastic theory

using the elastic modulus calculated in this study. The results of this fundamental analysis show that the developed stress is higher than the tensile strength of all concretes that can cause cracking in concrete. The application of shrinkage reducing admixtures (SRAs) to improve dimensional stability will be discussed in the next chapter.

CHAPTER 6 THE AUTOGENOUS SHRINKAGE OF PLC-MK PASTE AND THE SHRINKAGE REDUCING ADMIXTURES INTERACTIONS

6.1.Introduction

In cement-based materials, autogenous deformation is defined as the bulk deformation that occurs under sealed conditions at a constant temperature [239]. Autogenous shrinkage results from ongoing cement hydration and pore refinement after initial set. Autogenous shrinkage is most prevalent in low w/b systems (e.g., $\leq$ 0.42). In such systems, most of the free water is consumed by the time surrounding initial set and if no additional curing water is available, water extracted is progressively extracted from the capillary pores as the unhydrated cement undergoes hydration. As the capillary pores are emptied, surface tension is generated in the pores. Through restraint to this shrinkage, localized tensile stresses are generated in the past and can cause cracking.

The capillary tension in a pore is related to the surface tension of the pore solution and is inversely related to the pore radius (Equation 6.1), meaning that smaller pores will experience higher capillary tension in shrinkage, as described by the Young-Laplace equation:

$$\sigma_{cap} = \frac{2\gamma}{r} \qquad 6\text{-}1$$

Where σ_{cap} (Pa),

γ is the surface tension of the pore solution (N/m), and

r is the radius of the largest water-filled cylindrical pore (m).

The reduction in water-to-binder ratio, the incorporation of finely divided SCMs (e.g., silica fume, metakaolin), and the increase in binder fraction of high-performance concretes all results in increase in the autogenous shrinkage. Autogenous shrinkage is typically more significant in cases where the w/b is 0.42 or lower, as less water is available for cement hydration, leading to higher capillary stresses at earlier ages. However, it can also be observed for cement pastes with denser microstructures containing SCMs, even if sufficient water is available; here, the narrow pores restrict water mobility through the paste and create localized regions of low relative humidity [240]. It was reported that the use silica fume particles (<1 μm in diameter) that are much finer than cement creates a much finer pore structure within the hydrating cement paste can consequently increase the surface tension and shrinkage of concrete [239, 241].

As the use of finer SCMs has increased in the concrete, problems with greater shrinkage and early-age cracking have become more prominent. Whiting et al. [242] showed that silica fume (SF) increased the early-age cracking shrinkage of concrete, while it has a little effect on the ultimate (long-term) shrinkage of concrete. Another study [243] showed that the use of SF decreased the age of cracking, compared to that of concrete with OPC and fly ash, suggesting the role of accelerated hydration on the development of autogenous shrinkage cracks. However, it was observed that if the specimens are subjected to 7 days of moist curing prior to exposure to a drying environment, the SF concrete might not crack earlier. Brooks et al. [65] showed that the addition of MK at 5% replacement increased the autogenous shrinkage of concrete while 10 and 15% additions reduced the autogenous shrinkage. The autogenous shrinkage can be up to 40-50% of the total shrinkage in concrete for concrete with the w/b of 0.3-0.4 and the contribution of autogenous shrinkage to the

concrete shrinkage increases with the lower w/b ratio or with the use of finer SCMs such as MK or SF. This higher shrinkage of concrete with SCMs and finer fillers should be considered and mitigated to prevent cracking in concrete.

Several strategies have been suggested to mitigate autogenous shrinkage in concrete. Mitigation strategies discussed include control of the cement particle size distribution, modification of the mineralogical composition of the cement, the use of shrinkage-reducing admixtures, the addition of internal curing agents, and the use of controlled permeability formwork. Changes in mixture design (e.g., decrease cement content, increased aggregate content, use of coarser or less reactive SCMs, etc.) can be used to reduce autogenous shrinkage. Also, because moisture provided by external curing can be difficult to penetrate into HPC, internal curing agents (e.g., saturated lightweight aggregate, superabsorbent polymers, wood-derived particulates and fibers) have been shown to mitigate autogenous shrinkage of concrete as well. However, in some cases where severe environmental conditions (e.g., high temperature and low humidity) exist or when derivable locally available materials are not available, changes to the concrete mix to control the concrete shrinkage can be impractical. Therefore, in practice, shrinkage-reducing admixtures are more commonly used to control shrinkage of concrete.

The mechanism by which most commercial SRAs control autogenous shrinkage of concrete is by decreasing the surface tension of pore solution [115, 116, 239]. The history and use of shrinkage-reducing admixtures (SRAs) has been reviewed by Nmai et al. [244]. The world's first shrinkage-reducing admixture (SRA) was developed in Japan in 1982 [245, 246]. The main component of many commercial SRAs is polyoxyalkylene alkyl ether, which is a nonionic surfactant[125].

In general, SRAs have been shown to reduce the shrinkage of concrete by as much as 50% [110, 247]. Rongbing and Jian [110] show that the use of SRA at 2% by mass of cement can decrease the autogenous shrinkage for mortar by about 20–30% at 90 days. Additionally, the SRA addition can reduce the capillary stresses generated by autogenous shrinkage in high performance concrete with contain finer SCMs or have a lower w/b [239, 248].

The effect of SRAs on the pore solution of concrete was evaluated by measuring the change in chemistry and surface tension of pore solution with and without SRAs addition [116]. It was reported that SRAs molecules accumulate at the pore solution-pore interface and can significantly reduce the interfacial tension by reducing the degree of dissimilarity (.g. between water and air) at the interface which can result in a reduction of the interfacial free energy [125]. The extent of surface tension reduction is limited by the number of SRAs can accommodate at the water-air interface and the self-agglomeration of SRA molecules [220]. The SRA surfactants can self-aggregate in the bulk solution by forming the micelles that limit the effectiveness of SRA in reducing the surface tension beyond a dosage known as the critical micelle concentration (CMC) [249]. For the concentrations below the CMC, surfactant molecules are mainly adsorbed at pore solution-pore interfaces, and thus the surface tension is continuously reduced with increasing surfactant concentration until reaching the CMC. Above the CMC, excess surfactant molecules form micelles (Figure 6.1) in the water and cannot further reduce the surface tension [250].

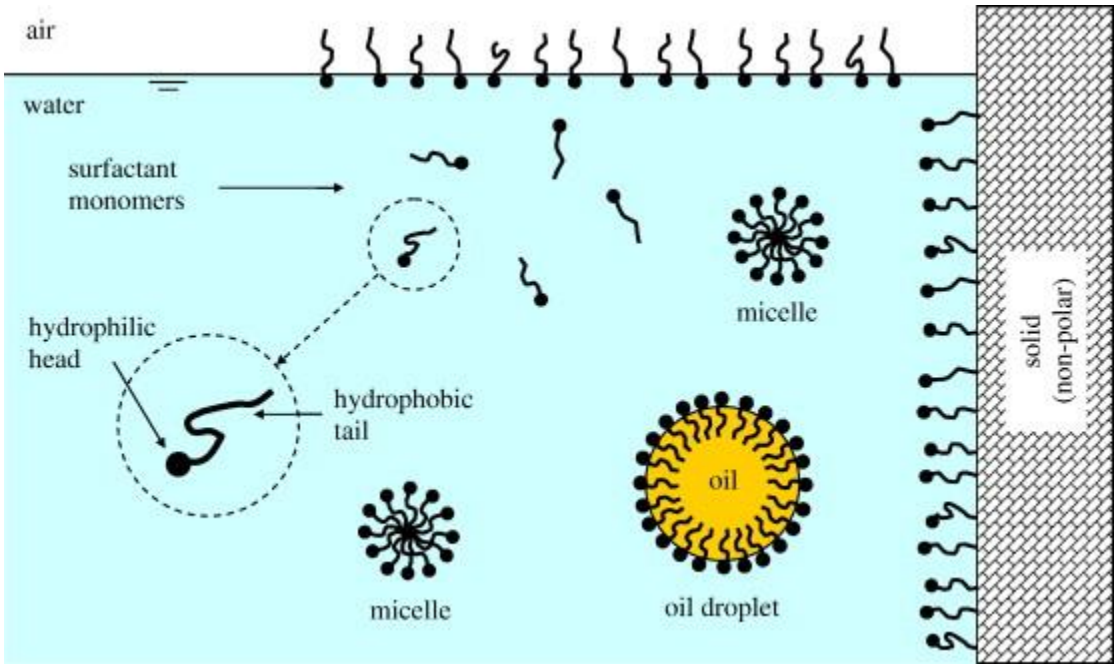

Figure 6.1. Interactions of surfactant (amphiphilic) molecules of SRAs with a polar solvent (e.g., water); adapted from [251]

Changes in the surface tension of the pore solution as a function of SRA dosage have been measured in the previous studies directly using tensiometer [115, 116] or indirectly by measuring the contact angle [252]. In the latter method, the surface tension is estimated from the contact angle measurement based on the Young-Laplace equation (Equation 6-2). Generically, the solid-liquid and solid-vapor interfacial energy depends on the solid, where values can be found in databases and published literature. SRA additions also showed to change the pore solution chemistry over the cement hydration process [116, 121]; pore solution composition can be measured on expressed or model pore solutions through a variety of analytical methods.

In this study, the autogenous shrinkage of PLC and PLC-MK pastes are measured to examine the effect of MK on the rate and overall autogenous shrinkage developed over the

first 28 days after the final setting time. For comparison, pastes prepared with quartz powder, which is essentially inert in this system, of a similar particle size distribution as the MK is also examined in combination with PLC. Moreover, the interaction and effectiveness of SRAs at different dosages with PLC-MK pastes with 10 and 30% MK is assessed.

6.2.Materials and methods

The cement used in this is ASTM C595 Type IL portland limestone cement (LS ≤ 15%) [41] provided by Argos where the clinker was produced in Calera, AL and finished in Roberta, GA. High purity metakaolin (Burgess Pigment Company, Sandersville, GA) was used as a replacement for cement at rates of 10% and 30% by mass of cement, denoted according to their MK contents as MK10 and MK30, respectively. The chemical composition and physical properties of the cement and MK are shown in Table 3.1.

A commercially produced quartz powder from Silica USA with a maximum particle size of 5 μm was selected to closely resemble the particle size distribution of MK powders. The particle size distribution of PLC, MK, and quartz (Figure 6.2) shows that MK and quartz have particle size distribution that is finer than the PLC powder. The WRA used in this study is PCE, which is a HRWRA. The shrinkage-reducing admixture used in this study is SIKA control 220 used at the dosages of 1% and 2% by mass of binder (cement+ metakaolin).

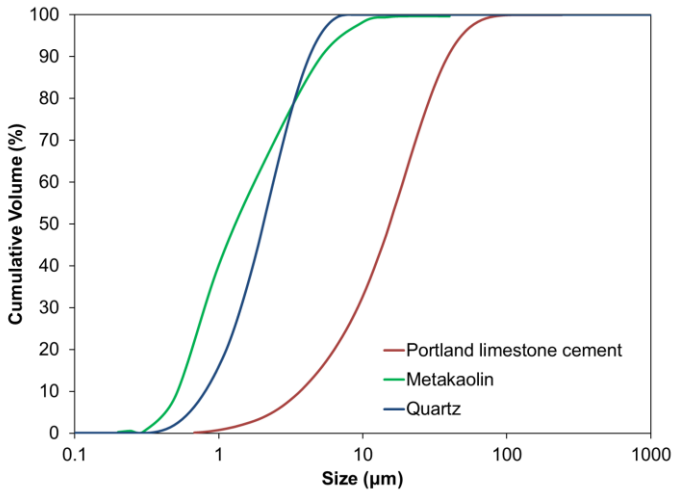

Figure 6.2. Comparison of particle size distributions of commercially produced quartz powders with portland limestone cement and metakaolin powders.

The autogenous shrinkage was measured on cement paste prepared with a w/b of 0.4 with PLC, PLC with MK, and PLC with quartz following ASMT C1698 [253]. This test method measures the bulk strain of a sealed cement paste or mortar specimen at a constant temperature and not subjected to external forces, from the time of final setting until a specified age with the negative strain corresponds to shrinkage and positive strain corresponds to expansion. The mixing procedure consisted of manual stirring of the cement with deionized water (containing HRWRA as determined in Chapter 3) for 30 s, and followed by mechanical mixing of the paste mixture with a 5-speed hand mixer at low speed for 60 s and at medium speed for 60 s. The PCE admixture was used in all mixes with the dosage determined by the mini-slump test shown in Chapter 3. Three specimens were cast for each mixture, poured in corrugated tube molds (Figure 6.3), and sealed with Parafilm tapes and stored in an environmental chamber at 23°C and 50% relative humidity (RH). The autogenous tubes were rotated every two hours for the first 6 hours as

recommended by Mohr and Hood [254] to avoid the potential for bleed water reabsorption and early age expansion.

Starting at the time of final setting, the length of the specimen is measured using a dilatometer. The time of final setting was determined by penetration of a Vicat needle in accordance with ASTM C191 [180]. Measurements of autogenous deformation were taken every 2 hr. for the first 6 hr., once daily until 7 days, bi-weekly until 28 days (see Figure 6.6).

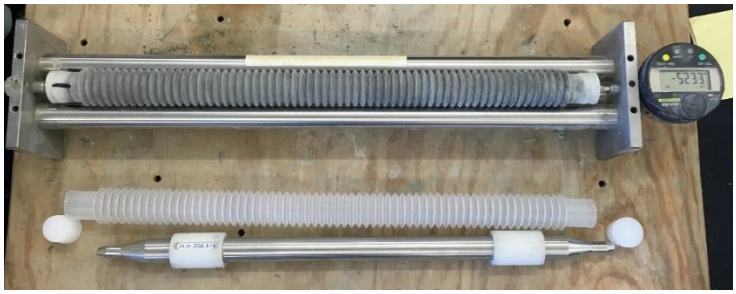

Figure 6.3. The autogenous shrinkage test apparatus, plastic tube, and the reference bar

Isothermal calorimetry was used to measure the heat release from cement paste with and without SRAs in the first 48 hours of hydration following ASTM 1679 [168] to examine the effect of SRAs on the cement hydration kinetics. The cement paste was mixed and cast following the method described for autogenous shrinkage paste.

A model pore solution was made in this study by mixing 10 g cementious materials and 20 g deionized water without and with SRAs at 0 to 20% by mass of binder (PLC+MK). The mix was then centrifuged at 400 rpm for 10 mins followed by filtering of the supernatant through a 45-μm pore size membrane attached to the top of a syringe. Goniometry (Ramé-hart Model 250, Figure 6.4) was used to measure the contact angle of

the pore solutions with different SRA concentrations. The surface tension of pore solution was then calculated, using Equation 6.2:

$$\gamma_{SG} - \gamma_{SL} - \gamma_{LG} \times \mathrm{Cos}\,\theta_C = 0 \qquad 6\text{-}2$$

Where:

γ_{SG} is the solid–vapor interfacial energy,

γ_{SL}, the solid–liquid interfacial energy,

γ_{LG}, the liquid–vapor interfacial energy (i.e. the surface tension), and

θ_C is the equilibrium contact angle

The solid surface used in this study is a silica wafer with a solid-vapor interfacial energy of 1240 erg/cm^2 (1.24 J/m2) [255]. The contact angle was measured by the static sessile drop method with the microliter syringe attached to add one drop of a sample on a wafer positioned on a small movable table. The contact angle was measured from captured camera data, using software developed by Pavel [256].

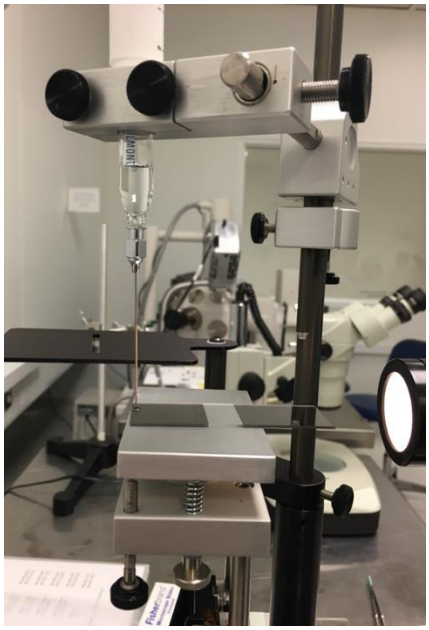

Figure 6.4. Goniometer (Ramé-hart Model 250) used for contact angel measurement

The ion concentrations in pore solution with and without SRAs were measured using Optical Emission Spectroscopy (ICP-OES) over time to determine the effect of SRAs on the pore solution chemistry. The filtered pore solution were diluted 100X and stored in sealed polypropylene vials until analysis. The ICP-OES Perkin Elmer Spectrometer Optima 7300DV was used to analyze the diluted pore solution. Inductively coupled plasma atomic emission spectroscopy (ICP-OES) is an analytical technique used to detect the element concentrations in a solution. This method has been used in previous studies to detect the elements in the pore solutions of concrete [257] and determine the ions present in leachates from cements [258].

Nitrogen gas adsorption and desorption were used to measure the porosity of the PLC pastes without and with 2 and 10% SRA dosages. Paste specimens were prepared at w/b = 0.40, using the mixing procedure described in Chapter 3 and after 1 day of hydration fragments of

paste were removed from each specimen and crushed until they were 0.595-1.00 mm in size (passing No. 18 sieve and retained on No. 30 sieve). The crushed fragments were submerged in liquid nitrogen for 15 min to stop hydration, then freeze-dried at -48℃ and 0.02 mbar pressure for 48 hr to sublimate the frozen pore water. Approximately 1.5 g of crushed material was analyzed in a Micrometrics ASAP 2020 specific surface area gas analyzer. Specimens were degassed at 10-μm Hg pressure and 105℃ for 12 hr prior to analysis. Analysis was performed at 77 K (-196°C) using nitrogen gas adsorbate over a relative pressures range of 0.01 to 0.99. Specific surface area was determined by Brunauer, Emmett, Teller (BET) theory [259] using the adsorption isotherm between relative pressures of 0.05 and 0.30. Pore size distributions, total pore volume, and average pore diameter were determined using the Barrett, Joyner, Halenda (BJH) method [260] on data obtained from the desorption isotherm

6.3.Results

In this section, first the autogenous shrinkage of PLC with MK is presented to show the effect of MK on PLC paste shrinkage and evaluate the risk of early-age cracking of concrete. Next, the effectiveness of SRAs at different dosages on mitigating the shrinkage of MK10 and MK30 paste was evaluated, and mechanisms for control are explored through complementary assessments by ICP-OES, contact angle measurements, and isothermal calorimetry tests.

6.3.1. The autogenous shrinkage of PLC-MK blended cement pastes

The measurement of autogenous shrinkage of cement paste was started after the final setting time of paste mixes. The setting times for PLC and PLC with quartz, MK10, and MK30 with and without SRAs are shown in Figure 6.5. The results show that 1% SRAs can have a slight effect on delaying the initial and final setting time of mortar mixes by 20-

30 min, while the use of SRA at 2% showed to increase both initial and final setting time of PLC-MK30 sample up to 3 hours showing the strong retardation effect of SRAs at this dosage that will be evaluated in this chapter. Moreover, the setting time of PLC-MK30 paste is shorter than that of PLC-quartz paste, while both mixes have longer setting time than that of PLC paste. The shorter setting time of PLC-MK30 with the same cement content as of the PLC-Q30 shows some interaction occurs between MK and cement even at these early ages of hydration.

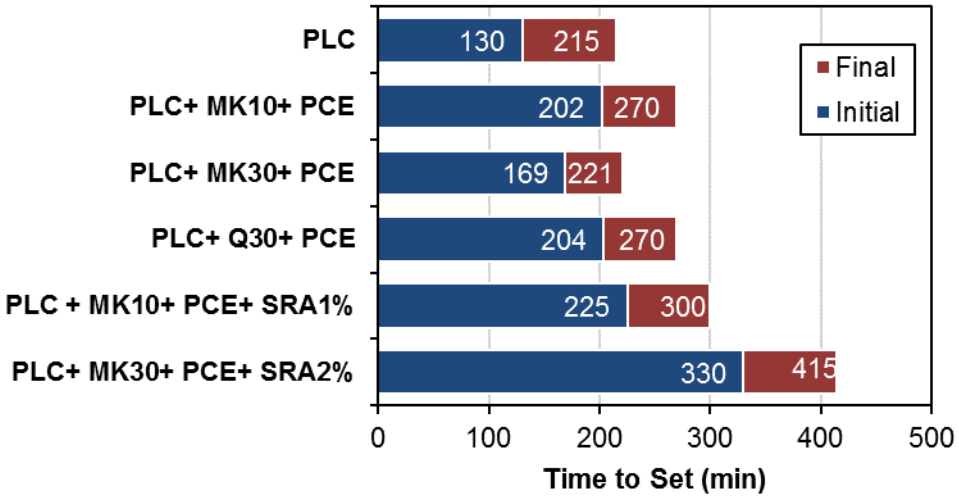

Figure 6.5. The initial and final setting time of PLC and PLC with MK10 and MK30 with and without SRAs. The autogenous shrinkage tests started after the final setting time for each mix.

The autogenous shrinkage of PLC, PLC-MK10, PLC-MK30, and PLC-Q30 are shown in Figure 6.6. The autogenous shrinkage of PLC-MK10 is close to that of PLC in the first days of hydration, but increased over time, ultimately achieving values up to 120% higher than the shrinkage of PLC paste at 21 and 28 days, similarly observed in a previous

study [138]. The higher shrinkage of MK10 can be due to the improved cement hydration provided by the nucleation effect, and largely due to the pozzolanic reaction of the MK itself. The introduction of fine particles also refines the pore structure and decrease the pore sizes, which contributes importantly to autogenous shrinkage.

Similarly, the autogenous shrinkage of PLC-MK30 was higher than that of PLC paste, even in the first days of hydration. As noted for the 10% case, this higher shrinkage can be in part due to the finer pores in the MK paste that according to Equation 6.1 can lead to increase in the surface tension and consequently greater autogenous shrinkage. It was shown in previous studies that the self-desiccation and autogenous shrinkage start to develop as soon as cement hydration begins and menisci rapidly develop into small capillaries if no external water is added [261, 262]. The drying of the very fine capillaries can generate high tensile stresses that shrink the hydrated cement paste that is referred to as autogenous shrinkage [263]. The shrinkage of MK30 paste plateaus after about 7 days, which can reflect a dilution effect in that there is less cement to hydrate.

The PLC paste with 30% quartz showed similar shrinkage to that of PLC paste for the first 3 days, but increased to be higher than the shrinkage of PLC afterward up to 14 days, trending at later ages similar to the MK30 case. The early age behavior suggests that any dilution effect by the introduction of quartz is compensated at early ages by nucleation and filler effects. At later ages, the pore size refinement – due in this case to particle packing alone with the fine quartz particles filling between the cement grains – compensate the dilution effect that results in a shrinkage similar to that of PLC paste.

The higher early shrinkage observed with MK30 paste and not in quartz paste at less than 7 days suggest that some additional interactions occur between hydrating cements

and MK. Previous studies [264] showed that in cement containing limestone powder or high aluminate content cement, formation of carboaluminate hydrates phases as early as 1 day can contribute to greater chemical shrinkage of the paste and increase the autogenous shrinkage [264, 265]. Therefore, it is proposed that the formation of aluminate phases such as calcium alumina hydrates, monocarboaluminate or hemicarboaluminate, or calcium aluminosilicate, such as gehlenite $Ca_2Al_2SiO_7$, in the PLC-MK pastes contributes to their greater early autogenous shrinkage, compared to PLC and PLC-30Q. The PLC-MK30 paste exhibits a higher shrinkage in the first 7 days of hydration with up to 1.5 times higher than the PLC paste shrinkage. This higher shrinkage of PLC-MK30 can cause potential cracking in concrete at early age.

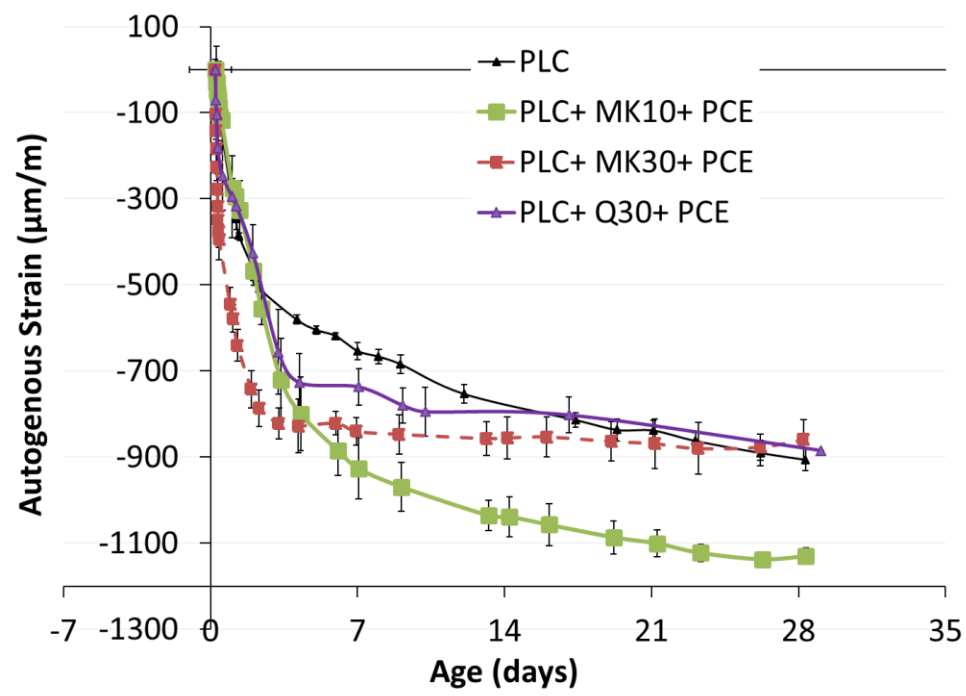

Figure 6.6. Autogenous shrinkage of PLC, Q-PLC and PLC-MK pastes

6.3.2. Effect of SRAs on controlling the shrinkage of PLC-MK paste

The higher shrinkage of MK-containing paste demonstrates the need to mitigate and control early shrinkage. The effectiveness of SRAs in controlling the shrinkage of PLC-MK at 10 and 30% replacement for cement is evaluated in this section.

The use of SRAs at 1% by mass of binder was used with PLC-MK10 and showed that it was capable of controlling the shrinkage of PLC with MK10 to be even lower than the shrinkage of PLC cement paste (Figure 6.7). It should be noted that in both mixes the same dosage of PCE was used to improve the workability of cement paste. The slight early expansion of cement paste observed in this study was also reported in previous studies and was contributed to the early formation of ettringite or reabsorption of bleed water [121, 266].

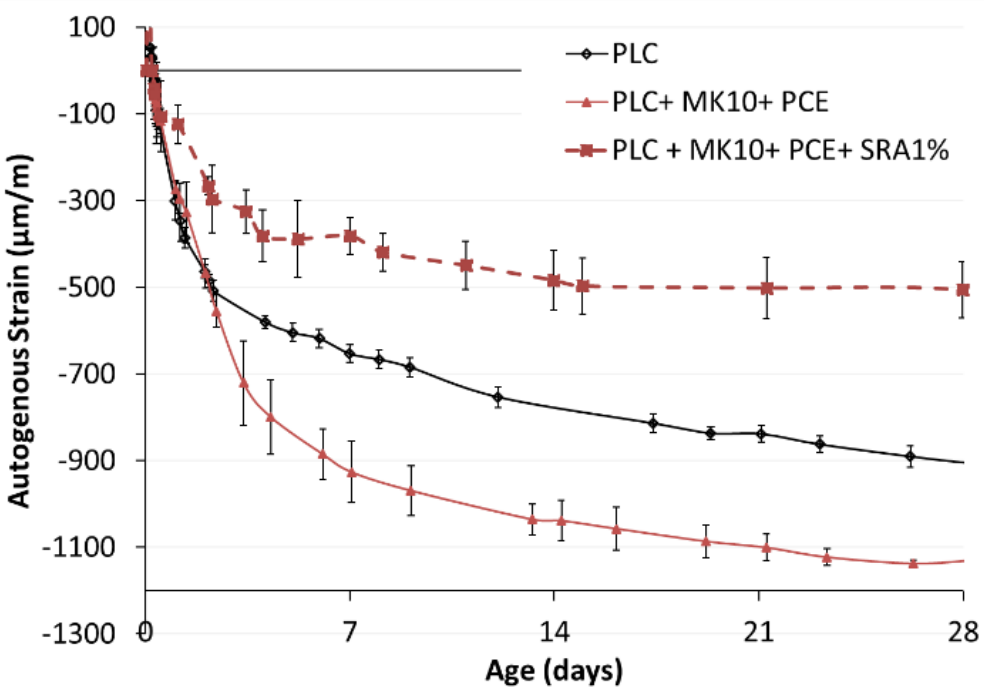

Figure 6.7. Autogenous shrinkage of PLC and PLC with MK and the effect of SRA at 1% on shrinkage mitigation of PLC with MK10.

The autogenous shrinkage of PLC with MK30 paste is shown in Figure 6.8. The shrinkage of PLC-MK30 paste was higher (up to 1.5 times) than that of PLC-MK10 paste, and therefore the SRA was first used at the rate of 2% by mass of binder. The use of SRA 2% with PLC with MK30 was shown to control the shrinkage of paste, but the shrinkage was unusually low that suggested the potential for a strong delay or inhabitation of cement hydration, as a 3-hour delay was observed it was observed in the setting time. The SRA dosage was then lowered to 1% and the results (Figure 6.8) showed that the shrinkage of MK30 paste was effectively controlled, with lower values than the PLC paste at up to 28 days. It should be also noted that a lower early expansion was observed in samples with SRAs as it was observed in previous studies [267].

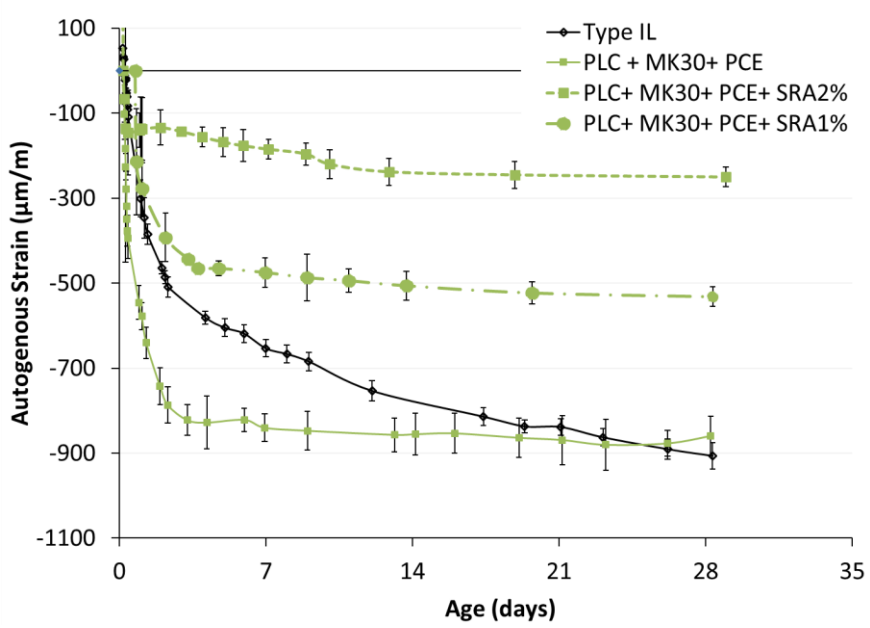

Figure 6.8. The autogenous shrinkage of PLC and PLC with MK30 paste and the effect of SRAs at 1 and 2% on the autogenous shrinkage of MK30 paste

6.3.3. Effect of SRAs on the pore solution chemistry

Previous research provides a good understanding of the time-dependent concentration of different ions in cement paste's pore solution without SRAs. However, the addition of SRAs can change the chemistry of portland cement pore solution, as shown in a previous study [116]. The results of this study showed that the presence of SRAs can noticeably decrease the concentrations of K^+ and SO_4^{2-} ions in the pore solutions of Type I ordinary portland cement. This observation was explained by a hypothesis that addition of SRA (which is a mixture of surfactant and non-polar oil) reduces the polarity of mixing water, and therefore, the affinity of salts (e.g., K_2SO_4) to dissolve and ionize into this "less polar" solvent is reduced [116].

Although the use of SRAs with the finer SCMs such as MK is necessary, the effect of SRAs on the pore solution of SCM blended cements is not yet evaluated and understood. Therefore, analysis here focused on examination of pore solution chemistry of PLC-MK30 without and with SRAs at 2%. The higher MK content and SRA dosage was used to signify the SRAs effect.

The concentrations of cement alkali cations in the PLC-MK30 paste pore solution with and without SRAs are shown in Figure 6.9. During initial mixing, a significant portion of alkalis dissolve in the pore solution, and upon increasing degrees of cement hydration further dissolution can occur that results in an increase in the concentration of K^+ and Na^+ as a function of time during the first hours of hydration (Figure 6.9).[1] These results show that the use of SRA at 2% can lower the concentration of the alkalis potassium (K^+) and sodium (Na^+) by 25-35% during the first few hours of hydration. The concentration of calcium (Ca^{++}) was also decrease by about 12%, but its total concentration is too low as to make this change negligible.

It was shown by previous researchers that the alkali sulfate are effective in accelerating the cement hydration [74, 268]. Thus, an ancillary effect of SRAs on

[1] Potassium (K+) and sodium (Na+) ions originate mainly from dissolution of alkali sulfates (K_2SO_4 and Na_2SO_4) into the pore solution [74] H.F. Taylor, Cement chemistry, Thomas Telford1997.. Taylor [74] ibid. showed that the concentration of K^+ and Na^+ in the pore solution can be calculated with a reasonable accuracy from the alkali content (K_2O and Na_2O) of the cement powder. The concentration of K_2O is 0.48% in the cement studied; given the 92 g/mole molecular weight of K_2O, that would be equal to 88 mmole/lit of K_2O if K_2O is totally dissolved. The Na_2O concentration is 0.09% in cement that will be equal to 26 mmol/l concentration in the pore solution if Na_2O is totally dissolved. ***Comment – are the results in Figure 6.9 reasonable?***

suppressing the alkali sulfate dissolution may be the retardation of the cement hydration. This effect will be discussed in the next session.

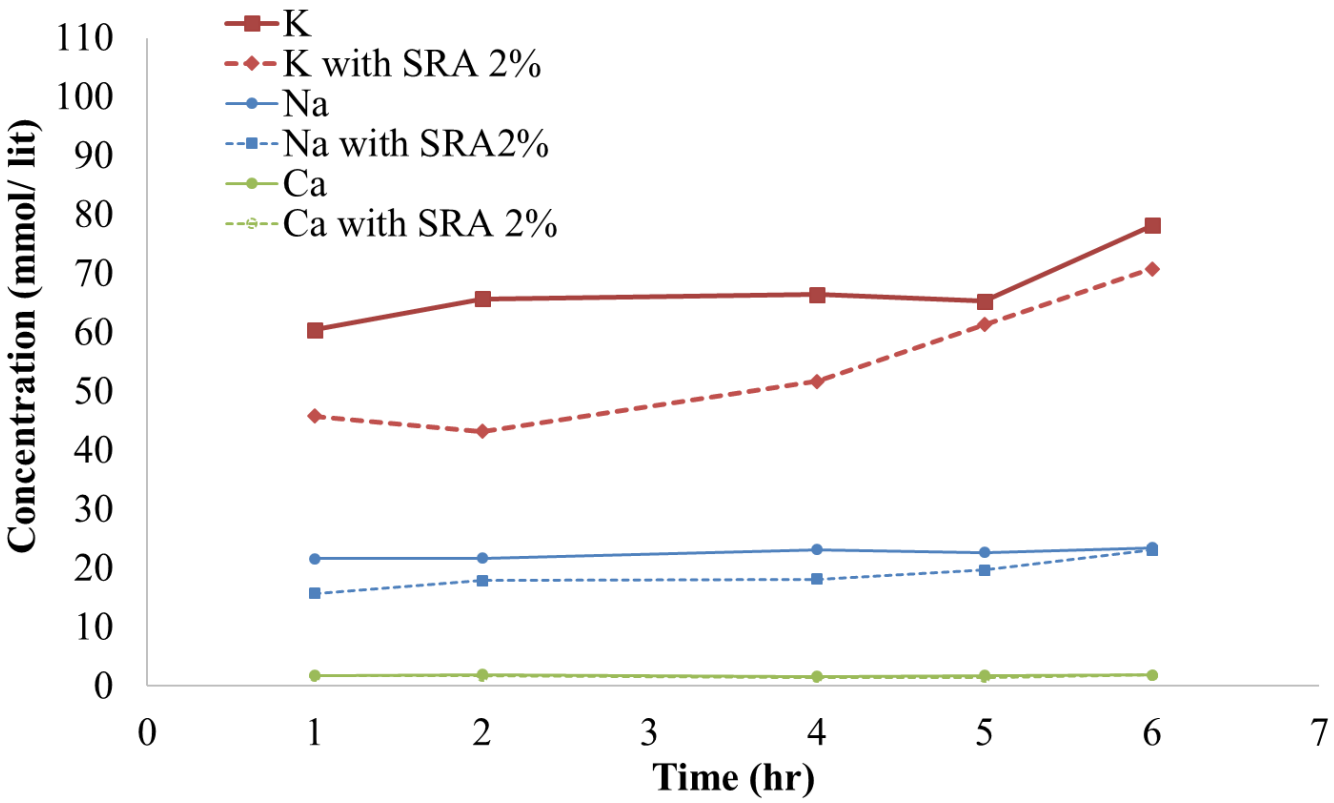

Figure 6.9. The concentration of cations in pore solution in PLC-MK30 over the first 6 hours of hydration measured by ICP-EAS

6.3.4. Effect of SRAs on cement hydration kinetics

The effects of SRAs on the cement hydration rate and total hydration heat are assessed by isothermal calorimetry and shown in Figure 6.10. The use of SRA at 1% was found to delay the rate peaks for hydration heat by about 3 hours. The delay in the cement hydration can be because of the apparent in the decrease the alkali content in the first hours of hydration, as shown in the previous section (Figure 6.9). The total heat of hydration was lower in the first 24 hour but it is similar to that of paste with no SRA by 60 hours.

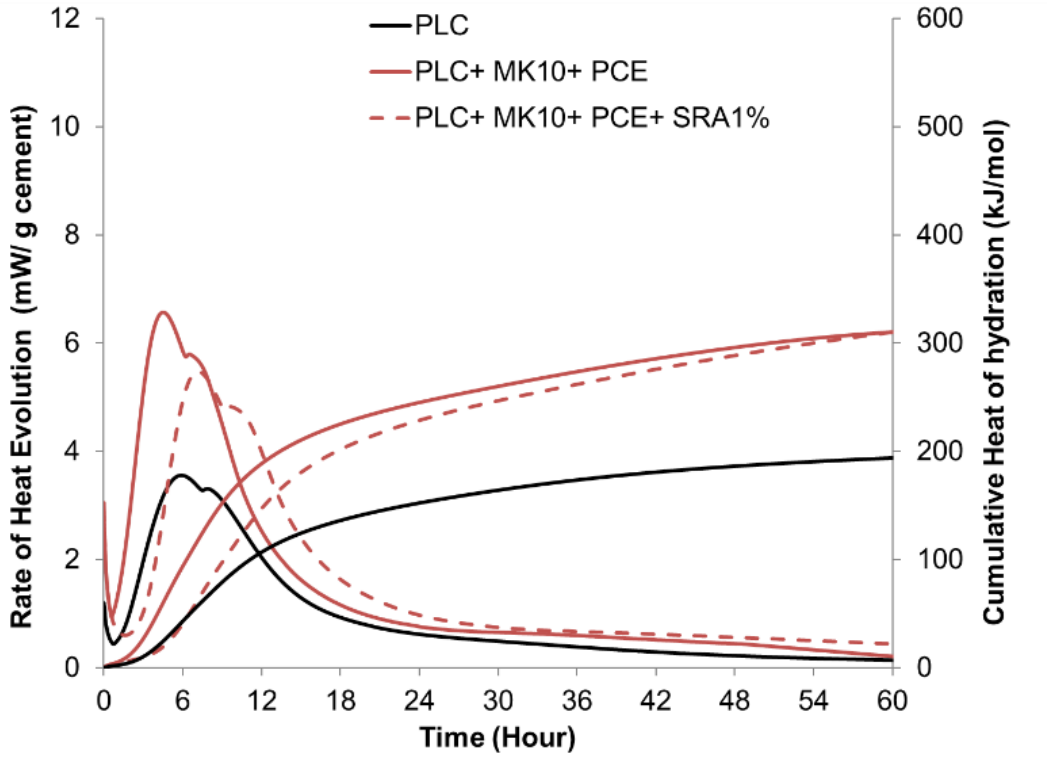

Figure 6.10. The rate and total heat of hydration of PLC, PLC-MK10, and PLC-MK10 with SRAs to show the effect of SRAs on the rate and total cement heat of hydration

The effect of SRAs on the hydration of PLC-MK30 is shown in Figure 6.11. The addition of SRA at 2% delays the cement hydration by about 5 hours and suppresses the hydration heat significantly (by 50%). This delay is evident as the total heat of hydration starts to increase at about 30 hours and become higher than the PLC cement paste at 60 hours, but still lower than the PLC-MK30 paste with no SRA. This strong delay can play a significant role in causing the lower early autogenous shrinkage of paste with 2% SRA.

The use of SRA at 1% in the MK30 system did not delay the hydration peaks as the 2% case experienced, but decreases in the hydration peak heights by about 30% were

observed when comparing to the PLC-MK30 paste without SRA. The total heat of hydration with 1% SRA is similar to that of the neat PLC paste.

The generally lower heat of hydration in SRA-containing pastes can result from a variety of admixture-cement interactions and admixture incompatibilities. As SRAs and PCE are both surfactants, they might also compete with each other to adsorb on the cement surface. This can lead to unanticipated excessive retardation in cement hydration, as was observed for the PLC-MK30 case with 2% SRA. This competition for surface adsorption can also decrease the efficiency of PCE in dispersing the cement and MK particles, particularly with higher MK content. As a result, a decrease in early age degree of hydration occurs, as observed here.

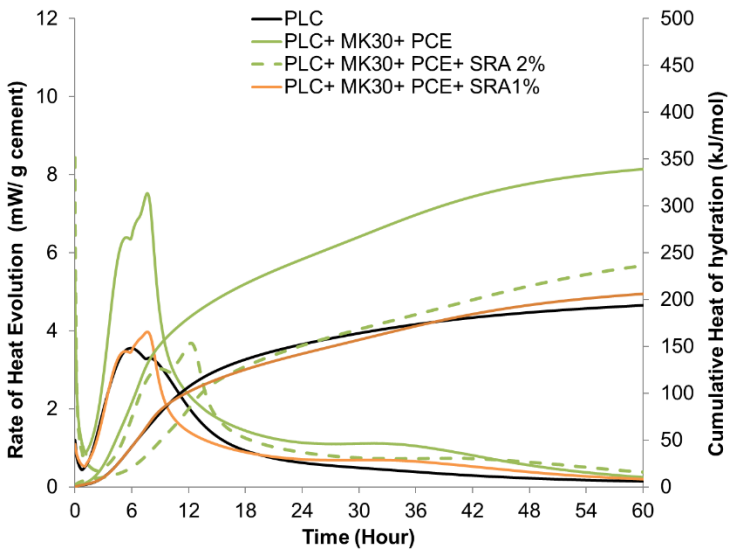

Figure 6.11. The rate and total heat of hydration of PLC, PLC-MK30, and PLC-MK30 with SRAs to show the effect of SRAs on the rate and total cement heat of hydration

6.3.5. Effect of SRAs on the pore solution surface tension

The effect of SRAs on the pore solution surface tension was evaluated by measurement of the pore solution of PLC-MK30 contact angle. Different SRA dosages after 6 hours of hydration were considered. The contact angle of each pore solution with different SRA content is shown in Table 6.1. The surface tension of the pore solution is calculated using Equation 6.2 and trends with SRA dosage are presented in Figure 6.12.

Table 6.1. The contact angle and surface tension of the PLC-MK30 pore solution with 0.1-20% SRA by mass of cement

SRA (%)	Contact angle (θ_c)	Y_{SG} (J/m^2)	Y_{SL} (J/m^2)	YLG (Surface tension, J/m^2)
0.1	28.84	1.24	0.45	0.90
0.3	25.80	1.24	0.45	0.88
0.5	24.46	1.24	0.45	0.87
1	18.11	1.24	0.45	0.83
3	13.12	1.24	0.45	0.81
5	13.14	1.24	0.45	0.81
10	11.24	1.24	0.45	0.81
15	11.00	1.24	0.45	0.80
20	9.05	1.24	0.45	0.80

With increases in the SRA dosage, a decrease in the pore solution surface tension results, up to 3% SRA. After that, increases in the SRA content do not change the surface tension significantly. This concentration appears to be what is also referred to critical micelle concentration (CMC) defined as the concentration of surfactants above which micelles form and all additional surfactants added to the system go to micelles [269]. That can be the reason that the increase in the SRA content after a specific concentration does

not change the pore solution surface tension significantly. This concentration can vary for different pore solutions and SRA types.

The behavior of surface tension with increase in the SRA content follows the Freundlich adsorption isotherm as shown in Equation 6.3. The best-fitted equation is shown in Figure 6.11. The negative value for 1/n shows that the surface reduction is adversely related to the surfactant adsorption as a higher adsorption further reduce surface tension up to the CMC.

$$\frac{x}{m} = Kc^{1/n} \qquad 6\text{-}3$$

where

x = mass of adsorbate

m = mass of adsorbent

p = Equilibrium pressure of adsorbate

c = Equilibrium concentration of adsorbate in solution.

K and n are constants for a given adsorbate and adsorbent at a particular temperature.

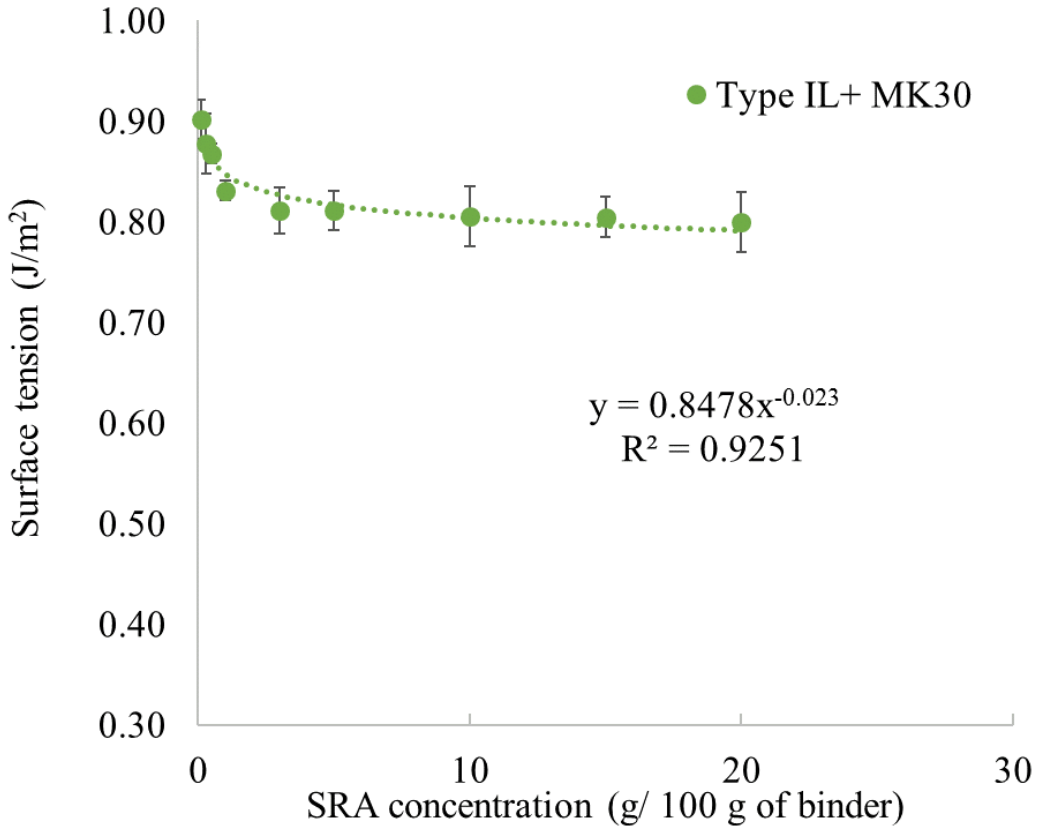

Figure 6.12. The surface tension of the PLC-MK30 pore solution with different SRA dosages

6.3.6. Nitrogen gas adsorption

Nitrogen gas adsorption and desorption were used to measure the porosity of the cement pastes without and with 2 and 10% SRA dosages. The results of the pore volumes (Figures 6.13 and 6.14) are separated into small having diameters between 1-10 nm, and large mesopores, having diameters 10-100 nm. The large mesopores primarily control transport properties and early-age shrinkage at high internal relative humidity (> 80%), while the small mesopores primarily control long-term creep and early-age shrinkage behavior at lower relative humidity [270]. In this study, SRAs dosage of 10% increases the pore volume of smaller pores and thus reduce the early age shrinkage while the pore volume of larger mesopores is almost constant in all

samples. The volume of smaller pores in PLC with 2% SRA is slightly lower than the PLC that can be due the smaller difference between these two samples that falls into the variations of the tests results and the lower accuracy of BET in showing the small difference.

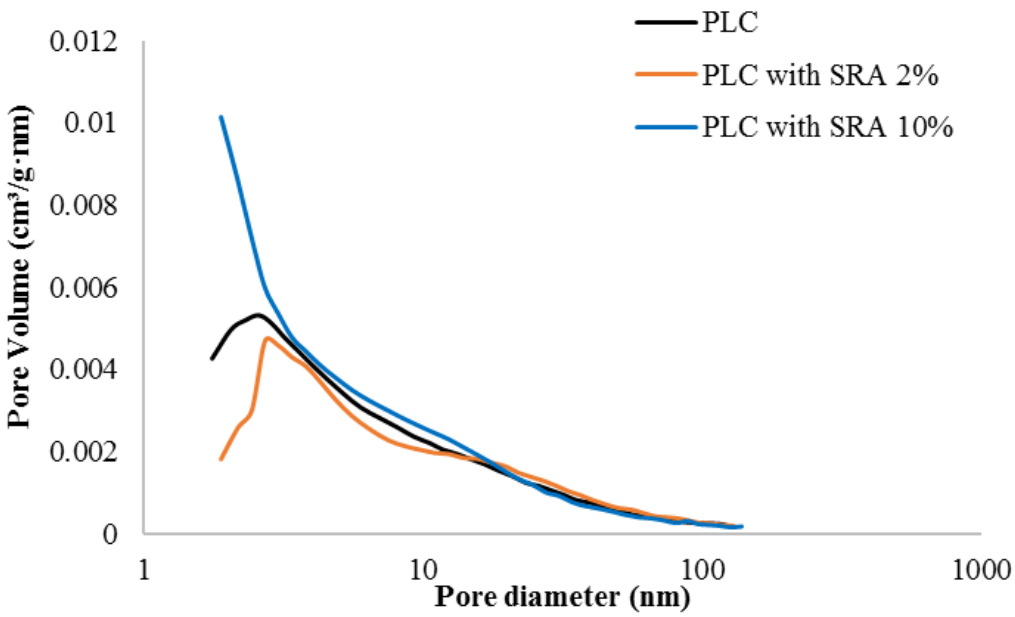

Figure 6.13. The pore volume per gram per diameter of PLC paste without and with SRA 2 and 10%

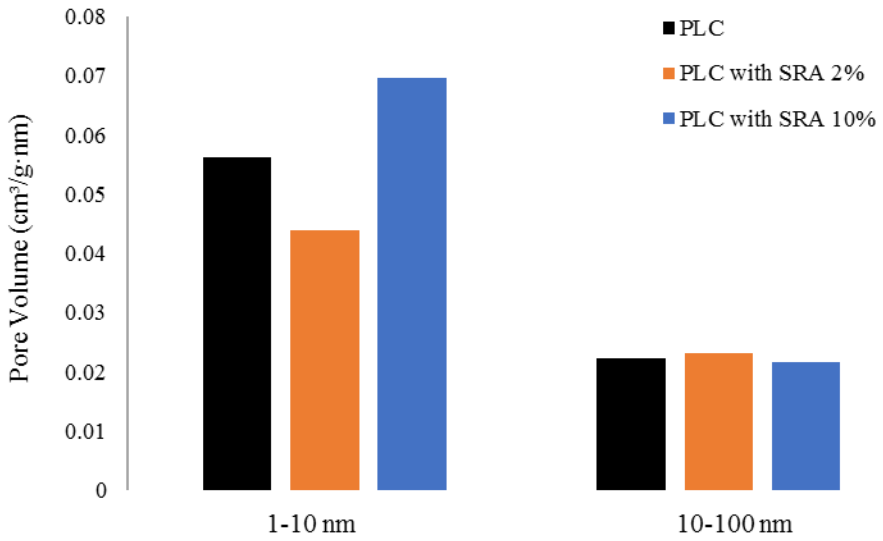

Figure 6.14. Capillary porosity in small (1-10 nm) and large (10-100 nm) mesoporous size ranges for PLC pastes without and with SRA 2 and 10%

6.4.Conclusion and discussion

The autogenous shrinkage of cement-based materials can be considerable when a w/b of lower than 0.42 or when finer SCMs such as MK or SF are used. This study evaluated the effect of MK substitution at 10 and 30% by mass of cement on PLC autogenous shrinkage. The results show that use of MK at 10% does not appreciably change the autogenous shrinkage of the paste at early ages but increases the shrinkage after 7 days. The use of MK30 increases the autogenous shrinkage as early as one day, likely due to pore refinements and contributions due to the chemical interaction of MK with hydrated cement to form carboaluminate and calcium aluminosilicate hydrates products.

SRAs can mitigate autogenous shrinkage of PLC-MK blends. Using 1% SRA by mass of binder was found to be sufficient for both 10% and 30% MK replacement levels. The use of 2% SRA showed to reduce the autogenous shrinkage of paste significantly, but also delayed the cement hydration by 5 hours and delay the initial and final setting time by 3 hours. The use of SRA at 1% delays the MK10 hydration by 3 hours and did not delay the MK30 cement hydration, but decreased the total heat of hydration.

The use of SRAs was found to change the pore solution chemistry, specifically the alkali content. The use of 1% SRA decreases the alkali cation content, Na^+ and K^+, at the early hours of hydration by 25-35%. However, with further cement hydration, their concentrations increased to be similar to those of control sample with no SRA by 6 hours.

As has been previously demonstrated in OPC, the addition of SRAs decreased the contact angle and surface tension of the pore solution for PLC-MK30. This was found up to 3% SRA dosage. The surface tension did not decrease above that concentration that can be due to the limited availability of air-water interfaces sites for SRAs and potential of SRA surfactants in forming micelles after that critical concentration that is referred to critical micelle concentration (CMC). The concentration used in this study for shrinkage mitigation is 1% that is lower than the CMC.

The retardation effect of SRAs on cement hydration and delaying the setting time can suggest a retardation effect on the concrete strength development as it was observed in previous studies [271, 272]. Therefore, further research is needed to examine the effect of SRAs on the mechanical properties of concrete particularly when higher dosages of SRAs are used.

The pore size volume of PLC paste without and with SRAs show that the use of SRAs increase the pore volume of mesoporous with smaller pore diameter, 1-10nm, while does not change the volume of larger pore diameters, 10-100 nm.

CHAPTER 7 CONCLUSIONS AND RECOMMENDATIONS

7.1.Conclusions

The primary objective of this research was to understand the early and later age properties of PLC-MK blended paste and concrete and their interaction with different chemical admixtures. To evaluate the effect of combined use of metakaolin (MK) at higher replacement levels (i.e., 10, 20, and 30% by mass) with portland limestone cement (PLC), with up to 15% limestone interground with cement, this investigation examines

(1) Early age hydration and microstructure development of PLC-MK paste with 10, 20, and 30% MK with each four type of water-reducing admixtures

(2) Mechanical properties including compressive and tensile strength and elastic modulus, of PLC-MK concrete with 10 and 30% MK with PMS and PCE admixture

(3) Durability of PLC-MK including permeability and propensity for shrinkage-induced cracking in the context of understanding the interactions and compatibility of water-reducing and shrinkage-reducing chemical admixtures with PLC-MK blended cements and concrete. Studies were performed at water-to-binder ratio (w/b) of 0.40.

Experimental and modeling investigations helped to understand the interaction of MK with PLC and its effect on the early age properties of cement paste and later age durability and mechanical properties of concrete. The evaluated effect of chemical admixtures such as water reducer and shrinkage reducer admixtures on the properties of PLC-MK based materials help to understand and predict the behavior of concrete with MK and each type of those admixtures.

7.1.1. Early age behaviour of PLC-MK paste

Previous studies showed the effect of MK up to 10-15% on cement hydration, as it was reviewed in Chapter 2, to be mainly related to the nucleation and dilution effects. This study investigated the effect of MK at higher replacement levels (>10%) on the PLC hydration and showed the influence of MK reaction itself on the early age properties of PLC paste. Moreover, the influence of each four types of water-reducing admixtures (WRAs), calcium lignosulfonate (LS), naphthalene formaldehyde condensate (PNS), polymelamine sulfonate (PMS), and polycarboxylate ether (PCE), on the PLC-MK hydration and microstructure was evaluated. The results of this study shows that:

- Metakaolin inclusion accelerates the cement hydration and increases the rate and total heat of hydration of the cement through physical effect that is the nucleation effect of MK being dominant in the first 48 hours of cement hydration, and the chemical effect that is the reaction of MK with limestone in presence of water to produce monocarboaluminate and calcium-aluminate silica phases. The chemical effect of MK was verified by replacing the MK with quartz (Q) and comparing the hydration kinetics of Q-PLC and PLC-MK mixes.
- The WRAs generally delay the cement hydration with the exception of the LS mix that the hydration was highly accelerated that shows the accelerated cement reaction in presence of LS.
- The results of the characterization techniques, XRD and TGA, show that the delay in the cement hydration is attributed to the decrease in the C_3S dissolution rate in the presence of WRAs. The highly accelerated peak in PLC-MK paste with LS can be interpreted as a result of accelerated C_3A hydration and

catalyzed formation of ettringite at early ages. The increased solubility of gypsum in pore solution in presence of LS could also accelerates the ettringite formation.

- Of the four admixture chemistries examined, the PCE that appears to be the most effective admixture in increasing the workability of metakaolin-portland limestone cement blends paste and dispersing the cementitious materials while it delays the hydration of both silicate and aluminate phases by about 2-3 hours in the first 6 hours of hydration.
- The Vicat test results on the initial and final setting time of MK mortars show that the use of MK without WRAs shortens the initial and particularly the final setting times. The use of WRAs showed to increase the setting time of PLC-MK blends mortars to be close to that of control sample with PMS showing the longest setting time and mixes with LS showed the shortest. The delay in the setting time of mortars with PMS can be due to the delay effect of PMS on the C_3S hydration as it was shown in XRD and TGA data and the shorter setting time of LS can be related to the accelerated cement phase reaction in presence of LS as it was observed in calorimetry and TGA data. The use of LS for MK10 and MK20 and PNS for MK30 mortars did not meet the ASTM C494 and cannot be used in combination.
- The LCA results show that the replacement of cements by MK can save the GHG emissions and embodied energy up to 20% when MK30 is used. The contribution of MK and PCE admixture to GHG emissions and embodied energy is much lower than that of portland cement.

- An empirical model based on the calorimetry data on different types of cements, Types I/II, IL, V, and II/V, without and with MK at 10, 20, and 30% by mass with PCE admixture. The developed model shows that cement silicate phase content, cement Blaine fineness, and MK content are important in determining the ultimate degree of and time of hydration of neat and blended cements. Besides, the slope of hydration is a factor of PCE dosage, the cement alkali content, and the cement Blaine fineness. The developed model helps to estimate the degree and rate of cement hydration and can be used to predict the total heat of hydration of MK-blended cements to prevent extreme heat development in MK concrete and avoid potential cracking.

7.1.2. The hardened properties of metakaolin-portland limestone cement concrete

One of the primary goals of this investigation is to evaluate the effects of MK use in concrete at higher substitution rates (>10%) when combined with PLC. The use of MK in PLC concrete was found to affect the fresh and hardened concrete properties. Two HRWRAs, PCE and PMS, based on their higher effectiveness in addressing workability were compared in this study.

- In terms of fresh concrete properties, the PLC-MK concrete in general exhibited slightly lower air content, potentially due to improved workability and improved packing. The MK concrete with PCE had a higher air content than that of PMS concrete, likely due to the foaming properties of PCE.
- The compressive of strength of concretes increase in general with MK addition. The MK concrete with PMS showed similar compressive strength to PLC concrete at 1 day but the strength increased to be higher than PLC concrete at later ages. The

delay in the strength development of PMC MK concrete can be due to the retardation effect of PMS. The MK concretes with PCE have a higher compressive strength as much as 90% higher than PLC concrete as early as one day and increased to be 150% higher at 7 days. The higher compressive strength of MK concrete at early age was related to the combination of the filler and nucleation effect of MK while the extension of these improvements to the later age can be due to the pozzolanic reaction of MK with CH produced from the cement hydration.

- The tensile strength of MK concrete showed to be dependent of on the efficiency of a WRA. Concrete with MK10 and MK30 and PCE showed to have tensile strength higher than PLC concrete by up to 40% while the MK concrete with PMS showed to have lower tensile strength than that of PLC concrete by 22%. The lower tensile strength of PMS MK-concretes can be due to the weaker ITZ and lower bond of cement paste with the aggregates in concrete. The ACI equations showed to overestimate the tensile strength of MK concrete in this study and therefore, this study developed a new equation to predict the tensile strength of MK concrete based on the results of this study.
- The elastic modulus of MK concrete showed to be a dependent of MK content and the admixture chemistry. While the elastic modulus of all MK concretes are higher than the PLC concrete, MK concretes with PCE showed a significantly higher (up to 80% higher) elastic modulus compared to that of PLC concrete, and this increases with increasing MK content. The elastic modulus of MK10 and MK30 concrete with PMS are higher than the PLC concrete up to 77% and 35% higher, respectively. The addition of MK densifies the paste matrix and reduces the porosity of paste and thus increases the elastic modulus. Moreover, the higher

elastic modulus with higher MK content can be because of the better packing due to the filler effect of fine MK particles, especially in the ITZ.

- The effect of MK on the durability and stability of concrete was revaluated through permeability and drying shrinkage. The results of the rapid chloride penetration test (RCPT) and surface resistivity show that the addition of MK decrease the permeability of concrete significantly from moderate for PLC concrete to low and very low PLC with MK. This lower permeability of MK concrete can be due to the effect of MK on densifying the concrete through filler and pozzolanic effects by filling the pores and densifying the concrete. The WRA chemistry showed to affect the MK concrete permeability as the MK concrete with PCE showed to have lower permeability than that of MK concrete with PMS. A great correlation was observed between the RCPT and SR results.
- The effect of MK on drying shrinkage of concretes showed that the MK addition decreased the concrete shrinkage, but that the concrete still had likely high cracking potential. The lower shrinkage of MK concrete may be because of the pozzolanic activity of MK that as a result, there is less evaporable water available in the mixes as hydration and pozzolanic reactions used up most of the free water and because of decreased moisture migration due to matrix densification. The MK10 concrete with PCE exhibited similar shrinkage to that of PLC concrete, while with increase in the MK content to 30% the shrinkage decreased to be as low as 47% of the PLC concrete at 90 days. The MK10 and MK30 concrete with PMS showed a lower drying shrinkage at 60 and 90 days. The stress developed in concrete due to the shrinkage was calculated by linear-elastic theory using the elastic modulus calculated in this study. The results of this fundamental analysis show that the

developed stress is higher than the tensile strength of all concretes that can cause cracking in concrete.

7.1.3. The autogenous shrinkage of PLC-MK paste and the effect of SRAs

- The results of autogenous shrinkage of MK pastes show that use of MK at 10% does not appreciably change the autogenous shrinkage of the paste at early ages but increases the shrinkage after 7 days that can be due to the reactions of MK. The use of MK30 increases the autogenous shrinkage as early as one day, likely due to pore refinements and the chemical interaction of MK with hydrated cement to form carboaluminate and calcium aluminosilicate hydrates products.
- SRAs can mitigate autogenous shrinkage of PLC-MK blends. Using 1% SRA by mass of binder was found to be sufficient for both 10% and 30% MK replacement levels. The use of 2% SRA showed to reduce the autogenous shrinkage of paste significantly, but also delayed the cement hydration by 5 hours and delay the initial and final setting time by 3 hours. The use of SRA at 1% delays the MK10 hydration by 3 hours and did not delay the MK30 cement hydration, but decreased the total heat of hydration. The use of SRAs was found to change the pore solution chemistry, specifically the alkali content. The use of 1% SRA decreases the alkali cation content, Na^+ and K^+, at the early hours of hydration by 25-35%. However, with further cement hydration, their concentrations increased to be similar to those of control sample with no SRA by 6 hours.
- Moreover, the addition of SRAs decreased the contact angle and surface tension of the pore solution for PLC-MK30 with up to 3% SRA dosage. The surface tension did not decrease above that concentration that can be due to the limited availability

of air-water interfaces sites for SRAs and potential of SRA surfactants in forming micelles after that critical concentration that is referred to critical micelle concentration (CMC). The concentration used in this study for shrinkage mitigation is 1% that is lower than the CMC.

7.2. Recommendations for practice

7.2.1. The early age behaviour

The use of MK showed to decrease the workability of fresh concrete with about 11% decrease for each 10% increase in the metakaolin level. The lower workability of MK concrete can become challenging particularly for pumping and used in highly reinforced concrete. Four types of water-reducing admixtures (WRAs) was evaluated and the results suggest that the use of PCE admixture as a WRA PLC-MK cements particularly when MK is used at higher rates (>10% by mass). The use of PMS admixture is capable of improving the workability of MK concretes but a potential delay in cement hydration and concrete strength development was observed particularly when higher dosages is required with higher MK content.

The MK addition showed to increase the cement heat of hydration at early age that can cause cracking when used in mass concrete construction or in hot temperatures. Therefore, when MK used at higher rates, the heat of hydration should be estimated and controlled. One solution to control the heat development of MK-blended cements is to use with cements with lower heat development (Type II or V) or blended with other SCMS with a lower heat production such as Class F fly ash.

7.2.2. The use of MK concretes

The use of MK in concrete showed to increase the compressive strength of concrete with PCE or PMS admixture. The compressive strength of MK10 and MK30 concrete with PCE showed to be 10,700 and 15,500 ksi at 28 days respectively that meets the compressive strength requirement of 9000 psi (62 MPa) for high strength concrete (HSC) according to

ACI 363 [222]. The MK concretes also meet 10,000 to 14,000 psi compressive strength at 28 to 91 days for high performance concrete (HPC) Grade 3 according to Federal Highway Administration classifications (FHWA) [273]. Besides, the MK concrete can be also used as a Class AAA concrete in GDOT section 500 specification for prestressed concrete [274].

The tensile strength of MK concrete depends on the type of admixture and the MK content. The tensile strength of MK concrete with PCE showed a higher tensile (up to 1.03 ksi) than that of PLC concrete (0.72 ksi). Therefore, when a concrete with both higher tensile and compressive strength is required, the use of MK10 and MK30 with PCE is recommended.

The elastic modulus of MK concrete showed to be generally higher than the PLC concrete showing the higher ductility of MK concrete due to lower porosity in the MK-containing paste. The elastic modulus of MK concrete showed to be in the range of 5.4-7.2 $\times 10^6$ psi that meets the FHWA requirement for Grade 3 HPC. Therefore, MK10 and MK30 concretes with PCE or PMS can be used when a higher elastic modulus of concrete is required.

The shrinkage of MK concrete in general showed to be similar to PLC concrete in the first 14 days and lower afterwards. The lower shrinkage of MK concrete shows their great potential to use in infrastructures such as bridges that shrinkage and potential cracking is critically important.

7.2.3. Use in aggressive environments

The results of this study show that a significant improvement in the impermeability and lower shrinkage of PLC concrete is made when combined with MK. The lower permeability and shrinkage of MK concretes show that an improved resistance to the ingress of contaminants such as chloride intrusion. Therefore, PLC-MK concrete can used as a suitable alternative in structural applications requiring low permeability to contaminants and might be susceptible to harsh environments such as foundations, slabs on grade, or bridge substructures in direct contact with soil or groundwater, or the bridges and pavement where anti-icing salts are used.

The lower permeability of MK concretes suggested that they have lower water penetration and less interconnected pores. Therefore, MK concretes can be used in cold environments to reduce the freezing and thawing damages.

7.2.4. Methods for characterizing and modelling PLC-MK systems

The research presented in this study revealed several areas where conventional approaches to characterizing and modeling neat OPC systems did not suitably apply to PLC-MK blended systems. One of them is to predict and estimate the heat of hydration PLC-MK blended cements where the conventional models underestimate the heat of hydration of PLC-MK cements. This study developed a non-linear regression model to predict the heat of hydration of PLC-MK cements based on the cement physical and chemical properties, the MK content, and WRAs dosages. This model helps to estimate the heat development of PLC-MK, avoid heat accumulation, and prevent potential cracking in concrete.

Another area where the use of conventional models for OPC does not apply for PLC-MK is in predicting the tensile strength of MK concretes. The conventional models, i.e. ACI equations, that are commonly used for OPC concretes showed to overestimate the tensile strength of MK concretes. This study developed an empirical equation to predict the splitting tensile strength of MK concrete based on the compressive strength. This model was tested on the data from other studies and showed acceptable results.

7.3. Recommendations for future research

- This study explored the use of dehydroxylated kaolinite as a pozzolanic material in concrete, while other studies can explore the use of other calcined clays such as calcined Bentonite, calcined montmorillonite) in structural concrete
- This study evaluated the effect of WRAs on the PLC-MK cement paste hydration and phase development; however, WRAs can also intercalate in cement phases such as ettringite and alter their morphologies. One area for future study will be the assessments of WRAs effect on morphology of cement phases over time.
- The retardation effect of SRAs on cement hydration and delaying the setting time can suggest a retardation effect on the concrete strength development. Therefore, further research can be focused on examining the effect of SRAs on the mechanical properties of concrete particularly when higher dosages of SRAs are used.
- This study evaluated the early and later age properties of pure high quality MK-blended cements while the use of lower quality MK due to their higher availability and lower energy-intense process is becoming more common. One study can focus on the effect of lower quality MK from different sources on the properties of MK paste and concretes.
- This study focused on the MK blended cement with only source of PLC with a specific particle size and surface area. Other studies can evaluate the effect of PLC mineralogy and physical properties on the properties of PLC-MK early and late age properties.
- This study evaluated the effect of SRAs as a mitigation way to control the shrinkage of PLC-MK blended paste. However, the other methods to control the PLC-MK shrinkage such as use of saturated light aggregates can be evaluated in another study.

- The w/b ratio used for PLC-MK in this study was 0.4 for paste and 0.445 for concrete. The higher w/b of 0.5 for concrete and paste can reduce the required dosages of WRAs and reduce their adverse effect but also lower the mechanical properties and impermeability of concrete. One study can evaluate the effect of MK at higher replacement rates (> 10%) with different w/b and different admixtures on the properties of paste and concrete.
- The lower permeability of and lower interconnectivity of pores in MK concrete can potentially increase their freezing and thawing resistance. One area for future studies can be evaluating the freeze and thaw resistance of non-air-entrained and air-entrained MK concrete. The effectiveness of air-entrainers in MK-concretes and their compatibility and interaction of WRAs with air-entrainers can be examined.
- Other studies can explore the potential of MK in UHPC instead of SF and compare the properties to that of UHPC with SF.
- With increase in the use of MK at higher rates, there is a need for developing new generation of chemical admixtures that are designed for the use with cements blended with SCMs.

APPENDIX A. Comparison of heat of hydration models results

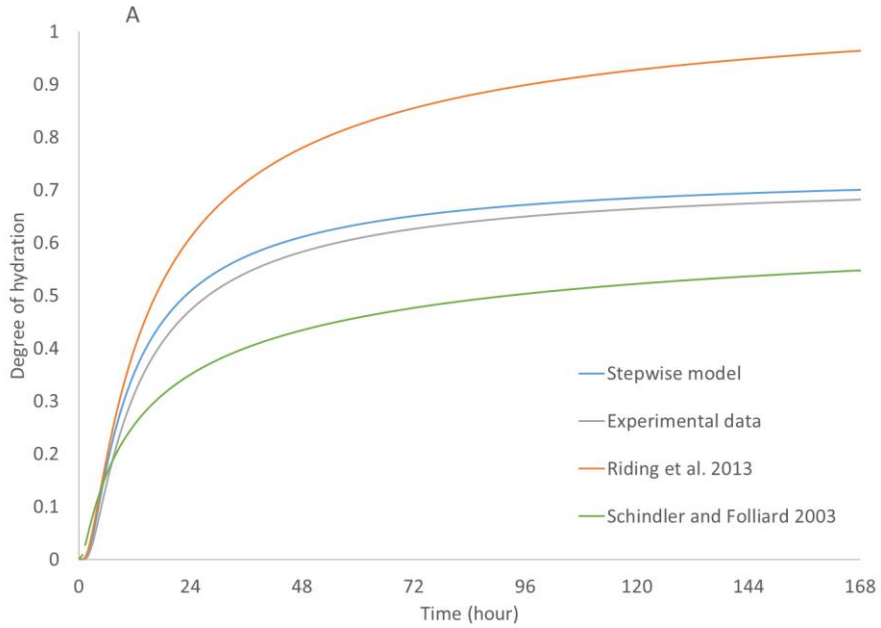

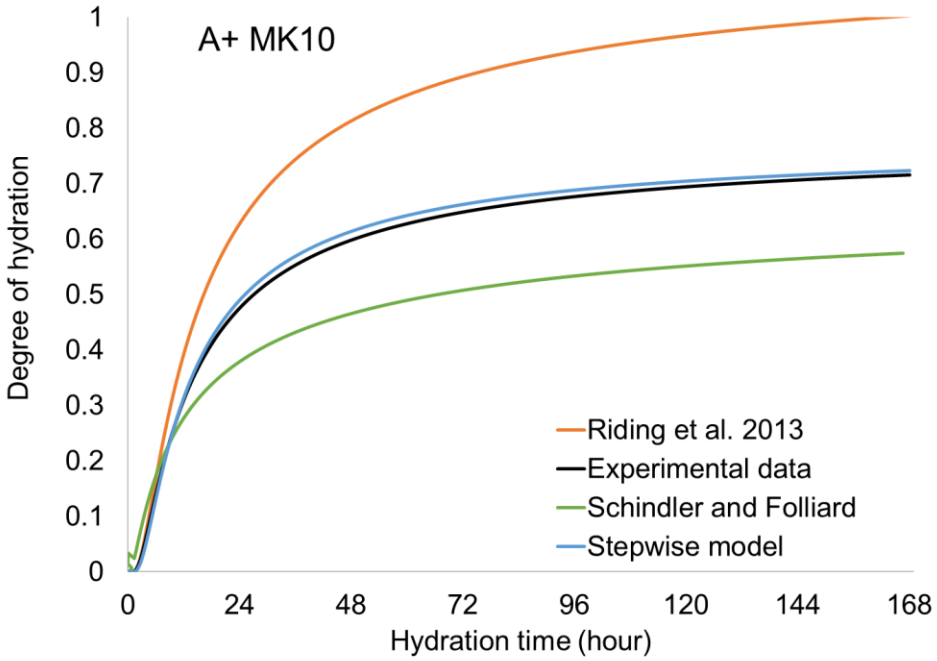

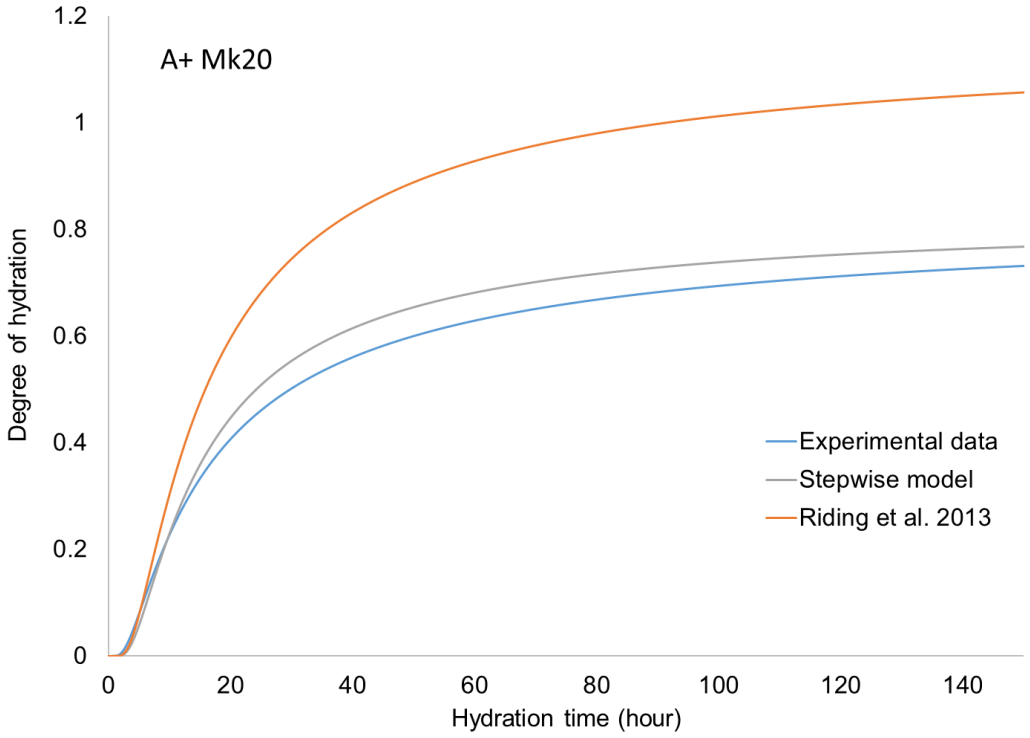
A+ Mk20
Degree of hydration
Hydration time (hour)
Experimental data
Stepwise model
Riding et al. 2013
0
0.2
0.4
0.6
0.8
1
1.2
0
20
40
60
80
100
120
140

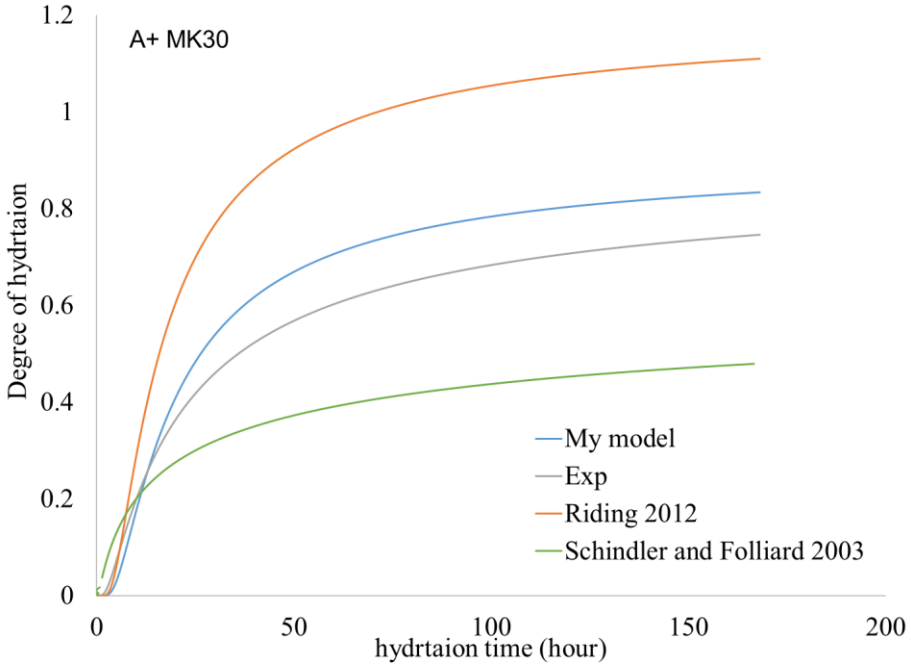
A+ MK30
Degree of hydrtaion
hydrtaion time (hour)
My model
Exp
Riding 2012
Schindler and Folliard 2003
0
0.2
0.4
0.6
0.8
1
1.2
0
50
100
150
200

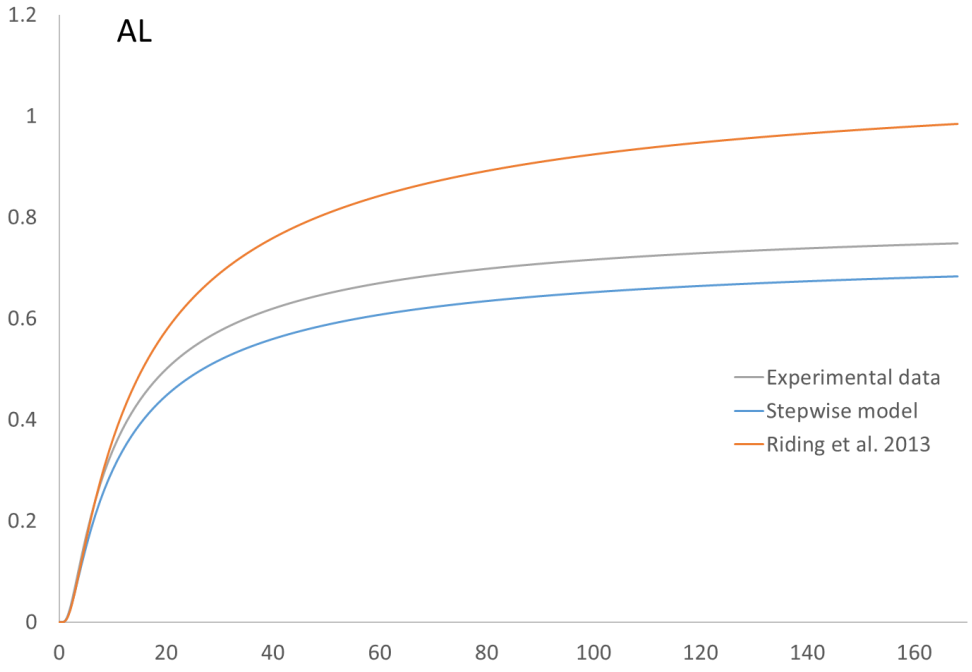
AL
1.2
1
0.8
0.6
0.4
0.2
0
0
20
40
60
80
100
120
140
160
Experimental data
Stepwise model
Riding et al. 2013

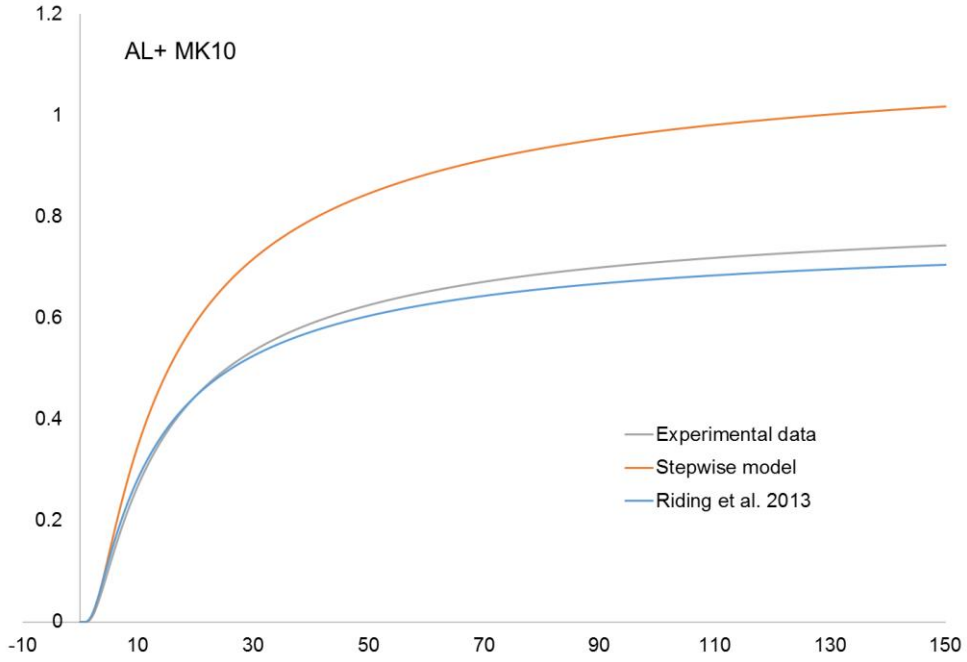
AL+ MK10
1.2
1
0.8
0.6
0.4
0.2
0
-10
10
30
50
70
90
110
130
150
Experimental data
Stepwise model
Riding et al. 2013

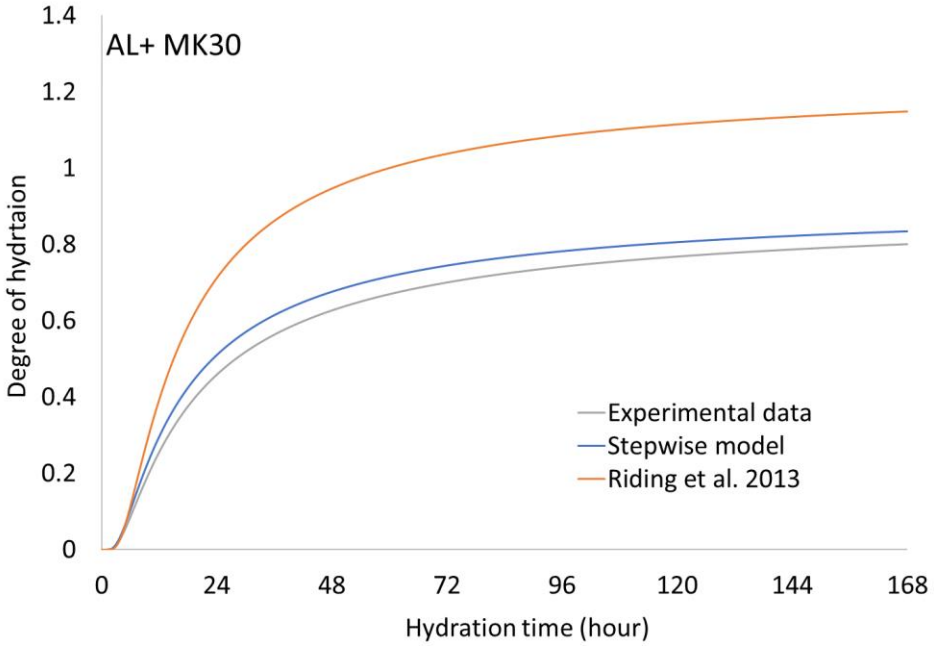
AL+ MK30
Degree of hydrtaion
1.4
1.2
1
0.8
0.6
0.4
0.2
0
0
24
48
72
96
120
144
168
Hydration time (hour)
Experimental data
Stepwise model
Riding et al. 2013

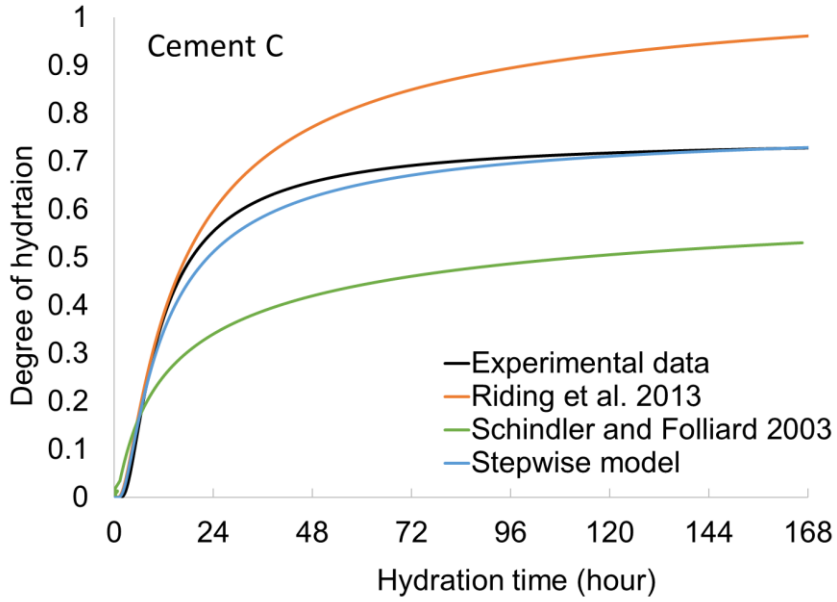
Cement C
Degree of hydrtaion
1
0.9
0.8
0.7
0.6
0.5
0.4
0.3
0.2
0.1
0
0
24
48
72
96
120
144
168
Hydration time (hour)
Experimental data
Riding et al. 2013
Schindler and Folliard 2003
Stepwise model

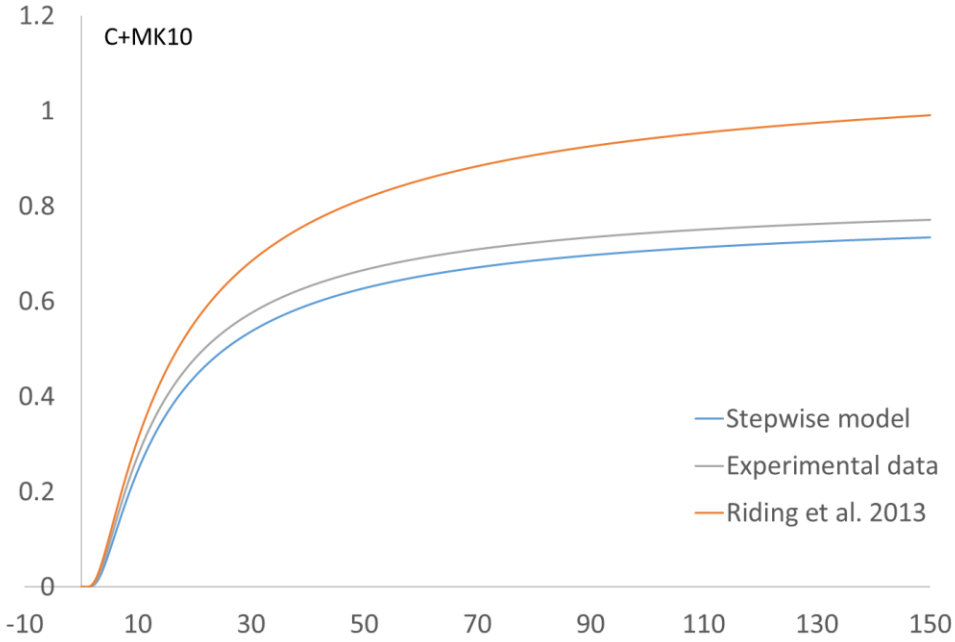
C+MK10
1.2
1
0.8
0.6
0.4
0.2
0
-10
10
30
50
70
90
110
130
150
Stepwise model
Experimental data
Riding et al. 2013

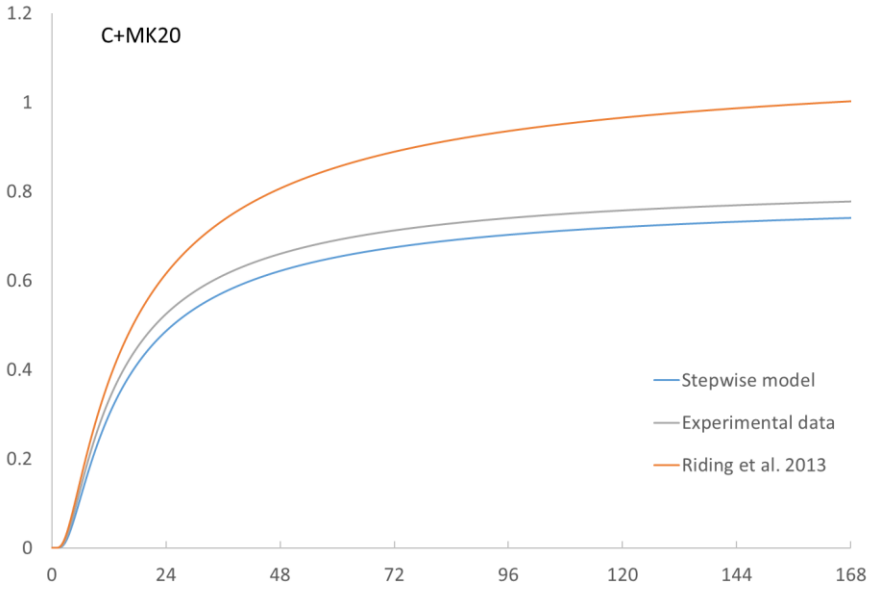
C+MK20
1.2
1
0.8
0.6
0.4
0.2
0
0
24
48
72
96
120
144
168
Stepwise model
Experimental data
Riding et al. 2013

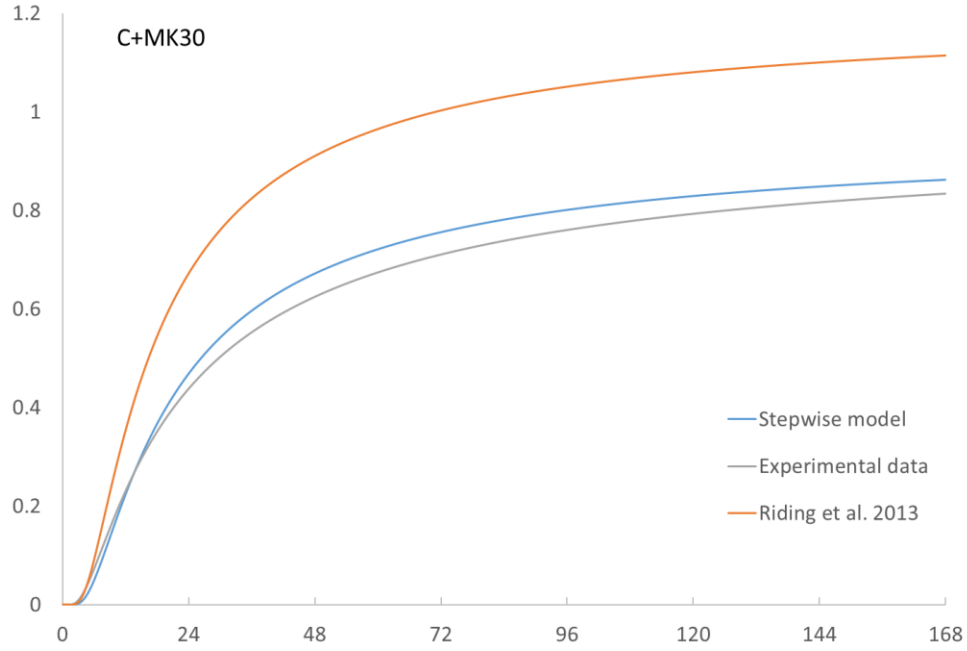
C+MK30
1.2
1
0.8
0.6
0.4
0.2
0
0
24
48
72
96
120
144
168
Stepwise model
Experimental data
Riding et al. 2013

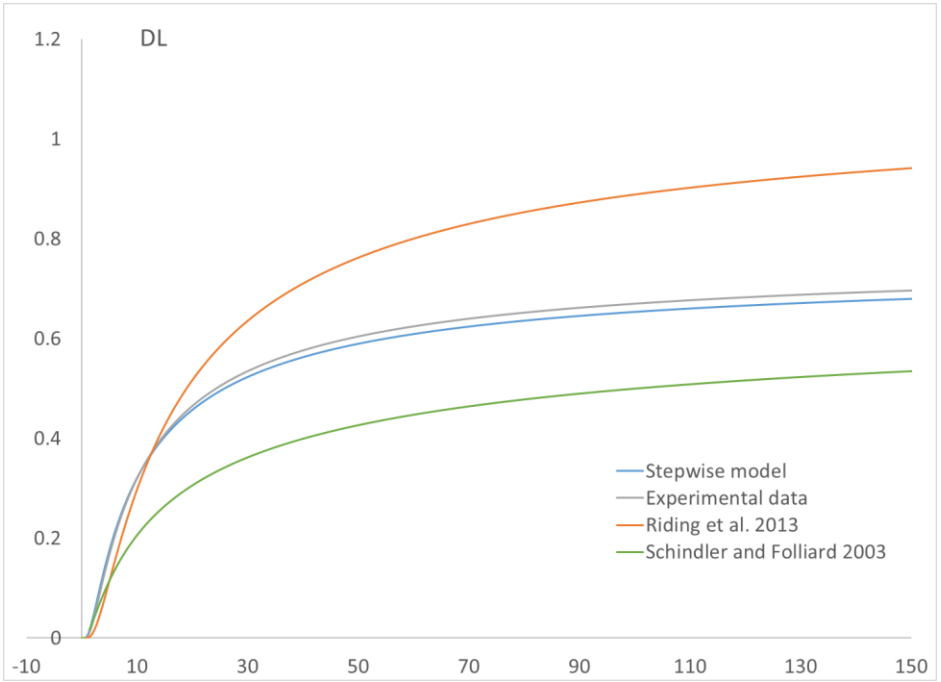
DL
1.2
1
0.8
0.6
0.4
0.2
0
-10
10
30
50
70
90
110
130
150
Stepwise model
Experimental data
Riding et al. 2013
Schindler and Folliard 2003

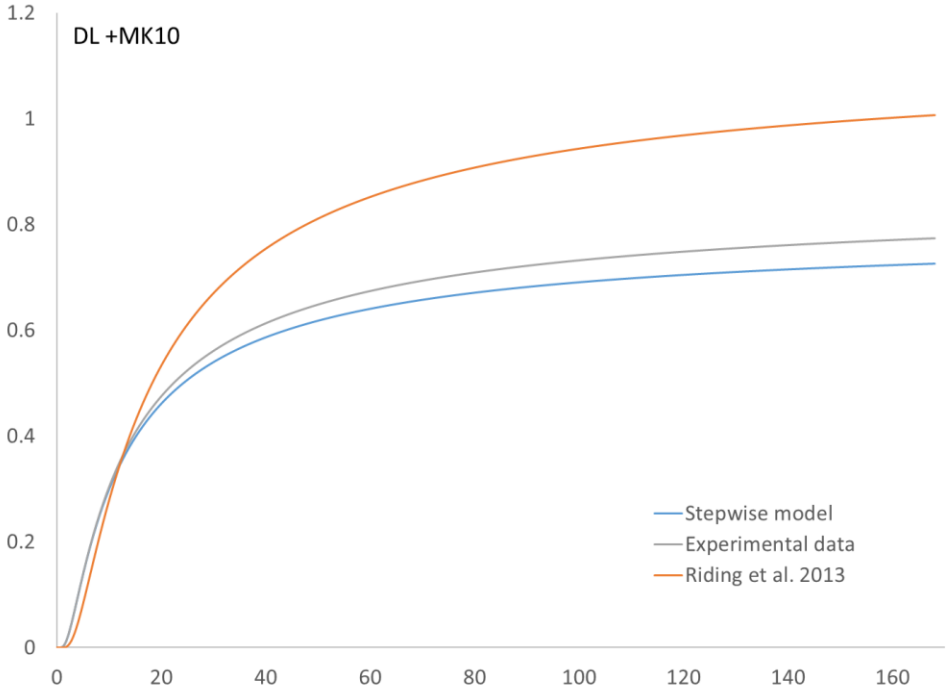
DL +MK10
1.2
1
0.8
0.6
0.4
0.2
0
0
20
40
60
80
100
120
140
160
Stepwise model
Experimental data
Riding et al. 2013

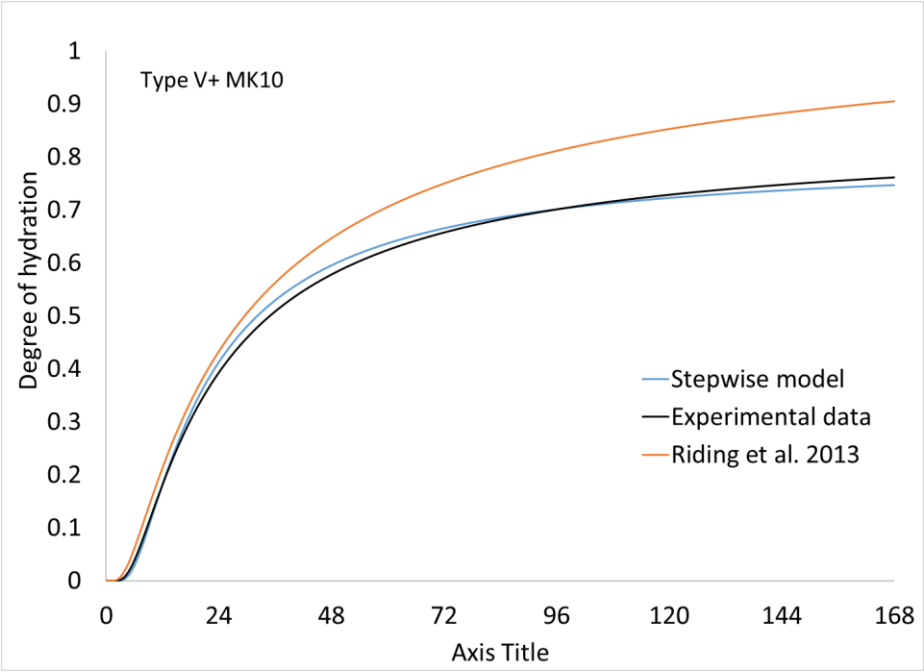
Type V+ MK10
Degree of hydration
1
0.9
0.8
0.7
0.6
0.5
0.4
0.3
0.2
0.1
0
0
24
48
72
96
120
144
168
Axis Title
Stepwise model
Experimental data
Riding et al. 2013

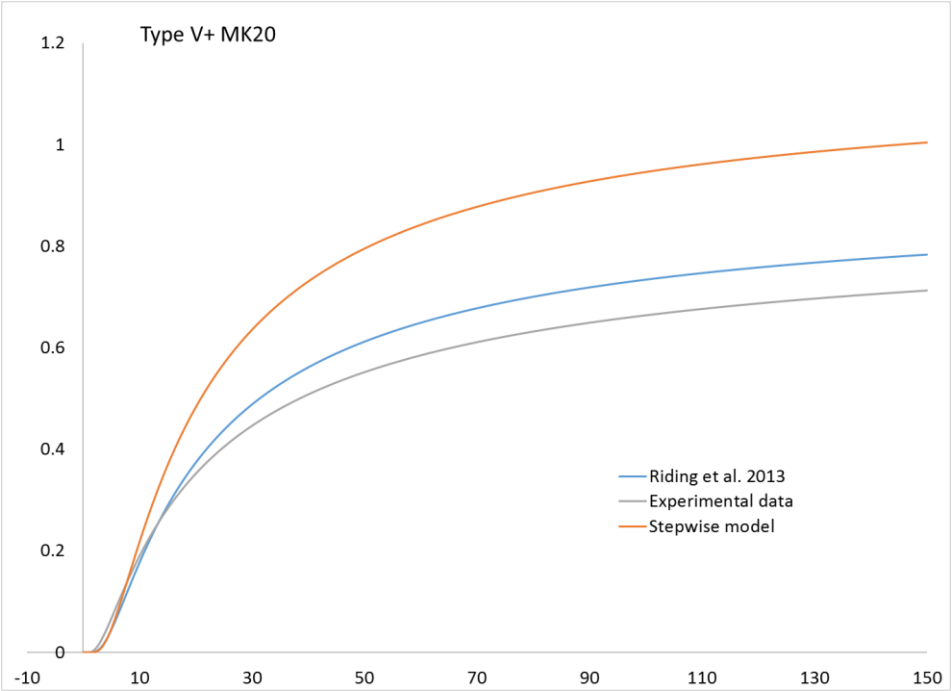
Type V+ MK20
1.2
1
0.8
0.6
0.4
0.2
0
-10
10
30
50
70
90
110
130
150
Riding et al. 2013
Experimental data
Stepwise model

APPENDIX B. THE DEFORMATIONS, STRAINS, ELASTIC MODULUS, AND POISSON'S RATIO OF EACH CONCRETE AT 10,000 LBS LOADING INTERVALS

PLC+ MK10+ PCE							
Load (lbs)	Stress (psi)	Longitudinal Deformation (in)	Transversal Deformation (in)	Longitudinal Ɛ	Transversal Ɛ	E (ksi)	Poisson´s Ratio
0							
10,000	353.68	0.0009	0.0001	0.0001	0.0000	6,130	0.13
20,000	707.36	0.0018	0.0001	0.0001	0.0000	6,407	0.18
40,000	1,296.82	0.0032	0.0002	0.0002	0.0000	6,468	0.21
60,000	1,768.39	0.0041	0.0003	0.0003	0.0001	6,979	0.22
80,000	2,239.96	0.0053	0.0004	0.0003	0.0001	6,841	0.22
100,000	2,829.42	0.0066	0.0004	0.0004	0.0001	6,877	0.22
120,000	3,300.99	0.0076	0.0006	0.0005	0.0001	6,941	0.24

PLC+ MK10+ PMS							
Load (lbs)	**Stress (psi)**	**Longitudinal Deformation (in)**	**Transversal Deformation (in)**	**Longitudinal Ɛ**	**Transversal Ɛ**	**E (ksi)**	**Poisson´s Ratio**
0	0	0.0007	0.0000	0.0000	0.0000	0	0
10,000	354	0.0034	0.0001	0.0002	0.0000	2,088	0.041
20,000	707	0.0041	0.0001	0.0002	0.0000	3,308	0.052
40,000	1,297	0.0048	0.0001	0.0003	0.0000	4,970	0.080
60,000	1,768	0.0056	0.0001	0.0003	0.0000	5,741	0.082
80,000	2,240	0.0063	0.0002	0.0004	0.0000	6,345	0.092
100,000	2,829	0.0069	0.0001	0.0004	0.0000	7,178	0.099
120,000	3,301	0.0075	0.0002	0.0004	0.0000	7,619	0.110

PLC+ MK30+PCE							
Load (lbs)	**Stress (psi)**	**Longitudinal Deformation (in)**	**Transversal Deformation (in)**	**Longitudinal ε**	**Transversal ε**	**E (ksi)**	**Poisson´s Ratio**
0	0	0.0000	0.0000	0.000000	0.000000		
10,000	354	0.0020	0.0000	0.000125	0.000000	2,829	0.00
20,000	707	0.0032	-0.0001	0.000200	-0.000012	3,537	0.06
30,000	1,061	0.0042	-0.0003	0.000263	-0.000024	4,042	0.09
40,000	1,415	0.0054	-0.0007	0.000338	-0.000060	4,192	0.18
50,000	1,768	0.0064	-0.0009	0.000400	-0.000072	4,421	0.18
60,000	2,122	0.0074	-0.0010	0.000463	-0.000084	4,588	0.18
70,000	2,476	0.0083	-0.0014	0.000519	-0.000120	4,773	0.23
80,000	2,829	0.0094	-0.0014	0.000588	-0.000120	4,816	0.20
90,000	3,183	0.0103	-0.0020	0.000644	-0.000168	4,945	0.26
100,000	3,537	0.0113	-0.0022	0.000706	-0.000180	5,008	0.25
110,000	3,890	0.0122	-0.0024	0.000763	-0.000200	5,102	0.26
120,000	4,244	0.0130	-0.0025	0.000813	-0.000210	5,224	0.26
130,000	4,598	0.0138	-0.0026	0.000863	-0.000220	5,331	0.26
140,000	4,951	0.0147	-0.0028	0.000919	-0.000230	5,389	0.25
150,000	5,305	0.0155	-0.0029	0.000969	-0.000240	5,476	0.25
160,000	5,659	0.0162	-0.0030	0.001013	-0.000250	5,589	0.25
170,000	6,013	0.0170	-0.0031	0.001063	-0.000260	5,659	0.24
180,000	6,366	0.018	-0.0034	0.001125	-0.000280	5,659	0.25

PLC+ MK30+PMS							
Load (lbs)	**Stress (psi)**	**Longitudinal Deformation (in)**	**Transversal Deformation (in)**	**Longitudinal ε**	**Transversal ε**	**E (ksi)**	**Poisson´s Ratio**
0	0	0.0000		0.000000		0	
10,000	354	0.0020	0.0000	0.000125	0.000000	2,829	0.00
20,000	707	0.0027	-0.0001	0.000169	-0.000010	4,192	0.06
30,000	1,061	0.0038	-0.0002	0.000238	-0.000020	4,468	0.08
40,000	1,415	0.0050	-0.0006	0.000313	-0.000050	4,527	0.16
50,000	1,768	0.0062	-0.0007	0.000388	-0.000060	4,564	0.15
60,000	2,122	0.0070	-0.0008	0.000438	-0.000070	4,850	0.16
70,000	2,476	0.0080	-0.0012	0.000500	-0.000100	4,951	0.20
80,000	2,829	0.0089	-0.0012	0.000556	-0.000100	5,087	0.18
90,000	3,183	0.0098	-0.0017	0.000613	-0.000140	5,197	0.23
100,000	3,537	0.0108	-0.0018	0.000675	-0.000150	5,240	0.22
110,000	3,890	0.0118	-0.0020	0.000738	-0.000167	5,275	0.23
120,000	4,244	0.0127	-0.0021	0.000794	-0.000175	5,347	0.22
130,000	4,598	0.0135	-0.0022	0.000844	-0.000183	5,449	0.22
140,000	4,951	0.0148	-0.0023	0.000925	-0.000192	5,353	0.21
150,000	5,305	0.0158	-0.0024	0.000988	-0.000200	5,372	0.20
160,000	5,659	0.0168	-0.0025	0.001050	-0.000208	5,389	0.20
170,000	6,013	0.0176	-0.0026	0.001100	-0.000217	5,466	0.20
180,000	6,366	0.0186	-0.0028	0.001163	-0.000233	5,476	0.20

REFERENCES

[1] Portland Cement Association, Global Cement Consumption on the Rise, 2015.

[2] H.G. Van Oss, U.S. Geological Survey: Mineral Commodity Summaries, 2016.

[3] M. Schneider, M. Romer, M. Tschudin, H. Bolio, Sustainable cement production—present and future, Cement and Concrete Research, 41 (2011) 642-650.

[4] N. Tanaka, B. Stigson, Cement Technology Roadmap 2009, World business council for sustainable development and the international energy agency technical report, (2009).

[5] L. Szabó, I. Hidalgo, J.C. Císcar, A. Soria, P. Russ, Energy consumption and CO2 emissions from the world cement industry, European Commission Joint Research Centre, Report EUR, 20769 (2003).

[6] Energy Research Centre of Netherland., Carbon Capture and Storage ClimateTechWiki, 2013.

[7] R. Snellings, Assessing, Understanding and Unlocking Supplementary Cementitious Materials, RILEM Technical Letters, 1 (2016) 50-55.

[8] N. Ghafoori, J. Bucholc, Investigation of lignite-based bottom ash for structural concrete, Journal of Materials in Civil Engineering, 8 (1996) 128-137.

[9] K. Scrivener, V.M. John, E. Gartner, Eco-efficient cements: Potential, economically viable solutions for low-CO2, cement based materials industry, UNEP, 2016.

[10] Headwaters Construction Materials, About Fly Ash, http://flyash.com/about-us/.

[11] M.L. Hall, W.R. Livingston, Fly ash quality, past, present and future, and the effect of ash on the development of novel products, Journal of Chemical Technology and Biotechnology, 77 (2002) 234-239.

[12] M. Ahmaruzzaman, A review on the utilization of fly ash, Progress in energy and combustion science, 36 (2010) 327-363.

[13] Z. Tang, S. Ma, J. Ding, Y. Wang, S. Zheng, G. Zhai, Current status and prospect of fly ash utilization in China, Proc. of World of Coal Ash Conference (WOCA), 2013, pp. 1-7.

[14] J. Lau, China's construction sector forecast to slump to historic lows: no recovery expected until 2030, South China Morning Post, 2015.

[15] SMITHERS APEX, The Future of Ferrous Slag to 2025, 2015.

[16] L. Turanli, B. Uzal, F. Bektas, Effect of material characteristics on the properties of blended cements containing high volumes of natural pozzolans, Cement and Concrete Research, 34 (2004) 2277-2282.

[17] G. Rodríguez de Sensale, Strength development of concrete with rice-husk ash, Cement and Concrete Composites, 28 (2006) 158-160.

[18] World Kaolin Producing Countries, http://www.mapsofworld.com/minerals/world-kaolin-producers.html.

[19] J. Ambroise, S. Maximilien, J. Pera, Properties of Metakaolin blended cements, Advanced Cement Based Materials, 1 (1994) 161-168.

[20] S. Wild, J.M. Khatib, A. Jones, Relative strength, pozzolanic activity and cement hydration in superplasticised metakaolin concrete, Cement and concrete research, 26 (1996) 1537-1544.

[21] H. Meissner, Pozzolans used in mass concrete, Symposium on Use of Pozzolanic Materials in Mortars and Concretes, ASTM International, 1950.

[22] C. Müller, S. Palm, C. Graubner, T. Proske, S. Hainer, M. Rezvani, W. Neufert, I. Reuken, Cements with a high limestone content–durability and practicability, Cement International, 12 (2014) 78-85.

[23] J. Fernández-Caliani, E. Galán, P. Aparicio, A. Miras, M. Márquez, Origin and geochemical evolution of the Nuevo Montecastelo kaolin deposit (Galicia, NW Spain), Applied Clay Science, 49 (2010) 91-97.

[24] X. Wang, M. Zhang, W. Zhang, J. Wang, Y. Zhou, X. Song, T. Li, X. Li, H. Liu, L. Zhao, Occurrence and origins of minerals in mixed-layer illite/smectite-rich coals of the Late Permian age from the Changxing Mine, eastern Yunnan, China, International Journal of Coal Geology, 102 (2012) 26-34.

[25] R.M. IMERYS, Metakaolin for concrete, Paris, France, 2014.

[26] A.A. Ramezanianpour, Metakaolin, Springer2014.

[27] B. Kaolin, 432 Park Avenue: The sky is the limit for this all-white concrete New York City skyscraper, 2013.

[28] ACI 301, 301-Specifications for Structural Concrete for Buildings, American Concrete Institute International, 32 (2005) 1313-1312.

[29] R. Toledo Filho, J. Gonçalves, B. Americano, E. Fairbairn, Potential for use of crushed waste calcined-clay brick as a supplementary cementitious material in Brazil, Cement and Concrete Research, 37 (2007) 1357-1365.

[30] D. Nied, C. Stabler, M. Zajac, Assessing the Synergistic Effect of Limestone and Metakaolin, in: K. Scrivener, A. Favier (Eds.) Calcined Clays for Sustainable Concrete: Proceedings of the 1st International Conference on Calcined Clays for Sustainable Concrete, Springer Netherlands, Dordrecht, 2015, pp. 245-251.

[31] S. Salvador, Pozzolanic properties of flash-calcined kaolinite: a comparative study with soak-calcined products, Cement and concrete research, 25 (1995) 102-112.

[32] ASTM C618, Standard Specification for Coal Fly Ash and Raw or Calcined Natural Pozzolan for Use in Concrete, ASTM International, 2015.

[33] H.H. Murray, Traditional and new applications for kaolin, smectite, and palygorskite: a general overview, Applied clay science, 17 (2000) 207-221.

[34] J. Justice, Evaluation of metakaolins for use as supplementary cementitious materials, Georgia Institute of Technology, 2005.

[35] R. Mejía de Gutiérrez, J. Torres, C. Vizcayno, R. Castelló, Influence of the calcination temperature of kaolin on the mechanical properties of mortars and concretes containing metakaolin, Clay minerals, 43 (2008) 177-183.

[36] S. Sperinck, P. Raiteri, N. Marks, K. Wright, Dehydroxylation of kaolinite to metakaolin—a molecular dynamics study, Journal of Materials Chemistry, 21 (2011) 2118-2125.

[37] P. Hawkins, P. Tennis, R. Detwiler, The use of limestone in Portland cement: a state-of-the-art review, Portland Cement Association, Skokie, Illinois, USA, 2003.

[38] C. Cement, Part 1: Compositions, specifications and conformity criteria for common cements, European standard EN, (2000) 197-191.

[39] ASTM C150, Standard Specification for Portland Cement, ASTM International, 2016.

[40] AASHTO M240, Standard specification for blended hydraulic cement, American Association of State Highway and Transportation Officials, 2016.

[41] ASTM C595, Standard Specification for Blended Hydraulic Cements, ASTM International, ASTM West Conshohocken, PA, 2014.

[42] C.S. A3001., Cementitious materials for use in concrete, Canadian Standards Association, Mississauga, Ontario, Canada, , 2013., 2013.

[43] M. Caldrone, K. Gruber, R. Burg, High reactivity MEtakaolin: a new generation mineral admixture for high performance concrete, Concrete International, 16 (1994) 11.

[44] P. Lawrence, M. Cyr, E. Ringot, Mineral admixtures in mortars: effect of inert materials on short-term hydration, Cement and concrete research, 33 (2003) 1939-1947.

[45] W. Stumm, Chemistry of the solid-water interface: processes at the mineral-water and particle-water interface in natural systems, John Wiley & Son Inc.1992.

[46] H. El-Diadamony, A. Amer, T.M. Sokkary, S. El-Hoseny, Hydration and characteristics of metakaolin pozzolanic cement pastes,, HBRC Journal, (2016).

[47] D.P. Bentz, E.J. Garboczi, on the Cement Paste-Aggregate lnterfacial Zone, ACI Materials Journal, 88 (1991).

[48] C.S. Poon, L. Lam, S.C. Kou, Y.L. Wong, R. Wong, Rate of pozzolanic reaction of metakaolin in high-performance cement pastes, Cement and Concrete Research, 31 (2001) 1301-1306.

[49] N. Coleman, W. McWhinnie, The solid state chemistry of metakaolin-blended ordinary Portland cement, Journal of materials science, 35 (2000) 2701-2710.

[50] R.D. Moser, A.R. Jayapalan, V.Y. Garas, K.E. Kurtis, Assessment of binary and ternary blends of metakaolin and Class C fly ash for alkali-silica reaction mitigation in concrete, Cement and Concrete Research, 40 (2010) 1664-1672.

[51] S. Greenberg, Reaction between Silica and Calcium Hydroxide Solutions. I. Kinetics in the Temperature Range 30 to 85 1, The Journal of Physical Chemistry, 65 (1961) 12-16.

[52] ASTM C311, Standard Test Methods for Sampling and Testing Fly Ash or Natural Pozzolans for Use in Portland-Cement Concrete, ASTM International, 2013.

[53] D.P. Bentz, A. Durán-Herrera, D. Galvez-Moreno, Comparison of ASTM C311 strength activity index testing versus testing based on constant volumetric proportions, Journal of ASTM International, 9 (2011) 1-7.

[54] G. Cochet, F. Sorrentino, Limestone filled cements: Properties and uses, Mineral admixtures in cement and concrete, 4 (1993) 266-295.

[55] S. Tsivilis, E. Chaniotakis, E. Badogiannis, G. Pahoulas, A. Ilias, A study on the parameters affecting the properties of Portland limestone cements, Cement and concrete composites, 21 (1999) 107-116.

[56] H.F.W. Taylor, A. Turner, Reactions of tricalcium silicate paste with organic liquids, Cement and Concrete Research, 17 (1987) 613-623.

[57] (!!! INVALID CITATION !!! [61-63]).

[58] K. De Weerdt, M.B. Haha, G. Le Saout, K.O. Kjellsen, H. Justnes, B. Lothenbach, Hydration mechanisms of ternary Portland cements containing limestone powder and fly ash, Cement and Concrete Research, 41 (2011) 279-291.

[59] M. Moesgaard, D. Herfort, M. Steenberg, L.F. Kirkegaard, Y. Yue, Physical performances of blended cements containing calcium aluminosilicate glass powder and limestone, Cement and Concrete Research, 41 (2011) 359-364.

[60] M. Antoni, J. Rossen, F. Martirena, K. Scrivener, Cement substitution by a combination of metakaolin and limestone, Cement and Concrete Research, 42 (2012) 1579-1589.

[61] J. Justice, K. Kurtis, Influence of metakaolin surface area on properties of cement-based materials, Journal of materials in civil engineering, 19 (2007) 762-771.

[62] A. Williams, A. Markandeya, Y. Stetsko, K. Riding, A. Zayed, Cracking potential and temperature sensitivity of metakaolin concrete, Construction and Building Materials, 120 (2016) 172-180.

[63] M. Frías, M.I.S. de Rojas, J. Cabrera, The effect that the pozzolanic reaction of metakaolin has on the heat evolution in metakaolin-cement mortars, Cement and Concrete Research, 30 (2000) 209-216.

[64] F. Lagier, K.E. Kurtis, Influence of Portland cement composition on early age reactions with metakaolin, Cement and Concrete Research, 37 (2007) 1411-1417.

[65] J. Brooks, M.M. Johari, Effect of metakaolin on creep and shrinkage of concrete, Cement and Concrete Composites, 23 (2001) 495-502.

[66] R. Siddique, J. Klaus, Influence of metakaolin on the properties of mortar and concrete: A review, Applied Clay Science, 43 (2009) 392-400.

[67] A. Al Menhosh, Y. Wang, Y. Wang, The mechanical properties of the concrete using metakaolin additive and polymer admixture, Journal of Engineering, 2016 (2016).

[68] J.M. Khatib, S. Wild, Pore size distribution of metakaolin paste, Cement and Concrete Research, 26 (1996) 1545-1553.

[69] J. Khatib, S. Wild, Pore size distribution of metakaolin paste, Cement and Concrete Research, 26 (1996) 1545-1553.

[70] P.J. Gleize, M. Cyr, G. Escadeillas, Effects of metakaolin on autogenous shrinkage of cement pastes, Cement and Concrete Composites, 29 (2007) 80-87.

[71] J. Kinuthia, S. Wild, B. Sabir, J. Bai, Self-compensating autogenous shrinkage in Portland cement—metakaolin—fly ash pastes, Advances in cement research, 12 (2000) 35-43.

[72] S. Wild, J. Khatib, L. Roose, Chemical shrinkage and autogenous shrinkage of Portland cement—metakaolin pastes, Advances in Cement Research, 10 (1998) 109-119.

[73] K.A. Riding, J.L. Poole, K.J. Folliard, M.C. Juenger, A.K. Schindler, Modeling hydration of cementitious systems, ACI Materials Journal, 109 (2012) 225-234.

[74] H.F. Taylor, Cement chemistry, Thomas Telford1997.

[75] A. Zayed, A. Sedaghat, A. Bien-Aime, N. Shanahan, Effects of portland cement particle size on heat of hydration, (2014).

[76] ASTM C150, Standard Specification for Portland Cement, ASTM International, 2007.

[77] ASTM C186, Standard Test Method for Heat of Hydration of Hydraulic Cement, ASTM International, 2015.

[78] A.K. Schindler, & Folliard, K. J., Influence of supplementary cementing materials on the heat of hydration of concrete, advances in Cement and Concrete IX ConferenceCopper Mountain Conference Resort, Colorado, 2003.

[79] A. 207.2R-07, Report Report on Thermal and Volume Change Effects on Cracking of Mass Concrete, 2007.

[80] ACI Committee 207, 207.2R-07: Report on Thermal and Volume Change Effects on Cracking of Mass Concrete, Technical Documents.

[81] S.B. Adnan A. Basma, A.-O. Salim, Prediction of Cement Degree of Hydration Using Artificial Neural Networks, Materials Journal, 96.

[82] A.K. Schindler, K.J. Folliard, Influence of supplementary cementing materials on the heat of hydration of concrete, Advances in Cement and Concrete IX Conference, Copper Mountain Conference Resort in Colorado, 2003.

[83] T. Kishi, K. Maekawa, Thermal and mechanical modelling of young concrete based on hydration process of multi-component cement minerals, in: E.E.S. R. Springenschmid (Ed.) RILEM Symposium on Thermal Cracking in Concrete at Early AgesLondon, UK., 1995.

[84] Z. Ge, Predicting temperature and strength development of the field concrete, (2005).

[85] ASTM C494, Standard Specification for Chemical Admixtures for Concrete, ASTM International, 2016.

[86] B. Bharatkumar, R. Narayanan, B. Raghuprasad, D. Ramachandramurthy, Mix proportioning of high performance concrete, Cement and Concrete Composites, 23 (2001) 71-80.

[87] P.J. Sandberg, L.R. Roberts, Cement-admixture interactions related to aluminate control, Journal of ASTM International, 2 (2005) 1-14.

[88] K.C. Hover, Concrete mixture proportioning with water-reducing admixtures to enhance durability: a quantitative model, Cement and Concrete Composites, 20 (1998) 113-119.

[89] R.L. Hill, S.L. Sarkar, R.F. Rathbone, J.C. Hower, An examination of fly ash carbon and its interactions with air entraining agent, Cement and Concrete Research, 27 (1997) 193-204.

[90] ASTM C494, Standard Specification for Chemical Admixtures for Concrete, West Conshohocken, PA, 2015.

[91] K.C. Hover, Concrete mixture proportioning with water-reducing admixtures to enhance durability: A quantitative model, Cement and Concrete Composites, 20 (1998) 113-119.

[92] L.E.C.J.C.H. T. C. Powers, H.M. Mann, Permeablity of Portland Cement Paste, Journal Proceedings, 51.

[93] Ş. Erdoğdu, Compatibility of superplasticizers with cements different in composition, Cement and Concrete Research, 30 (2000) 767-773.

[94] P. Hewlett, Lea's chemistry of cement and concrete, Butterworth-Heinemann2003.

[95] H. Uchikawa, S. Hanehara, T. Shirasaka, D. Sawaki, Effect of admixture on hydration of cement, adsorptive behavior of admixture and fluidity and setting of fresh cement paste, Cement and Concrete Research, 22 (1992) 1115-1129.

[96] A. Pierre, R. Mercier, A. Foissy, J. Lamarche, The Adsorption of Cement Superplasticizers on to Mineral Dispersions, Adsorption Science & Technology, 6 (1989) 219-231.

[97] N. Mikanovic, M.-A. Simard, C. Jolicoeur, Interaction Between Poly-Napthalene Sulfonate-Type Superplasticizers and Cements During Initial Hydration, Special Publication, 195 (2000) 561-584.

[98] W. Prince, M. Edwards-Lajnef, P.C. Aïtcin, Interaction between ettringite and a polynaphthalene sulfonate superplasticizer in a cementitious paste, Cement and Concrete Research, 32 (2002) 79-85.

[99] P.-C. Aitcin, C. Jolicoeur, J.G. MacGregor, Superplasticizers: how they work and why they occasionally don't, Concrete International, 16 (1994) 45-52.

[100] T. Danner, H. Justnes, M. Geiker, R.A. Lauten, Phase changes during the early hydration of Portland cement with Ca-lignosulfonates, Cement and Concrete Research, 69 (2015) 50-60.

[101] P. Gu, P. Xie, J.J. Beaudoin, C. Jolicoeur, Investigation of the retarding effect of superplasticizers on cement hydration by impedance spectroscopy and other methods, Cement and concrete research, 24 (1994) 433-442.

[102] M. Collepardi, Admixtures used to enhance placing characteristics of concrete, Cement and concrete composites, 20 (1998) 103-112.

[103] B. Lothenbach, F. Winnefeld, R. Figi, The influence of superplasticizers on the hydration of Portland cement, Empa, Dübendorf, Switzerland, (2007).

[104] A. Zingg, F. Winnefeld, L. Holzer, J. Pakusch, S. Becker, R. Figi, L. Gauckler, Interaction of polycarboxylate-based superplasticizers with cements containing different C3A amounts, Cement and Concrete Composites, 31 (2009) 153-162.

[105] W. Perenchio, D. Whiting, D. Kantro, Water Reduction, Slump Loss, and Entrained Air-Void Systems as Influenced by Superplasticizers, Special Publication, 62 (1979) 137-156.

[106] B.H. Zaribaf, B. Uzal, K. Kurtis, Compatibility of Superplasticizers with Limestone-Metakaolin Blended Cementitious System, Calcined Clays for Sustainable Concrete, Springer2015, pp. 427-434.

[107] T. Goto, T. Sato, K. Sakai, M. Ii, Cement-shrinkage-reducing agent and cement composition, Google Patents, 1985.

[108] S. Shh, M. Krguller, M. Sarigaphuti, Effects of shrinkage-reducing admixtures on restrained shrinkage cracking of concrete, Materials Journal, 89 (1992) 289-295.

[109] T. Zhang, S. Shang, F. Yin, A. Aishah, A. Salmiah, T.L. Ooi, Adsorptive behavior of surfactants on surface of Portland cement, Cement and Concrete Research, 31 (2001) 1009-1015.

[110] B. Rongbing, S. Jian, Synthesis and evaluation of shrinkage-reducing admixture for cementitious materials, Cement and Concrete Research, 35 (2005) 445-448.

[111] P. Hansson, B. Lindman, Surfactant-polymer interactions, Current opinion in colloid & interface science, 1 (1996) 604-613.

[112] R. Zana, Dynamics of surfactant self-assemblies: micelles, microemulsions, vesicles and lyotropic phases, CRC press2005.

[113] H. Wennerström, D. Evans, The colloidal domain: where physics, chemistry, biology, and technology meet, Wiley-VCH: New York, 1999.

[114] M. Palacios, F. Puertas, Effect of shrinkage-reducing admixtures on the properties of alkali-activated slag mortars and pastes, Cement and concrete research, 37 (2007) 691-702.

[115] D.P. Bentz, M.R. Geiker, K.K. Hansen, Shrinkage-reducing admixtures and early-age desiccation in cement pastes and mortars, Cement and concrete research, 31 (2001) 1075-1085.

[116] F. Rajabipour, G. Sant, J. Weiss, Interactions between shrinkage reducing admixtures (SRA) and cement paste's pore solution, Cement and Concrete Research, 38 (2008) 606-615.

[117] K.J. Folliard, N.S. Berke, Properties of high-performance concrete containing shrinkage-reducing admixture, Cement and Concrete Research, 27 (1997) 1357-1364.

[118] P. Juilland, E. Gallucci, R. Flatt, K. Scrivener, Dissolution theory applied to the induction period in alite hydration, Cement and Concrete Research, 40 (2010) 831-844.

[119] I. Jawed, J. Skalny, Alkalies in cement: a review: II. Effects of alkalies on hydration and performance of Portland cement, Cement and Concrete Research, 8 (1978) 37-51.

[120] A. Borsoi, M. Collepardi, S. Collepardi, R. Troli, Influence of chemical admixtures on the drying shrinkage of the concrete, this Symposium, 2009.

[121] G. Sant, F. Rajabipour, P. Lura, J. Weiss, Examining time-zero and early age expansion in pastes containing shrinkage reducing admixtures (SRA's), Proc., 2nd RILEM Symp. on Advances in Concrete through Science and Engineering, 2006.

[122] J. Weiss, P. Lura, F. Rajabipour, G. Sant, Performance of shrinkage-reducing admixtures at different humidities and at early ages, ACI Materials Journal, 105 (2008) 478-486.

[123] W.J. Weiss, B.B. Borichevsky, S.P. Shah, The influence of a shrinkage reducing admixture on early-age shrinkage behavior of high performance concrete, 5th International Symposium on Utilization of High Strength/High Performance Concrete, 1999, pp. 1339-1350.

[124] A. Balogh, New admixture combats concrete shrinkage, Concrete construction, 41 (1996) 546-551.

[125] D.P. Bentz, Influence of shrinkage-reducing admixtures on early-age properties of cement pastes, Journal of Advanced Concrete Technology, 4 (2006) 423-429.

[126] E. Badogiannis, V. Papadakis, E. Chaniotakis, S. Tsivilis, Exploitation of poor Greek kaolins: strength development of metakaolin concrete and evaluation by means of k-value, Cement and Concrete Research, 34 (2004) 1035-1041.

[127] C.S. Poon, S.C. Kou, L. Lam, Compressive strength, chloride diffusivity and pore structure of high performance metakaolin and silica fume concrete, Construction and Building Materials, 20 (2006) 858-865.

[128] J.M. Khatib, Metakaolin concrete at a low water to binder ratio, Construction and Building Materials, 22 (2008) 1691-1700.

[129] Z. Li, Z. Ding, Property improvement of Portland cement by incorporating with metakaolin and slag, Cement and Concrete Research, 33 (2003) 579-584.

[130] C.-S. Poon, L. Lam, S. Kou, Y.-L. Wong, R. Wong, Rate of pozzolanic reaction of metakaolin in high-performance cement pastes, Cement and Concrete Research, 31 (2001) 1301-1306.

[131] H.A. Razak, H. Wong, Strength estimation model for high-strength concrete incorporating metakaolin and silica fume, Cement and Concrete Research, 35 (2005) 688-695.

[132] X. Qian, Z. Li, The relationships between stress and strain for high-performance concrete with metakaolin, Cement and Concrete Research, 31 (2001) 1607-1611.

[133] A.H. Asbridge, C.L. Page, M.M. Page, Effects of metakaolin, water/binder ratio and interfacial transition zones on the microhardness of cement mortars, Cement and Concrete Research, 32 (2002) 1365-1369.

[134] T. Ramlochan, M. Thomas, K.A. Gruber, The effect of metakaolin on alkali–silica reaction in concrete, Cement and Concrete Research, 30 (2000) 339-344.

[135] L. Courard, A. Darimont, M. Schouterden, F. Ferauche, X. Willem, R. Degeimbre, Durability of mortars modified with metakaolin, Cement and Concrete Research, 33 (2003) 1473-1479.

[136] P. Mehta, P. Monteiro, Effect of aggregate, cement, and mineral admixtures on the microstructure of the transition zone, MRS Proceedings, Cambridge Univ Press, 1987, pp. 65.

[137] M. Thomas, K. Gruber, R. Hooton, The use of high reactivity metakaolin in high performance concrete, First Engineering Foundation Conference on High Strength Concrete, 1999.

[138] J. Justice, L. Kennison, B. Mohr, S. Beckwith, L. McCormick, B. Wiggins, Z. Zhang, K. Kurtis, Comparison of two metakaolins and a silica fume used as supplementary cementitious materials, SP-228, ACI, Farmington Hills, Mich, (2005) 213-236.

[139] G. Batis, P. Pantazopoulou, S. Tsivilis, E. Badogiannis, The effect of metakaolin on the corrosion behavior of cement mortars, Cement and Concrete Composites, 27 (2005) 125-130.

[140] J. Cabrera, S. Nwaubani, The microstructure and chloride ion diffusion characteristics of cements containing metakaolin and fly ash, Fly Ash, Silica Fume, Slag and Natural Pozzolans in Concrete, 1 (1998).

[141] J. Khatib, S. Wild, Sulphate resistance of metakaolin mortar, Cement and Concrete Research, 28 (1998) 83-92.

[142] D. Roy, P. Arjunan, M. Silsbee, Effect of silica fume, metakaolin, and low-calcium fly ash on chemical resistance of concrete, Cement and Concrete Research, 31 (2001) 1809-1813.

[143] W.A. Gutteridge, J.A. Dalziel, Filler cement: the effect of the secondary component on the hydration of Portland cement: part I. A fine non-hydraulic filler, Cement and Concrete Research, 20 (1990) 778-782.

[144] T. Matschei, B. Lothenbach, F.P. Glasser, The role of calcium carbonate in cement hydration, Cement and Concrete Research, 37 (2007) 551-558.

[145] J. Brooks, M.M. Johari, M. Mazloom, Effect of admixtures on the setting times of high-strength concrete, Cement and Concrete Composites, 22 (2000) 293-301.

[146] E. Badogiannis, G. Kakali, G. Dimopoulou, E. Chaniotakis, S. Tsivilis, Metakaolin as a main cement constituent. Exploitation of poor Greek kaolins, Cement and Concrete Composites, 27 (2005) 197-203.

[147] K. Yamada, T. Takahashi, S. Hanehara, M. Matsuhisa, Effects of the chemical structure on the properties of polycarboxylate-type superplasticizer, Cement and concrete research, 30 (2000) 197-207.

[148] F. Winnefeld, S. Becker, J. Pakusch, T. Götz, Effects of the molecular architecture of comb-shaped superplasticizers on their performance in cementitious systems, Cement and Concrete Composites, 29 (2007) 251-262.

[149] N. Singh, R. Sarvahi, N. Singh, Effect of superplasticizers on the hydration of cement, Cement and Concrete Research, 22 (1992) 725-735.

[150] M. Şahmaran, H.A. Christianto, İ.Ö. Yaman, The effect of chemical admixtures and mineral additives on the properties of self-compacting mortars, Cement and Concrete Composites, 28 (2006) 432-440.

[151] A. Zingg, F. Winnefeld, L. Holzer, J. Pakusch, S. Becker, R. Figi, L. Gauckler, Interaction of polycarboxylate-based superplasticizers with cements containing different C 3 A amounts, Cement and Concrete Composites, 31 (2009) 153-162.

[152] S. Pourchet, C. Comparet, L. Nicoleau, A. Nonat, Influence of PC superplasticizers on tricalcium silicate hydration, 12th International Congress on the Chemistry of Cement-ICCC 2007., 2007, pp. 000.

[153] M. Bishop, A.R. Barron, Cement hydration inhibition with sucrose, tartaric acid, and lignosulfonate: analytical and spectroscopic study, Industrial & engineering chemistry research, 45 (2006) 7042-7049.

[154] ASTM D2940-03, Standard specification for graded aggregate material for bases or subbases for highways or airports, American Society for Testing and Materials, USA, 2003.

[155] A. Korpa, R. Trettin, The influence of different drying methods on cement paste microstructures as reflected by gas adsorption: comparison between freeze-drying (F-drying), D-drying, P-drying and oven-drying methods, Cement and Concrete Research, 36 (2006) 634-649.

[156] L. Zhang, F. Glasser, Critical examination of drying damage to cement pastes, Advances in cement research, 12 (2000) 79-88.

[157] ISO 13320-1. 1999, Particle size analysis—Laserdiffraction methods—Part 1: General principles International Organization for Standardization:Geneva, CH.

[158] J. Zhang, G.W. Scherer, Comparison of methods for arresting hydration of cement, Cement and Concrete Research, 41 (2011) 1024-1036.

[159] E. Knapen, Ö. Cizer, K. Van Balen, D. Van Gemert, Comparison of solvent exchange and vacuum drying techniques to remove free water from early age cement-based materials, Proceedings of 2nd International RILEM Symposium on Advances in Concrete through Science and Engineering, Quebec, Canada, September 11-13, Rilem Publications SARL, 2006, pp. CD-rom.

[160] A. Michoel, N. De Jaeger, R. Sneyers, W. De Wispelaere, E. Geladeé, J. Kern, W. Gorter, P. van Amsterdam, Y.D. Tandt, E. Houtmeyers, Influence of porosity on the

electrical sensing zone and laser diffraction sizing of silicas. A collaborative study, Particle & Particle Systems Characterization, 11 (1994) 391-397.

[161] F. Cassagnabere, M. Lachemi, G. Escadeillas, M. Mouret, P. Broilliard, M. Joorabchian, Flash Metakaolin/slag/cement binder: An environmental and performantial alternative for steam-cured mortar for precast use, Annual Conference of the Transportation Association of Canada, 2010, pp. 1-10.

[162] ASTM C114, Standard Test Methods for Chemical Analysis of Hydraulic Cement, ASTM International, 2015.

[163] ASTM C1365, Standard Test Method for Determination of the Proportion of Phases in Portland Cement and Portland-Cement Clinker Using X-Ray Powder Diffraction Analysis, ASTM International, 2011.

[164] ASTM C150 / C150M-12, Standard Specification for Portland Cement, ASTM International, West Conshohocken, PA, 2012.

[165] T. Wriedt, Mie theory: a review, The Mie Theory, Springer2012, pp. 53-71.

[166] D. Kantro, Influence of water-reducing admixtures on properties of cement paste: A miniature slump test, Portland Cement Association1982.

[167] ASTM C143, Standard Test Method for Slump of Hydraulic-Cement Concrete, ASTM International, 2015.

[168] ASTM C1679-14, Standard Practice for Measuring Hydration Kinetics of Hydraulic Cementitious Mixtures Using Isothermal Calorimetry, ASTM International, West Conshohocken, PA, 2014.

[169] ASTM C305-14, Standard Practice for Mechanical Mixing of Hydraulic Cement Pastes and Mortars of Plastic Consistency, ASTM International, 2014.

[170] K. Scrivener, R. Snellings, B. Lothenbach, A Practical Guide to Microstructural Analysis of Cementitious Materials, Crc Press2016.

[171] J. Payá, J. Monzó, M.V. Borrachero, S. Velázquez, Evaluation of the pozzolanic activity of fluid catalytic cracking catalyst residue (FC3R). Thermogravimetric analysis studies on FC3R-Portland cement pastes, Cement and Concrete Research, 33 (2003) 603-609.

[172] L. Alarcon-Ruiz, G. Platret, E. Massieu, A. Ehrlacher, The use of thermal analysis in assessing the effect of temperature on a cement paste, Cement and Concrete research, 35 (2005) 609-613.

[173] D. Damidot, F.P. Glasser, Investigation of the CaO-Al2O3-SiO2-H2O system at 25 °C by thermodynamic calculations, Cement and Concrete Research, 25 (1995) 22-28.

[174] S. St Stöber, H. Pöllmann, Crystalchemistry of organic sulfonates used as cement additives, InMaterials Science Forum, Trans Tech Publications, 1998, pp. 904-908.

[175] M.F. Rojas, amp, x, as, M.I. Sánchez de Rojas, The effect of high curing temperature on the reaction kinetics in MK/lime and MK-blended cement matrices at 60 °C, Cement and Concrete Research, 33 (2003) 643-649.

[176] ASTM C191-13, Standard Test Methods for Time of Setting of Hydraulic Cement by Vicat Needle, ASTM International, West Conshohocken, PA, 2014.

[177] ASTM C191, Standard Test Methods for Time of Setting of Hydraulic Cement by Vicat Needle, ASTM International, 2013.

[178] ASTM C109, Standard Test Method for Compressive Strength of Hydraulic Cement Mortars (Using 2-in. or [50-mm] Cube Specimens), ASTM International, West Conshohocken, PA, , 2013.

[179] ASTM C305, Standard Practice for Mechanical Mixing of Hydraulic Cement Pastes and Mortars of Plastic Consistency, ASTM International, 2014.

[180] ASTM C191-13, Standard Test Methods for Time of Setting of Hydraulic Cement by Vicat Needle, ASTM International, West Conshohocken, PA.

[181] L.R. Roberts, P.J. Sandberg, Cement-admixture interactions related to aluminate control, Journal of ASTM International, 2 (2005) 1-14.

[182] A.K. Shrivastava, M. Kumar, Compatibility issues of cement with water reducing admixture in concrete, Perspectives in Science, 8 (2016) 290-292.

[183] ASTM C1679, Standard Practice for Measuring Hydration Kinetics of Hydraulic Cementitious Mixtures Using Isothermal Calorimetry, ASTM International, 2014.

[184] M. Collepardi, Admixtures used to enhance placing characteristics of concrete, Cement and Concrete Composites, 20 (1998) 103-112.

[185] T.A. Danner, H. Justnes, M.R. Geiker, R.A. Lauten, Effect of Lignosulfonate Plasticizers on the Hydration of C3A, 14th International Congress on the Chemistry of Cement, Beijing, China, 2015.

[186] G. Le Saout, K. Scrivener, Early hydration of Portland cement with corundum addition, 16, Internationale Baustofftagung (ibausil). Weimar, Germany, (2006) 409-416.

[187] J.W. Bullard, H.M. Jennings, R.A. Livingston, A. Nonat, G.W. Scherer, J.S. Schweitzer, K.L. Scrivener, J.J. Thomas, Mechanisms of cement hydration, Cement and Concrete Research, 41 (2011) 1208-1223.

[188] W. Prince, M. Edwards-Lajnef, P.-C. Aïtcin, Interaction between ettringite and a polynaphthalene sulfonate superplasticizer in a cementitious paste, Cement and Concrete Research, 32 (2002) 79-85.

[189] J. Young, Hydration of tricalcium aluminate with lignosulphonate additives, Magazine of Concrete Research, 14 (1962) 137-142.

[190] M.F. Rojas, M.I. Sánchez de Rojas, Influence of metastable hydrated phases on the pore size distribution and degree of hydration of MK-blended cements cured at 60 °C, Cement and Concrete Research, 35 (2005) 1292-1298.

[191] G. Habert, J.B. d'Espinose de Lacaillerie, N. Roussel, An environmental evaluation of geopolymer based concrete production: reviewing current research trends, Journal of Cleaner Production, 19 (2011) 1229-1238.

[192] A. Sharma, A. Saxena, M. Sethi, V. Shree, Life cycle assessment of buildings: a review, Renewable and Sustainable Energy Reviews, 15 (2011) 871-875.

[193] A.P. Gursel, E. Masanet, A. Horvath, A. Stadel, Life-cycle inventory analysis of concrete production: a critical review, Cement and Concrete Composites, 51 (2014) 38-48.

[194] V.S. Ramachandran, Concrete admixtures handbook: properties, science and technology, William Andrew1996.

[195] E. Sakai, K. Raina, K. Asaga, S. Goto, R. Kondo, Influence of sodium aromatic sulfonates on the hydration of tricalcium aluminate with or without gypsym, Cement and Concrete Research, 10 (1980) 311-319.

[196] E. Sakai, T. Kasuga, T. Sugiyama, K. Asaga, M. Daimon, Influence of superplasticizers on the hydration of cement and the pore structure of hardened cement, Cement and concrete research, 36 (2006) 2049-2053.

[197] F.A. Branco, P. Mendes, E. Mirambell, Heat of hydration effects in concrete structures, Materials Journal, 89 (1992) 139-145.

[198] J. Taplin, A method for following the hydration reaction in portland cement paste, Australian Journal of Applied Science, 10 (1959) 329-345.

[199] F. Lin, C. Meyer, Hydration kinetics modeling of Portland cement considering the effects of curing temperature and applied pressure, Cement and Concrete Research, 39 (2009) 255-265.

[200] D.P. Bentz, E.J. Garboczi, C.J. Haecker, O.M. Jensen, Effects of cement particle size distribution on performance properties of Portland cement-based materials, Cement and Concrete Research, 29 (1999) 1663-1671.

[201] K.A. Riding, J.L. Poole, K.J. Folliard, M.C. Juenger, A.K. Schindler, Modeling hydration of cementitious systems, ACI Materials Journal, 109 (2013) 225-234.

[202] G. Dul'Nev, N. Pilipenko, A method of determining the heat of cement hydration, Journal of Engineering Physics and Thermophysics, 23 (1972) 901-903.

[203] K. Van Breugel, Simulation of hydration and formation of structure in hardening cement-based materials, (1991).

[204] A.A. Ramezanianpour, Metakaolin, Cement replacement materials, Springer Berlin Heidelberg2014, pp. 225-255.

[205] Georgia Department of Transportation (GDOT), Standard Specifications for Construction of Transportation Systems, Section 500., Concrete Structures.Georgia Department of Transportation., 2015.

[206] ASTM C138, Standard Test Method for Density (Unit Weight), Yield, and Air Content (Gravimetric) of Concrete, ASTM International, 2016.

[207] ASTM C231, Standard Test Method for Air Content of Freshly Mixed Concrete by the Pressure Method, ASTM International, 2014.

[208] ASTM C39, Standard Test Method for Compressive Strength of Cylindrical Concrete Specimens, ASTM International, 2017.

[209] A. C496., Standard Test Method for Splitting Tensile Strength of Cylindrical Concrete Specimens, ASTM International, 2004.

[210] ASTM C469, Standard Test Method for Static Modulus of Elasticity and Poisson’s Ratio of Concrete in Compression, ASTM International, 2014.

[211] ASTM 1202, Standard Test Method for Electrical Indication of Concrete's Ability to Resist Chloride Ion Penetration, ASTM International, 2012.

[212] AASHTO T277, Standard Method of Test for Rapid Determination of the Chloride Permeability of Concrete, Standard Specifications-Part II Tests, Washington, DC., 1990.

[213] A. T-259-02, Standard method of test for resistance of concrete to chloride ion penetration, American Association of State Highway and Transportation Officials, Washington, DD, USA 2002.

[214] A.T. 358-15, Standard method of test for surface resistivity indication of concrete's ability to resist chloride ion penetration, American Association of State Highway and Transportation Officials, 2011.

[215] ASMT C157, Standard Test Method for Length Change of Hardened Hydraulic-Cement Mortar and Concrete, ASTM International, 2014.

[216] D. Whiting, D. Stark, Control of air content in concrete, NCHRP report, (1983).

[217] H.A. Razak, H.S. Wong, Effect of Incorporating Metakaolin on Fresh and Hardened Properties of Concrete, Special Publication, 200.

[218] A. Lange, J. Plank, Study on the foaming behaviour of allyl ether-based polycarboxylate superplasticizers, Cement and Concrete Research, 42 (2012) 484-489.

[219] A. Dubey, N. Banthia, Influence of high-reactivity metakaolin and silica fume on the flexural toughness of high-performance steel fiber-reinforced concrete, ACI Materials Journal, 95 (1998) 284-292.

[220] P. Monteiro, Concrete: Microstructure, Properties, and Materials, McGraw-Hill Publishing2006.

[221] ACI Committee 318, Building code requirements for structural concrete (ACI 318-08) and commentary, American Concrete Institute, International Organization for Standardization., 2008.

[222] ACI Committee 363, State-of-the-Art Report on High-Strength Concrete (ACI 363R),, American Concrete Institute, Farmington Hills, Mich.

[223] J.D. Dewar, The Indirect Tensile Strength of Concrete of High Compressive Strength, in: T.R.N. 42.377 (Ed.) Cement and Concrete AssociationWexham Springs, England, 1964.

[224] N.J. Carino, H. Lew, Re-examination of the relation between splitting tensile and compressive strength of normal weight concrete, Journal Proceedings, 1982, pp. 214-219.

[225] J.M. Raphael, Tensile strength of concrete, Journal Proceedings, 1984, pp. 158-165.

[226] N. Gardner, P. Sau, M.S. Cheung, Strength development and durability of concretes cast and cured at 0 C, Materials Journal, 85 (1988) 529-536.

[227] E. Arıoglu, C. Girgin, N. Arıoglu, Re-evaluation of ratio of tensile strength to compressive strength for normal-strength concrete, Journal of Ready Mix Concrete, (2002) 58-63.

[228] N. Arıoglu, Z.C. Girgin, E. Arıoglu, Evaluation of ratio between splitting tensile strength and compressive strength for concretes up to 120 MPa and its application in strength criterion, ACI Materials Journal, 103 (2006) 18-24.

[229] S.H. Ahmad, S.P. Shah, Structural properties of high strength concrete and its implications for precast prestressed concrete, PCI Journal, 30 (1985) 92-119.

[230] H.-S. Kim, S.-H. Lee, H.-Y. Moon, Strength properties and durability aspects of high strength concrete using Korean metakaolin, Construction and building materials, 21 (2007) 1229-1237.

[231] P. Dinakar, P.K. Sahoo, G. Sriram, Effect of metakaolin content on the properties of high strength concrete, International Journal of Concrete Structures and Materials, 7 (2013) 215-223.

[232] E. Güneyisi, M. Gesoğlu, K. Mermerdaş, Improving strength, drying shrinkage, and pore structure of concrete using metakaolin, Materials and Structures, 41 (2008) 937-949.

[233] P.K. Mehta and P.J.M. Monteiro, Concrete: Microstructure, Properties, and Materials,, McGraw-Hill, , 2014.

[234] AASHTO-LRFD Bridge Design Specifications, American Association of State Highway and Transportation Officials, Washington DC, 20001 (2007).

[235] I. Janotka, T. Nürnbergerová, Effect of temperature on structural quality of the cement paste and high-strength concrete with silica fume, Nuclear Engineering and Design, 235 (2005) 2019-2032.

[236] B. Persson, Poisson's ratio of high-performance concrete, Cement and Concrete Research, 29 (1999) 1647-1653.

[237] E. Nadelman, Ph.D dissertation: Hydration And Microstructural Development Of Portland Limestone Cement-Based Materials, School of Civil and Environmental Engineering, Georgia Institute of Technology, 2016.

[238] C. Shi, Effect of mixing proportions of concrete on its electrical conductivity and the rapid chloride permeability test (ASTM C1202 or ASSHTO T277) results, Cement and Concrete Research, 34 (2004) 537-545.

[239] D.P. Bentz, O.M. Jensen, Mitigation strategies for autogenous shrinkage cracking, Cement and Concrete Composites, 26 (2004) 677-685.

[240] D.P. Bentz, M.A. Peltz, Reducing thermal and autogenous shrinkage contributions to early-age cracking, ACI Materials Journal, 105 (2008) 414.

[241] H.W. Brewer, R.W. Burrows, Coarse-ground cement makes more durable concrete, Journal Proceedings, 1951, pp. 353-360.

[242] D.A. Whiting, R.J. Detwiler, E.S. Lagergren, Cracking tendency and drying shrinkage of silica fume concrete for bridge deck applications, Materials Journal, 97 (2000) 71-77.

[243] T.H.W. H. Li, S.F. Wong, Early-Age Creep and Shrinkage of Blended Cement Concrete, Materials Journal, 99.

[244] R.T.F.H. Charles Nmai, B. Julie, Shrinkage-Reducing Admixtures, Concrete International, 20.

[245] T. Sato, T. Goto, K. Sakai, Mechanism for reducing drying shrinkage of hardened cement by organic additives, CAJ Rev, 5 (1983) 52-55.

[246] M. Collepardi, A. Borsoi, S. Collepardi, J.J.O. Olagot, R. Troli, Effects of shrinkage reducing admixture in shrinkage compensating concrete under non-wet curing conditions, Cement and Concrete Composites, 27 (2005) 704-708.

[247] A.B. Ribeiro, A. Gonçalves, A. Carrajola, Effect of shrinkage reduction admixtures on the pore structure properties of mortars, Materials and Structures, 39 (2006) 179-187.

[248] E.-i. Tazawa, S. Miyazawa, Influence of cement and admixture on autogenous shrinkage of cement paste, Cement and Concrete Research, 25 (1995) 281-287.

[249] J.N. Israelachvili, Intermolecular and surface forces, Academic press2011.

[250] D.F. Evans, H. Wennerstrom, Colloidal domain, Wiley-Vch1999.

[251] R. Zana, Introduction to surfactants and surfactant self-assemblies, Dynamics of Surfactant Self-Assemblies: Micelles, Microemulsions, Vesicles and Lyotropic Phases, CRC Press2005, pp. 1-35.

[252] P. Lura, O.M. Jensen, K. van Breugel, Autogenous shrinkage in high-performance cement paste: An evaluation of basic mechanisms, Cement and Concrete Research, 33 (2003) 223-232.

[253] ASTM C1698-09, Standard Test Method for Autogenous Strain of Cement Paste and Mortar, , ASTM International, West Conshohocken, PA,, 2014.

[254] B.J. Mohr, K.L. Hood, Influence of bleed water reabsorption on cement paste autogenous deformation, Cement and Concrete Research, 40 (2010) 220-225.

[255] J.J. Gilman, Direct measurements of the surface energies of crystals, Journal of Applied Physics, 31 (1960) 2208-2218.

[256] F. Hejda, P. Solar, J. Kousal, Surface free energy determination by contact angle measurements–A comparison of various approaches, WDS, 2010, pp. 25-30.

[257] C.Y. Rha, J.W. Seong, C.E. Kim, S.K. Lee, W.K. Kim, Properties and interaction of cement with polymer in the hardened cement pastes added absorbent polymer, Journal of Materials Science, 34 (1999) 4653-4659.

[258] J. Camilleri, A. Cutajar, B. Mallia, Hydration characteristics of zirconium oxide replaced Portland cement for use as a root-end filling material, Dental Materials, 27 (2011) 845-854.

[259] S. Brunauer, P.H. Emmett, E. Teller, Adsorption of gases in multimolecular layers, Journal of the American chemical society, 60 (1938) 309-319.

[260] E.P. Barrett, L.G. Joyner, P.P. Halenda, The determination of pore volume and area distributions in porous substances. I. Computations from nitrogen isotherms, Journal of the American Chemical society, 73 (1951) 373-380.

[261] S. Weber, H.W. Reinhardt, Improved Durability of High-Strength Concrete Due to Autogenous Curing, Special Publication, 170.

[262] P.C. Aïtcin, The durability characteristics of high performance concrete: a review, Cement and Concrete Composites, 25 (2003) 409-420.

[263] P.-C. Aitcin, A. Neville, P. Acker, Integrated view of shrinkage deformation, Concrete International, 19 (1997) 35-41.

[264] B. Lothenbach, G. Le Saout, E. Gallucci, K. Scrivener, Influence of limestone on the hydration of Portland cements, Cement and Concrete Research, 38 (2008) 848-860.

[265] P. Hawkins, P.D. Tennis, R.J. Detwiler, The use of limestone in Portland cement: a state-of-the-art review, Portland Cement Association Skokie2003.

[266] S. Slatnick, K.A. Riding, K.J. Folliard, M.C. Juenger, A.K. Schindler, Evaluation of Autogenous Deformation of Concrete at Early Ages, ACI Materials Journal, 108 (2011).

[267] G. Sant, B. Lothenbach, P. Juilland, G. Le Saout, J. Weiss, K. Scrivener, The origin of early age expansions induced in cementitious materials containing shrinkage reducing admixtures, Cement and Concrete Research, 41 (2011) 218-229.

[268] E. Gartner, J. Young, D. Damidot, I. Jawed, Hydration of Portland cement, Structure and performance of cements, 13 (2002) 978-970.

[269] T. Zhang, S. Shang, F. Yin, A. Aishah, A. Salmiah, T. Ooi, Adsorptive behavior of surfactants on surface of Portland cement, Cement and Concrete Research, 31 (2001) 1009-1015.

[270] S. Mindess, J.F. Young, D. Darwin, Concrete 2nd Edition, Upper Saddle River, NJ: Pearson Education, Inc, 2003.

[271] B.L. Cope, G.E. Ramey, Reducing drying shrinkage of bridge-deck concrete, Concrete International, 23 (2001) 76-82.

[272] J. Brooks, X. Jiang, The influence of chemical admixtures on restrained drying shrinkage of concrete, Special Publication, 173 (1997) 249-266.

[273] H.G. Russell, R. Miller, H. Ozyildirim, M. Tadros, Compilation and Evaluation of Results from High-Performance Concrete Bridge Projects, Volume I: Final Report, 2006.

[274] Georgia department of transportation (GDOT), SUPPLEMENTAL SPECIFICATION, Section 500—Concrete Structures, 2013.